CHAOS, CONTROL AND SYNCHRONIZATION IN EXCITATORY-INHIBITORY NEURAL NETWORK MODELS

Sitabhra Sinha

Machine Intelligence Unit
Indian Statistical Institute
Calcutta 700035, India

A thesis submitted to the *Indian Statistical Institute*
in partial fulfillment of the requirements for the degree of
Doctor of Philosophy
1998

ACKNOWLEDGEMENTS

I would like to take this opportunity to express my heartfelt gratitude and indebtedness to my supervisor, Prof. Sankar K. Pal, for his constant support and guidance during the tenure of my research work. I am thankful to him for the confidence he placed on me, and his encouragement throughout the last four years.

I am also indebted to Prof. Bikas K. Chakrabarti, who was not only my co-author, but has also helped in developing my analytical thinking through his valuable comments and suggestions. I cherish the memories of the time spent in discussing different aspects of my work with both Prof. Pal and Prof. Chakrabarti.

I thank my co-authors Dr. Jayanta Basak, Sambhunath Biswas and Suvranshu Kar, for not only allowing me to include the joint research work in this thesis, but also to enrich my knowledge through numerous discussions.

Heartfelt thanks are due to my former teachers, Dr. Indrani Bose and Dr. Ranjan Roy, who have encouraged me throughout to continue research in the somewhat unconventional field of chaotic neural modeling. I have benefited greatly by my discussions with Prof. Jayanta K. Bhattacharjee, whose knowledgeable comments have shed new light on several points. I also take this opportunity to express sincere gratitude to my former teachers Pinaki Mitra, Dr. Sisir Bhanja and Dr. Albert C. Gomes, who have inculcated in me the spirit of learning.

It is a pleasure to thank Mrs. Deepavati Sen, who, as director of Jagadis Bose National Science Talent Search, made it possible for me to experience the real world of academic research during my undergraduate days. I am also grateful to Prof. Chandan Dasgupta and Prof. Deepak Dhar for spending their valuable time in discussing physical problems, which allowed me a glimpse of how scientists think about a problem.

To my friends Saugata Bhattacharya, Rudra Dutta, Aviroop Moulik and Nirmalya Chakrabarty, I would like to express my appreciation for their assistance throughout these years.

Among MIU colleagues, I would like to thank B. Umashankar, for his assistance in computational problems, as well as providing a quotation for the concluding chapter. A special note of thanks to Dr. M. K. Kundu, Dr. N. R. Pal, Dr. C. A. Murthy, Dr. D. P. Mandal, Dr. S. Mitra, Dr. A. Ghosh and my research colleagues Rajat De, Suman Mitra, Sanghamitra Bandyopadhyay, Mousumi Acharyya, Pabitra Mitra and Arunima Banerjee. I also acknowledge the office staff of Machine Intelligence Unit, especially Mr. Indranil Dutta, for providing a friendly environment and the staff of the reprography unit for careful photocopying.

This thesis could not have been completed in time without the assistance of my wife, Indrani, who actively helped me during the writing and preparation of the manuscript. Her encouragement and constant support have kept me going through several discouraging moments. Words are inadequate to express my gratitude to my parents for their warm support and encouragement in all my undertakings. Their constant encouragement, enthusiasm and support have helped me face the challenges of life. I would also like to express my indebtedness to Bina-di, who did not live to see my thesis completed. Thanks are due to my in-laws, who urged me constantly to finish my work in time.

Finally, I express my sincere thanks to the authorities of ISI for the facilities extended to carry out my research work.

ISI, Calcutta
November, 1998.

Contents

List of Figures

Chapter 1

Introduction

Who traces life and seeks to give
Descriptions of the things that live
Begins with 'Killing to Dissect'
He gets the pieces to inspect
The lifeless limbs beneath his knife
All parts - but link which gave them life.
Goethe

The answer to the question of life, the universe
and everything is twenty-two.
Douglas Adams

Since the development of the electronic computer in the 1940s, the serial processing computational paradigm has successfully held sway. It has developed to the point where it is now ubiquitous. However, there are many tasks which are yet to be successfully tackled computationally. A case in point is the multifarious activities that the human brain performs regularly, including pattern recognition, associative recall, etc. which is extremely difficult, if not impossible to do using traditional computation.

This problem has led to the development of non-standard techniques to tackle situations at which biological information processing systems excel. One of the more successful of such developments aims at "reverse-engineering" the biological apparatus itself to find out why and how it works. The field of neural network models has grown up on the premise that the massively parallel distributed processing and connectionist structure observed in the brain is the key behind its superior performance. By implementing these features in the design of a new class of architectures and algorithms, it is hoped that machines will approach human-like ability in handling real-world situations.

Network models of computation have been enjoying a period of revival for quiet some time now, from the perspective of both theory and applications [85]. These

models comprise networks of large numbers of simple processing elements, usually having continuously varying activation values and stochastic threshold dynamics. The activity of these elements, x_i ($i = 1, 2, ..., N$) at some time instant t, are determined by the temporal evolution equation:

$$x_i\ (t)\ =\ \mathrm{F}\ (\ \Sigma_j\ W_{ij}\ x_j\ (t-1)\ -\ \theta_i\ ),$$

where, θ_i is an internal threshold (usually taken as zero), W_{ij} is the connection weight from element j to element i, and F is a nonlinear activation function. If $W_{ij} > 0$, the synaptic connection between neurons i and j is called *excitatory*; if $W_{ij} < 0$, it is called *inhibitory*. The activation function, F, usually has a sigmoid form, which may be of the following type:

$$\mathrm{F}(z)\ =\ \tanh(\frac{z}{a}),$$

a being the slope. For a= 0, F is a "hard limiting" or step function,

$$x_i\ =\ \mathrm{sgn}\ (\ \Sigma_j\ W_{ij}\ x_j\ -\ \theta_i\ ).$$

Different neural network models are specified by

- network topology, i.e. the pattern of connections between the elements comprising the network,
- characteristics of the processing element, e.g. the explicit form of the nonlinear function F, and the value of the threshold, θ,
- learning rule, i.e. the rules for computing the connection weights W_{ij} appropriate for a given task, and,
- updating rule, e.g. the states of the processing elements may be updated in parallel (synchronous updating), sequentially or randomly.

One of the limitations of most network models at present is that they are basically static, i.e., once an equilibrium state is reached, the network remains in that state, until the arrival of new external input [8]. In contrast, real neural networks show a preponderance of dynamical behavior. Once we recall a memory, our minds are not stuck to it, but also recall other associated memories without being prompted by any additional external stimuli. This ability to 'jump' from one memory to another in the absence of appropriate stimuli is one of the hallmarks of the brain. It is an ability which one should try to recreate in a network model if it is ever to come close to human-like performance in intellectual tasks. One of the possible ways of simulating such behavior is through models guided by non-equilibrium dynamics, in particular, chaos. This is because of the much richer dynamical possibilities of such networks, compared to systems governed by convergent dynamics [86, 7].

There is as yet no universally accepted definition of the term "chaos", but the following working definition is adequate for our purpose [188]:

> Chaos is *aperiodic* long-term behavior in *deterministic* systems that exhibit *sensitive dependence* on initial conditions.

"Aperiodic long-term behavior" means that there are trajectories which do not settle down to fixed points, periodic orbits, or quasiperiodic orbits as time, $t \rightarrow \infty$. Aperiodic behavior is marked by a broad frequency spectrum. "Deterministic" implies that the system has no random/ noisy inputs or parameters. The irregular behavior arises from the system's inherent nonlinearity. "Sensitive dependence on initial conditions" indicates that nearby trajectories separate exponentially fast. As a result, any error in our knowledge of the initial conditions of the system will amplify rapidly, making its behavior effectively unpredictable.

In this thesis, we present some results of theoretical and simulation studies exploring the occurrence and utility of chaotic dynamics in network computation, particularly in the case of networks of nonlinear devices ("neurons") of 2 specific classes: excitatory and inhibitory. Section 1 discusses the biological evidence for chaotic activity in the brain. The necessity of modeling to resolve the controversy of interpreting the biological data is briefly outlined. Even if chaos exists, its role in the functioning of the brain will need to be established. The possible advantages of chaos for information processing is discussed in Section 2. Section 3 contains a brief survey of the work done in the general area of chaotic neural networks. However, so many papers in this area have appeared over the past decade, that any review can at best be partial. We have stressed on work which leads directly to the model network studied in the thesis. We have also tried to trace the "ancestry" of our model. Finally, in Section 4, the scope of the thesis is outlined.

1.1 Neurobiological evidence of chaos

Evidence of deterministic chaos in neuronal systems was found within a very short time of the emergence of the field of chaotic dynamics. Experiments on excitable biological membranes, supplemented by physiologically plausible models of neurons showed that chaos occurs in the presence of periodic stimulation (either chemical or electrical). Hayashi *et al* [79] investigated the nonperiodic behavior in self-sustained oscillation of the internodal cell of *Nitella* under sinusoidal stimulation. The analysis of the nonperiodic oscillations revealed chaotic behavior. Chaotic oscillations was also observed in the molluscan neuron [88]. Another group of researchers [3] studied the self-sustained oscillation of action potentials in a model axon immersed in calcium-deficient sea water, whose dynamics was modeled by the Hodgkin-Huxley equations. The oscillations were analyzed by stroboscopic plots revealing both periodic and chaotic behavior, determined by the amplitude and the frequency of the stimulating current. The results corroborated similar studies carried out previously in squid giant axons (for an overview, see [121] or the article by Aihara and Matsumoto in [87]). The group of Glass and Guevara [72] showed that recurrent inhibition and

periodic forcing of neural oscillators can produce chaos and explored its implications in modeling normal and abnormal function in neurophysiology. However, most of the experimental work was done with the membranes in artificial circumstances, the electrical and/or chemical stimulations being far from the physiological state. The occurrence of chaos in equations for membrane excitability even in the absence of stimulation was shown in [34].

After demonstrating chaos in the case of single neurons, the obvious next step was to show it in macroscopic neural assemblages, and in particular, the brain. However, this progression was far from simple. For one thing, the complementary approaches of experimental observations and modeling used successfully in the case of single neuron studies, could not be used in the case of the brain. In the absence of any good model for large-scale brain activity, the evidence for chaos in the brain has to be searched for in such coarse-grained variables as the EEG. One of the complicating factors in studying EEG is the continuous presence of background "spontaneous" neural activity, seemingly random in appearance. One has to therefore devise a test to determine whether this apparent randomness is truly stochastic or owes its origin to deterministic chaos. Analysis of human EEG in various mental states have put forward several candidates for chaotic activity. Evidence of low-dimensional chaos was found in some sleep stages [15] and in 'petit mal' epileptic seizures of small duration [14]. However, any claim based on time-series analysis of EEG data depends on the efficiency of the tests for determining chaotic activity [65, 67, 27, 138]. Such methods usually require large data sets recorded under constant conditions and relatively free of noise. As all three requirements are hard to satisfy in the case of biological data, the detection of low dimensional chaos in brain activity has often been questioned [62]. The dependence of the results of such tests on the brain site at which recording occurs and on the state of the subject (wakeful, resting, or moving) have been shown by Pijn *et al* [145]. Several attempts have been made to devise new tests which will provide unequivocal results when applied to such data sets, including nonlinear forecasting techniques, but as yet no one has come up with an universally accepted method.

It has been suggested that the use of chaos control techniques to suppress and enhance aperiodic activity in brain-slice preparations [155] is a clear-cut evidence in favor of the presence of chaotic dynamics in the brain. However, such control methods have been shown to be effective even in non-chaotic systems [37]. The presence of unstable periodic orbits (UPOs) in chaotic trajectories has suggested a new method, relying on the detection of such UPOs in the biological time series. Statistically significant evidence of the existence of UPOs in a crayfish sensory neuron [142] have been reported, with experimental parameters being kept in ranges typically found in the animal's natural environment.

Chaos has also been implicated in certain 'dynamical diseases' - medical problems that have their roots in some underlying dynamical effect [89]. In the neurological context, abnormal oscillations and complex rhythms often pose clinical problems. There may be significant oscillation in a neurological control system that does not

normally have a rhythm, e.g., ankle tremor in patients with corticospinal tract disease, various movement disorders like Parkinson's tremors, and abnormal paroxysmal oscillations in the discharge of neurons that occur in many seizures. Otherwise, there may be qualitative changes in the oscillations within an already rhythmic process, resulting in waking abnormality, alerted sleepwake cycles, or rapidly cycling manic depression. Epileptic seizures, which recur in an apparently random manner, may be yet another manifestation of such pathological dynamics. However, in the absence of any reasonable models of such complex neural processes, the role of chaos in these dynamical diseases cannot be established beyond doubt.

1.2 Chaos and information processing

Even if chaos does exist in the brain, the issue of whether it plays any role in the overall cognitive functioning of the brain needs to be looked into. The possible uses of chaos in the biological world has been discussed in [38]. In the context of brain functioning, chaos may have the multiple roles of generating and preserving diversity, maintenance of network activity through disentrainment, dissipation of disturbance and facilitating learning. All these different functions enable the nervous system to be adaptive, and continue to function in the face of an uncertain and unknown environment.

The role of chaos in higher brain functions is discussed in [75]. In the context of information processing, it would appear at first that chaos can play only a negative role. However, the brain is *not* a conventional processor of information, in the sense of classical information theory, as developed by Shannon, Wiener and others. In the case of a highly nonlinear and interconnected system such as the brain, chaotic dynamics might play a counter intuitive role by enhancing the robustness, reliability and overall functionality of neural information processing. The particular case of thalamocortical interactions as a generator of chaotic activity [129] and its possible role for generating self-referential logic and short-term memory, were explored in [130].

Tsuda [192] has suggested several other possible roles of cortical chaos in brain functioning:

- Interpreter for input stimuli via thalamo-cortical interactions.
- Efficient search mechanism in memory.
- Robust information transfer channel for periodically oscillating stimuli.
- Providing dynamic storage of long-term memory.

The work on human EEG analysis has suggested a further possible functional role of chaos [14]. Chaos seems to increase the resonance capacity of the brain, enabling

an extremely rich response to an external stimulus, as compared to stable periodic oscillations.

However, the most well-known work to obtain empirical physiological evidence for the possible relevance of chaos to brain function is probably that of W. J. Freeman. Through his work on the large-scale collective behavior of neurons in the perception of olfactory stimuli [51], [177], [52], a concrete link between chaos and cognition has been built up through a successful combination of biological experiments and computational modeling. Olfactory stimuli are detected by receptor neurons in the nasal passage. The number of receptors excited by a smell is a measure of the intensity of the stimulus, while the spatial pattern of activated receptors is dependent on the nature of the scent. On trapping molecules carrying specific odors these receptors fire action potentials which are transmitted to the olfactory bulb in the cortex. The bulb then transmits signals to the olfactory cortex which, in its turn, sends information to many regions of the brain. The test animals used by Freeman were trained to recognize several different odors and were then subjected to smells, both familiar and unfamiliar. EEG data was recorded by a grid-like array of electrodes placed over the surface of the olfactory bulb. Most of the time, the EEGs showed irregular oscillations. However, when an animal inhaled, a "burst" occurred in each EEG tracing as all the waves in the array became more regular for a brief period until the animal exhaled. These waves, named gamma waves, had a higher amplitude and frequency than usual and varied in frequency from 20 - 90 Hz, mostly occurring in the neighborhood of 40 Hz. Each set of burst recordings had a common carrier waveform, although the average amplitude of the different recordings varied widely. It was inferred that, as the carrier waveform changed during each inhalation, even for the same stimulus, the information about a particular scent was not encoded in the shape of the waveform but rather, in the spatial pattern of the carrier-wave amplitudes across the bulb, which remained invariant over trials. On plotting the different amplitudes of the carrier waves in different regions of a surface representing the locations in the grid-like array over the olfactory bulb from which they were obtained, a contour diagram was produced. This remained the same for a specific scent throughout the testing period. However, if the reinforcement associated with a scent was altered, then the amplitude contour map representing it also changed. This indicated that the olfactory bulb is involved in the assigning of meaning to stimuli. One of the early pointers to chaotic activity was the aperiodicity of the common carrier wave in the bulb both during and between bursts. Another clue was the sudden transitions of neuronal networks in the bulb and the cortex from a non-burst to a active, bursting state. These factors prompted the development of a model for the olfactory system having cells in a network connected by both excitatory and inhibitory synapses. Computer simulations of the model showed that it recreated all the observed behavior of the olfactory system and, thus, was an accurate representation of it. The network was then made to produce EEGs of extended bursts and of inter burst activity for a longer period than is possible in actual EEGs. The

attractor [1] of the underlying dynamics, reconstructed from the EEG data using the delay-coordinate technique was found to be chaotic in nature. The primary findings suggested that a separate chaotic attractor is maintained for each stimulus and the act of perception consists of a transition of the system from the domain of influence of one attractor to another. Later findings led Freeman to hypothesize that each brain area (rather than each stimulus) has a chaotic attractor. A specific sensory stimulus drives the system into a localized region within the attractor, which can be identified with the appearance of specific spatial patterns of carrier waveform amplitudes, associated with a specific stimulus. Further, the attractors themselves would have to change as a result of new experience and continued development of the brain.

This description of non equilibrium nervous activity has suggested several possible functions of chaos:

- providing rapid and unbiased access to a number of possible attractors, one of which is selected dependent upon the stimulus,
- acting as a "novelty filter" by failing to converge to any of the existing attractors in the presence of a significant but unidentified stimulus, and,
- allowing the system to escape from the existing set of attractors and add a new response to a novel stimulus under reinforcement

Thus, according to this picture, chaotic activity is fundamental to the general process of perception.

1.3 A brief survey of chaotic neural network models

Extremely simplified models of neurons connected in a network via suitable connection weights were known to implement various logical functions since the 1940s [124]. The subject received fresh impetus a decade and half ago due to some breakthroughs, e.g., the identification of a class of globally connected network models with 'spin glass' models [126] of condensed matter physics by Hopfield [90] (see also [159]). These developments were however restricted to networks subject to equilibrium dynamics. Such systems converge to a time-independent solution (a "fixed-point" attractor) after starting off from some initial condition. On the other hand, the brain never settles down to a steady state but appears to exhibit a rich variety of non-periodic behavior.

[1] *Attractor* of a dynamical system is a set to which all neighboring trajectories converge. Stable fixed points and stable limit cycles are examples. An attractor that exhibits sensitive dependence on initial conditions is a chaotic attractor.

The development of nonlinear dynamical systems theory - in particular, the discovery of "deterministic chaos" in extremely simple systems - has furnished the theoretical tools necessary for analyzing non-equilibrium network dynamics. Neurobiological studies indicating the presence of chaotic dynamics in the brain and its possible role in biological information processing has provided further motivation. Thus, the ability to design networks with aperiodic behavior promises to add a new dimension to our understanding of how the brain works.

Several efforts in designing and applying chaotic neural networks have been reported. One of the first such studies was on a continuous time randomly connected network [108], whose individual elements are inherently stable. The high dimensionality of this example precludes a theoretical understanding. However, numerical studies showed the occurrence of chaos.

Chaotic dynamics in a globally connected network with Gaussian distribution of connection weights was theoretically established by Sompolinsky *et al* [180] in the thermodynamic limit (i.e., $N \rightarrow \infty$, N= the number of neurons). This was extended to networks with variable connectivity in [49], which showed through numerical simulations that the connectivity is not a determinant parameter for the behavior of such nets.

Aihara *et al* [4] developed a neural network model where each neuron behaved as a chaotic system, due to the introduction of delayed interactions [127]. This model was shown to be effective in solving optimization problems [35], as the chaotic behavior could be used as to perform a deterministic version of *simulated annealing* [103]. The network can also be used for image segmentation [77] and associative recall [1].

Recurrent neural networks with a single hidden layer have been proposed as a realization of one-dimensional maps of an interval onto itself which show chaotic behavior [9]. By encoding images as strings and relating them to stable limit cycles of a chaotic map [10], such networks have been used to store and retrieve images.

Destexhe [44] has studied two-dimensional networks of excitatory and inhibitory neurons which evolve in continuous time, with time-delayed interactions. As the number of neurons, connectivity and synaptic weights are varied, the model exhibits a transition from spatially uniform oscillations to spatiotemporal chaos. Several properties of the spatiotemporal phase and the information transport in such a system was studied. Hayashi [80] has also examined a continuous-time evolving network of excitatory and inhibitory neurons, with the aim of implementing a model of dynamical associative memory.

Associative recall through non-equilibrium dynamics has also been explored (in the discrete time evolution context) by Thomas *et al* [191], who use a network with randomly connected excitatory neurons with an inhibitory interneuron that adjusts their threshold, and Yamakawa *et al* [205].

Wang [197, 24] has studied the simple system of an excitatory and inhibitory neuron evolving in discrete time to analytically establish the occurrence of chaos. A similar

system has been studied in [149] to see how onset of chaos occurs as a function of stimulus intensity. Variants of the model have been used for demonstration of chaos control methods in the neural context [179, 186].

Coupled map lattices [99] [100] which are networks of chaotic systems coupled to each other, either locally or globally, share several common features with neural networks. The relation of a globally coupled map lattice to neural network models has been explored in [101]. Such systems have, in fact, been proposed as plausible models of neural computation for performing optimization [94] and associative recall [96].

The Hopfield model, which shows only equilibrium dynamics, has been shown to exhibit chaos when a nonlinear self-feedback term is introduced [33]. The chaotic dynamics prevents the network from staying at a local minima indefinitely and therefore, the system can be used to solve combinatorial optimization problems.

Other network models which show chaos include higher order networks [196], 'dynamical perceptron' [102], stochastic dynamics networks [57] [192] and networks of coupled Hindmarsh-Rose neurons [74].

In the present thesis, a particularly simple model comprising excitatory and inhibitory neurons, which are updated in parallel after discrete time intervals, is considered. The 'simplicity' of this model has enabled a detailed theoretical understanding of its behavior, which could not be achieved in many of the aforementioned models, owing to their relative complexity. The origin of this model may be traced back to the work of other investigators as follows:

- Wilson and Cowan [204] derived coupled nonlinear differential equations for the dynamics of spatially localized populations containing both *excitatory and inhibitory model neurons*. The model showed simple and multiple hysteresis phenomena as well as limit cycles. However, it evolves in continuous time, as a result of which the original 2-variable autonomous system is not capable of exhibiting chaos. As pointed out by Choi and Huberman [36] and explored in depth later by Wang and Blum [198], the discretisation of time can often lead to qualitatively different behavior in a network model.

- Amari [5] used an *additive model* of a neuron to study the dynamics of randomly connected neuron-like elements.

- Hopfield [91] used *graded-response* (i.e., continuous valued) neurons in a globally coupled network to study the process of associative recall of patterns previously stored in the network, extending his work on a similar model comprising binary state neurons [90]. As the connections are symmetric (i.e., $W_{ij} = W_{ji}$), the network always converges to an equilibrium state. Chaotic activity, which is a non-equilibrium state, is therefore absent in this model. The network evolves in continuous time with asynchronous updating of neurons.

- Little [113] described a network of binary neural elements, similar to the one used by Hopfield, but the neurons being *updated in parallel.*

- Marcus and Westervelt [117] studied a *discrete time* version of the Hopfield model referred above. The stability of the equilibrium states of this 'iterated map neural network' was guaranteed by having a symmetric connection weight matrix.

- Wang's model [197] involves only a pair of excitatory and inhibitory neurons coupled to each other, with the dynamics evolving in discrete time. It is a very simple model which can show chaotic behavior. It is the closest relative of the network model that will be described in the thesis. Note that, one needs to impose severe restrictions on the model of Wang, as compared to the one required by the proposed one, to make it analytically tractable. These restrictions prevented a full exploration of various interesting features of the system, even in the limited case of an asymmetric, sigmoid activation function.

1.4 Scope of the thesis

The present thesis reports some results of investigation on the behavior of simple excitatory-inhibitory network models. Almost throughout, a strict form of Dale's hypothesis (i.e., a neuron has exclusively excitatory or inhibitory synaptic connections) is assumed. The resultant discrete-time dynamics (with synchronous or parallel updating of the neural elements) has shown a variety of interesting features. The underlying motivation is to look at the simplest neural module capable of showing chaotic behavior and to use the knowledge gained from studying this system to obtain a broader understanding of the possible relevance of chaotic dynamics to brain functioning.

In Chapter 2, we introduce and analyze the basic module of the excitatory-inhibitory neural network, which is the main topic of our investigation [169, 170]. As a first step towards understanding the behavior of such a network, the intrinsic properties of an excitatory-inhibitory pair is studied in detail. If $x(n)$ and $y(n)$ represent the activation states of the excitatory and inhibitory elements at the nth time instant, respectively, then the discrete-time evolution equations are:

$$x(n+1) = \mathbf{F}_{\mu_1}(\, a\, x(n) \,-\, b\, y(n) \,+I(n)),\; y(n+1) = \mathbf{F}_{\mu_2}(\, c\, x(n) \,-\, d\, y(n) \,+I'(n))$$

where $\mathbf{F}_{\mu}(z)$ can be a asymmetric/ anti-symmetric, sigmoidal/ 'piecewise linear' activation function with parameter μ, (a, b, c, d) are the self- and interconnection weights for the excitatory and inhibitory elements and I, I' denote magnitude of external stimuli. The model is analytically treated under the restrictive assumption of $b/a = d/c = k$ (say). For $k = 1$, the 2-dimensional system reduces to an equivalent 1-dimensional system with the corresponding variable being $z = x - y$ (absorbing a

and b in μ_1 and μ_2 respectively), defined in the interval [-1,1]. For sigmoidal activation functions, this system exhibits a period-doubling route to chaos for sigmoidal activation function. The piecewise linear activation function also leads to chaotic behavior following a route similar to that of the "tent" map, defined over the unit interval [0,1] as:

$$\begin{aligned} x(n+1) &= ax(n), \text{ for } 0 < x(n) < 0.5, \\ &= a(1-x(n)), \text{ for } 0.5 < x(n) < 1, \end{aligned}$$

where $a \in [0, 2]$ is a parameter.

The presence of chaos can be analytically demonstrated for a range of values of (μ_1, μ_2). For $k \leq 1$ the chaos is symmetry-broken. There are two chaotic intervals corresponding to $I_1 : [0, 1]$ and $I_2 : [0, -1]$ which are disconnected, i.e., if $z(0) \epsilon I_1$, then $z(n) \epsilon I_1 \ \forall \ n$ necessarily and similarly for I_2. However, for $k > 1$ the symmetry is restored and a trajectory starting from any initial z can go to both I_1 and I_2. The introduction of a threshold, θ, in this picture enables one to go from chaos to order through the variation of θ. The concept of a dynamical threshold is motivated by the existence of refractory period in biological neural network. A detailed study of the dependence of chaotic activity on the magnitude of threshold has been done.

In Chapter 3, the nonlinear resonance phenomenon exhibited by a chaotic neural pair, on stimulation with weak periodic signal, is studied [174]. This is remarkably similar to "stochastic resonance" (SR) seen in non-deterministic systems. SR is a recently observed nonlinear phenomena in noisy systems, whereby the noise helps in amplifying a sub threshold signal (which would have been otherwise undetected) when the signal frequency is close to a critical value. As the output of a chaotic process is indistinguishable from that of a noisy system, the question of whether a similar process occurs in the former case is studied in this chapter.

Before looking at the behavior of the excitatory-inhibitory neural pair, we study a simpler model for analytical convenience. The model chosen is a anti-symmetric piecewise linear map defined in the interval [-1,1]. The behavior of the system is controlled by a parameter, a $(0 < a < 4)$. Onset of chaos is seen to occur at $a = 1$. The chaos is symmetry broken, i.e., the system is restricted to either of the two sub-intervals (0,1] and (0,-1], depending on initial condition. Symmetry is restored at $a = 2$.

To observe SR, the value of a is kept close to 2, and then modulated sinusoidally with amplitude δ and frequency ω. The response of the system shows a non-monotonic behavior as ω is varied, attaining a peak value at ω_c, a "critical frequency", which depends on a_0 and δ - a clear signature of a SR-type phenomenon. Some analytical calculations have also been done - in particular obtaining the invariant probability density and the dominant time scale of the time-varying processes. The implication of the above study is that chaotic neural networks can amplify weak signals in a noisy background, thus enhancing its information processing capabilities. We have also studied kinetic aspects, such as hysteresis, of the above model.

The one-dimensional map equivalent to the excitatory- inhibitory neural model exhibits SR-type behavior similar to that reported above for the anti-symmetric chaotic map. The dependence of such 'resonance' on the relative magnitudes of μ_1 and μ_2 and other parameters has been studied. Analytical results have been obtained in the case of piecewise linear activation function. For sigmoidal function, numerical studies have been done.

Having studied in Chapter 2 the existence of chaotic activity in our proposed model, in Chapter 4 we proceed to control it [167, 166, 168]. With this objective, piecewise linear maps are studied as approximations of excitatory-inhibitory neural pairs, for analytical convenience. In principle, any piecewise linear map can be represented by a recurrent neural network with properly connected excitatory and inhibitory elements having appropriate thresholds and linear activation functions with a cutoff.

The "tent" map, defined above, is subjected to dynamical variable feedback control. In this method, a particular interval $I : (x_0 - \delta, x_0 + \delta)$ of the unit interval is chosen and whenever $x(n+1) \epsilon I$, a feedback of magnitude $k\ |x(n+1) - x_0|$ is applied to the system (k is a constant). The dependence of control on the parameter set (x_0, δ, k) is studied in detail and a geometrical understanding of the control process is obtained.

Control is also achieved through the use of a dynamical threshold (as outlined in Chapter 2). This is same as subjecting the model to small-amplitude periodic perturbations. Various periodic cycles can be stabilized by periodically varying the threshold. A numerical study of the control method has been done.

The chaos control method is then implemented on a network model comprising N excitatory and N inhibitory elements. The model exhibits both periodic and chaotic behavior, depending on parameter values. Numerical simulations are carried out for N=3, the number being kept low for ease of visual representation. The control process made the chaotic trajectories converge to any one of a large number of possible unstable periodic attractors. The potentially high storage capacity, as well as, the extremely rapid speed of convergence, are notable features of the network. The model also attempts to explain the occurrence of olfactory hallucinations in certain types of epileptic seizures.

In Chapter 5, the collective dynamics and synchronization in assemblies of coupled chaotic neural pairs is studied [176, 174, 171]. In the brain, synchronization of neural assemblies seems to be employed in "visual binding". The question of what happens if competitive synchronizing interactions occur among different neural assemblies is the motivation to study such interaction among coupled chaotic systems.

Synchronization can be achieved through both unidirectional and bidirectional coupling among chaotic elements. In the case of unidirectional coupling, an n-dimensional autonomous system is divided into two parts, a 'driving' and a 'responding' subsystem. A replica of the 'responding' subsystem is then created and driven with the x_d variables of the original system. The two systems will synchronize only if the 'conditional Lyapunov exponents' of the 'responding' subsystem are all negative. For

bidirectional coupling, the coupling magnitude should be at least greater than half the magnitude of the Lyapunov exponent of the uncoupled system, for synchronization to occur.

Synchronization of chaotic activity among small assemblies of coupled neural pairs has been numerically studied. In the case of bidirectional coupling of two neural pairs, on-off intermittency phenomena is observed. For three neural pairs (A,B,C) coupled to each other, such that (A,B) and (B,C) are connected, but not (A,C), we find synchronization to occur between (A,C), although neither (A,B) nor (B,C) synchronize. We call this 'mediated synchronization', as B appears to be mediating the synchronization process, without itself taking part in it. For unidirectional coupling, a particularly interesting feature is the effect of competitive interactions on the synchronization dynamics. To obtain a theoretical understanding of some of the numerical observations, we study the effect of two 'driving' systems driving a single 'responding' system, each system being governed by the well-known Lorenz equations. One of the variables (y) of the 'responding' system is defined in terms of the corresponding variables of the two 'driving' systems as:

$$y = ay_1 + (1-a)y_2$$

where a is the 'competition' parameter. For a=0 or 1, the conventional Lorenz attractor is obtained. However, as $a \rightarrow 0.5$, the resultant chaotic attractor is found to be qualitatively different and more complex than the conventional Lorenz attractor. The results of linear stability analysis suggests that the trajectory of the system moves among the stable and unstable manifolds of a large number of unstable fixed points. This is responsible for the observed complicated dynamics of the system. We define a 'desynchronization parameter', δ and have obtained a scaling relation of δ with a.

In Chapter 6, we have used excitatory-inhibitory networks to study certain problems of early vision, the stage of visual processing at which the primitive features of an image are extracted. Two models have been studied: a two-layer network for segmentation (in particular, object-background discrimination) and a three-layer network for adaptive smoothing and edge detection.

The segmentation network model consists of a layer of excitatory and a layer of inhibitory neurons coupled to each other. On presenting the network with a noisy image, the object and the background portions are found to have different dynamical behavior, enabling segmentation to be done [172].

In the three-layer network model, contrast enhancement, followed by edge detection, is studied. A layered network with a sigmoidal activation function is found to give high contrast when a gray-level image is processed through it. The interaction between excitatory and inhibitory neurons results in a filtering process whereby edges of the image are obtained. This has motivated the designing of a model of retinal processing. The model consists of an input layer of excitatory neurons (analogous to the photoreceptor layer in the retina), followed by a layer of coupled pairs of inhibitory and excitatory neurons (analogous to the horizontal and bipolar cell layers

of the retina, respectively). The lateral connections among the inhibitory neurons and the inter-layer connections between all three layers allows the local gradient of the image to be computed, the information being fed back to the input layer. An iterative process is then used to adaptively smooth the image. From the resulting enhanced image, one can obtain the edges, either by employing an additional pair of excitatory-inhibitory neuronal layer, or with a conventional gradient thresholding technique. The proposed model has been implemented on different types of images, and its performance compared with some existing models for image enhancement and edge-extraction (namely, Perona-Malik diffusion method and the Canny operator). Although the model compares favorably with some standard methods of edge detection, its main contribution lies in the area of adaptive smoothing.

A concluding summary with an outlook on further work that can be done extending the aforesaid ideas is presented in Chapter 7.

Chapter 2

Intrinsic Dynamics of an Excitatory-Inhibitory Neural Pair

A pair of an excitatory and an inhibitory neurons, coupled to each other and evolving in discrete time intervals, is one of the simplest systems capable of showing chaotic behavior. This has guided the choice of this system for extensive study in this thesis. The present chapter examines the discrete-time dynamics of such coupled neuron pairs with four different types of nonlinear activation functions. The complex dynamical behavior of the system is generic for the different types of activation functions considered here. Features specific to each of the functions, were also observed. For example, in the case of piecewise linear functions, border-collision bifurcations and multifractal fragmentation of the phase space occurred for a range of parameter values. Anti-symmetric activation functions show a transition from symmetry-broken chaos (with multiple coexisting but disconnected attractors) to symmetric chaos (when only a single chaotic attractor exists). The model can be extended to a larger number of neurons, under certain restrictive assumptions, which makes the resultant network dynamics effectively one-dimensional. Possible applications of the network for information processing have been outlined. These include using the network for auto-association, pattern classification, nonlinear function approximation and periodic sequence generation.

The rest of the chapter is organized as follows. The basic features of the neural model used is described in section 1, along with the biological motivation for such a model. The next section is devoted to analyzing the dynamics of a pair of excitatory and inhibitory neurons, with self- and inter-connections. Two specific types of activation functions are chosen for detailed investigation, with either (*i*) asymmetric, piecewise linear, or, (*ii*) anti-symmetric, sigmoid characteristics. This simple system shows a wide range of behavior including periodic cycles and chaos. In section 3, we discuss the effect of introducing a non-zero threshold (or "bias"), which is equivalent (in the present model) to subjecting the system to a constant external input. Section 4 extends the model to larger networks under certain restrictive conditions. This is followed by a discussion of the possible application of the model

to various information processing tasks, such as associative memory and nonlinear function approximation. The rich dynamics of the system allows it to respond to specific inputs with periodic or aperiodic responses (in contrast with convergent networks, which give time-independent constant output) and also to act as a *central pattern generator*. We conclude with a short discussion on possible ramifications of the model.

2.1 Single 'neuron' behavior

Let u_n denote the activation state of a model neuron at the $n-$th time interval. If $u_n = 1$, the neuron is considered to be active (firing), and if $u_n = 0$, it is quiescent. Then, if v_n is the input to the neuron at the nth instant and θ be the threshold, the discrete-time neural dynamics is described by the equation

$$u_n = \mathcal{F}(v_n - \theta), \tag{2.1}$$

assuming there to be no effects of delay. The input v_n is the weighted sum of the activation states of all other neurons, at the $(n-1)$-th instant, that are connected to the neuron under consideration, together with external stimulus (if any). The form of $\mathcal{F}$ is decided by the input-output behavior of the neuron. Usually, it is taken to be the *Heaviside step function*, i.e.,

$$\begin{aligned} \mathcal{F}(z) &= 1, \text{ if } z > \theta, \\ &= 0, \text{ otherwise,} \end{aligned} \tag{2.2}$$

where θ is known as the *threshold*.

If the *mean firing rate*, i.e., the activation state averaged over a time interval, is taken as the dynamical variable, then a continuous state space is available to the system. If X_n be the mean firing rate at the $n-$th time interval, then

$$X_{n+1} = F_\mu(\Sigma_j W_j X_n^j + I_n - \theta_n). \tag{2.3}$$

Here, F is known as the *activation function* and μ is the parameter associated with it. The first term of the argument represents the weighted sum of inputs from all neurons connected with the one under study. W_j is the synaptic weightage for the connection to the jth neuron. I_n and θ_n represent the external stimulus and threshold respectively, at the nth instant.

Considering the detailed biology of a neuron, there are two transforms occurring at the threshold element. At the input end, the impulse frequency coded information is transformed into the amplitude modulation of the neural current. For single neurons, this pulse-wave transfer function is linear over a small region, with nonlinear saturation at both extremities. At the output end, the current amplitude is converted back to impulse frequency. The wave-pulse transfer-function for single neurons is zero below a threshold, then rises linearly upto a maximum value. Beyond this maximum,

the output falls to zero due to "cathodal block". These relations are time-dependent. For example, the slope of the wave-pulse transfer function decreases with time when subjected to sustained activation - this is known as "adaptation" [53].

The net transformation of a input by a neuron is therefore given by the combined action of the two transfer-functions. Let us approximate the nonlinear pulse-wave transfer function F_1 with a piecewise linear function, such that

$$\begin{aligned} F_1(z) &= -c, \text{ if } z < -c/m, \\ &= m\,z, \text{ if } -c/m \leq z \leq 1/m, \\ &= 1, \text{ if } z > 1/m. \end{aligned} \tag{2.4}$$

The wave-pulse transfer function F_2 is represented as

$$\begin{aligned} F_2(z) &= 0, \text{ if } z < \theta, \\ &= m'\,(z-\theta), \text{ if } \theta \leq z \leq \theta + (1/m'), \\ &= 0, \text{ if } z > \theta + (1/m'), \end{aligned} \tag{2.5}$$

where m, m' are the slopes of F_1, F_2 respectively, c is the inhibitory saturation value and θ represents a threshold value.

It is easily seen that the combined effect of the two gives rise to the resultant transfer function, G, defined as

$$\begin{aligned} G(z) &= 0, \text{ if } z < \theta, \\ &= m\,m'\,(z-\theta), \text{ if } \theta \leq z \leq \theta + (1/m), \\ &= m'\,(1-\theta), \text{ if } \theta + (1/m) < z \leq \theta + (1/m'), \\ &= 0, \text{ if } z > \theta + (1/m'). \end{aligned} \tag{2.6}$$

In the present work we will assume that $m'\,(1-\theta) << \theta + (1/m')$. This condition ensures that the operating region of the neuron does not go into the "cathodal block" zone. This allows us to work with the following simplified, piecewise linear neural activation function (upon rescaling) throughout the rest of the thesis:

$$\begin{aligned} F_a(z) &= 0, \text{ if } z < \theta, \\ &= a\,(z-\theta), \text{ if } \theta \leq z \leq \theta + (1/a), \\ &= 1, \text{ if } z > \theta + (1/a), \end{aligned} \tag{2.7}$$

where a (> 0) is called the *gain parameter* of the function (Figure 2.1 (a)). Note that, this activation function is *asymmetric* as it corresponds to an input-output mapping of the form $(-\infty, \infty) \rightarrow [0, 1]$. For infinite gain ($a \rightarrow \infty$), the activation function reverts to the hard-limiting Heaviside step function.

The piecewise linear nature of the model neuron used, not only makes detailed theoretical analysis possible, but also enables an intuitive understanding of the dynamics, at least for a small number of connected elements. This makes it easier to extrapolate to larger networks and suggest possible applications. The proposed model is also particularly suitable for hardware implementation using operational amplifiers (owing to their piecewise linear characteristics).

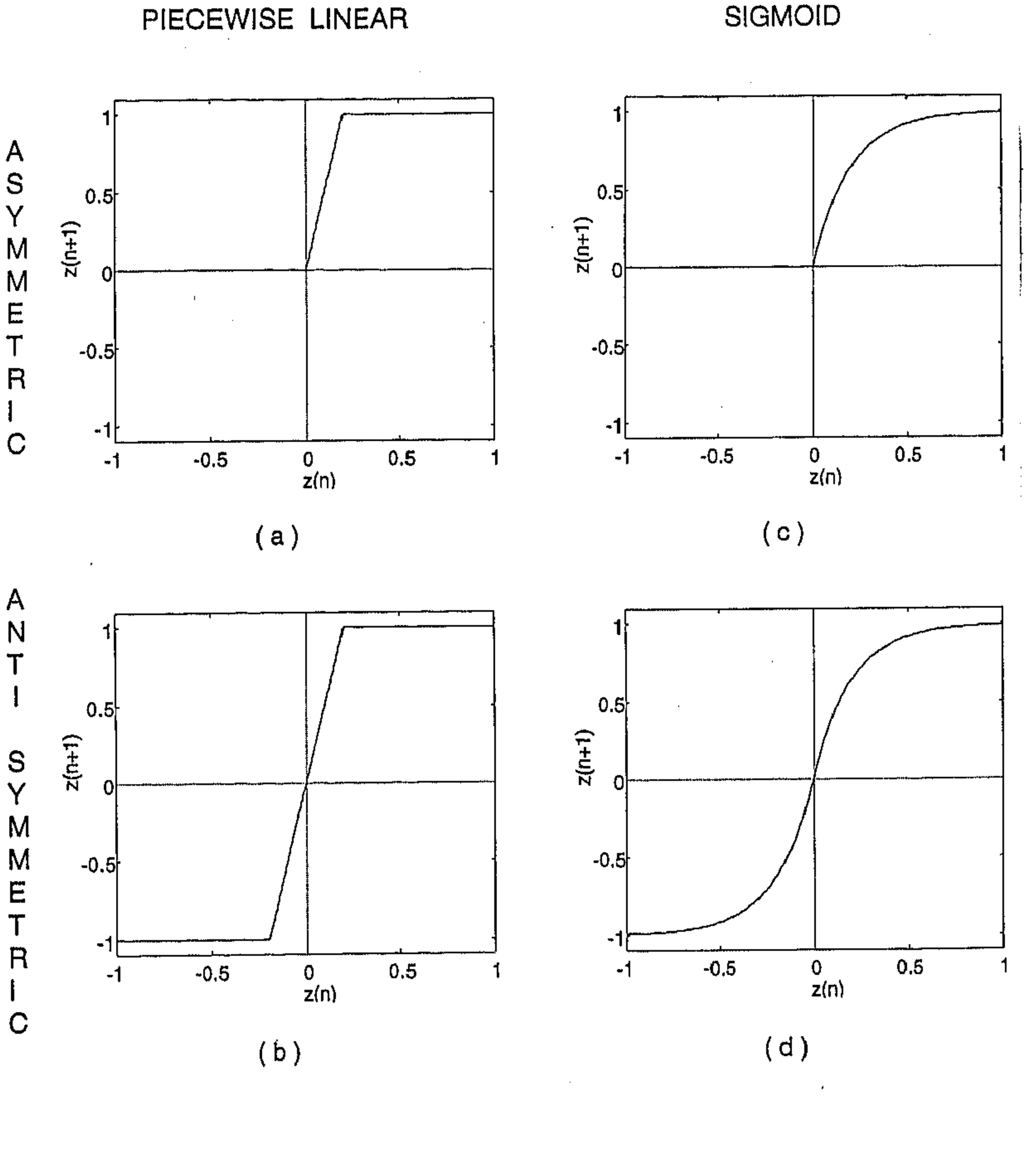

Figure 2.1: The different activation functions (F_a) for a single neuron (gain parameter, $a = 5$) having (a) asymmetric, piecewise linear, (b) anti-symmetric, piecewise linear, (c) asymmetric, sigmoid, and (d) anti-symmetric, sigmoid characteristics.

On translation and scaling, we obtain an *antisymmetric* form of this activation function, viz.

$$\begin{aligned} F_a(z) &= -1, \text{ if } z < \theta - (1/a), \\ &= a\,(z-\theta), \text{ if } \theta - (1/a) \leq z \leq \theta + (1/a), \\ &= 1, \text{ if } z > \theta + (1/a), \end{aligned} \tag{2.8}$$

so that the input-output mapping is now of the form $(-\infty, \infty) \rightarrow [-1, 1]$ (Fig. 2.1 (b)).

Although, in the present study, the gain parameter, a, of the transfer function is considered constant, in general it will be a time-varying function of the activation state, decreasing under constant external stimulation until the neuron goes into a quiescent state. The threshold θ is also a dynamic parameter, changing as a result of external stimulation. We have also assumed that the neuron state at the nth instant is a function of the state value at the previous instant only. Introducing delay effects into the model, such that,

$$X_{n+1} = F(X_n, X_{n-1}, \ldots, X_{n-\tau}),$$

might lead to novel behavior. This is discussed briefly in the concluding section.

If we now consider neural populations, instead of single neurons, then sigmoidal activation functions of the form

$$\begin{aligned} F_a(z) &= 1 - e^{-az}, \text{ if } z > 0, \\ &= 0, \text{ otherwise,} \end{aligned} \tag{2.9}$$

are the appropriate choice (Fig. 2.1 (c)). Note that, the output of a neural population is not a train of pulses (as in single neuron) but a continuous pulse density. By varying a, transfer functions with different slopes are obtained. In the neurobiological situation, the slope is both state-dependent (e.g., it increases with the behavioral arousal of a subject) and input-dependent (increasing with sensory excitation). In this work, we have taken a to be constant.

As in the piecewise linear case, here also we can define an antisymmetric form of the activation function (Fig. 2.1 (d)) as follows:

$$\begin{aligned} F_a(z) &= 1 - e^{-az}, \text{ if } z > 0, \\ &= -(1 - e^{az}), \text{ otherwise.} \end{aligned} \tag{2.10}$$

Note that for all the activation functions defined so far (i.e., Eqns. (2.7), (2.8), (2.9) and (2.10)), the following common features hold:

- $F(0) = 0$, i.e., 0 is a 'fixed-point' of the function, and
- the functions saturate at an output value, arbitrarily set to unity.

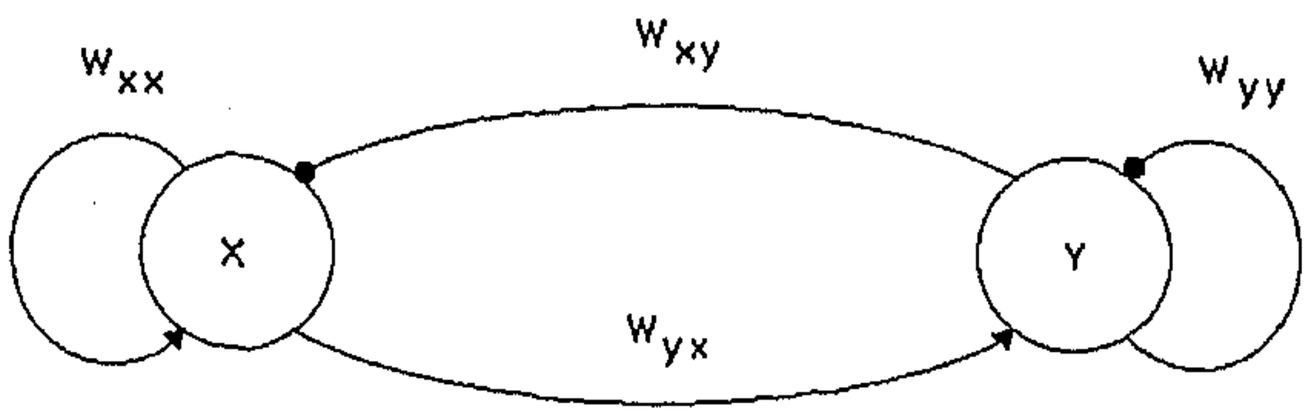

Figure 2.2: The pair of excitatory (x) and inhibitory (y) neurons. The arrows and circles represent excitatory and inhibitory synapses, respectively.

2.2 Excitatory-inhibitory pair dynamics

Having established the response properties of single neurons, we can now study the dynamics when they are connected. It is observed that, even connecting only an excitatory and an inhibitory neuron with each other leads to a rich variety of behavior, including high period oscillations and chaos. The continuous-time dynamics of pairwise connected excitatory-inhibitory neural populations (with sigmoidal nonlinearity) have been studied before [204]. However, an autonomous two-dimensional system (i.e., one containing no explicitly time-dependent term), evolving continuously in time, cannot exhibit chaotic phenomena, by the Poincare-Bendixson theorem [188]. In the present case, the resultant system is updated in discrete-time intervals and the dynamics is governed by one of the nonlinear activation functions defined in the previous section. This makes chaotic behavior possible in the proposed neural network model.

If X and Y be the mean firing rates of the excitatory and inhibitory neurons, respectively, then their time evolution is given by the coupled difference equations:

$$X_{n+1} = F_a(W_{xx}X_n - W_{xy}Y_n), \tag{2.11}$$

$$Y_{n+1} = F_b(W_{yx}X_n - W_{yy}Y_n).$$

The network connections are shown in Fig. 2.2. The W_{xy} and W_{yx} terms represent the synaptic weights of coupling between the excitatory and inhibitory elements, while W_{xx} and W_{yy} represent self-feedback connection weights. Although a neuron coupling to itself is biologically implausible, such connections are commonly used in neural network models to compensate for the omission of explicit terms for synaptic and dendritic cable delays [53].

Without loss of generality, the connection weightages W_{xx} and W_{yx} can be absorbed into the gain parameters a and b and the correspondingly rescaled remaining connection weightages, W_{xy} and W_{yy}, are labeled k and k' respectively. For convenience,

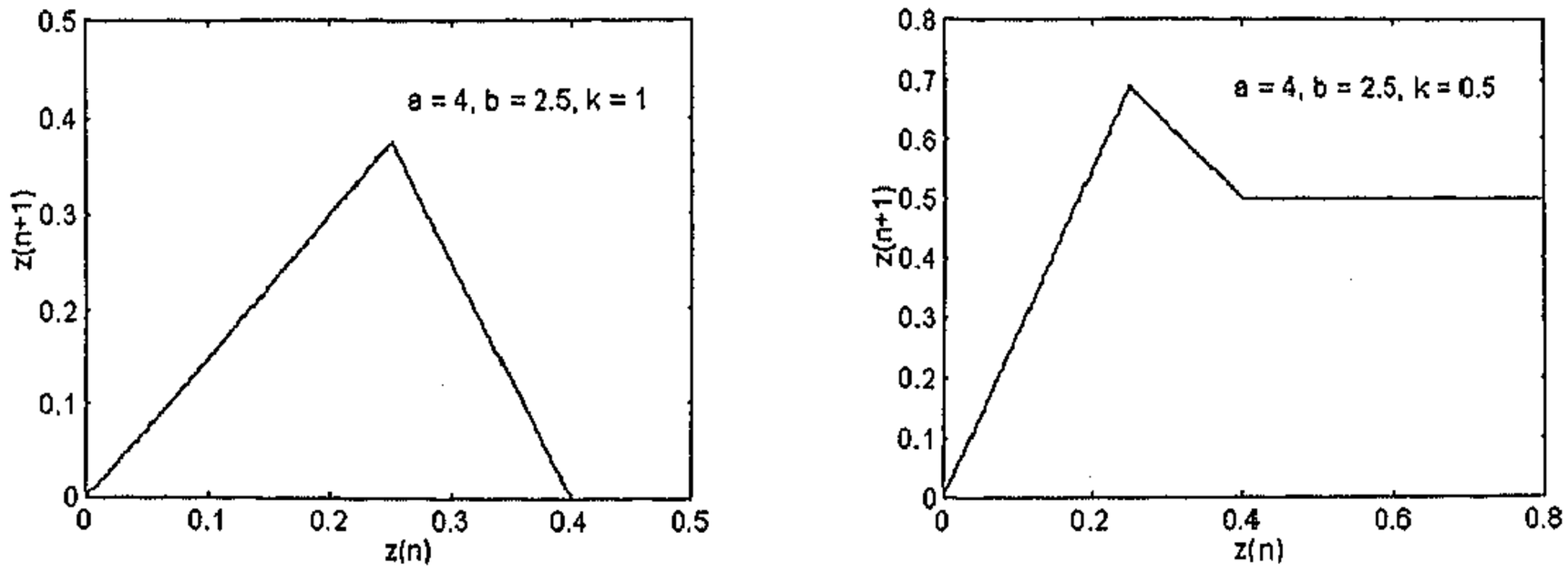

(a) (b)

Figure 2.3: The one-dimensional map representing neural pair dynamics with asymmetric, piecewise linear F for (a) $k = k' = 1$ and (b) $k = k' \neq 1$.

a transformed set of variables, $Z_n = X_n - k\ Y_n$ and $Z'_n = X_n - k'\ Y_n$, is used. The dynamics is now given by

$$Z_{n+1} = F_a(Z_n) - k\ F_b(Z'_n), \tag{2.12}$$

$$Z'_{n+1} = F_a(Z_n) - k'\ F_b(Z'_n).$$

Note that, if $k = k'$, the two-dimensional dynamics is reduced effectively to that of an one-dimensional difference equation ("map"), simplifying the analysis. We shall now consider in detail the dynamics of the map, when F has either (i) asymmetric, piecewise linear nature, or (ii) anti-symmetric, sigmoid character.

2.2.1 Asymmetric, piecewise linear activation function

Chaotic activity has been previously observed in piecewise linear systems, for both continuous-time [157] as well as discrete-time evolution [132, 133] of the system. In the following investigation, we shall examine the cases: $(i) k = k' = 1$, $(ii) k = k' \neq 1$, and $(iii) k \neq k'$, in detail. Throughout the present section, the threshold, θ, will be taken as 0 (a non-zero value of θ introduces some new phenomena, which will be investigated in the next Section).

Case I: $k = k' = 1$

This represents the condition when the connection weights $W_{xy} = W_{xx}$ and $W_{yy} = W_{yx}$, $(a > b)$. The dynamics is that of an *asymmetric tent map* (Fig. 2.3 (a)):

$$\begin{aligned} Z_{n+1} &= (a - b)\ Z_n, \text{ if } 0 \leq Z_n \leq 1/a, \\ &= 1 - bZ_n, \text{ if } 1/a < Z_n \leq 1/b, \\ &= 0, \text{ otherwise.} \end{aligned} \tag{2.13}$$

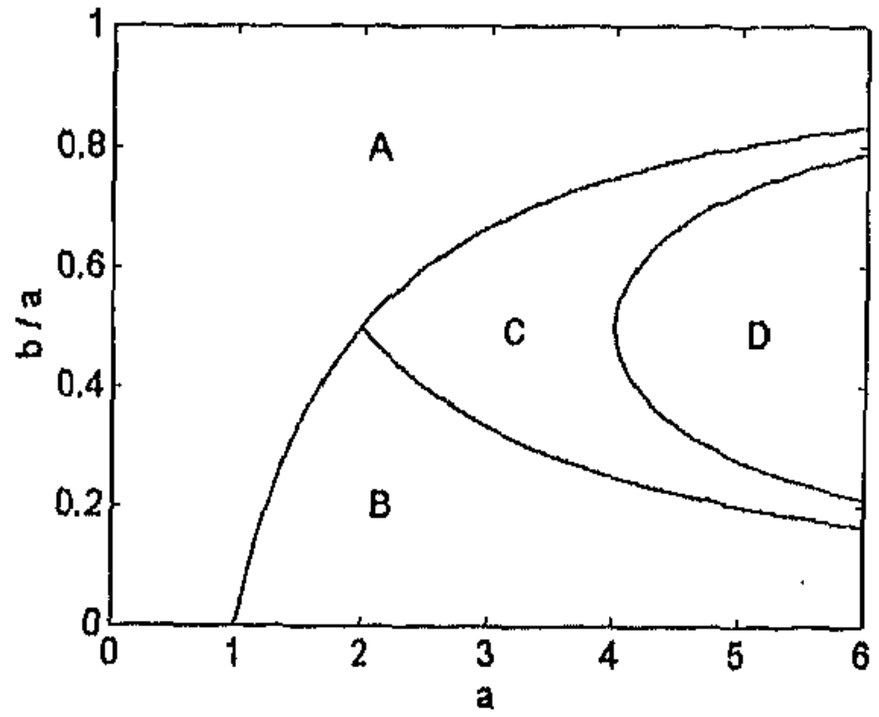

Figure 2.4: The activation gain a vs. (b/a) parameter space for $k = k' = 1$. Region A: $z^* = 0$ stable, B: $z^* = 1/(1+b)$ stable, C: chaos, D: coexistence of $z^* = 0$ and a fractal chaotic invariant set.

The fixed points of this system are, $Z_1^* = 0$ and $Z_2^* = 1/(1+b)$. Z_1^* is stable for $a - b < 1$, whereas Z_2^* exists only when $a - b > 1$, and is stable for $b < 1$. Beyond this, chaotic behavior is observed unless the maximum output value, i.e., $1 - (b/a)$, maps to $Z > 1/b$. The parameter space diagram is shown in Fig. 2.4. Along the line $b/a = 0.5$, we get the symmetric tent map scenario. So the Lyapunov exponent [1] along this curve grows as $\lambda = \log_e(b)$ for $0 < a < 4$. This is one of the two special cases where an analytical expression for λ can be obtained. The other instance is when the map's invariant probability distribution, $P(Z) = 1$. This occurs when

$$F\ (1/a) = 1 - (b/a) = 1/b. \tag{2.14}$$

Along the curve defined by the above relation, the Lyapunov exponent evolves with the parameter b/a according to

$$\lambda = -b/a\ \log_e(b/a) - (1 - (b/a))\log_e(1 - (b/a)). \tag{2.15}$$

In general, λ has to be obtained computationally. Fig. 2.5 shows λ plotted against b/a for $a = 4$, when the map is in the chaotic region. A sharp drop to zero is observed in both the terminal points, indicating sharp transition between chaotic and fixed-point behavior at $b/a = 0.25$ and 0.75. At $b/a = 0.5$, the entire interval $[0, 1/b]$ is uniformly visited by the chaotic trajectory $(P(Z) = 1)$. This corresponds to "fully-developed chaos" in the symmetric tent map for which $\lambda = \log_e(2) \simeq 0.693$.

[1] Lyapunov exponent (λ) is a quantitative indicator of chaotic behavior. It is defined for a one-dimensional mapping F as:

$$\lambda = \mathrm{Lim}_{N\to\infty} \frac{1}{N} \log_e \left| \sum_{i=0}^{N-1} \frac{dF}{dx}|_{x=x_i} \right|.$$

Chaotic behavior is indicated by a positive value of λ.

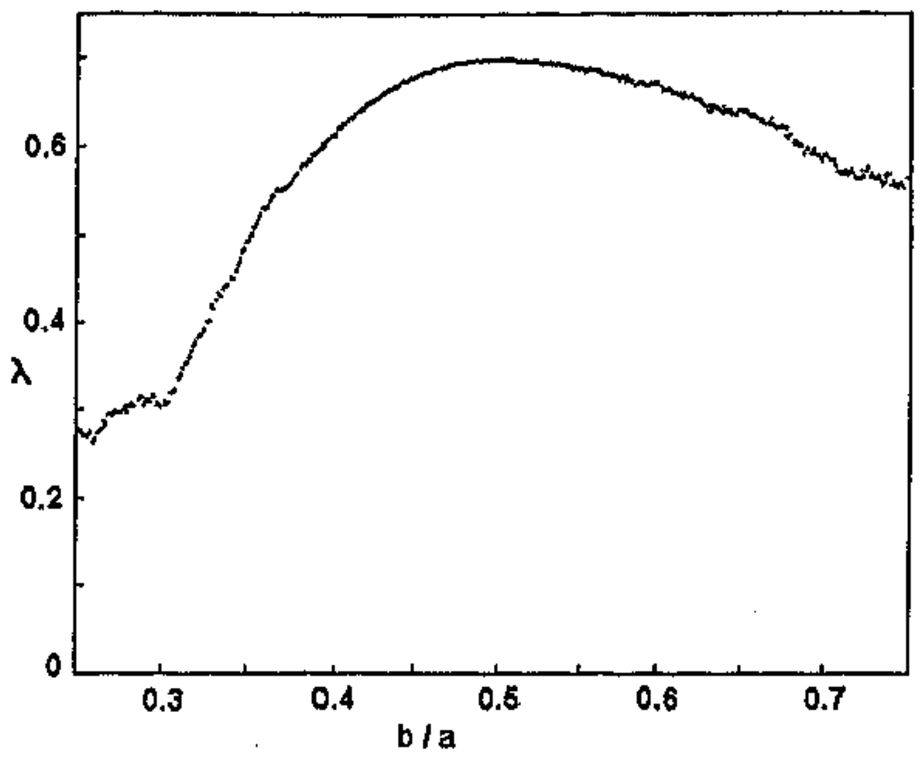

Figure 2.5: Lyapunov exponent of the chaotic dynamics for $k = k' = 1$ and $a = 4.0$. At $b/a = 0.5$, the entire interval $[0, 1/b]$ is uniformly visited.

When $F(1/a) > 1/b$, the interval $[0, 1/b]$ is divided into a chaotic region of measure zero, defined on a non-uniform Cantor set (in general) and an "escape set" which maps to $Z_1^* = 0$. This is because, for $Z \in (1/b(a-b), (b-1)/b^2)$, F(Z)=0. Any time an iterate of Z falls in this region, in the next iterate the trajectory will converge to Z_1^*. The points left invariant after one iteration, will be in the two intervals $[0, 1/b(a-b)]$ and $[(b-1)/b^2, 1]$. The phase space is thus fragmented into two invariant regions. After n iterations, there will be 2^n fragments of the chaotic invariant set, with $n!/r!(n-r)!$ $(r = 0, 1, \ldots, n)$ intervals of length $(a-b)^r(1-b)^{r-n}$. The fragmentation of the phase space, therefore, has a *multifractal* nature [123].

The presence of multiple length scales is due to the fact that the slope magnitude of the map is not constant throughout the interval $[0, 1/b]$. It is to be noted that, even for Z not belonging to the fractal invariant set, the trajectory might show long *chaotic transients* until at some iterate it maps to $Z^* = 0$. For $b/a = 0.5$, the map has a constant slope. As a result, the Cantor set is uniform, having exact geometrical self-similarity and a fractal dimension, $D = \log_e(2)/\log_e(b)$. So, the phase space of the coupled system has a fractal structure in this parameter region, i.e., where $1 - (b/a) > 1/b$.

Fig. 2.6 shows the bifurcation structure of the map for $a = 4$. For $b/a < 0.25$, the fixed point Z_2^* is stable. At $b/a = 0.25$ it becomes unstable, leading to bands of chaotic behavior. The chaotic bands collide with the unstable fixed point Z_2^* at $b/a \simeq 0.2985...$ and merge into a single chaotic band. This band-merging transition is an example of *crisis* [69] and has been studied in detail for the symmetric tent map [206]. The b-value at which the band-merging occurs for a given value of a, can be obtained analytically by solving the quartic equation:

$$b^4 + (1-2a)b^3 + (a^2-a)b^2 + ab + (a-a^2) = 0. \tag{2.16}$$

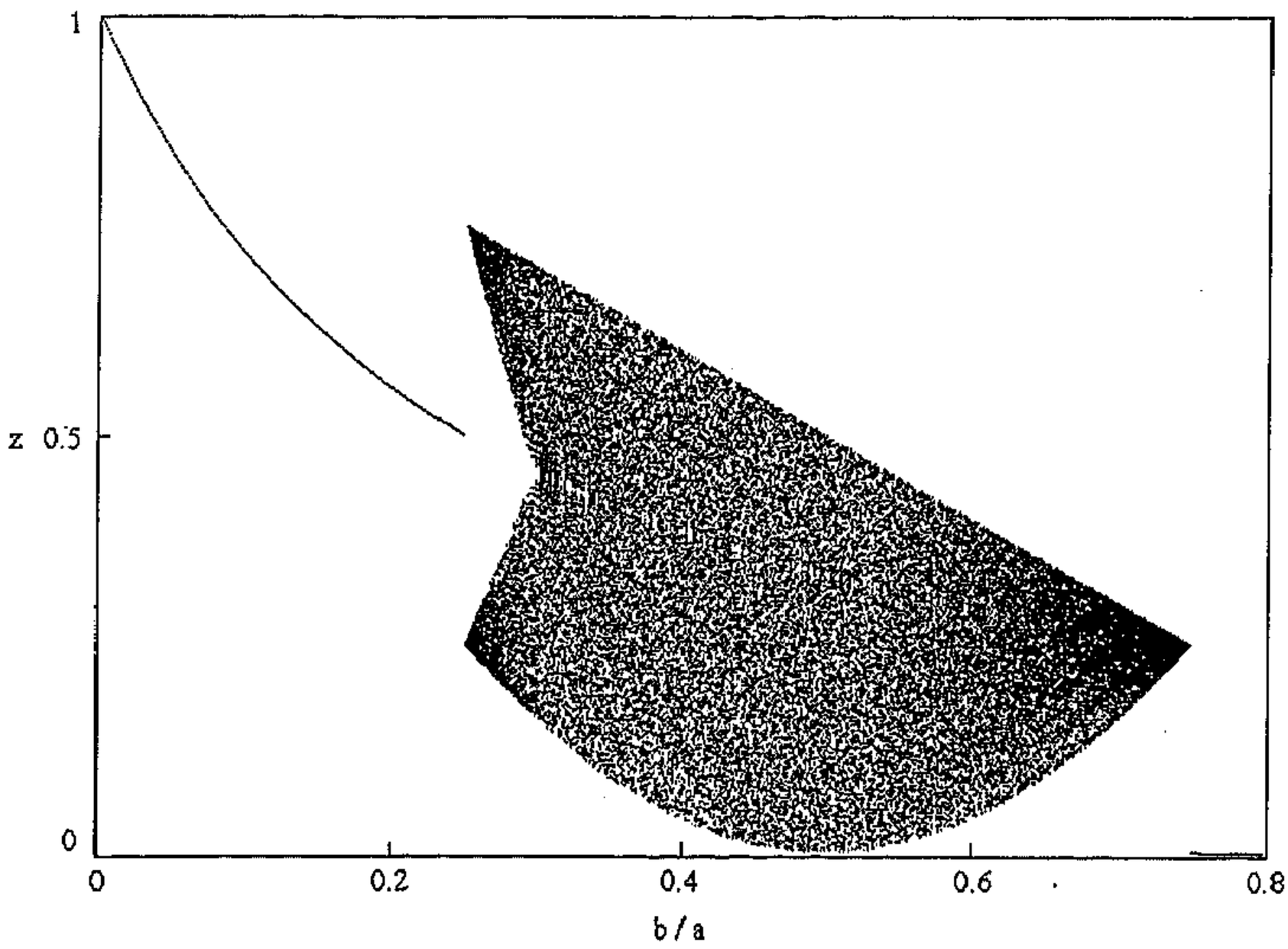

Figure 2.6: Bifurcation diagram for $k = k' = 1$ at $a = 4.0$.

For $2 < a < 2.5$, all the roots are complex, implying that band-merging does not occur over this range of a-values.

Uniform chaotic behavior occurs at $b/a = 0.5$ (the entire interval [0,1/b] is uniformly visited by the chaotic trajectory). The chaotic band collides with the unstable Z_2^* again at $b/a = 0.75$. This boundary crisis destroys chaos and stabilizes the fixed point $Z_1^* = 0$.

Case II: $k = k' \neq 1$

This represents the condition when the connection weightages are such that, $W_{xy}/W_{xx} = W_{yy}/W_{yx} = k$, $(a > b)$. The dynamics is given by the following map (Fig. 2.3 (b))

$$\begin{aligned} Z_{n+1} &= (a - kb)\, Z_n, \text{ if } 0 \leq Z_n \leq 1/a, \\ &= 1 - kbZ_n, \text{ if } 1/a < Z_n \leq 1/b, \\ &= 1 - k, \text{ otherwise.} \end{aligned} \tag{2.17}$$

The key difference with the earlier case is that, now, the dynamics supports superstable period-m orbits ($m \geq 2$). This is a result of the existence of a region of zero slope ($Z > 1/b$) giving a non-zero output. There are two fixed points of the map, $Z_1^* = 0$ (as before), and,

$$\begin{aligned} Z_2^* &= 1 - k, \text{ if } 0 < k < 1 - (1/b), \text{ or,} \\ &= 1/(1 + kb), \text{ if } (a-1)/b > k > 1 - (1/b). \end{aligned}$$

$Z_2^* = 1 - k$, if it exists, is superstable, as the local slope is zero. On the other hand, $Z_2^* = 1/(1 + kb)$ is stable, only if $bk < 1$. If the fixed points are unstable, but iterates of Z fall in the region $Z > 1/b$, superstable periodic cycles occur. The fixed point, $Z_1^* = 0$, becomes stable when $(a - bk) < 1$. Chaotic behavior occurs if none of the fixed points are stable, and no iterate of Z falls in the region $Z > 1/b$. The (b/a) vs. k parameter space diagram in Fig. 2.7 (for $a = 4$) shows the different dynamical regimes that are observed.

The bifurcation diagram for $a = 4, b = 2$ (Fig. 2.8) shows how the dynamics changes with k. For $0 \leq k < 0.5$, $Z_2^* = 1 - k$, is the stable fixed point. At $k = 0.5$, Z_2^* becomes unstable, giving rise to a superstable period-2 cycle. A periodic regime is now observed, which was absent in the previous case. The periodic orbits initially follow a *period-doubling* sequence until a period-32 ($= 2 \times 2^4$) orbit gives rise to a period-48 ($= 3 \times 2^4$) one. This occurs as a result of a border-collision bifurcation by which "period-2 to period-3" bifurcations have been seen to occur [132, 133]. In the above instance, each of the sixteen period-2 orbits give rise to a period-3 orbit. The structure of the superstable periodic orbits is quite complex. The length of the cycles is plotted against k in Fig. 2.9. The remarkable self-similar structure of the intervals is to be noted. Numerical studies indicate that cycles of all periods exist having the following ordering: between any superstable period-m and period-$(m+1)$ cycle, there exists an interval of k for which a period-$(m + 2)$ orbit is superstable. At $k = 1.0$ all periodic orbits become unstable, leading to onset of chaos. The chaotic behavior persists till $k = 1.5$, when $Z_1^* = 0$ becomes stable. The sequence of the periodic cycles

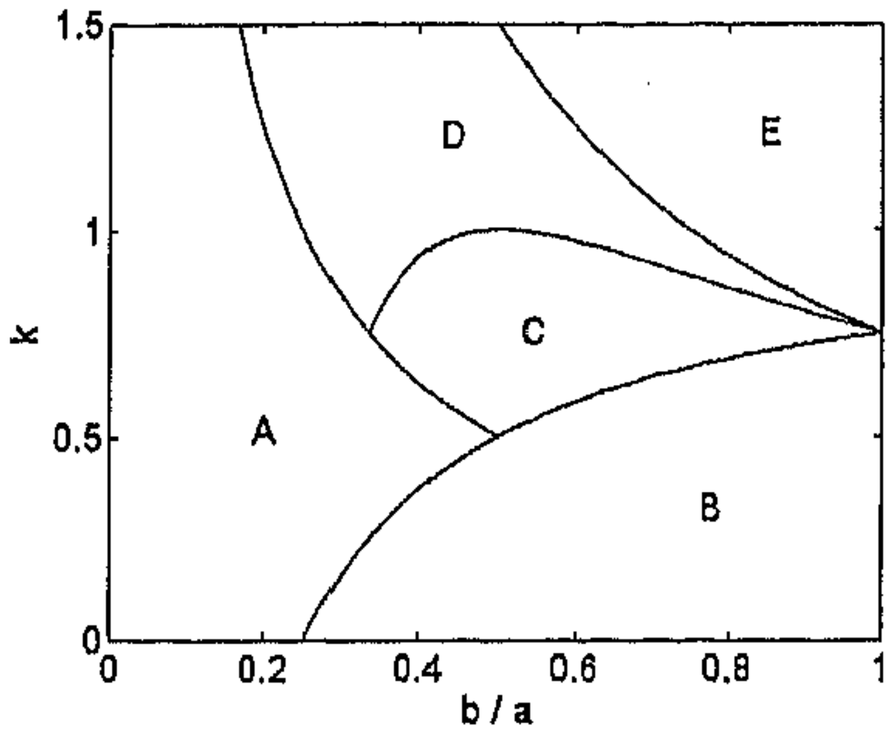

Figure 2.7: The (b/a) vs. k parameter space for $k = k' \neq 1$ at $a = 4.0$. Region A: $z^* = 1/(1+kb)$ stable, B: $z^* = 1-k$ stable, C: superstable periodic cycles, D: chaos, E: $z^* = 0$ stable.

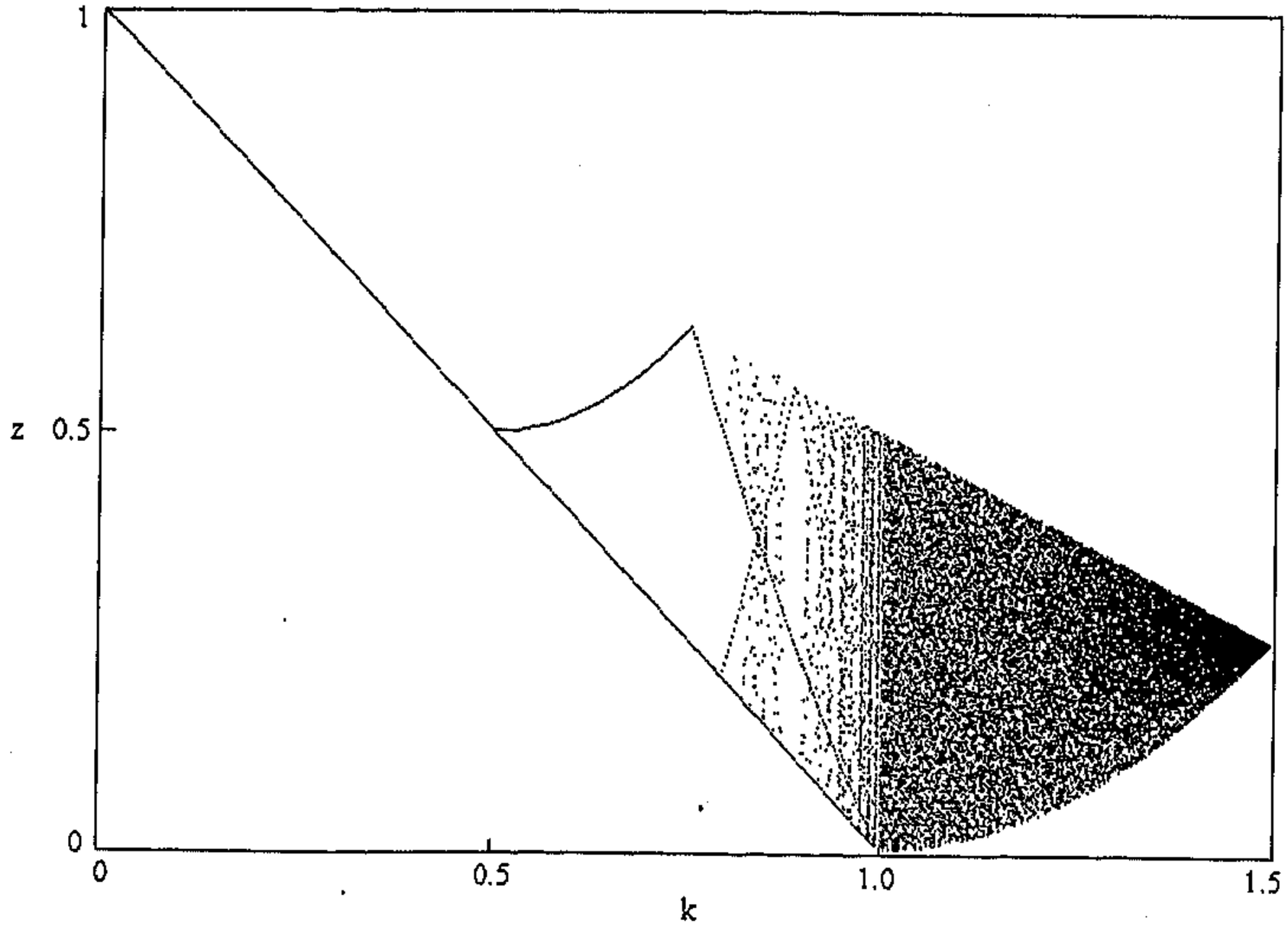

Figure 2.8: Bifurcation diagram for $k = k' \neq 1$ at $a = 4.0, b = 2.0$.

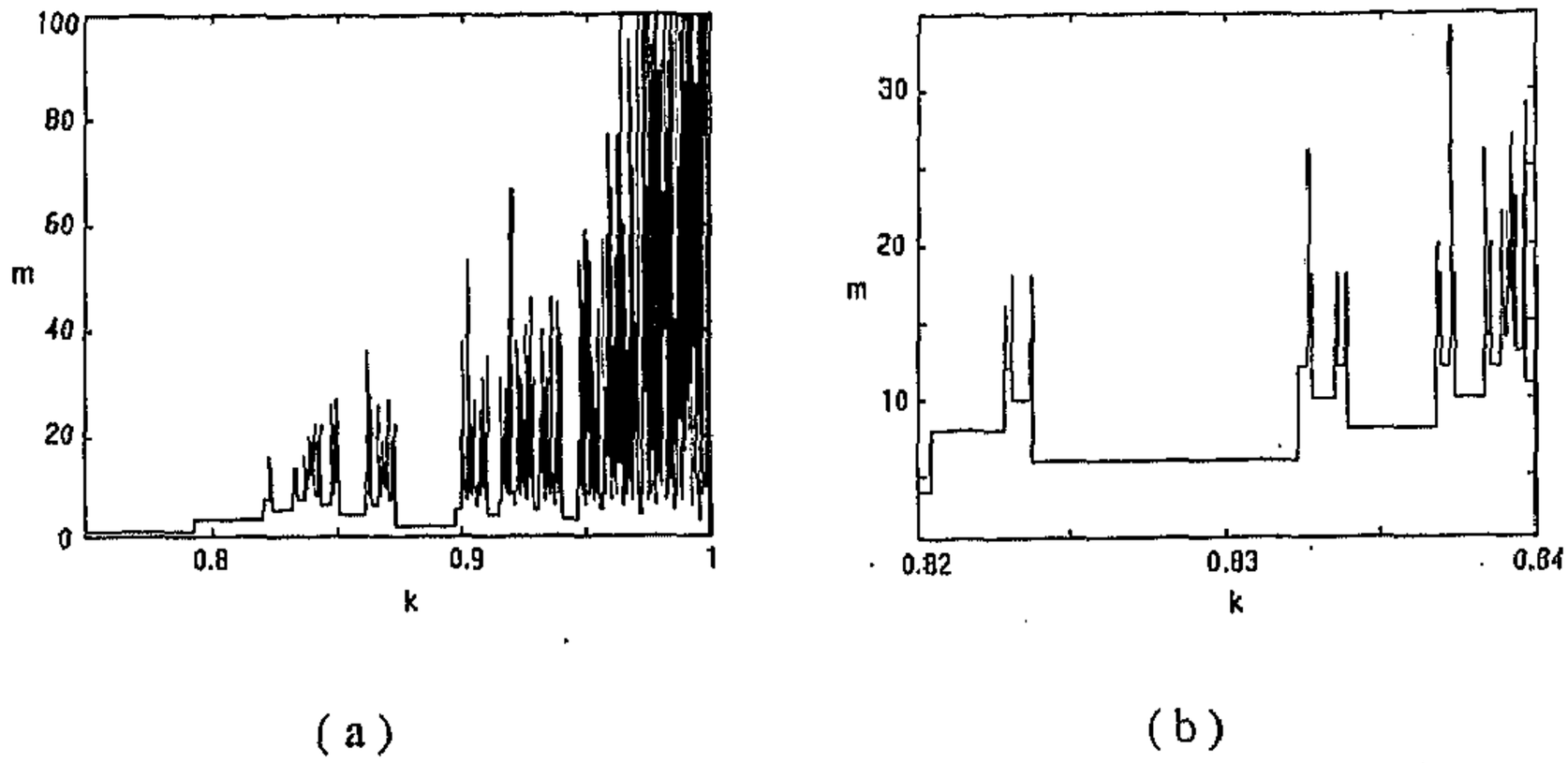

(a) (b)

Figure 2.9: Length of superstable periodic cycles, m, of the excitatory-inhibitory neural pair ($a = 4$, $b = 2$) for (a) $0.75 \leq \mathrm{k} < 1$, and (b) $0.82 \leq \mathrm{k} < 0.84$. Note the self-similar structure of the intervals.

is remarkably similar to that seen in the case of unidirectional, adaptive dynamics on a lattice of chaotic maps [165].

Case III: $k \neq k'$

This corresponds to the condition when all the connection weights are different. The dynamics is irreducible to 1-dimension. We need to consider only the positive (Z, Z') region, as otherwise, $(0, 0)$ is the stable fixed point. In the non-zero region, different dynamical behavior may occur depending on the region where the fixed point occurs and on its stability. One of the fixed points is $(Z, Z') = (0, 0)$, whose stability is determined by obtaining the eigenvalues of the corresponding Jacobian,

$$\mathrm{J} = \begin{vmatrix} a & -kb \\ a & -k'b \end{vmatrix} .$$

Evaluating the above matrix, gives the following condition

$$-2 < (a - k'b) \pm [(a - k'b)^2 - 4ab(k - k')]^{1/2} < 2, \tag{2.18}$$

for stability of the fixed point.

The other fixed point may occur in any one of the four following regions of the (Z, Z')-space:

Region I: $0 < Z < 1/a$, $0 < Z' < 1/b$.
$(Z, Z') = (0, 0)$ is the only fixed point.

Region II: $0 < Z < 1/a$, $Z' > 1/b$.
The fixed point is $(Z, Z') = (k/(a-1), (a(k-k') + k')/(a-1))$, which is stable if $-1 < a < 1$.

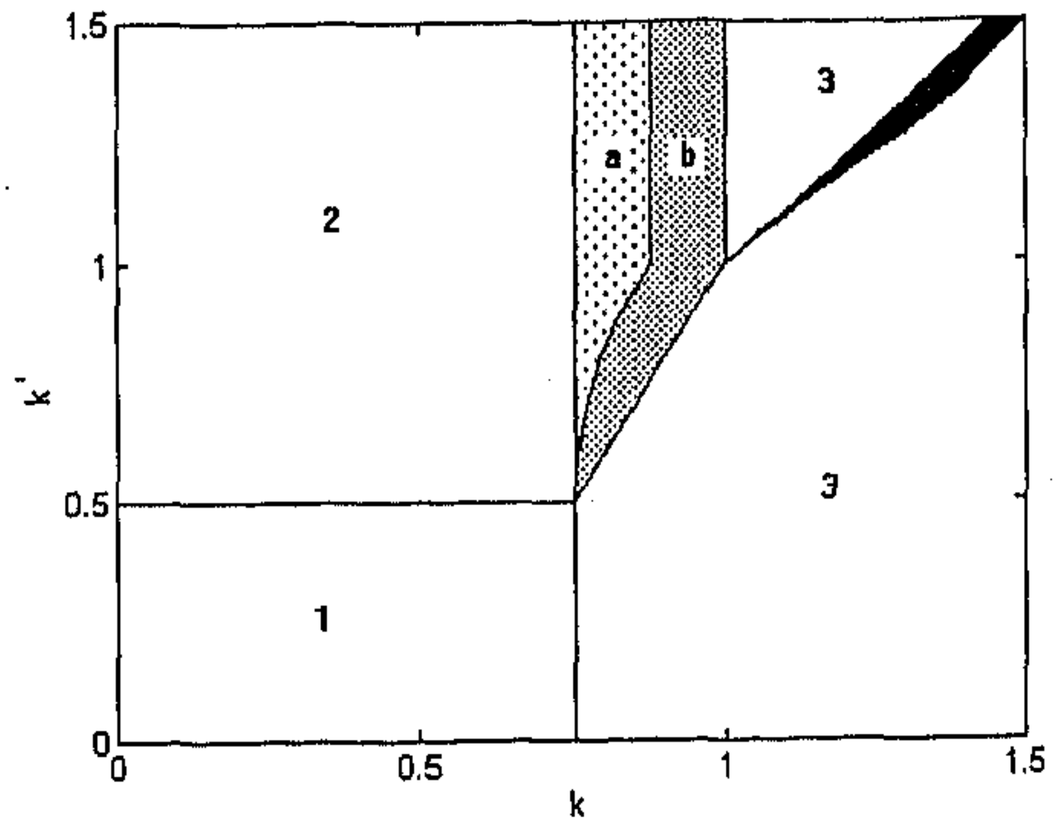

Figure 2.10: The (k, k') parameter space for $a = 4.0$ and $b = 2.0$. Region 1: x^*=1, y^*=1 stable, 2: x^*=1, y has period-2 cycles, 3: x^*=0, y^*=0 stable, *a*: Both x and y have period-2 cycles, *b*: x and y show period-m cycles (m>2). Fully chaotic behavior occurs in the dark wedge-shaped region in 3. In addition, fractal intervals showing chaos occur in region *b*.

Region III: $Z > 1/a$, $0 < Z' < 1/b$.
The fixed point is $(Z, Z') = ((1 + b(k' - k))/(1 + bk'), 1/(1 + bk'))$, which is stable if $-1 < k'b < 1$.

Region IV: $Z > 1/a$, $Z' > 1/b$.
The fixed point is $(Z, Z') = (1 - k, 1 - k')$. This is a superstable root, as the local slope is zero under all conditions.

The abundance of tunable parameters in this case, makes detailed simulation study extremely difficult. However, some preliminary studies in the (k, k') parameter space (keeping the other parameters fixed) gives indication of dynamics similar to that seen in cases (i) and (ii). The (k, k') parameter space is shown in Fig. 2.10 for $a = 4$, $b = 2$. A variety of dynamical behaviors is observed - from fixed points to periodic cycles to chaos, as indicated by the different regions. In addition, there are regions exhibiting periodic behavior which have fractal intervals of chaotic activity embedded within them.

2.2.2 Anti-symmetric, sigmoid activation function

We will now look at the dynamics of the excitatory-inhibitory neural pair when the activation function F is of the form (2.10). If $k = k'$, the resultant dynamics is that of a one-dimensional bimodal map, whose phase space is disconnected into two halves for $k \leq 1$. We shall consider first the case when $k = k' = 1$, and then investigate the change in the behavior of the system when $k = k' \neq 1$.

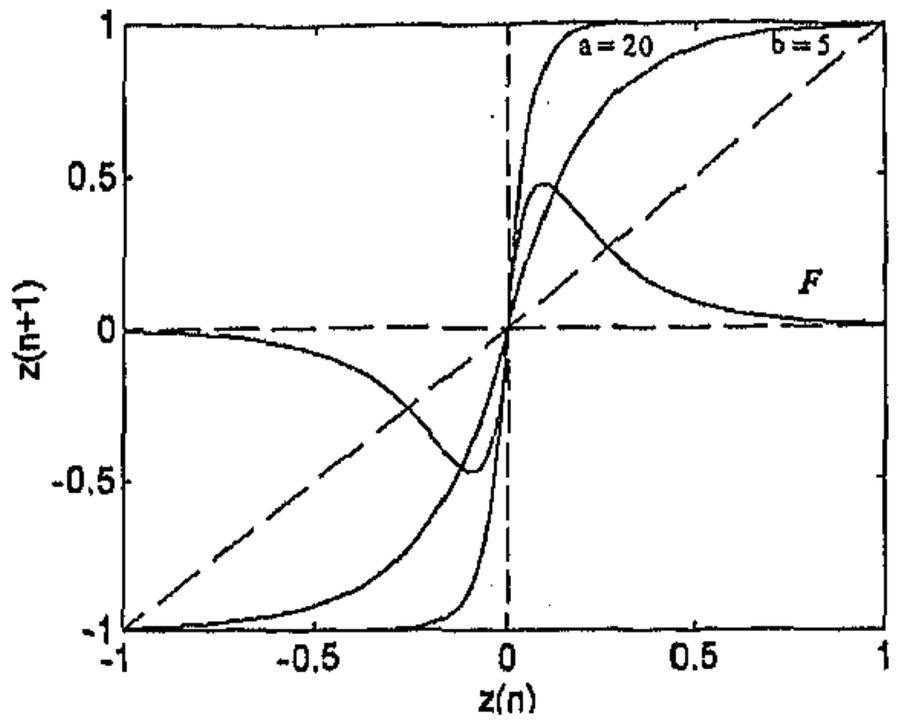

Figure 2.11: The sigmoid activation functions (F) for slopes, a=20 and b=5, and the resulting one-dimensional map.

For $k = 1$, the two halves of the phase space ($L : (-\infty, 0)$ and $R : [0, \infty)$ are not connected - i.e., a trajectory starting with an initial condition belonging to L, can never reach R in the course of time, and vice versa. The resulting dynamics is that of the following map:

$$\begin{aligned} Z_{n+1} &= \exp(-bZ_n) - \exp(-aZ_n), \text{ if } 0 \leq Z_n \leq \infty, \\ &= -\exp(bZ_n) + \exp(aZ_n), \text{ otherwise.} \end{aligned} \tag{2.19}$$

Fig. 2.11 shows the map, arising out of interaction between an excitatory neuron with slope, $a = 20$, and an inhibitory neuron with slope, $b = 5$. The bifurcation diagram of the map (Fig. 2.12), obtained by increasing the ratio b/a, keeping a fixed shows a transition from fixed point to periodic cycles and chaos, following a "period-doubling" route, an universal feature for an entire family of one-dimensional chaotic maps [188]. Fig. 2.13 shows a magnified image of the bifurcations, which clearly exhibits the successive doubling of the periodic cycles. The variation of a, keeping the ratio b/a fixed, also shows a transition to chaotic behavior, as is indicated in Fig. 2.14.

The map has 3 fixed points: $Z_1^* = 0$, Z_2^* and Z_3^* (by symmetry of the map, $Z_3^* = -Z_2^*$). The latter are the solutions of the transcendental equation $Z = \exp(-bZ) - \exp(-aZ)$. The fixed point Z_1^* is stable if the local slope ($\simeq (a - b)$) is less than 1. For $a > \frac{1}{1-\mu}$ (where, $\mu = \frac{b}{a}$), this condition no longer holds and Z_1^* loses stability while Z_2^* becomes stable by a transcritical bifurcation. On further increase of a, this fixed point also loses stability (by flip bifurcation) with the local slope becoming less than -1, and a 2-period cycle become stable. Increasing a further leads to cycles of higher and higher periods becoming stable, ultimately leading to totally aperiodic behavior.

The chaotic behavior can be quantified, as in the case of the piecewise linear function,

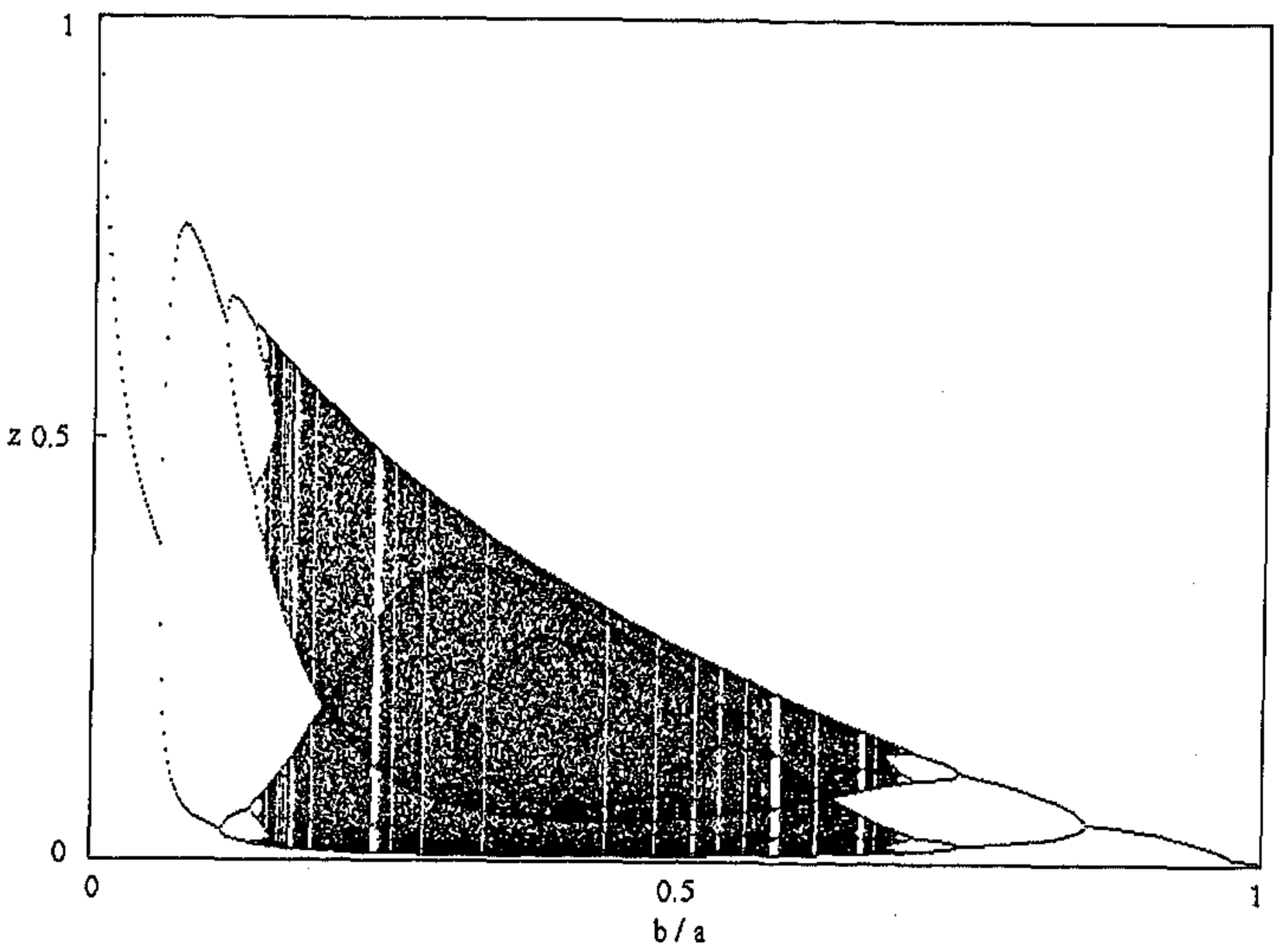

Figure 2.12: Bifurcation diagram of the map representing excitatory-inhibitory pair dynamics with sigmoid F for a=50.

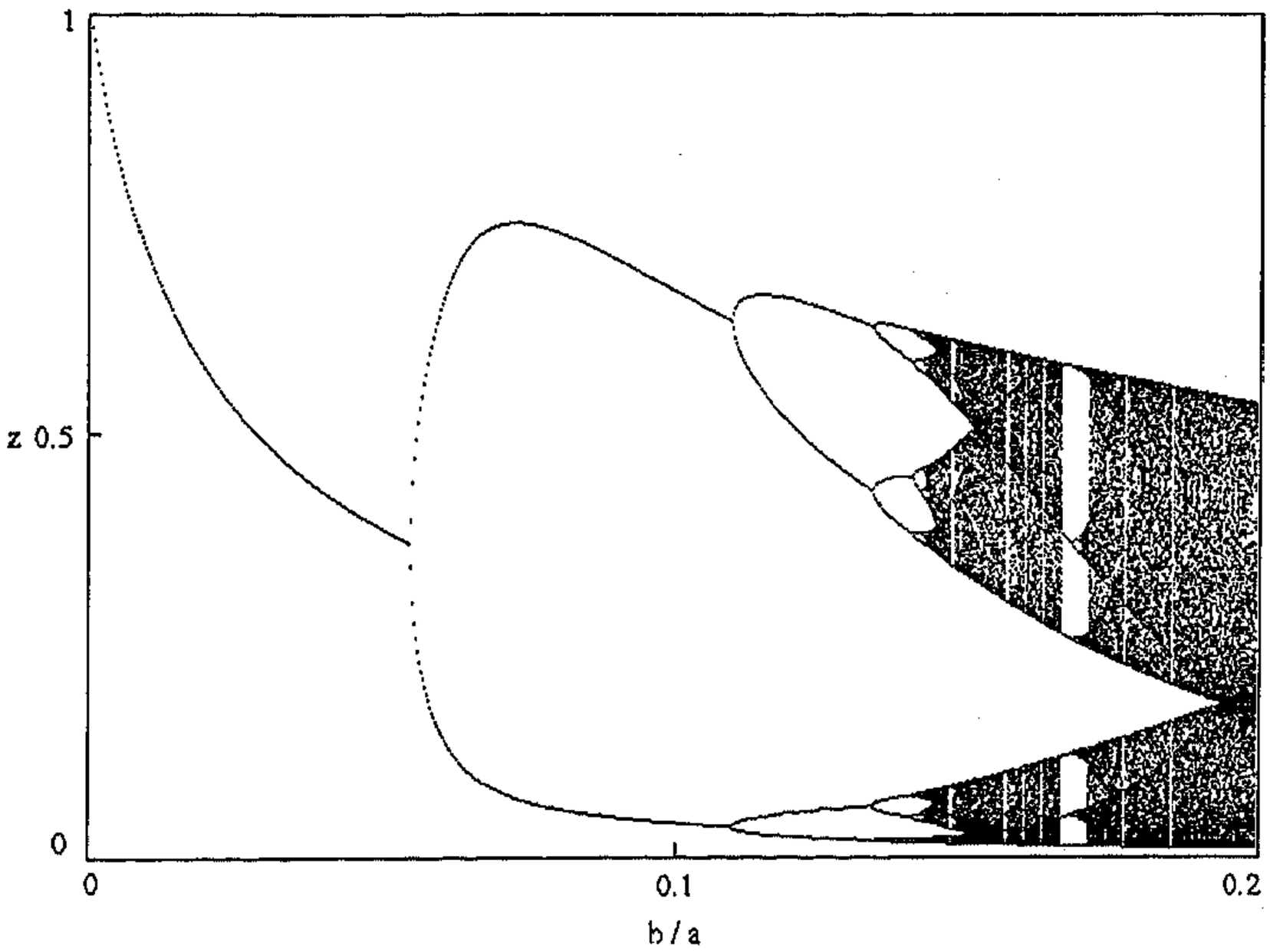

Figure 2.13: Magnified view of the preceding bifurcation diagram, over the interval $0 \leq b/a \leq 0.2$ (a=50).

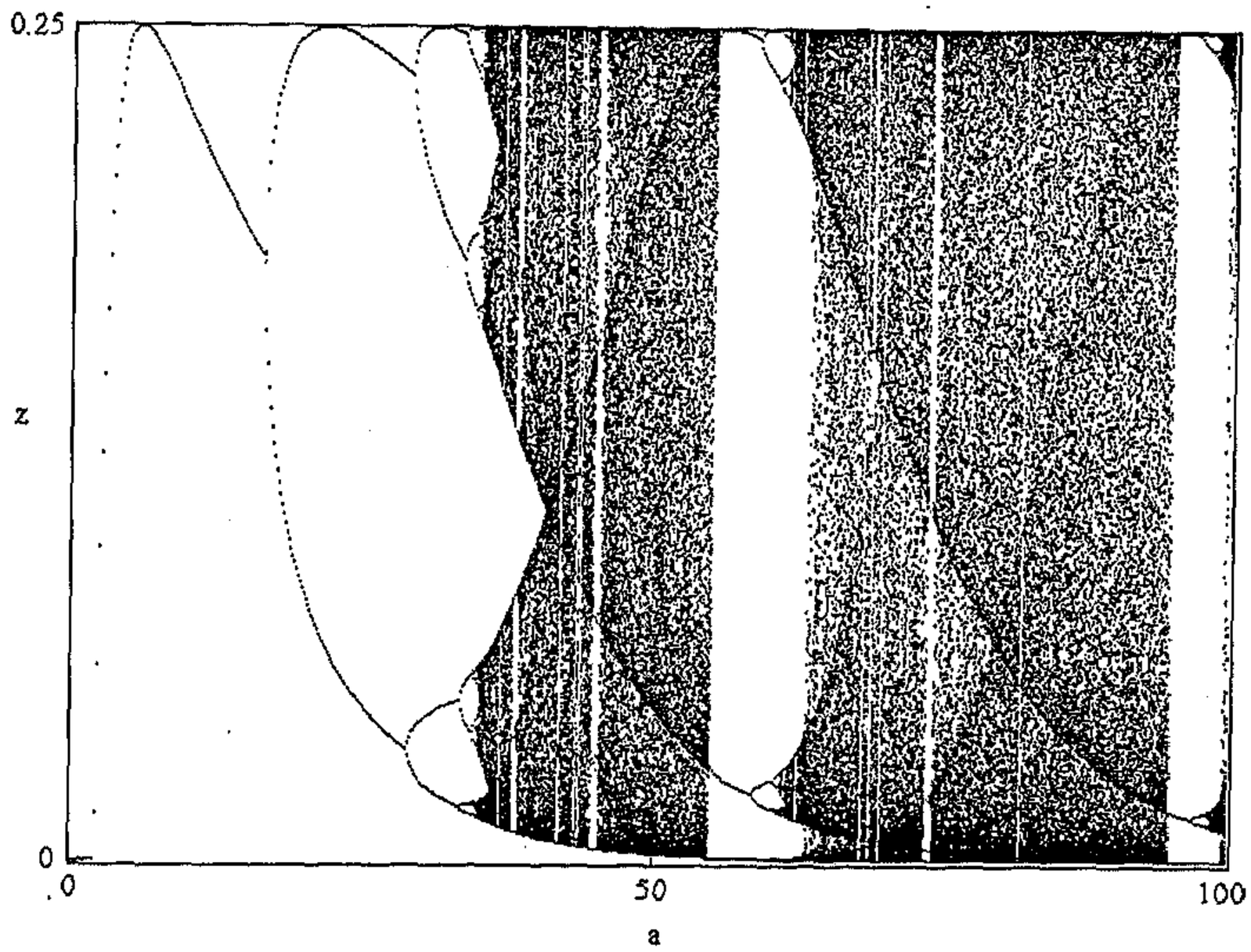

Figure 2.14: Bifurcation diagram of the map representing excitatory-inhibitory pair dynamics with sigmoid F for b/a=0.5.

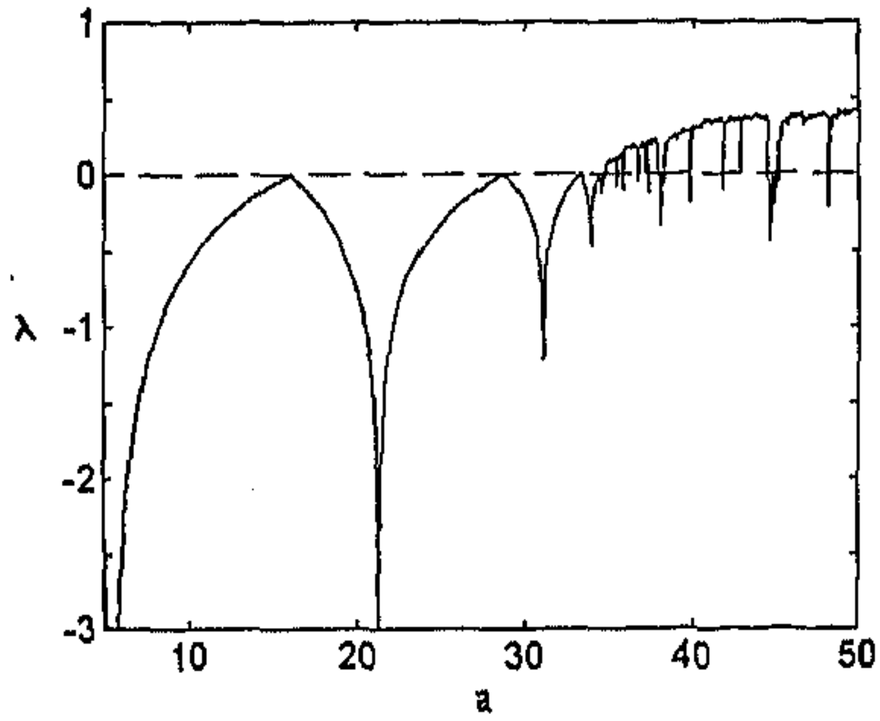

Figure 2.15: Lyapunov exponent (λ) plotted against a for $b/a = 0.5$.

by the Lyapunov exponent (λ). Fig. 2.15 shows the variation of λ with a ($b/a = 0.5$) and Fig. 2.16 exhibits the chaotic and non-chaotic regions on the basis of the sign of λ, with regions having $\lambda < 0$ (i.e., non-chaotic) indicated by black. Notice the "garlands" of periodic windows within the chaotic region. The isolated points of periodic behavior, interspersed throughout the chaotic region, are remnants of periodic windows too fine to be resolved at the present scale.

We shall now consider the case when $k = k' \neq 1$. Figs. 2.17 and 2.18 show the bifurcation diagrams at $a = 50$ and $b/a = 0.5$ over the intervals, $(0 \leq k \leq 1.5)$ and $(0.99 \leq k \leq 1.03)$, respectively. As k decreases from 1, the flatter end of the map rises, so that, very soon the local slope of the fixed point, Z_2^* (or, equivalently, Z_3^*), becomes greater than -1, making it stable. This is indicated by the long interval of non-chaotic behavior for $0 \leq k < 0.9$. When k increases from 1, the two disjoint chaotic attractors are dynamically connected - so that a transition from symmetry-broken chaos to symmetric chaos is observed. On further increase of k, chaos again gives rise to periodic, and finally, fixed point behavior.

2.3 Effect of threshold / bias

In the previous section, we have looked at the autonomous dynamics of the excitatory-inhibitory neural pair - i.e., in the absence of any external input. We had also assumed the threshold θ to be zero. We shall now look at the effect of both of these variables on the system variables. One of the simplifying features of the type of activation functions we have chosen is that introducing a threshold of magnitude θ is equivalent to subjecting the system to a constant external input of amplitude $|\theta|$. This is evident if we look at eqn. 2.12 for the case $k = k' = 1$, in the presence of

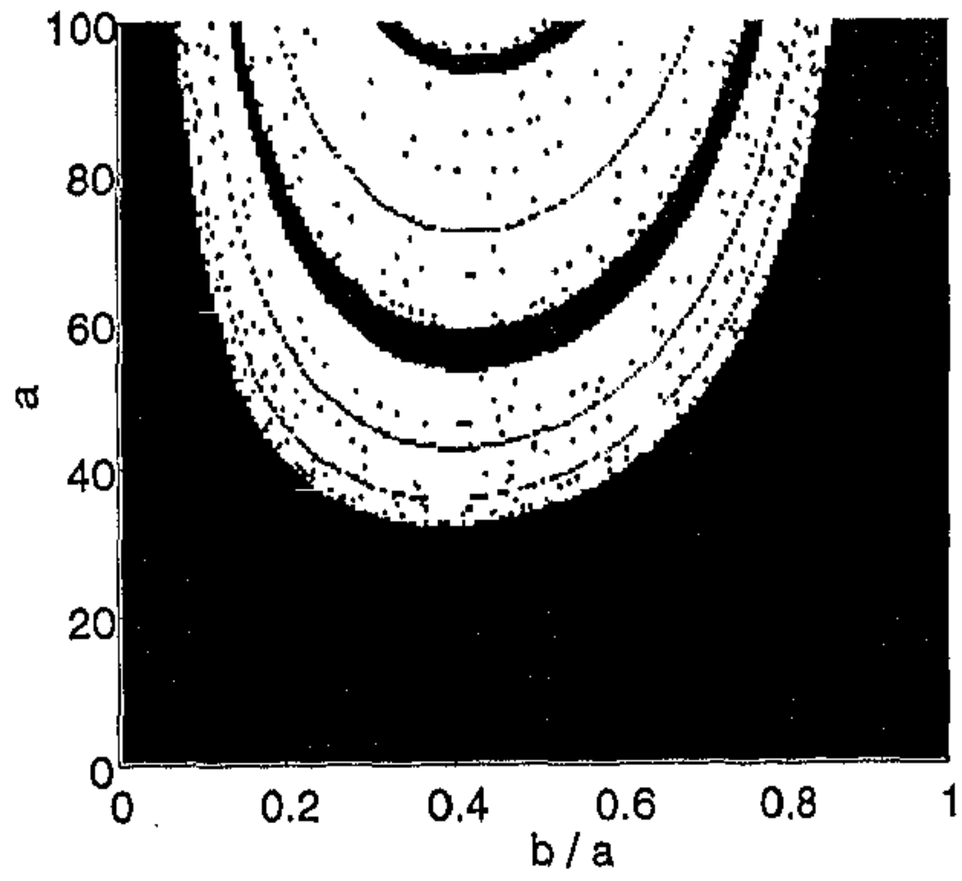

Figure 2.16: Stability diagram in the a vs (b/a) parameter space with ordered behavior indicated by black and chaotic behavior indicated by white.

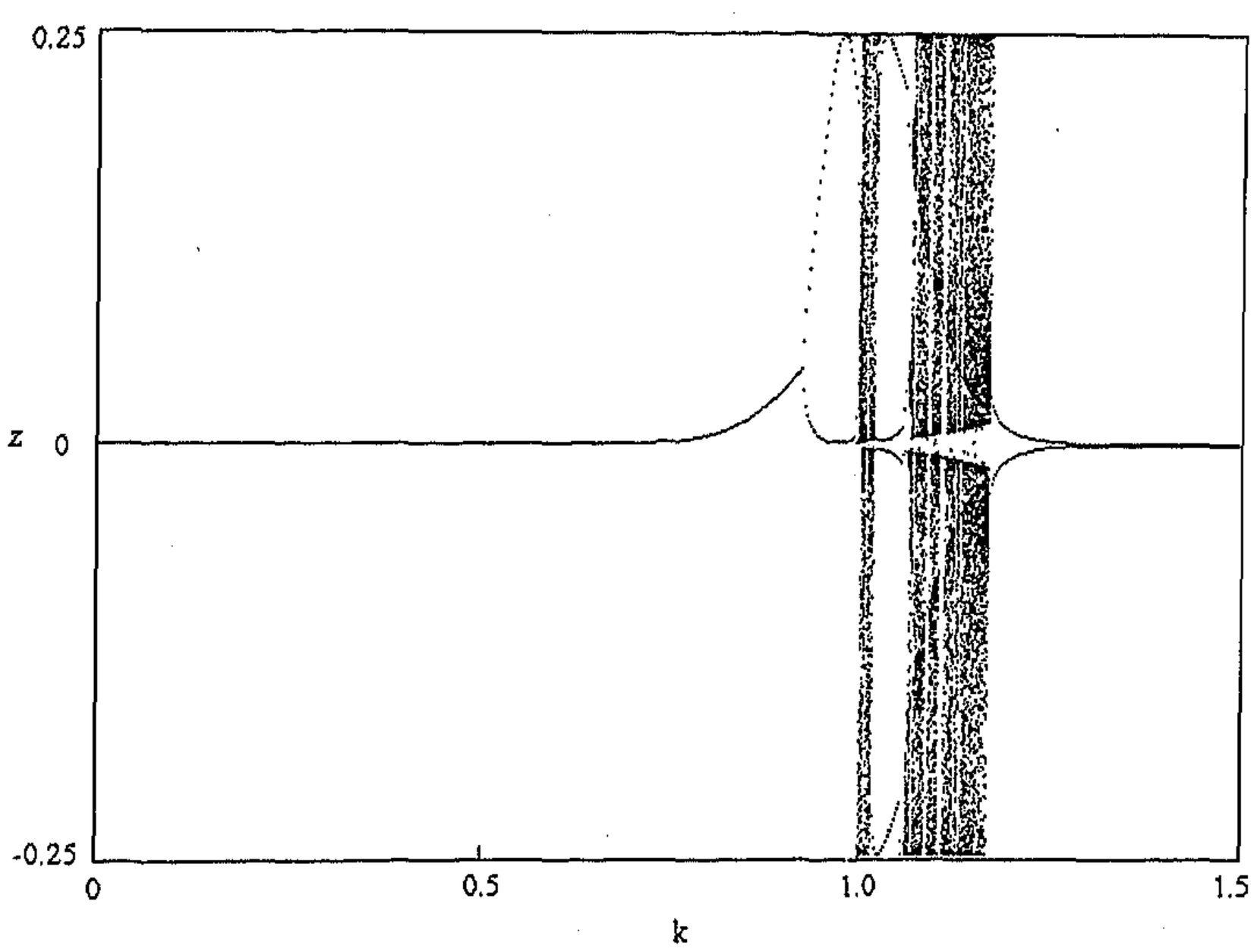

Figure 2.17: Bifurcation diagram for $k = k' \neq 1$ at $a = 50, b/a = 0.5$

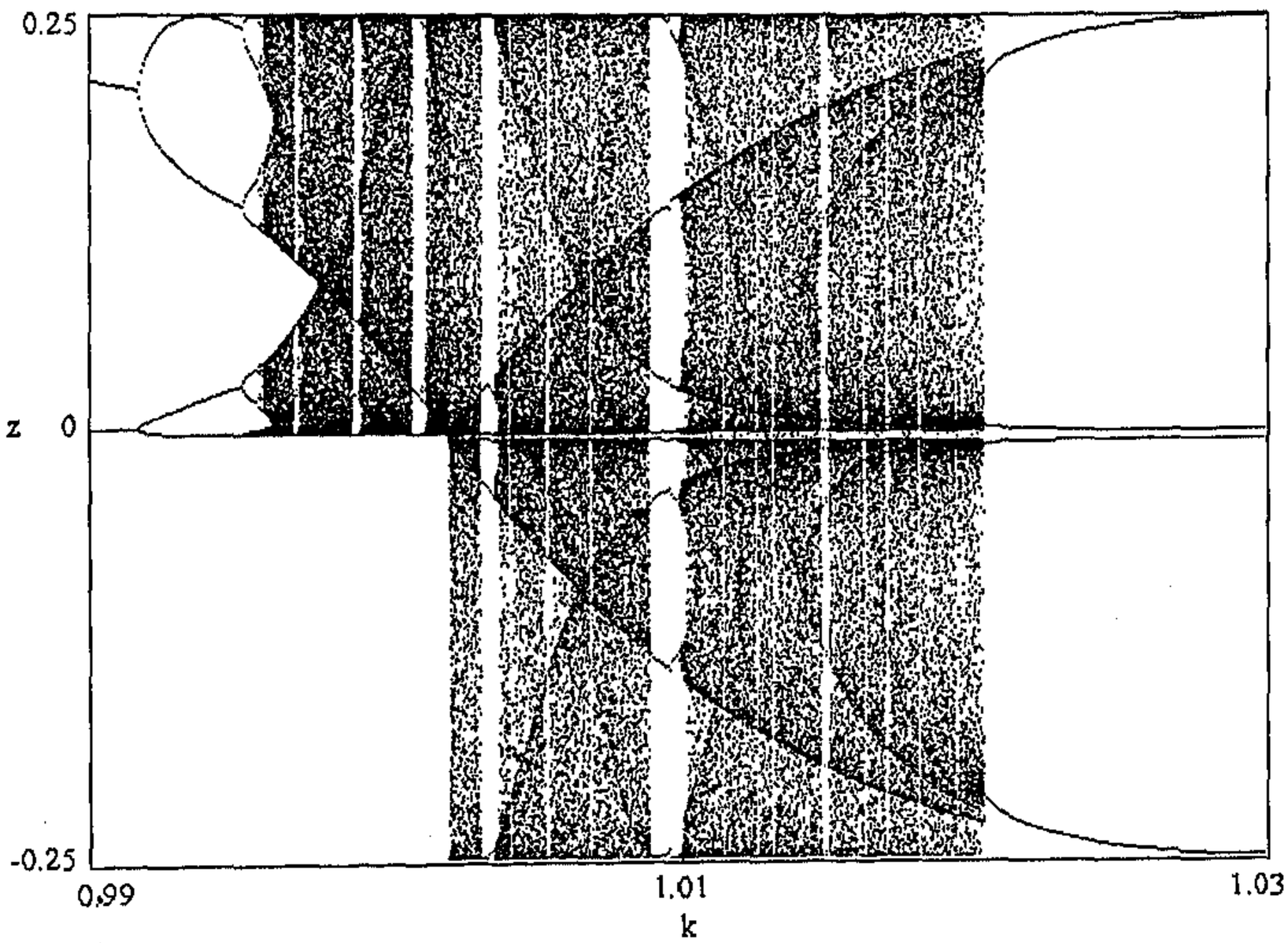

Figure 2.18: Magnified view of bifurcation diagram for $k = k' \neq 1$ at $a = 50, b/a = 0.5$ over the interval $0.99 \leq k \leq 1.03$

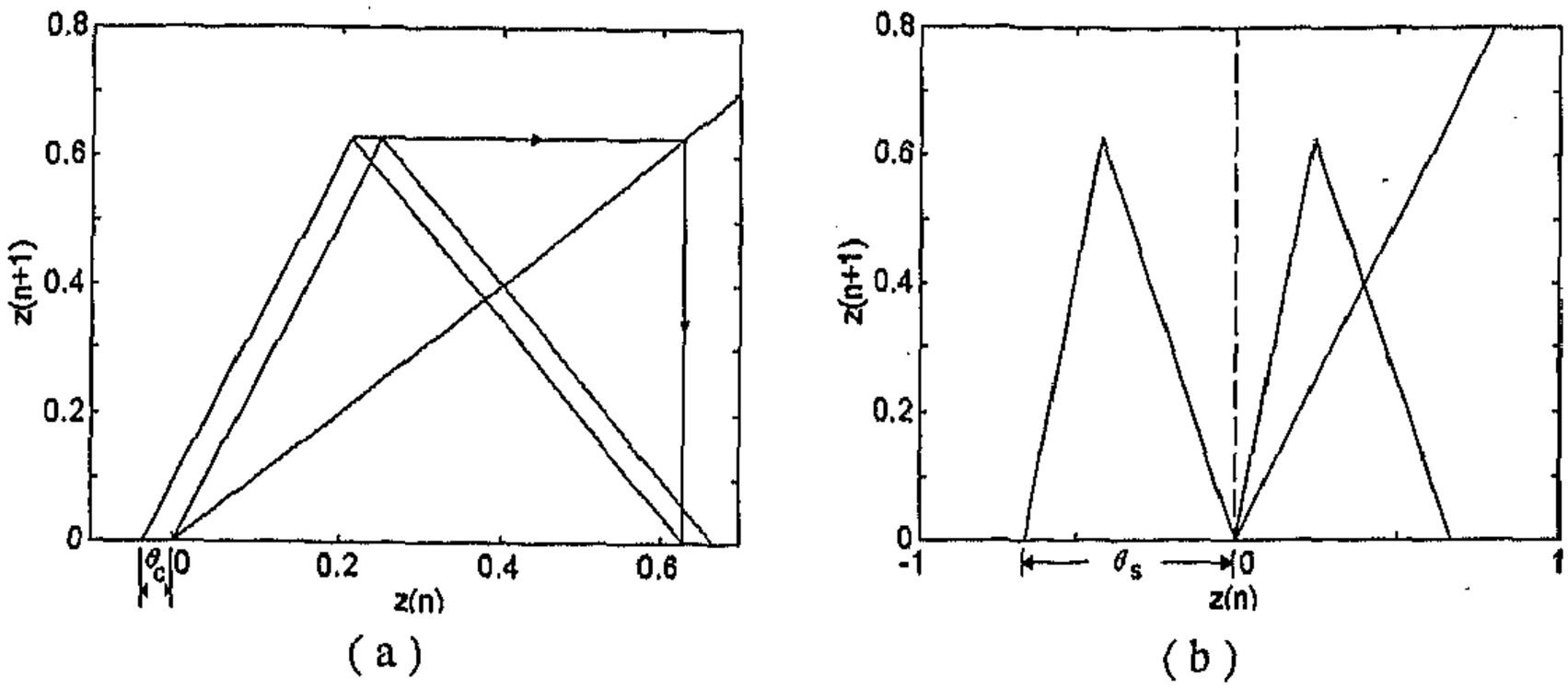

Figure 2.19: (a) The critical bias (θ_c) and (b) the saturation bias (θ_s).

external input

$$Z_{n+1} \doteq F_a(Z_n + \theta) - F_b(Z_n + \theta). \tag{2.20}$$

An identical equation is obtained if, instead of an external input, we had introduced a negative threshold (i.e., bias) of magnitude θ. In what is to follow, we will not therefore differentiate between bias/threshold and a constant amplitude external input. The effect of introducing a constant perturbation in simple chaotic maps, have been previously observed to give rise to 'non-universal' behavior (i.e., the nature of response differ from one map to another) [187, 175]

Let us first consider the case when $\theta > 0$ (we will refer to this as 'bias'). As θ increases from 0, the map shifts to the left, and the origin, $Z_1^* = 0$, is no longer a fixed point. Two values of θ are of interest in understanding what changes are made to the autonomous system dynamics by this modification.

- The *critical bias* (θ_c) is the bias value at which the critical point of the one-dimensional map (representing the dynamics of the system) is mapped to 0. This marks the transition point from chaotic behavior to superstable cycles (Fig. 2.19 (a)).
- The *saturation bias* (θ_s) is the bias value at which $Z_1^* = 0$ again becomes a fixed point, in fact, a stable one - i.e., for any initial value, Z_0, the trajectory terminates at $Z_1^* = 0$. This occurs when the entire non-zero portion of the map shifts to the left of the origin, so that the point $Z = 1/b$ in the original map, now coincides with the origin.

An expression for the critical bias is obtained, in the case of the asymmetric piecewise linear transfer function, by noting that for $\theta = \theta_c$, $F_a(\frac{1}{a} + \theta) - F_b(\frac{1}{a} + \theta) = 0$. So,

$$\theta_c = \frac{1}{b} + \frac{b}{a} - 1.$$

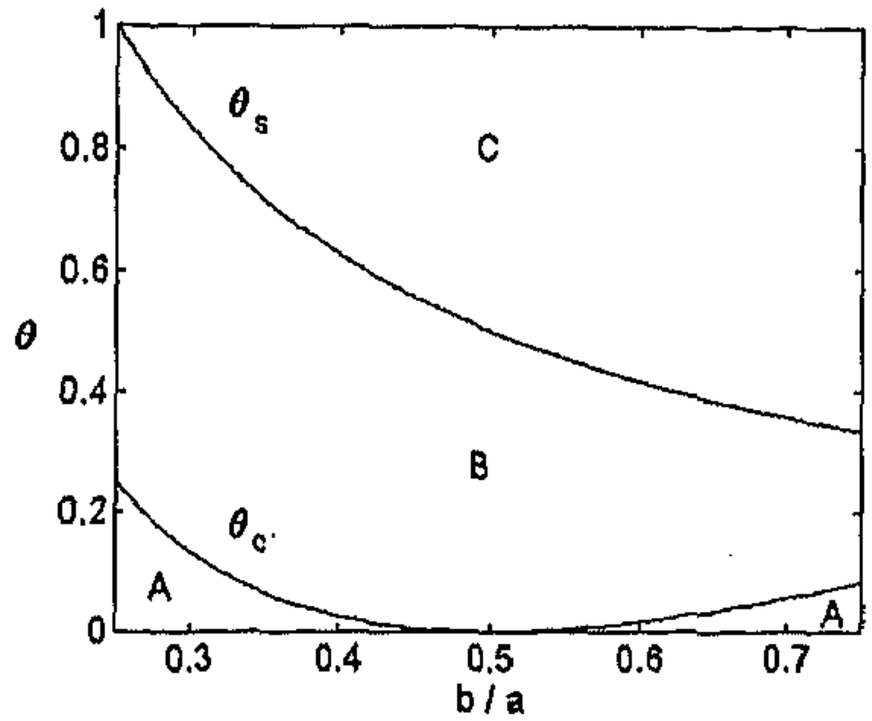

Figure 2.20: The μ vs θ parameter space indicating regions of (A) chaotic, (B) superstable period cycles and (C) fixed point ($Z^* = 0$) behavior, for $a = 4$.

The saturation bias, θ_s, is given as

$$\theta_s = 1/b.$$

These two expressions enable us to draw the (b/a) vs θ diagram in Fig. 2.20, showing the regions of different dynamical behavior.

When $\theta < 0$, coexistence of multiple attractors of different dynamical types is observed. Fig. 2.21 gives an example of the coexistence of a fixed point ($Z^* = 0$) and a chaotic attractor.

This allows the segmentation of activation state (X, Y)-space, according to dynamical behavior. For initial conditions lying in the region bounded by the two straight lines, $Y = (X - \theta)/k$ and $Y = (X - \theta)/(k - 1/ak)$, the trajectories are chaotic, provided the maximum point of the map, $F(Z) = 1 - (kb/a)$, does not iterate into the region $Z > \theta + (1/b)$. For the region, $Y > (X - \theta)/k$, any iterate will map to the fixed point, $Z^* = 0$. Initial conditions from $Y < (X - \theta)/(k - 1/ak)$ will map to the chaotic region, if the maximum point of the map does not iterate into $Z > \theta + (1/b)$. Otherwise, a fractal set of initial conditions will give rise to bounded chaotic motion, the remaining region falling in the "escape set", eventually leading to periodic orbits.

The condition for coexistence of multiple attractors, in the case of $k = k' = 1$, is obtained as follows. The one-dimensional map equivalent to the excitatory-inhibitory system now has an unstable fixed point at $Z_u = \frac{\theta(a-b)}{a-b-1}$. Note that $Z^* = 0$ will always be stable for any $\theta < 0$. For two attractors to exist, the critical point of this modified map should not belong to the basin of attraction of $Z^* = 0$, which can be written as:

$$F_a(1 - \frac{b}{a}) - F_b(1 - \frac{b}{a}) > Z_u.$$

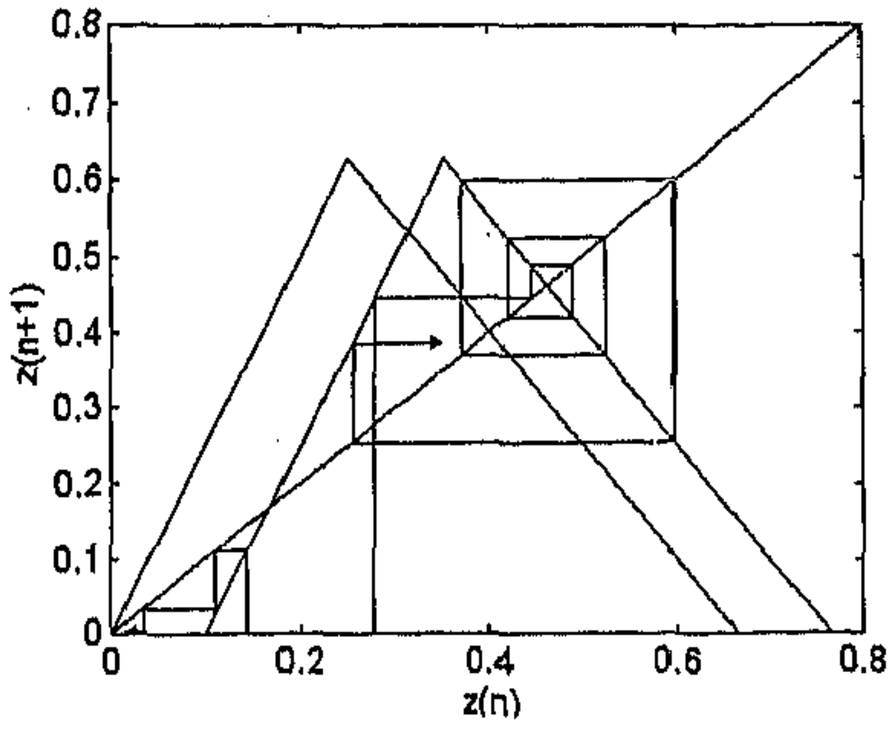

Figure 2.21: Coexistence of fixed point ($Z^* = 0$) and chaotic attractors, with trajectories in the two basins of attractions indicated, for $a = 4$, $b = 1.5$.

By simple algebraic manipulation, one obtains the following condition on the magnitude of θ:

$$\theta < \frac{(1 - b + \frac{b^2}{a})(a - b - 1)}{a - b - b(a - b - 1)}. \tag{2.21}$$

In the case of anti-symmetric activation functions, for a negative θ, $Z^* = 0$ is not a fixed point. Rather, under the condition mentioned above, the two disconnected chaotic attractors to be dynamically connected. This means, starting from an initial condition which belongs to one of the chaotic attractors, it is possible to visit the other attractor, provided the above condition is satisfied. This gives rise to hysteretic phenomenon in the model, as θ is monotonically increased or decreased.

Let us discuss the case of the anti-symmetric activation function given by Eqn. (2.10). As mentioned before, this has two coexisting chaotic attractors, in the two halves of the phase space: $L : (-\infty, 0)$ and $R : [0, \infty)$. In general, when $\theta > 0$, the trajectory remains in the attractor in R, whereas, if $\theta < 0$, it is confined to the attractor in L. Fig. 2.22 shows the bifurcations induced by varying θ, when the initial value, $Z_0 > 0$. It is apparent that the trajectory falls in the attractor in R, much before $\theta = 0$. On the other hand, for the initial value $Z_0 < 0$, a magnified view (Fig. 2.23) over the interval $(-0.01 < \theta < 0.01)$, shows that the trajectory remains in L even after θ has become positive.

Simple hysteresis loops have been demonstrated and discussed by Harth (reviewed in [75] and the article by Harth in [6]) in neural populations containing mostly excitatory elements. Wilson and Cowan [204] showed that excitatory- inhibitory networks can show more complex hysteresis phenomena. For instance, multiple separated or simultaneous loops are observed, which is an outcome essentially of the inclusion of inhibition in the model.

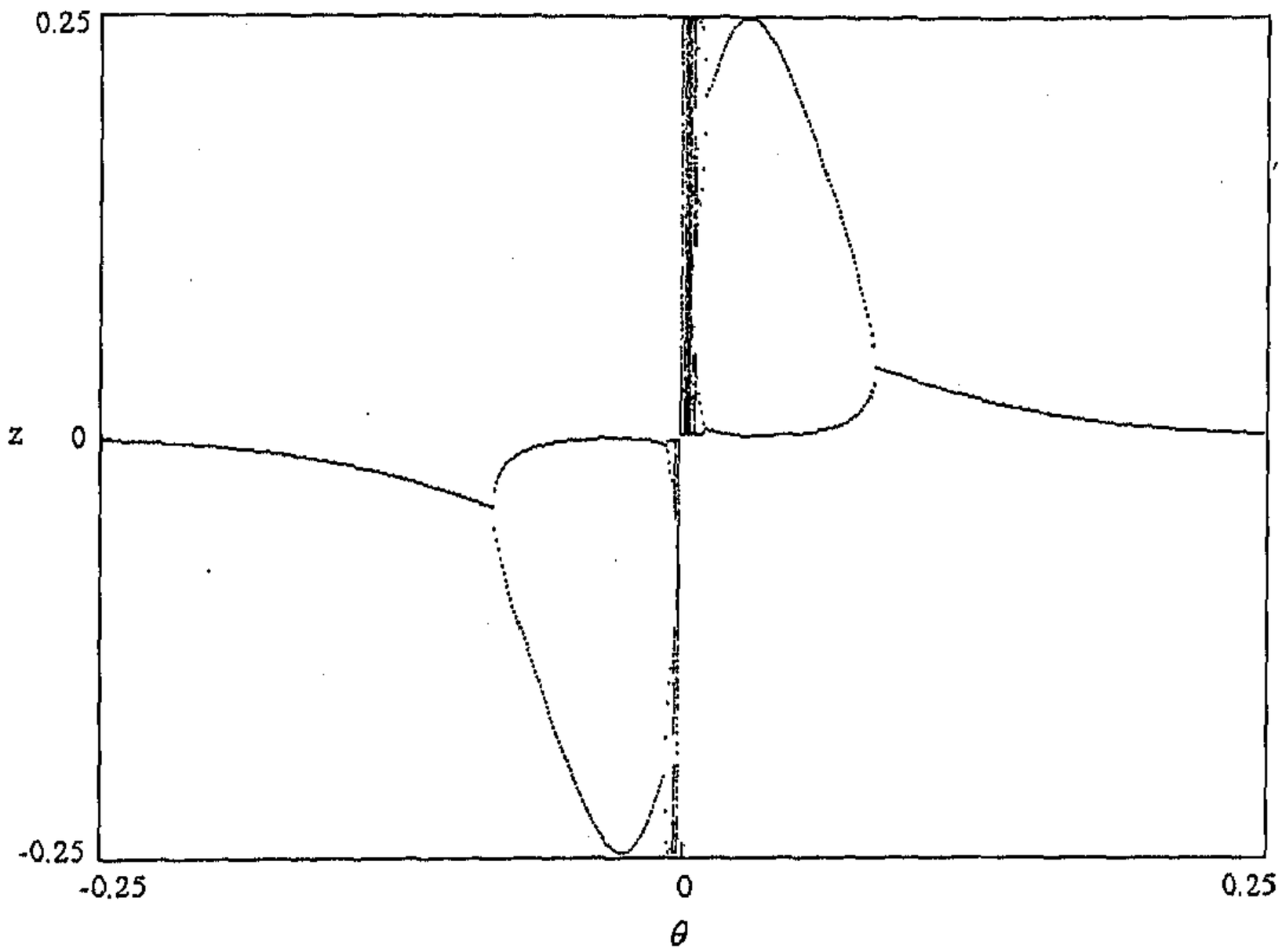

Figure 2.22: Bifurcation diagram for variation of threshold θ over the interval (-0.01, 0.01) for $a = 50, b/a = 0.5$ and $k = k' = 1$ (initial value, $Z_0 > 0$)..

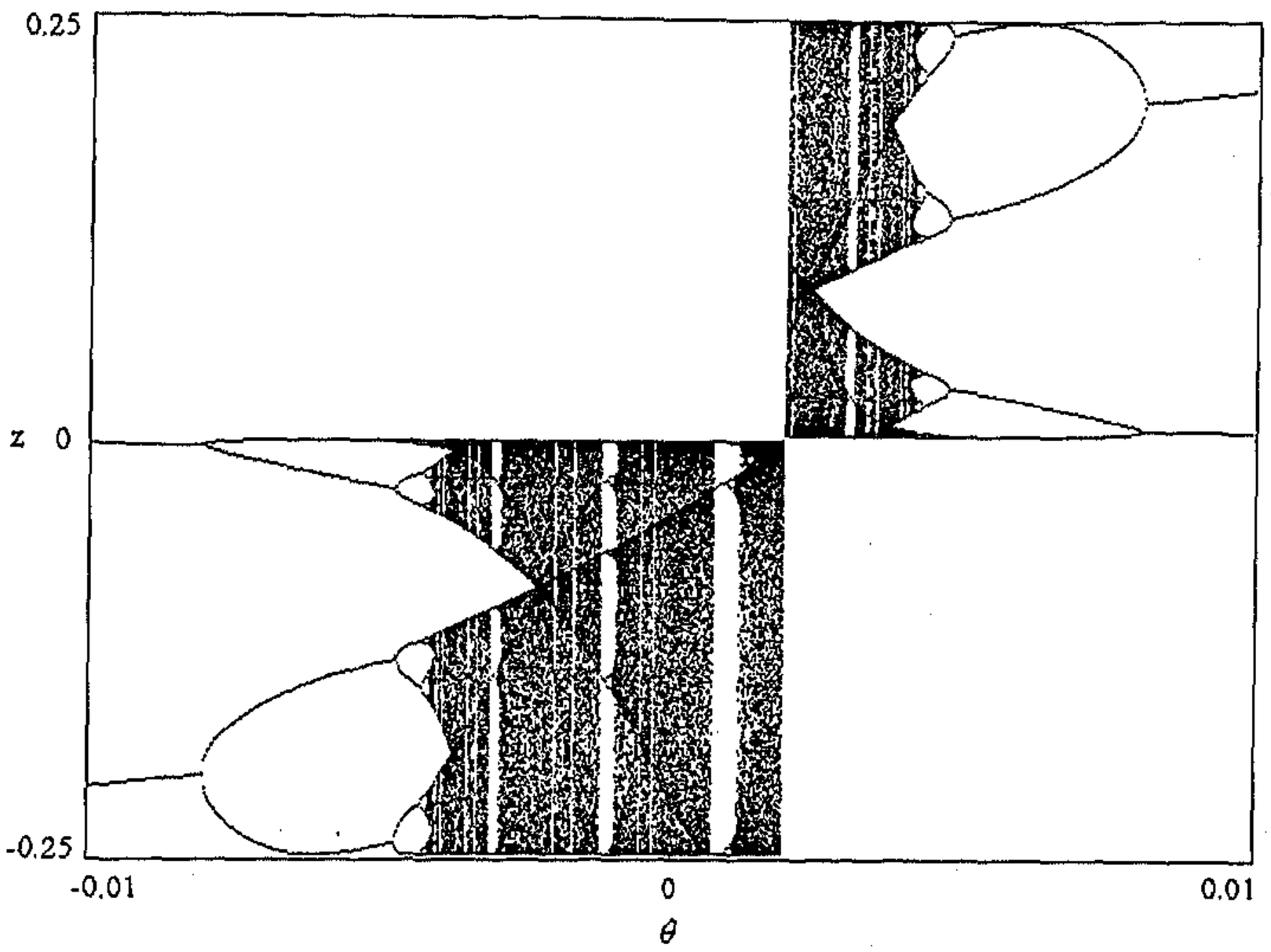

Figure 2.23: Magnified view of the bifurcation diagram for variation of θ over the interval (-0.25, 0.25) for $a = 50, b/a = 0.5$ and $k = k' = 1$ (initial value, $Z_0 < 0$).

Functionally, hysteresis may be a physiological basis for short-term memory. Any sufficiently strong stimulus is going to cause the activity to jump from a low level to a high level, and this activity will persist even after the input ceases. The existence of hysteresis in the central nervous system, specifically in the fusion of binocularly presented patterns to produce single vision, has also been experimentally verified. Hysteresis has the benefit of imparting robustness against noise. A large change in the external stimulus is needed to excite the element to a higher state, giving a threshold. For a complex system like the brain, that is immersed in a noisy environment, the advantage of such noise tolerance is obvious.

2.4 Extension to large networks

In the preceding sections, the behavior of a pair of excitatory-inhibitory neurons (number of neurons, $N = 2$) was shown to have sufficient complexity. The dynamics of a N-neuron network ($N >> 2$) described by

$$\mathbf{X_{n+1}} = F(\sum \mathbf{W}.\mathbf{X_n}),$$

where $\mathbf{X_n}$ is the set of N activation state values (both excitatory and inhibitory neurons), and $\mathbf{W}$ is the matrix of connection weights between different neurons. The full range of behavior shown by such a system will be impossible to study in detail, as the number of available tunable parameters are too large to handle. However, under certain restrictions, the dynamics of such large networks can be inferred.

Let W_{ij} denote the connection weight from jth to the ith neuron. Then, under the condition

$$W_{i\ j+1}/W_{i\ 1} = k_j, \quad (k_j = \text{constant for a given } j = 1, \ldots, N), \tag{2.22}$$

the N-neuron network dynamics is reducible to that of a 1-dimensional map with ($N+1$) linear segments (for $\theta = 0$). The occurrence of "folds" in a map have already been shown to be responsible for creation and persistence of localized coherent structures within a chaotic flow [162]. As in this case, the resultant map will have a number of such folds, the system might show coexistence of multiple chaotic attractors (isolated from each other). A simple example to illustrate this point is a fully connected network of four neurons: two excitatory (x_1,x_2) and two inhibitory (y_1,y_2). Let a_i and b_i represent the slope of the transfer functions for the ith excitatory and inhibitory neurons, respectively. The 4-dimensional dynamics is reducible to the 1-dimensional dynamics of $z = x_1 - k_1 y_1 + k_2 x_2 - k_3 y_2$. Simulations were carried out for the set of parameter values: ($a_1 = 4.6, a_2 = 4.0, b_1 = 3.6, b_2 = 1.6$) and ($k_1 = 0.7, k_2 = 1.0, k_3 = 1.1$). Furthermore, x_2,y_2 have a threshold equal to $1/b_1$. Fig. 2.24 (a) shows the return map and time evolution of z in the absence of any bias. There is only a single global chaotic attractor in this case. When a small negative bias is applied to the whole network, the previous attractor splits into two coexisting

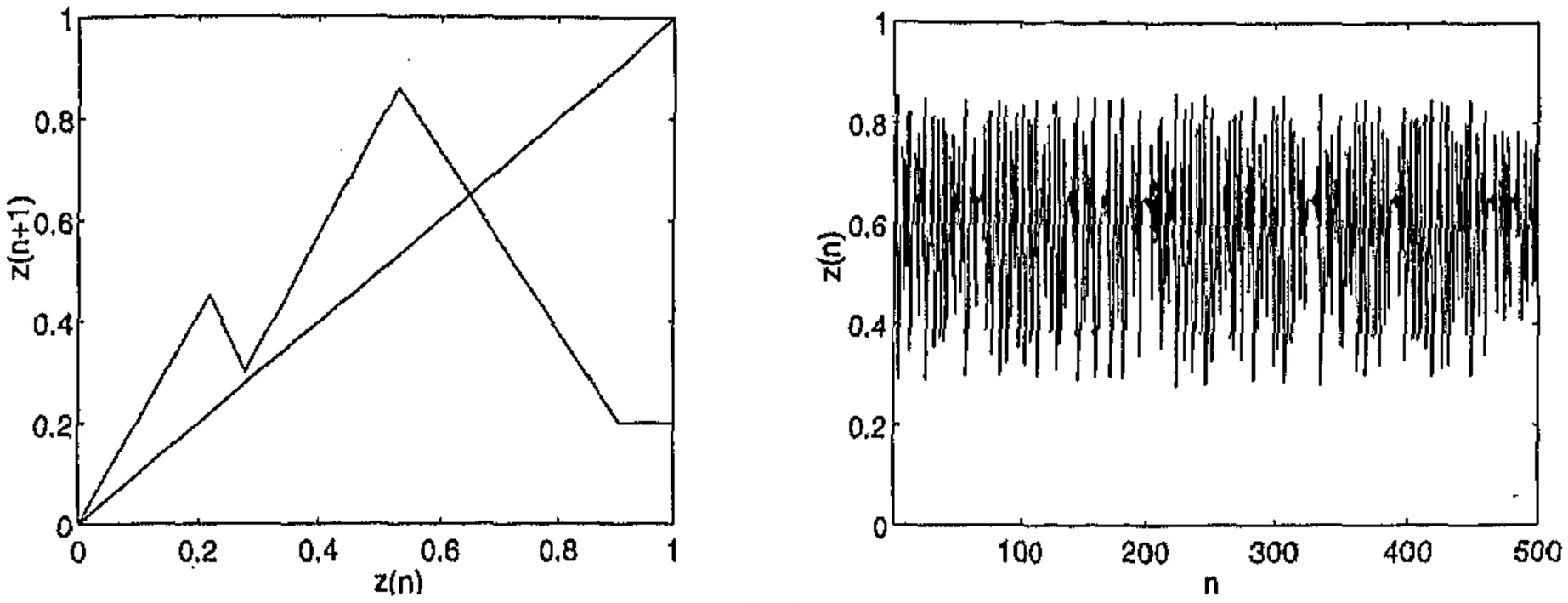

(a)

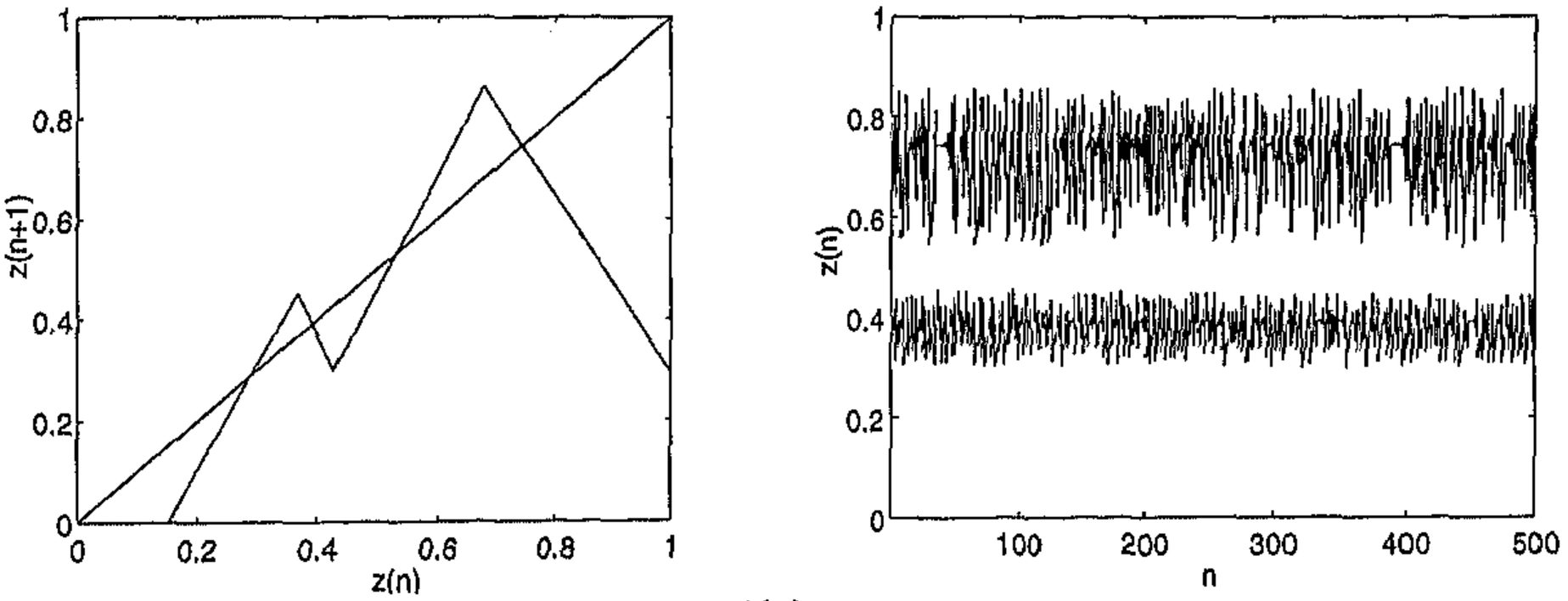

(b)

Figure 2.24: The return map and time evolution of the reduced variable, z, for a 4-neuron network (for details see text), with (a) bias = 0 and (b) bias = − 0.15. In the former there is a single global chaotic attractor. For non-zero bias, there are two co-existing chaotic attractors. Time evolution of z starting from two initial conditions belonging to different attractors are superposed.

isolated attractors having localized chaotic activity. Which attractor the system will be in, depends upon the initial value it starts from. Fig. 2.24 (b) shows the return map for a bias value of -0.15 and the superposed time evolutions of z starting from initial conditions belonging to two different attractors. So, an increase in bias, can cause transition from global chaos to localized chaotic regions.

This property can be used to simulate a proposed mechanism of olfactory information processing [53]. It has been suggested that the olfactory system maintains a global attractor with multiple "wings", each corresponding to a specific class of odorant. During each inhalation, the system moves from the central chaotic repeller to one of the wings, if the input contains a known stimulus. The continual shift from one wing to another via the central repelling zone has been termed as chaotic "itinerancy". This forms the basis of several chaotic associative memory models.

The above picture can be observed in the present model by noting that, if the external input has the effect of momentarily increasing the bias from a negative value to zero, then the isolated chaotic regions merge together into a single global attractor. In this condition, the entire region is accessible to any input state. However, as the bias goes back to a small negative value, the different isolated chaotic attractors re-emerge, and the system dynamics is constrained into one of these. Sustained external stimuli will cause the gain parameters to decrease (adaptation), thereby decreasing the local slope of the map. If the stimulus is maintained, the unstable fixed point in the isolated region will become stable leading to a fixed-point or periodic behavior. The above scenario, in fact, is the basis of using the proposed model as an associative memory network.

2.5 Information processing with chaos

Chaotic dynamics enables the microscopic sensory input received by the brain to control the macroscopic activity that constitutes its output. This occurs as a result of the selective sensitivity of chaotic systems to small fluctuations in the environment and their capacity for rapid state transitions. On the other hand, chaotic attractors are globally extremely robust. These properties indicate that the utilization of chaos by biological systems for information processing can indeed be advantageous. It has been suggested, based on investigations into cellular automata, that complex computational capabilities emerge at the "edge of chaos" [109].

Based on this notion, efforts are on to use chaos in neural network models to achieve human-like information processing capabilities. Chaotic neural networks have been already been applied in designing associative memory networks [96] and solving combinatorial optimization problems, using chaos to carry out an effective stochastic search [94]. The superposition of chaotic maps for information processing has also been suggested before [10, 9].

The model presented in this chapter can be used for a variety of purposes, classified

as follows:

Associative memory: A set of patterns (i.e., specific network state configurations) are stored in the network as attractors of the system dynamics, such that, whenever a distorted version of one of the patterns is presented to the network as input, the original is retrieved upon iteration. The distortion has to be small enough so that the input pattern is not outside the basin of attraction of the desired attractor. In networks using convergent dynamics, the stored patterns necessarily have to be time-invariant or at most, periodic.

Chaos provides rapid and unbiased access to all attractors, any of which may be selected on presentation of a stimulus, depending upon the network state and external environment. It also acts as a "novelty detector", classifying a stimulus as being previously unknown, by not converging to any of the existing attractors. This suggests the use of chaotic networks for *auto association.*

In the previous section, the basic mechanism for constructing an associative memory network has been described. In this proposed model, both constant and periodic sequences can be stored. This is made possible by introducing "folds" in the return map of the network, so that a large number of isolated regions are produced. The nature of the dynamics in a region can be controlled by altering the gain parameters of individual neurons. Accessibility to a given attractor depends upon the initial condition of the network and the input stimulus. So, regions with fixed-point or periodic attractors may be embedded within regions having chaotic behavior. In addition, chaotic trajectories confined within a specific region can also be generated when presented with a short-duration input stimulus belonging to that region. "Novelty detection" is implemented in the above model by making the basins of attractors (corresponding to the stored patterns) of some pre-specified size. Input belonging outside the region, therefore, cannot enter the basin and will not be able to converge to the stored pattern.

Pattern classification: In this information processing task, different input sets need to be classified into a fixed number of categories. Decision boundaries, i.e., boundaries between the different classes are constructed by a "training session" where the network is presented with a series of inputs and the corresponding class to which they belong. In the proposed model, classification can be on the basis of dynamical behavior. For example, input sets belonging to different input classes may give rise to different periodic sequences. Otherwise, the distinction can be made between categories of inputs which give rise to chaotic and non-chaotic trajectories. For a pair of neurons ($N = 2$), under the condition $k = k'$, linear separation of the (X, Y)-space can be done (as shown above). By varying the parameters k and b the orientation and size of the class regions can be controlled. If $k \neq k'$ and $N > 2$, nonlinear decision boundaries between different classes can be generated. By using suitably adjusted weights, any arbitrary classification can be achieved.

An example of nonlinear decision boundary generation is shown in Fig. 2.25. The network used for this purpose consists of 4 neurons - 2 excitatory (x_1, x_2) and 2

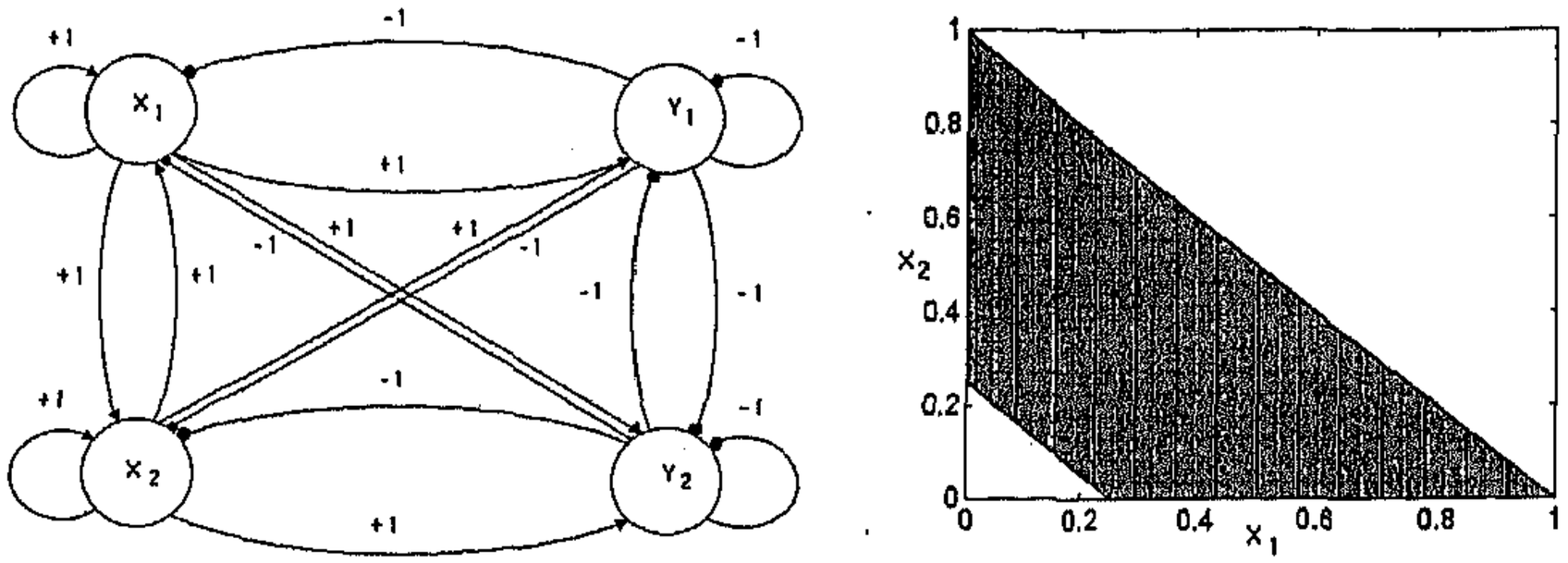

(a) (b)

Figure 2.25: (a) A fully connected 4-neuron network with 2 excitatory ($x_{1,2}$) and 2 inhibitory ($y_{1,2}$) neurons. The arrows and circles represent excitatory and inhibitory synapses, respectively. (b) The (x_1, x_2) phase space shows the basin of the chaotic attractor (shaded region) for threshold, θ=0.25. The unshaded region corresponds to fixed point behavior of the network.

inhibitory (y_1, y_2) (Fig. 2.25 (a)) with asymmetric, piecewise linear activation functions. The gain parameters are $a_{x_1,x_2} = 2$ and $b_{y_1,y_2} = 1$. All the neurons have a threshold, θ. The network is fully connected with all weightages equal to unity. The input stimulus is taken to be the initial value of the excitatory neurons and the inhibitory neuronal states are initially taken to be zero.

As shown in Fig. 2.25 (b), for $\theta = 0.25$, the (x_1, x_2) phase space is segmented into basins leading either to fixed point or to chaotic attractors. By increasing θ, the width of the chaotic band can be reduced. Changing the initial value of the inhibitory neurons will cause translation of the band and manipulating the connection weights gives a rotation to the band. Thus, any general transformation can be applied to the segment. More complex network connections might permit segmenting isolated box-like regions in the phase space. This possibility is currently under investigation.

System Dynamics Approximation: A system may be described by a nonlinear input-output relation,

$$Y = \mathbf{G}(X),$$

where the mapping function, **G**, is unknown. By having access to a limited set of input-output pairs, the function has to be approximated - in effect, building a system simulator. Jin *et al* have proposed a discrete-time recurrent neural network [97], which is non-chaotic but similar to the present model, in order to approximate discrete-time systems [98]. In the present model, a sufficient number of coupled neurons can be used to construct any arbitrary piecewise linear input-output relation. By use of a suitable learning rule, the available data set can be used to determine the

gain parameters, thresholds and connection weights of the network. A close approximation of the system dynamics will enable prediction and control of its behavior. The approximation's accuracy is not restricted to systems with piecewise linear functions - but can also give good qualitative reconstruction of smooth nonlinear systems.

Periodic sequence generation: Capability for periodic sequence generation can be exploited for modeling *central pattern generators*. These are a class of biological neural ensembles which control well-defined rhythmic muscle movements such as swimming, running, walking, breathing, etc. Usually they are found in the spinal cord, producing periodic sequences without feedback from the motor system or higher-level control. The ability to generate multiple sequences from the same neural assembly is another interesting feature. Postulating the existence of single pacemaker neurons acting as the 'system clock' to initiate periodic activity cannot explain all the observed phenomena. The existing network models for simulating this behavior mostly suffer from the drawback that they cannot generate multiple non-overlapping sequences. This shortcoming is overcome in the model presented here. For $N = 2$ and $k = k' \neq 1$, a rich variety of periodic sequences can be chosen from the same network, simply by altering the gain parameters by a very small amount. As mentioned above, numerical investigations indicate that cycles of any period can be generated by suitably altering the value of k.

2.6 Discussion

One notable feature of our investigations is the existence of the wide range of dynamical behavior in the simple system of a coupled neuron pair, which has been observed with a variety of nonlinear activation functions. In addition to the functions considered here, other types of nonlinear activation functions, e.g., $F_a(z) = tanh(z/a)$ and $F_a(z) = \frac{2}{\pi}\arctan(z/a)$ also show qualitatively similar features. In this context, it may be remarked that a related form of activation function: $F_a(z) = \frac{1}{1+exp(-az)}$ has been shown to be topologically conjugate to the chaotic logistic map by Wang [197]. The universality of the observed dynamical features argue strongly that the observations reported here are not merely artifacts of the specific type of function chosen, but in fact, have a broader relevance.

As mentioned previously, we have not considered delayed interactions in our model. The introduction of delays in a neural system can produce qualitatively different behavior. Such effects have been observed in continuous-time [16] and discrete-time [116, 43] updated neural networks. A particularly simple form of delay, viz., an unbounded, exponentially decreasing delay is amenable to simple theoretical analysis [39]. Including this type of delayed interaction in our model shows no new qualitative features. However, other types of delay might produce new, interesting behaviors in the system.

To summarize, the behavior of an excitatory-inhibitory neural pair has been studied

in detail for $N = 2$ (where N is the number of neurons). Nonetheless it shows capability for supporting extremely complex behavior. Under certain restrictions, the dynamics for $N >> 2$ networks can also be understood. Relaxation of these restrictions will provide a challenging task for the future.

Chapter 3

Nonlinear Resonance in a Chaotic Neural Pair

The autonomous behavior of the excitatory-inhibitory neural pair was investigated in the previous chapter. We shall now look at the response of such a system to periodic stimulus. Our observations indicate the occurrence of a nonlinear resonance phenomenon in such a situation. To simplify the theoretical analysis we have investigated an anti-symmetric, piecewise linear map, that shows a transition from symmetry-broken to symmetric chaos on increasing a system parameter. In the latter state, the chaotic trajectory switches between the two formerly disjoint attractors, driven by the map's inherent dynamics. This chaotic switching rate is found to 'resonate' with the frequency of an externally applied periodic perturbation (multiplicative or additive). By periodically modulating the parameter at a specific frequency ω we observe the existence of resonance where the response of the system (in terms of the residence-time distribution) is maximum. This is a clear indication that the resonance we have observed is a deterministic analogue of the phenomenon of Stochastic Resonance (SR) [59] - with thermal noise being replaced by one-dimensional chaos. The insights gained from the simple model is then used to study similar resonance behavior in an excitatory-inhibitory neural pair with anti-symmetric, piecewise linear activation functions.

In Section 1, we briefly review the previous investigations of stochastic resonance in chaotic systems. In Section 2, the model for studying deterministic SR is introduced and the experimental observation of resonance in computer simulations for parametric perturbation is described. In the following section, a theoretical analysis is undertaken of these observations. Additive perturbations also give rise to similar resonance and is described in Section 4. In Section 5, we consider an excitatory-inhibitory neural pair, for which experimental and theoretical results are given. We conclude with a discussion on the implication of such resonance phenomena for biological systems. We also mention the relation of the results of the present investigation with the process of deterministic diffusive and resonance in the kinetic Ising model.

3.1 Stochastic resonance in chaotic systems

"Stochastic Resonance" is a recently observed nonlinear phenomena in noisy systems, where the noise helps in amplifying a sub threshold signal (which would have been otherwise undetected) when the signal frequency is close to a critical value [19]. This occurs because of noise-induced hopping between multiple stable states of a system, locking on to an externally imposed periodic signal. The characteristic signature of SR is the non-monotonic nature of the Signal-to-Noise Ratio (SNR) as a function of the external noise intensity. A theoretical understanding of this phenomena in bistable systems, subject to both periodic and random forcing, has been obtained based on the rate equation approach [125]. As the output of a chaotic process is indistinguishable from that of a noisy system, the question of whether a similar process occurs in the former case has long been debated. In fact, Benzi *et al* [19] indicated that the Lorenz system of equations, a well-known paradigm of chaotic behavior might be showing SR. Later studies [128], [11] in both discrete-time and continuous-time systems seemed to support this view. However, it is difficult to guarantee that the response behavior is due to "resonance" and not due to "forcing". In the latter case, the periodic perturbation is of so large an amplitude, that the system is forced to follow the driving frequency of the periodic forcing. The ambiguity is partly because the SNR is a monotonically decreasing function of the forcing frequency and cannot be used to distinguish between resonance and forcing.

Signature of SR can also be observed in the residence time distribution. In the presence of a periodic modulation, the distribution shows a number of peaks superposed on an exponential background. However, this is observed both in the case of resonance as well as forcing. The ambiguity is, therefore, present in theoretical [40] and experimental [150] studies of noise-free SR, where regular and chaotic phases take the role of the two stable states in conventional SR. Although the distribution of the lengths of the chaotic interval shows a multi-peaked structure, this by itself is not sufficient to ensure that the enhanced response is not due to "forcing". In the present work this problem is avoided by measuring the response of the system in terms of the peaks in the normalized distribution of residence times [60]. For SR, the strength of the peaks shows non-monotonicity with the variation of both noise intensity and signal frequency.

Ippen *et al* [95] have used a chaotic driving term to show SR-like behavior in the SNR of the system response. However, in this case, the chaos is supplied from outside, and not inherent to the system. Indeed, this distinction between stochastic and chaotic driving is somewhat artificial as, e.g., random numbers for Monte Carlo simulations are generated using chaos. If SR is actually used for information processing by biological systems, then it is likely that organs producing chaotic behavior might enhance their survival capability through selective amplification of signals in a noisy background. In this case, the inherent chaos of the system itself could play the role of "noise". In the model proposed in this chapter, a simple one-dimensional map has been shown to use its inherent chaoticity to replicate SR-like phenomena. This

suggests a deep relation between stochastic resonance on the one hand, and crises in chaotic dynamics on the other, mentioned in [31]. The present work also supports this view.

3.2 The model

The simplest chaotic system to show SR-type behavior are one-dimensional maps with two critical points. The most commonly studied system of this kind is the cubic map [122, 190],

$$x_{n+1} = ax_n^3 + (1-a)x_n,$$

where a is a tunable parameter. The map is found to consist of two attractors, the initial condition determining the attractor into which the system settles. Various properties of such 'bimodal' maps differ from those observed for the well-studied class of maps with a single critical point (e.g., the logistic map).

Recently, SR has been studied in 1-D maps with two well-defined states (but not necessarily stable) with switching between them aided by either additive or multiplicative external noise [58]. However, dynamical contact of two chaotic 1-D maps can also induce rhythmic hopping between the two domains of the system [158]. The present work shows how the chaotic dynamics of a system can itself be used for resonant switching between two states, without introducing any external noise.

The model chosen here is a piecewise linear anti-symmetric map, henceforth referred to as the Discontinuous Anti-symmetric Tent (DAT) map, defined in the interval [-1,1]:

$$x(n+1) = \mathrm{F}(x_n) \begin{cases} 1 + a(0.5 - x(n)), & \text{if } x(n) \geq 0.5 \\ 1 - a(0.5 - x(n)), & \text{if } 0 < x(n) < 0.5 \\ -1 + a(0.5 + x(n)), & \text{if } -0.5 < x(n) < 0 \\ -1 - a(0.5 + x(n)), & \text{if } x(n) \leq -0.5. \end{cases} \tag{3.1}$$

The map has a discontinuity at $x = 0$. The behavior of the system was controlled by the parameter a ($0 < a < 4$). Onset of chaos occurs at $a = 1$. The chaos is symmetry-broken, i.e., the trajectory is restricted to either of the two sub-intervals R:(0,1] and L:(0,-1], depending on initial condition. Symmetry is restored at $a = 2$. The Lyapunov exponent of the map is a simple monotonic function of the parameter a. The piecewise-linear nature of the map makes its behavior simpler to study than, say, the cubic map described above. The map is shown in Fig. 3.1, the inset giving a detailed picture of the region around the discontinuity at $x = 0$. Fig. 3.2 shows the evolution of the map's attractor with a increasing from 0 to 4.

The map has a symmetrical pair of fixed points $x^*_{1,2} = \pm\frac{1+a/2}{1+a}$ which are stable for $0 < a < 1$ and unstable for $a > 1$. Another pair of unstable fixed points, $x^*_{3,4} = \pm\frac{1-a/2}{1-a}$ come into existence for $a > 2$. It is to be noted that as $a \to 2$ from above, $x^*_{3,4}$ both collide at $x = 0$ causing an interior crisis [69], which leads to symmetry-breaking of the chaotic attractor.

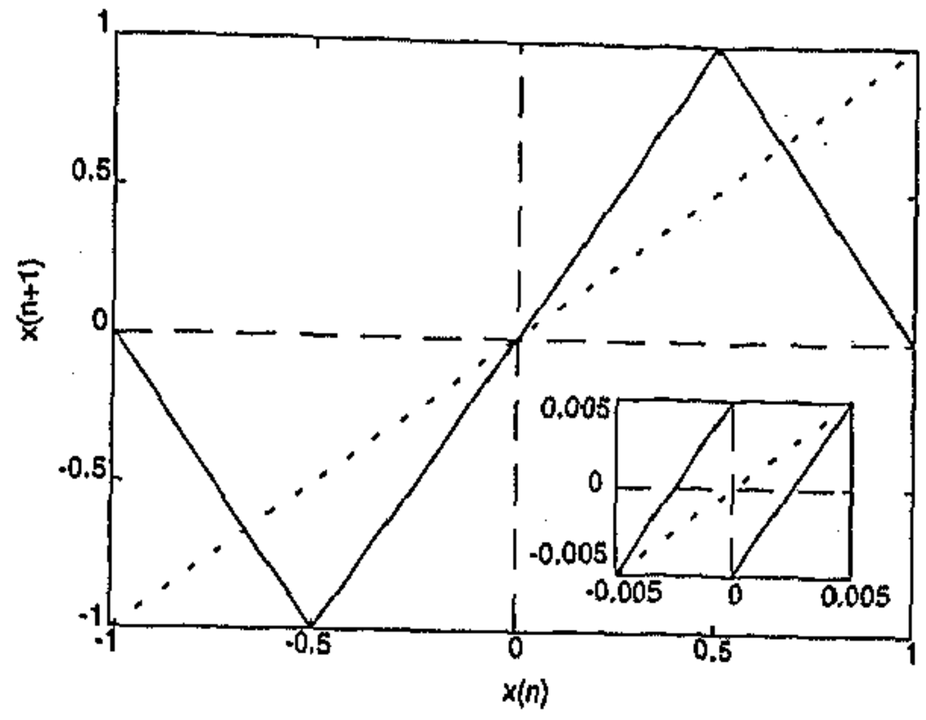

Figure 3.1: The DAT map for $a_0 = 2.01$. Inset: a magnified view of the map in the interval $[-0.005, 0.005] \times [-0.005, 0.005]$.

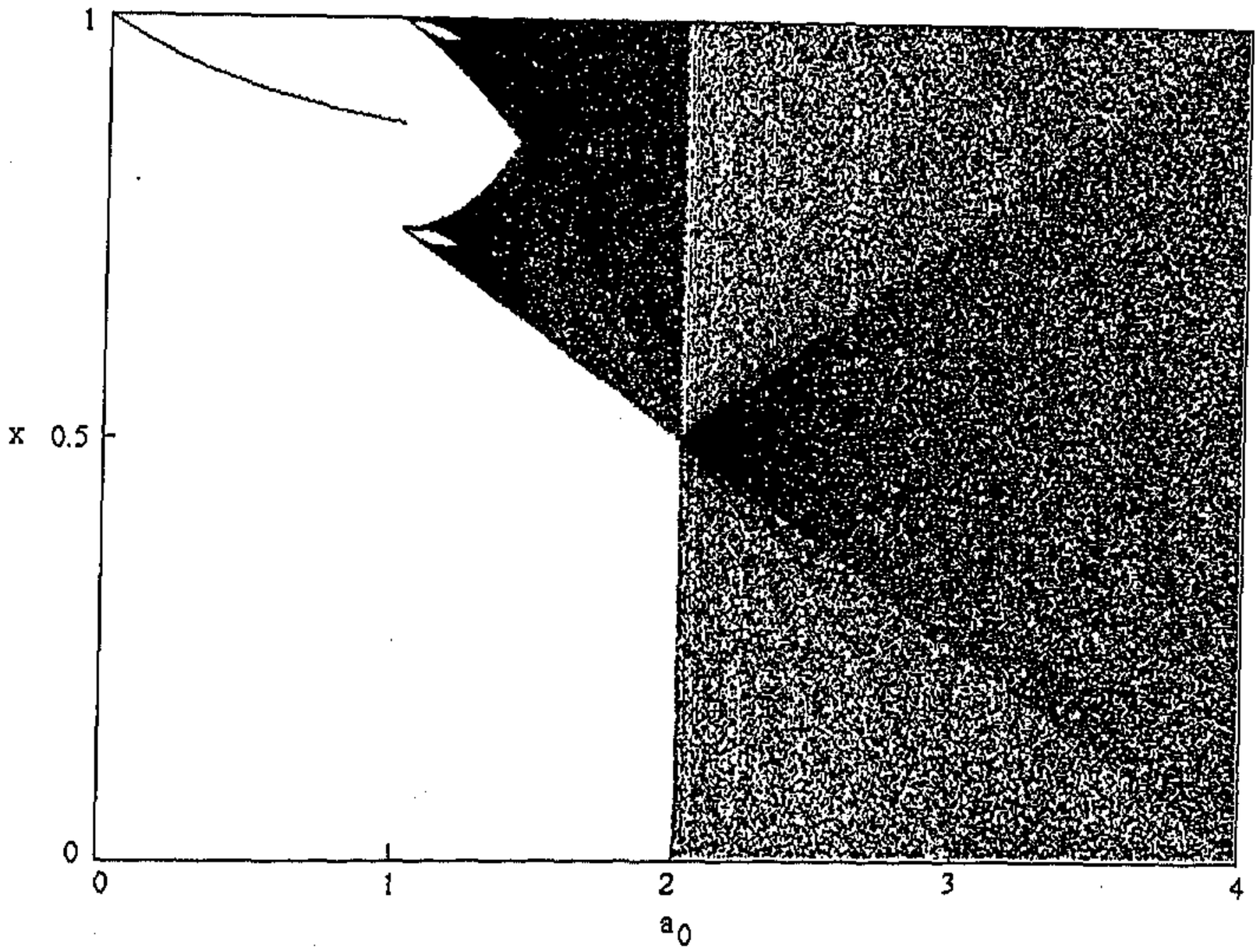

Figure 3.2: Attractor of the DAT map versus a_0. The figure was obtained for $x_0 \in \mathrm{R}$. For $x_0 \in \mathrm{L}$, the corresponding image is obtained by reflecting about x-axis.

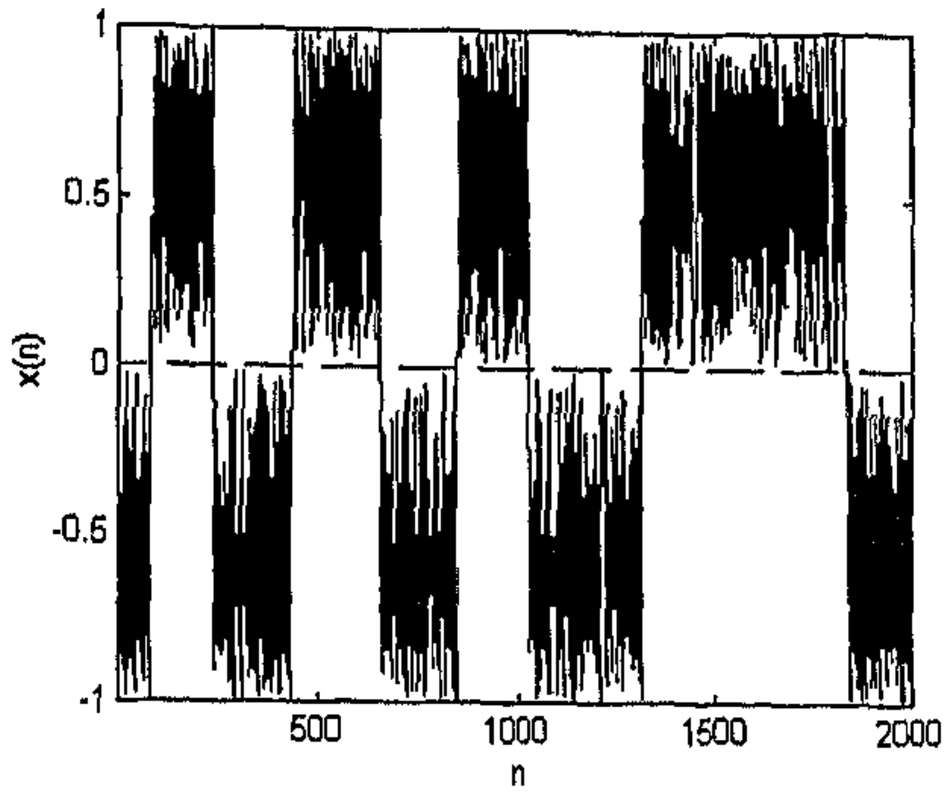

Figure 3.3: The time-evolution of the sinusoidally perturbed DAT map for $a_0 = 2.01$, $\omega = 1/400$ and $\delta = 0.05$. The broken line is the boundary between L and R.

3.3 Parametric perturbation

To observe SR, the value of a was kept close to 2, and then modulated sinusoidally with amplitude δ and frequency ω, i.e.,

$$a_{n+1} = \begin{cases} a_0 + \delta \sin(2\pi\omega n), & \text{if } x \in \mathrm{R} \\ a_0 - \delta \sin(2\pi\omega n), & \text{if } x \in \mathrm{L}. \end{cases} \tag{3.2}$$

We refer to this henceforth as multiplicative or parametric perturbation, to distinguish it from additive perturbation (discussed later).

The system immediately offers an analogy to the classical bistable well scenario of SR. The sub intervals L and R correspond to the two wells between which the system hops to and fro, aided by the inherent noise (chaos) and the external periodic forcing. In each positive (negative) half-cycle of the periodic signal, a portion of the map defined over R (L) overlaps into the domain of the other portion defined over L (R). This is analogous to the successive raising and lowering of the wells in synchronization with the signal frequency, allowing the system to escape from one well to the other. The resultant intermittent switching of the trajectory between L and R is shown in Fig. 3.3. If the dynamics of the system due to the internal noise (chaos) has some inherent time-scale (say n_k), as $\frac{1}{\omega} \to n_k$ the two time-scales may lock onto each other. This resonance should be observable through an increase in the response characteristics of the map.

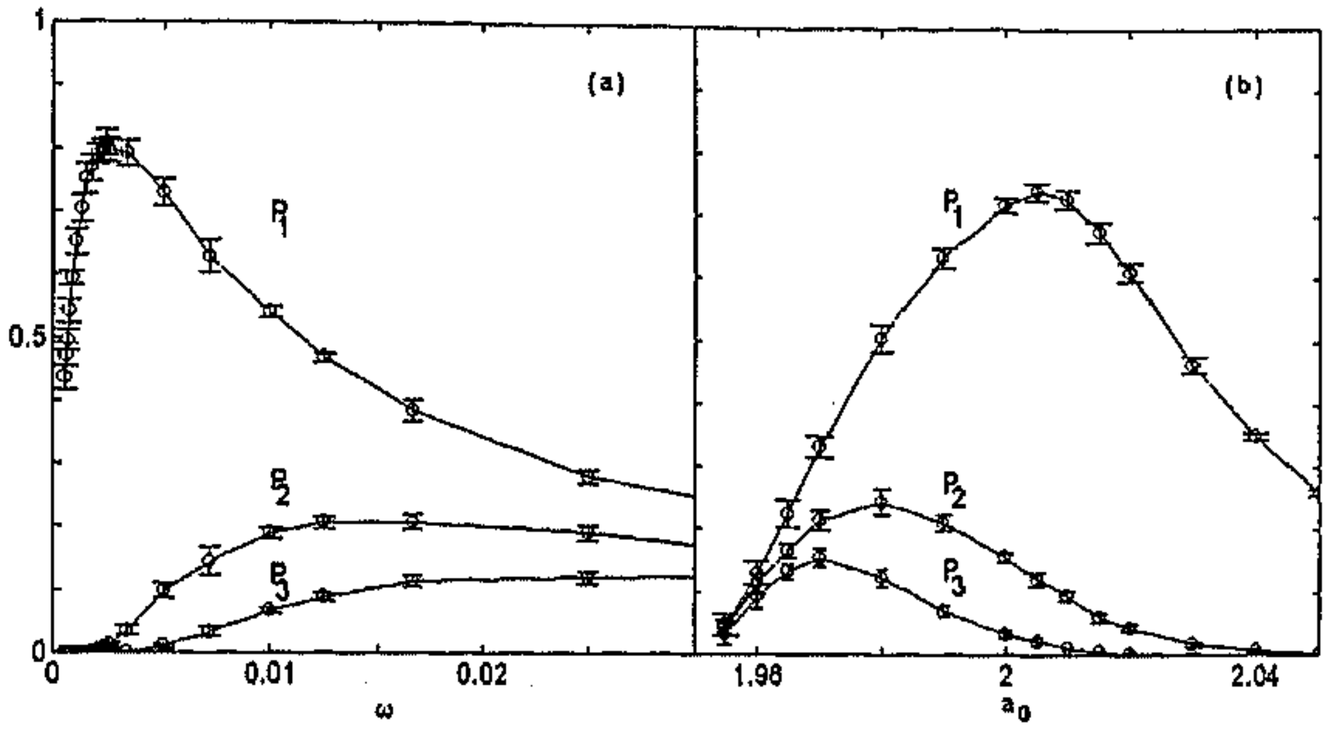

Figure 3.4: (a) P_n ($n = 1, 2, 3$) versus ω for $a_0 = 2.01$ and $\delta = 0.05$, (b) P_n ($n = 1, 2, 3$) versus a_0 for $\omega = 1/400$ and $\delta = 0.05$. The circles represent the average value of P_n for 18 different initial values of x, the bars representing the standard deviation. The data points are joined by solid lines for the reader's convenience.

3.3.1 Simulation results

The response of the system is measured in terms of the normalized distribution of residence times, $N(n)$ [60]. This distribution shows a series of peaks centered at $n_j = (j - \frac{1}{2})n_0$, i.e.,odd-integral multiples of the forcing period, $n_0 = \frac{1}{\omega}$. The strength of the j-th peak

$$P_j = \int_{n_j - \alpha n_0}^{n_j + \alpha n_0} N(n)dn \quad (0 < \alpha < 0.25), \tag{3.3}$$

is obtained at different values of ω, keeping a_0 fixed for j=1,2 and 3. To maximize sensitivity, α was taken to be 0.25. For $a_0 = 2.01$ and $\delta = 0.05$, the response of the system showed a non-monotonic behavior as ω was varied, with P_1 peaking at $\omega_1 \sim 1/400$, a value dependent upon a_0 – a clear signature of SR-type phenomenon. P_2 and P_3 also showed non-monotonic behavior, peaking roughly at odd-integral multiples of ω_1 (Fig. 3.4 (a)). For $a_0 < 2$, P_1 increases monotonically to 1 with decreasing ω, while, $P_j (j > 1)$ goes down to zero. So, 'true resonance', signified by the non-monotonic profile of P_1, occurs only for $a_0 > 2$.

Similar observations of P_j were done also by varying a_0, while keeping ω fixed. Fig. 3.4 (b) shows the results of simulations for $\omega = 1/400$ and $\delta = 0.05$. Here also a non-monotonicity was observed for P_1,P_2 and P_3. The broadness of the response curve and the magnitude of the peak-strengths are a function of the perturbation magnitude, δ. The variation of P_1 with a_0 for different values of δ were also studied (Fig. 3.5). As δ decreases, the response curve becomes more sharply peaked while the peak-strength decreases.

Note that, the parametric perturbation cannot be done without modulating the noise-

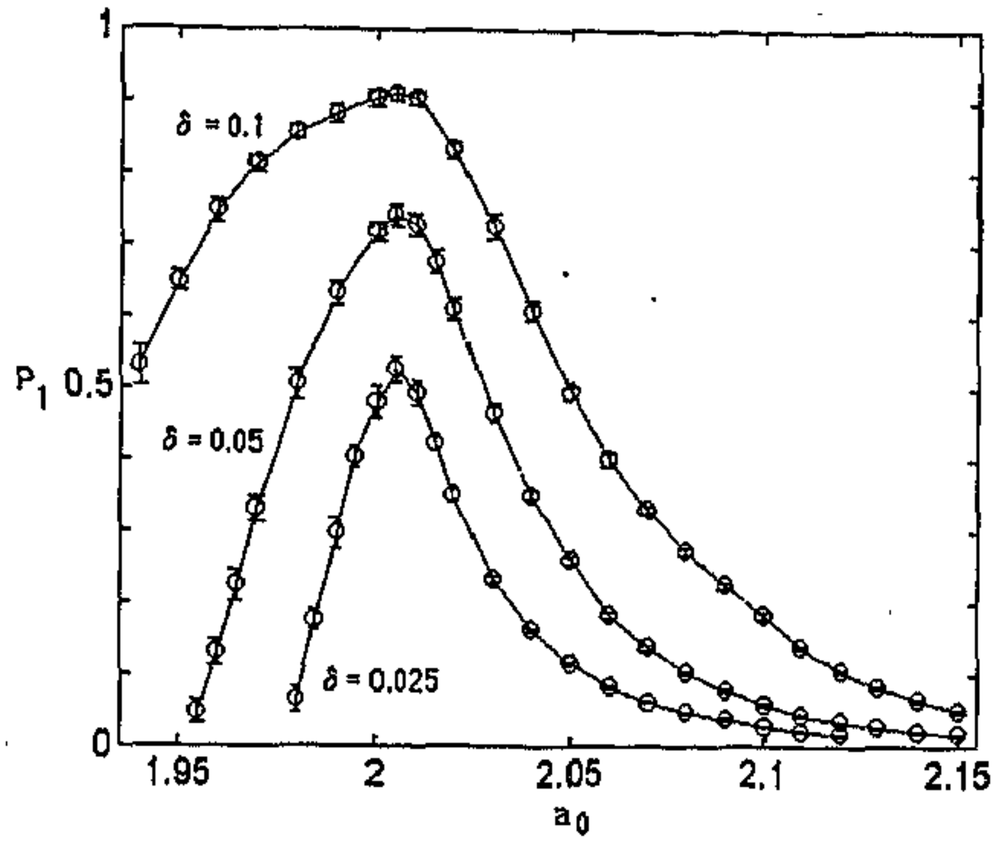

Figure 3.5: P_1 versus a_0 for $\omega = 1/200$ at $\delta = 0.01$, 0.05 and 0.025. The circles represent the average value of P_n for 18 different initial values of x, the bars representing the standard deviation.

intensity. This seems to be the principal difference between this type of 'chaotic resonance' and classical SR. As the local slope of the map, a, is varied periodically, the internal noise, whose intensity is a function of the Lyapunov exponent (and hence of a) also varies periodically. In contrast, for classical SR, the wells are raised or lowered periodically without affecting the external noise, which is independent of the geometry of the wells.

3.3.2 Theoretical analysis

Analytical calculations were done to obtain the invariant probability density and the dominant time-scale governing the residence-time distribution. This was done by proper partitioning of the domain of definition of the system and obtaining the eigenvalues of the corresponding transition matrix. From Fig. 3.2, it is clear that the system spends a longer time in the interval $[-\epsilon/2, \epsilon/2]$, where $\epsilon = a_0 - 2$. So a natural partitioning of the interval [-1,1] is into the four sub-intervals: $C_1 : [-1, -\epsilon/2]$, $C_2 : [-\epsilon/2, 0]$, $C_3 : [0, \epsilon/2]$ and $C_4 : [\epsilon/2, 1]$. This is an exactly Markov partition at integral values of ϵ, i.e., the partition boundaries, $\{p_i\}$ transform into each other on application of the map dynamics, ($f(p_j) \in \{p_i\}$) [18]. It is assumed that for $\epsilon \to 0$ the partitioning approximately retains its Markovian character, so that the process can be mapped onto a Markov process. Close to $\epsilon = 0$, the transition matrix

corresponding to the above partitioning is:

$$W = \begin{vmatrix} \frac{1-\epsilon/2-\epsilon^2/4}{1-\epsilon^2/4} & \frac{\epsilon}{4(1-\epsilon^2/4)} & \frac{\epsilon}{4(1-\epsilon^2/4)} & 0 \\ \frac{\epsilon}{2+\epsilon} & \frac{1}{2+\epsilon} & \frac{1}{2+\epsilon} & 0 \\ 0 & \frac{1}{2+\epsilon} & \frac{1}{2+\epsilon} & \frac{\epsilon}{2+\epsilon} \\ 0 & \frac{\epsilon}{4(1-\epsilon^2/4)} & \frac{\epsilon}{4(1-\epsilon^2/4)} & \frac{1-\epsilon/2-\epsilon^2/4}{1-\epsilon^2/4} \end{vmatrix} \tag{3.4}$$

where, $W_{ij} = P(C_i, C_j)$ is the probability of transition from C_i to C_j. The eigenvalues of the above matrix are $\lambda_1 = 1$, $\lambda_2 = \frac{1-\epsilon/2-\epsilon^2/4}{1-\epsilon^2/4}$, $\lambda_3 = \frac{1-\epsilon}{1-\epsilon^2/4}$ and $\lambda_4 = 0$. The largest eigenvalue, 1, corresponds to the invariant probability density over the four intervals. The next largest eigenvalue dominates any time-dependent phenomena. The relevant time-scale (i.e., the mean residence time) is given by [128]

$$n_k = \frac{-1}{\log(\frac{1-\epsilon/2-\epsilon^2/4}{1-\epsilon^2/4})} \simeq \frac{-1}{\log(1-\epsilon/2)}. \tag{3.5}$$

So, for $a_0 = 2.01$, $n_k \simeq 200$. This predicts that a peak in the response should be observed at a frequency $\frac{1}{2n_k} \simeq 1/400$, which agrees with the simulation results. For small ϵ, $\lambda_2 \simeq \exp(-\epsilon/2)$. Therefore, as $a_0 \to 2$ from above, the residence time diverges as

$$n_k \sim (a_0 - a_0^*)^{-1}, \quad a_0^* = 2. \tag{3.6}$$

The mean time spent by the trajectory in any one of the sub-intervals (L or R) can be calculated exactly for piecewise linear maps [50]. For $\epsilon > 0$, the intervals $\beta_1 = (0, \frac{\epsilon}{2(2+\epsilon)}]$ and $\beta_2 = [1-\frac{\epsilon}{2(2+\epsilon}, 1]$ of R maps to L, so that the trajectory escapes from one sub-interval to the other. Note the symmetrical placement of the two R $\to$ L 'escape regions' about $x = 0.5$, because of the symmetry $F(1/2-x) = F(1/2+x)$ of the DAT map. So the total fraction of R escaping to L after one iteration is $l_1 = \frac{2\epsilon}{2(2+\epsilon)}$. Let us now consider the first pre-image of β_1 and β_2, which escapes from R to L after two iterations. The total fraction of R belonging to this set is $l_2 = \frac{4\epsilon}{2(2+\epsilon)^2}$. Proceeding in this manner, we find from the geometry of the map that the total fraction of R which maps to L after n iterations is

$$l_n = \frac{2^n\epsilon}{2(2+\epsilon)^n}. \tag{3.7}$$

These are just the probabilities that the trajectory spends a period of n iterations in R before escaping to L ($\sum_{j=1}^{\infty} l_j = 1$). So the average lifetime of a trajectory in R is

$$< n >= \sum_{j=1}^{\infty}(j-1)l_j = \frac{2}{\epsilon}. \tag{3.8}$$

For $a_0 = 2.01$, $< n > = 200$, in good agreement with the result obtained using the approximate Markov partitioning (which ensures the validity of the latter approximation). The above equation also establishes exactly the linear scaling relation of

the mean lifetime about $\epsilon = 0$, with $< n >$ diverging at $a_0 = 2$. By symmetry of the map, identical results will be obtained if we consider the trajectory switching from L to R.

Another interesting quantity which also shows a scaling behavior around $\epsilon = 0$, is the drift rate, v, from one sub-interval to the other [71]. This measures the rate at which the chaotic trajectory switches between L and R. Owing to the symmetry $\mathrm{F}(-x) = -\mathrm{F}(x)$ of the DAT map, the net drift rate is zero, i.e., switching to either sub-interval occurs equally often. Let us consider switching from R to L (identical results will hold for switching in the opposite direction due to symmetry). The drift rate is measured by the fraction of R mapping to L per iteration. Hence,

$$v = \frac{\epsilon}{2+\epsilon}. \tag{3.9}$$

It is again a linear scaling relation as $a_0 \to 2$ from above. Note that, for $a_0 < 2$, $v = 0$ as the two sub-intervals are isolated from each other. Thus, v is analogous to an 'order parameter', having a finite (positive) value above $a_0 = 2$ and zero below it. This suggests that the merging of the chaotic attractors at $a_0 = 2$ is akin to a critical phenomena, with the local slope a_0 as the tuning parameter.

3.4 Additive perturbation

Similar study was also conducted with additive perturbation for the above map. In this case the dynamical system is defined as follows:

$$x_{n+1} = \mathrm{F}(x_n) \; + \; \delta \sin(2\pi\omega n). \tag{3.10}$$

For $a = 1.9$ (say), the map has two disconnected sub-intervals, L:[-1,0) and R:(0,1]. However, an additive perturbation of magnitude $\delta > 0.1$ causes a portion of L to diffuse into R in the positive half-cycle of the sinusoidal signal (of frequency ω). Similarly, in the negative half-cycle, a portion of the R interval diffuses into L. The long-term behavior of the map is described by a "smeared-out" DAT map with a width δ, rather than the "crisp" piecewise linear DAT map with $a_0 = 1.9$. This happens as the map performs a periodic vertical motion, causing a smearing-out over time. The simulation results showed non-monotonic behavior for the response, as either ω or a_0 was varied, keeping the other constant, but this was less marked than in the case of multiplicative perturbation (Fig. 3.6). This work can be seen in context with studies conducted on the dynamics of the logistic map under parametric perturbation [153].

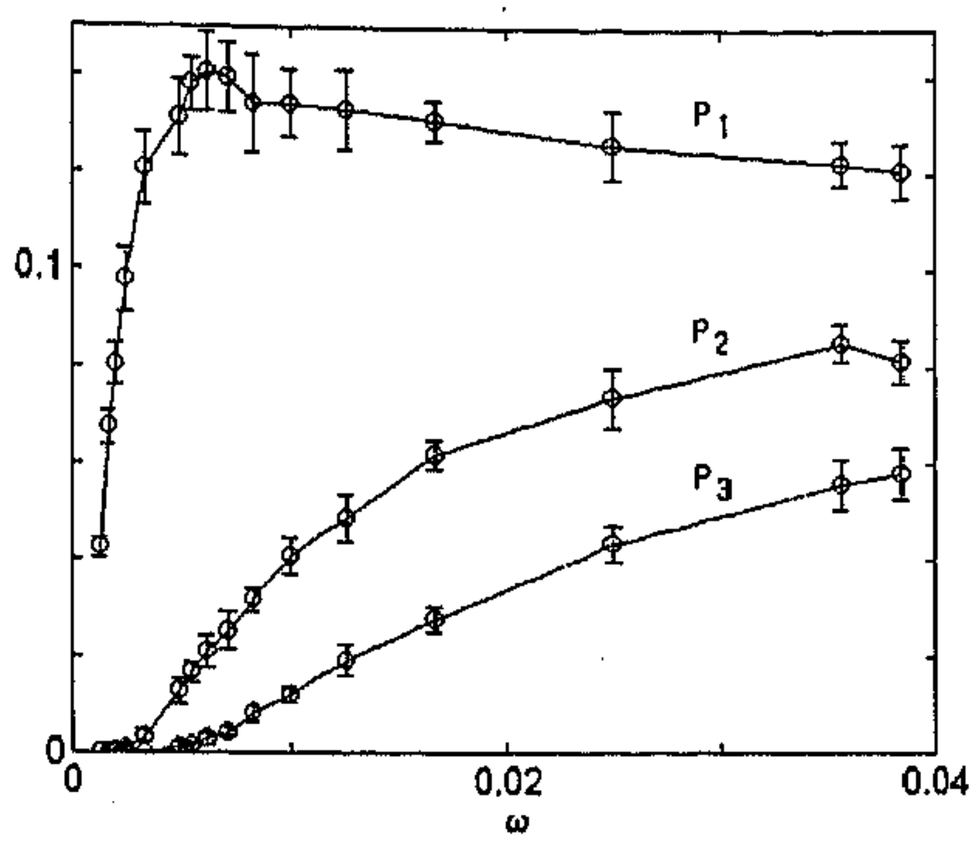

Figure 3.6: P_n ($n = 1, 2, 3$) versus ω for $a_0 = 2.01$ and $\delta = 0.05$, in the case of additive perturbation. The circles represent the average value of P_n for 18 different initial values of x, the bars representing the standard deviation.

3.5 Nonlinear resonance in a chaotic neural network model

The resonance phenomenon is also observed in an excitatory-inhibitory neural pair, with anti-symmetric, piecewise linear activation function. This type of activation function has been chosen for ease of theoretical analysis. However, sigmoidal activation functions also show similar resonance behavior. When a small amplitude periodic signal is given as external input, it is enhanced if the signal frequency is close to the "characteristic frequency" of the chaotic activity. This is due to resonance between the periodic signal and the chaotic switching. The frequency-sensitive enhanced response to stimuli allows the detection of signals which would otherwise have been undetected. As shown below by theoretical and simulation studies, proper choice of system parameters leads to resonant enhancement of signals of a desired frequency bandwidth.

If x_n and y_n ($x, y \in [-1, 1]$) be the state of the excitatory and inhibitory elements at the n-th iteration, respectively, then the discrete time-evolution equation of the system is given by

$$x_{n+1} = F_a(w_{xx}x_n - w_{yx}y_n + I_n),$$

$$y_{n+1} = F_b(w_{xy}x_n - w_{yy}y_n + I_n),$$

where w_{ij} is the connection weight from neuron j to neuron i, and I is an external input. The activation function is of anti-symmetric, piecewise linear nature, viz., $F_a(z) = -1, \text{if } z < -1/a$, $F_a(z) = az, \text{if } -1/a \leq z \leq 1/a$, and $F_a(z) = 1, \text{if } z > 1/a$.

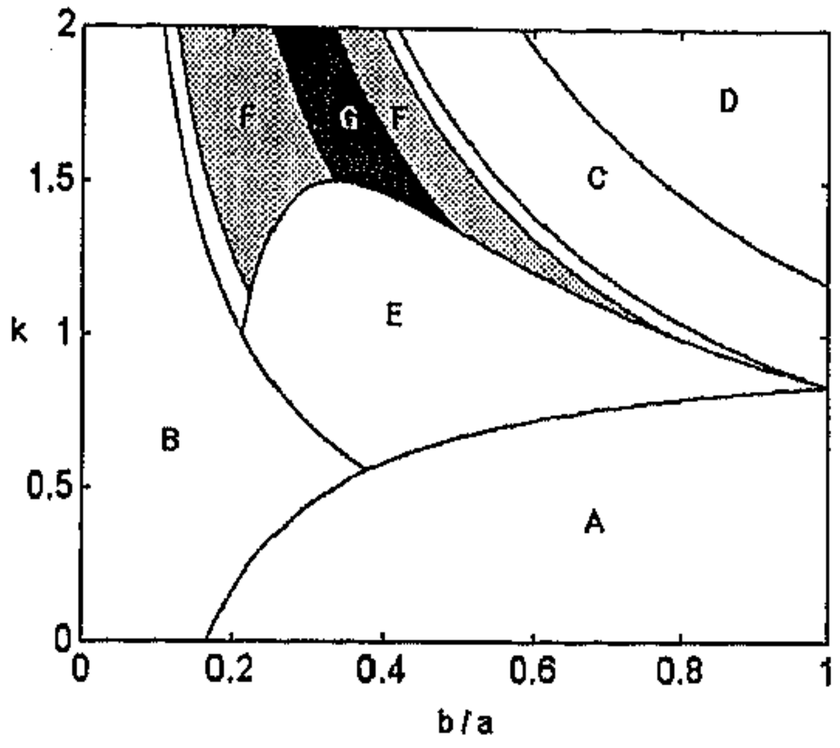

Figure 3.7: The (b/a) vs. k parameter space at a = 6.0, for neural pair dynamics governed by an anti-symmetric, piecewise linear activation function. Region A: $z^* = 1 - k$ stable, B: $z^* = 1/(1 + kb)$ stable, C: $z^* = 0$ stable, D: 2-period cycle between $[(1 - k), -(1 - k)]$, E: superstable periodic cycles, F: two-band symmetry-broken chaos, G: symmetric chaos. The two thin bands, between B and F, and again, between F and C, indicate regions of single-band symmetry-broken chaos.

Under the restriction $w_{yx}/w_{xx} = w_{yy}/w_{xy} = k$, the 2-dimensional dynamics reduces to a simple 1-dimensional form. The relevant variable is now the effective neural potential $z = x - ky$ $(z \in [-1, 1])$, whose dynamics is governed by

$$z_{n+1} = F_a(z_n) - kF_b(z_n),$$

where a, b are the suitably scaled transfer function parameters. The design of the network ensures that the phase space [-1,1] is divided into two well-defined and segregated sub-intervals L:[-1,0] and R:[0,1]. Analysis shows that for $a < 4$, there is no dynamical connection between the two sub-intervals. For $a > 4$, in a certain range of (b, k) values the system shows both symmetry-broken and symmetric chaos. In the former case, the trajectory, while chaotically wandering over one of the sub intervals, cannot enter the other sub interval. In the latter case, this restriction is removed and the trajectory visits both sub-intervals in turn. The parameter space diagram in Fig. 3.7 shows the various dynamical regimes occurring for different values of k and b/a, at $a = 6$. The curve in $(b/a, k)$-parameter space forming a boundary between the symmetric and symmetry-broken chaotic domains is given by the equation:

$$k = a(1 \pm \sqrt{1 - (4/a)})/2b. \tag{3.11}$$

For the simulations reported here, $a = 6$ and $b = 3.42$, for which the system shows symmetric chaos over a range of values of k.

The chaotic switching between the two sub-intervals occurs at random. However the average time spent in any of the sub-intervals before a switching event can be exactly

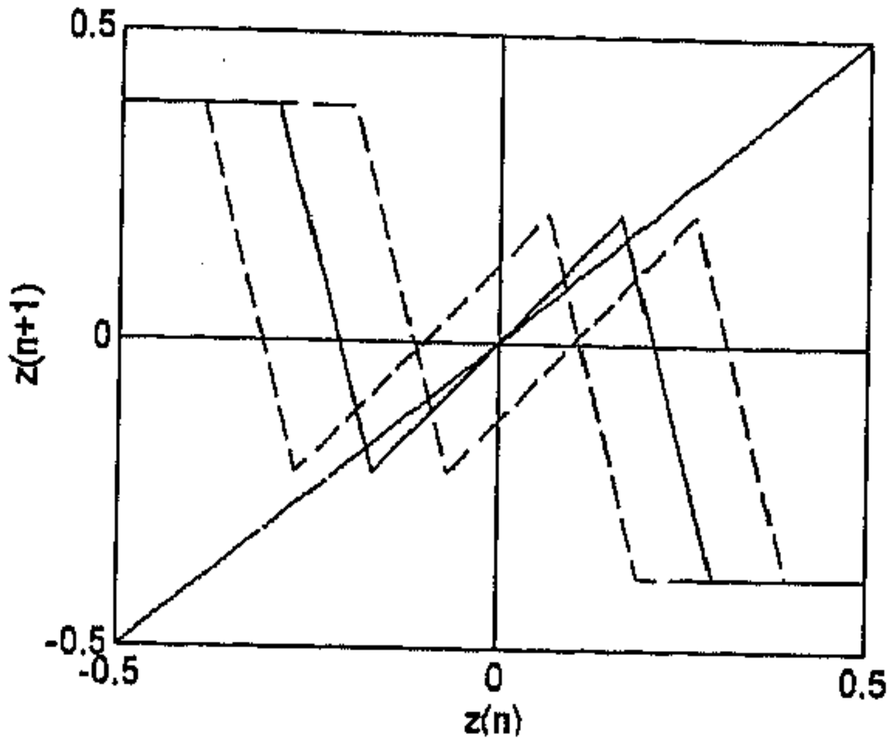

Figure 3.8: The map representing the dynamics of a neural pair for $a = 6.0, b = 3.42$ and $k = 1.3811$. The figure in solid lines represent the unperturbed map, while the figures in broken lines indicate the maximum displacement due to a periodic signal of peak amplitude, $\delta = 0.1$.

calculated for the present model:

$$n_k = 1/(bk(1 - (bk/a)) - 1). \tag{3.12}$$

As a complete cycle would involve the system switching from one sub-interval to the other and then switching back, the "characteristic frequency" of the chaotic process is $\omega_c = 1/2n_k$. E.g., for the system to have a "characteristic frequency" of $\omega = 1/400$ (say), the above relation provides the value of $k \simeq 1.3811$ for $a = 6, b = 3.42$. The system being symmetric, there is no net drift between L and R. However, in the presence of an external signal of amplitude ϵ, the symmetry is broken. The net drift rate, which measures the net fraction of phase space of one sub-interval mapped to the other after one iteration, is given by $v = \epsilon$, if $\epsilon < \epsilon_c$, and $v = 1 - (kb/a) - (1/bk)$, otherwise. The critical signal strength,

$$\epsilon_c = 1 - (k^2b^2 + a)/akb, \tag{3.13}$$

is a limit above which the net drift rate no longer varies in phase with the external signal. For the aforementioned system parameters (a, b, k), $\epsilon_c \simeq 0.001$. If the input to the system is a sinusoidal signal of amplitude $< \epsilon_c$ and frequency $\sim \omega_c$, we can expect the signal to be enhanced, as is borne out in the simulations described below. The effect of a periodic input (having peak amplitude δ, say) is to translate the map describing the dynamics of the neural pair, to the left and right, periodically. Fig. 3.8 shows the unperturbed map (solid lines) along with the maximum displacement to the left and right (broken lines) for $\delta = 0.1$.

As before, we verify the presence of resonance by looking at the peaks of the residence time distribution, where the strength of the jth peak is given by Eqn. (3.3). For maximum sensitivity, α is set as 0.25. As seen in Fig. 3.9, the dependence of $P_j (j = 1, 2, 3)$

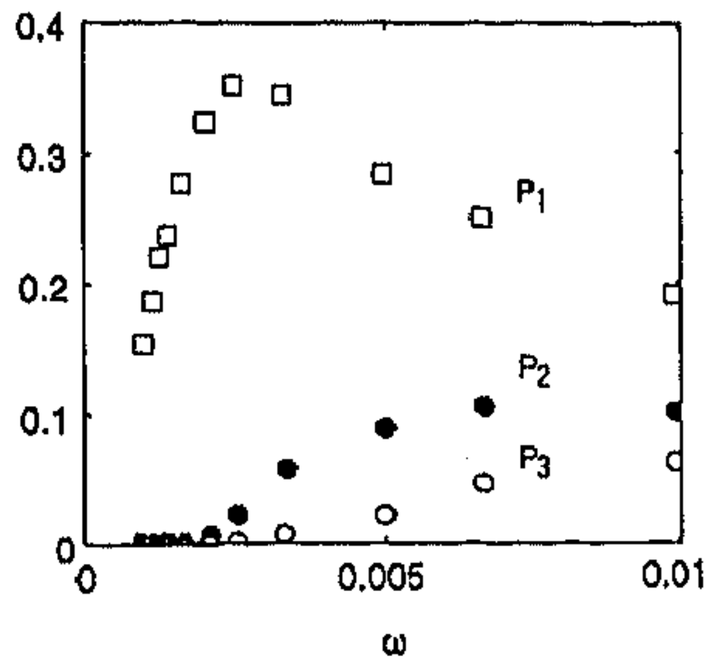

Figure 3.9: The peak strengths of the normalized residence time distribution, $P_n(n = 1, 2, 3)$, for periodic stimulation of the excitatory-inhibitory neural pair ($a = 6$, $b = 3.42$ and $k = 1.3811$). The peak amplitude of the periodic signal, $\delta = 0.001$. P_1 shows a maximum at a signal frequency $\omega_c \simeq 1/400$

on external signal frequency, ω, exhibits a characteristic non-monotonic profile, indicating the occurrence of resonance at $\omega \simeq 1/2n_k$. For the system parameters used in the simulation, $n_k = 200$. The results clearly establish that the switching between states is dominated by the sub-threshold periodic signal close to the resonant frequency.

The above results indicate that deterministic chaos can play a constructive role in the processing of sub-threshold signals. Experimental study involving crayfish mechanoreceptor cells have provided evidence of SR in the presence of external noise and periodic stimuli. The evidence of chaotic activity in neural processes of the crayfish [142] suggests that nonlinear resonance (as reported here) due to inherent chaos might also be playing an active role in such systems. The versatility of biological sensory apparatus could be partially emulated in artificial systems by using the proposed resonance mechanism for signal enhancement.

3.6 Discussion

Low-dimensional discrete-time dynamical systems are amenable to several analytical techniques and hence can be well-understood compared to other systems. The examination of resonance phenomena in this scenario was for ease of numerical and theoretical analysis. However, it is reasonable to assume that similar behavior occurs in higher-dimensional chaotic system, described by both maps and differential equations. In fact, SR has been reported for spatially extended systems (spatiotemporal SR) [112], e.g., in coupled map lattices [58]. A possible area of future work is the demonstration of phenomena analogous to spatiotemporal SR with a network of

coupled excitatory-inhibitory neural pairs.

The close resemblance of the merging of attractors with critical phenomena has possible relevance to SR in Ising systems. Although numerical studies have reported SR in kinetic Ising system, it seems to be inconclusive as the primary peak strength of the normalized residence-time distribution shows only a monotonic behavior [163], [164]. This response profile is identical to that observed in DAT Map for $a_0 < 2$. A study of kinetic aspects like hysteresis is planned to be undertaken, which should give information concerning the phase-dependence of the resonance behavior. The relation of nonlinear resonance to the phenomena of deterministic diffusion [66, 104] is another area of further study.

The observation of 'SR' in chaotic systems also has implications for the area of noisy information processing. It has been proposed that the sensory apparatus of several creatures use SR to enhance their sensitivity to weak external stimulus, e.g., the approach of a predator. Some experimental work on crayfish have provided supporting evidence to this assertion [48]. The above study indicates that external noise is not necessary for such amplification as chaos in neural networks can enhance weak signals. As chaotic behavior is extremely common in a recurrent network of excitatory and inhibitory neurons, such a scenario is not entirely unlikely to have occurred in the biological world. This can however be confirmed only by further biological studies and detailed modeling of the phenomena.

Chapter 4

Chaos Control in Simple Excitatory-Inhibitory Neural Network Models

Neurobiological studies have indicated that rapid transitions between chaotic and relatively more ordered states may be the key towards understanding how the brain performs cognitive tasks. This immediately suggests that methods of controlling chaos may be used to study similar phenomena in neural network models. In the work described in this chapter, control of chaotic behavior is investigated in chaotic neural network models. On imposition of control, transition of the network behavior from chaos to periodicity is observed. This has implications for both the explanation of observed neurobiological phenomena (e.g., olfactory hallucinations during epileptic seizures) as well as a more dynamic interpretation of associative recall performed by neural network models.

The next section reviews some existing techniques of chaos control which can drive a system from chaotic to ordered behavior. In Section 2, we analyze the physical mechanism of control in a chaotic neural pair, achieved through, either, a feedback to a system variable, or, through periodic forcing. Section 3 reports the results of applying control to a chaotic neural network comprising three pairs of excitatory and inhibitory neurons, while, in Section 4, the relevance of this type of research to explaining neurobiological phenomena is discussed. Finally, some observations on the possible applications of chaos control in neural computation are briefly mentioned.

4.1 Chaos control

One of the distinguishing features of chaotic attractors is that they have an infinite number of periodic attractors embedded within them. If the system state exists at any time on a region belonging to one of the periodic attractors then it will remain

within it. However, as the attractors are unstable, when perturbed by noise, the system diverges away from the periodic orbit at an exponential rate. In a chaotic attractor, the system state may be, at any given time, infinitesimally close to any one of the infinite periodic attractors but due to the highly unstable nature of the periodic orbits, the periodicity is never manifested over a measurable period of time.

Ott, Grebogi and Yorke have used this feature of chaotic attractors to construct a general method of controlling chaos, i.e. to convert the chaotic behavior of a system to a time-periodic one [135, 161]. Their method (referred to as OGY method henceforth) achieves this control by making small, carefully chosen time-dependent perturbations of one of the parameters of the system. To obtain a periodic orbit, a local map around the desired attractor is constructed by the method of delay-coordinate embedding. In this method, the experimentally obtained time-series of a system is used to construct a $(n+1)$-dimensional (say) delay-coordinate vector, whose time-evolution can be plotted to give a 3-dimensional projection of the trajectory. It has been mathematically demonstrated that such a projection is a good approximation of the dynamical attractor of the relevant system in $(n+1)$-dimensional space [138], [27]. The OGY control method relies upon the identification of saddle instabilities, i.e., unstable periodic points located on a surface having both stable and unstable directions. The system approaches the periodic point along a stable direction and diverges away from it along an unstable one. When the chaotic system state is in the neighborhood of the desired attractor, a perturbation is applied to a system parameter such that on the next iteration the system state falls on the stable direction. The state will then move towards the attractor in successive iterations. Using this principle, many physical systems exhibiting chaotic behavior has been subjected to control. However, one drawback of this method is that only low-period orbits can be stabilized, since, because of the exponential error magnification in chaotic systems, high-period stable orbits are extremely difficult to achieve by making only one correction in the long period. The OGY method has been used to control chaos in a biological neural network prepared from a hippocampal slice of a rat brain [155]. Using precisely timed electrical stimulation of the brain slice, the system was perturbed such that a trajectory coincided with a stable direction in the neighborhood of a periodic attractor. Thereafter the point moved towards the attractor with successive iterations and the resulting trajectories became periodic. In a similar way, anticontrol was achieved by perturbing a stable orbit, so that the next iterate falls close to the unstable direction, with a corresponding transition from periodic to chaotic behavior.

An alternative method of controlling chaos, called "occasional proportional feedback" (OPF), has been proposed by Hunt [93]. This allows stabilization of longer orbits than that possible through the OGY method. As higher period orbits visit most regions of the attractor, which correspond to different physical states of the system, it is desirable to have high-period orbits if one wishes to sample as many of the states as possible. In the OPF method, feedback is used to modulate the system parameter. The deviations of a chaotic variable within a specified window, centered

about a specified value of a chosen system variable, are fed back to the system. By varying the control parameters, different periodic orbits are stabilized. A theoretical framework for this control mechanism has been sought to be developed by Carr and Schwartz [30].

Both the methods mentioned above apply the control signal to the system parameter. Feedback to the system variable, has also been applied to control chaotic systems with success. One such method [120] is based on the application of a periodic proportional feedback to the system variable, such that, every p time steps (say), the system is modified by means of a proportional feedback. As a result, an unstable periodic orbit, of period equal to a multiple of p is found to be stabilized. This method has been used to control the chaotic behavior of small, discrete neural networks [179], where the control is applied to one of the neurons, the others being free of direct control.

4.2 Controlling chaos in a neural pair

In this section we demonstrate two different ways of controlling the discrete-time chaotic dynamics of an excitatory-inhibitory neural pair. The first method is based on the application of proportional feedback to the system variable (instead of the system parameter, as in the OPF method) described above. The second method involves subjecting the neural pair to an external periodic stimulus.

4.2.1 System variable feedback method

To observe the effect of applying occasional proportional feedback to the system variable, let us consider the case of a neural pair whose dynamics is governed by piecewise linear activation functions. As already mentioned in Chapter 2, the behavior of a neural pair, with function parameters, $a = 4$ and $b = 2$, is identical to that of the "tent" map:

$$\begin{aligned} z_{n+1} &= 2z_n, \quad \text{for } 0 < z_n < 0.5, \\ &= 2(1 - z_n), \quad \text{for } 0.5 < z_n < 1, \end{aligned} \tag{4.1}$$

with the difference being that the phase space of the neural system is confined to the interval $[0, 0.5]$, while the tent map is defined in the unit interval $[0, 1]$. However, this distinction can be removed by suitable rescaling. We shall therefore focus on the tent map as the system to which the proposed control mechanism is applied.

The tent map, as defined above, is chaotic over the entire unit interval. The Lyapunov exponent of the system is $\lambda = \log_e 2 \simeq 0.693$, and the expansion of small perturbations among nearby trajectories is uniform throughout the interval. The results obtained for this specific case, are easily generalizable to maps with a globally uniform stretching rate, and, with slight modifications, to piecewise uniform stretching rates.

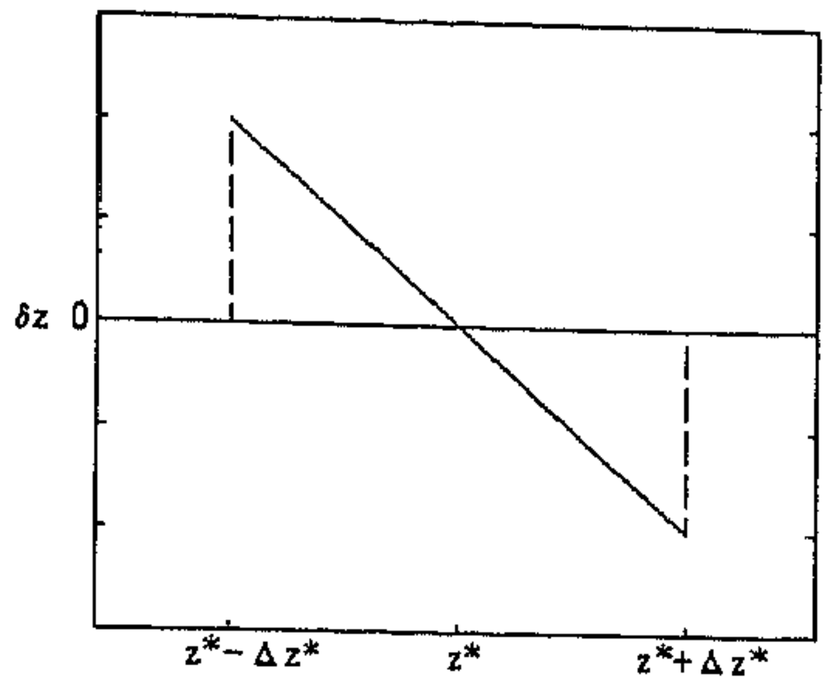

Figure 4.1: The input-output relation of the control signal, δz, with the control parameters, z^* and Δz^*. The feedback magnitude, α, gives the slope of the function.

If $z_{n+1} = I\!F(z_n)$ represent the system to be controlled (in the present case, $I\!F$ is given by Eqn. (4.1)), then the on applying control, we have the modified system:

$$z_{n+1} = I\!F(z_n) + \delta z_n, \tag{4.2}$$

where, δz_n, represents the control signal. For the proposed control method, the control signal is obtained by

$$\delta z_n = \alpha \mathcal{F}_{\Delta z^*}(z^* - I\!F(z_n)). \tag{4.3}$$

Here, z^* is the system state which is desired to be stabilized, α is a parameter governing the magnitude of feedback and $\mathcal{F}$ is a function, defined as,

$$\begin{aligned} \mathcal{F}_\mu(\xi) &= \xi, \text{ if } |\xi| < \mu, \\ &= 0, \text{ otherwise.} \end{aligned}$$

As is evident from the form of $\mathcal{F}$, the control signal is generated only on occasions when the system variable $z \in I\!F^{-1}(z^* \pm \Delta z^*)$ (see Fig. 4.1).

Let us now see the effect of the above control mechanism on the tent map. If $z_n = I\!F^{-1}(z^* + \Delta z)$, where $\Delta z < \Delta z^*$, then, on the next iteration, the system goes to

$$z_{n+1} = z^* + \Delta z + \alpha(z^* - z^* - \Delta z).$$

Now for the tent map, $I\!F^{-1}(z) = \frac{z}{2}$, so that,

$$\Delta z = 2z_n - z^*.$$

Therefore, one can write the resultant system dynamics, in the presence of control, as

$$z_{n+1} = 2z_n - 2\alpha z_n + \alpha z^*. \tag{4.4}$$

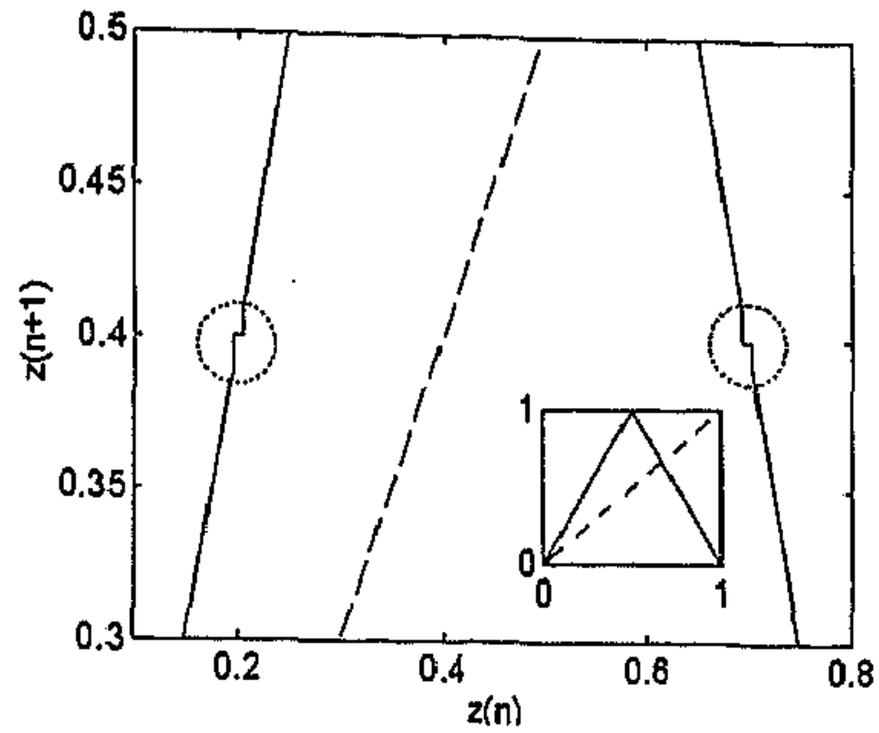

Figure 4.2: The effect of feedback control ($z^* = 0.4$, $\Delta z^* = 0.02$ and $\alpha = 1$) to the system variable of the tent map (inset), $\mathbb{F}$, is shown in a magnified view. The regions $\mathbb{F}^{-1}(z^*) \pm \Delta z^*$ have a slope of zero, the rest of the map remaining unchanged.

The above expression implies that, the slope of the map, in the region $\mathbb{F}^{-1}(z^* \pm \Delta z^*)$, has been modified to

$$\frac{dz_{n+1}}{dz_n} = 2(1-\alpha),$$

on the application of control. This is shown, for $z^* = 0.4, \Delta z^* = 0.02$ and $\alpha = 1$, in Fig. 4.2. Note that, the slope of the map is the system parameter governing the nature of the dynamics. This implies that the effect of feedback to the system variable is the same as local parametric perturbation around the desired region of the phase space to be controlled.

We shall now investigate the conditions under which a period-p cycle is stabilized by the control method. Let, the p-th iterate, $\mathbb{F}^p$, be the lowest order iterate of the map, to have a fixed point in the region $\mathbb{F}^{-1}(z^* \pm \Delta z)$. The stability of the fixed point is decided by the magnitude of its slope, m. In the case of the tent map,

$$m = 2^p(1-\alpha). \tag{4.5}$$

The p-th order cycle is stable only if $|m| < 1$, so that, by Eqn. (4.5), the critical value of α at which the cycle just becomes stable is:

$$\alpha_c = 1 - \frac{1}{2^p}. \tag{4.6}$$

For example, a fixed point can be stabilized for $\alpha > 0.5$, while a stable 2-cycle is obtained only for $\alpha > 0.75$, and similarly for higher order periodic cycles.

The time required for the system to converge to the stable state, on application of the control mechanism, is dependent upon Δz^*. The average time required for

convergence can be obtained analytically in the case of the tent map. The extent of the region in which control is activated is $2\Delta z^*$. As the map is defined in the unit interval, the probability that a trajectory is in this region is also $2\Delta z^*$. If the system is in another region, the probability that it enters the control region is $2\Delta z^*(1-2\Delta z^*)$. Proceeding in this manner, the probability for the trajectory to enter the control region after n iterations, is given by

$$P(n) = 2\Delta z^*(1 - 2\Delta z^*)^n. \tag{4.7}$$

Therefore, the average time required for convergence is

$$< n >= \Sigma_{n=0}^{\infty} nP(n) = 2\Delta z^* \Sigma_{n=0}^{\infty} n(1 - 2\Delta z^*)^n. \tag{4.8}$$

This is evaluated as

$$< n >= \frac{(1 - 2\Delta z^*)}{2\Delta z^*}, \tag{4.9}$$

which, comes out to be $\simeq 49$, for $\Delta z^* = 0.01$. An example of a controlled transition from chaos to a period-2 cycle is shown in Fig. 4.3, for the control parameters: z^*=0.4, $\Delta z^* = 0.01$ and $\alpha = 1$. The control mechanism is turned on at $n = 50$ (indicated by an arrow "a") and the periodic cycle is stabilized quite rapidly (indicated by an arrow "b"). The bottom panel of Fig 4.3 shows the magnitude of the control signal, δz.

Since the control perturbation, δz, is a function of the neuron state, z_n, and a desired system state, z^*, the control method can be implemented as a network of excitatory-inhibitory neural pairs with suitable connection weights and activation function parameters (Fig. 4.4). The combination of a chaotic neural pair with a controlling neural system provides a neuromodule for stabilizing various periodic orbits, as suggested in [186]. Note that, an entire periodic sequence can be stabilized if only one of its members is known. Therefore, for a system with uniform stretching rate (e.g., the tent map), there is no necessity for obtaining a time-series to generate a control signal - a single stationary input is sufficient. The method has the further advantage of being extremely simple to implement, as compared to, say, the OGY method, which involves intensive calculations.

4.2.2 External periodic stimulation

Periodic cycles can also be stabilized by applying a periodic external input. This had been observed in the case of chaotic nonlinear oscillators evolving in continuous time [25]. Similar phenomena has been observed in our neural model.

For an excitatory-inhibitory neural pair, with activation functions of sigmoid nature, the effect of applying a periodic signal has been observed. As already mentioned in Chapter 3, for low-frequency signals, nonlinear resonance occurs. However, if the signal is of higher frequency, periodic orbits of various orders are stabilized. The reason for this phenomena is as follows.

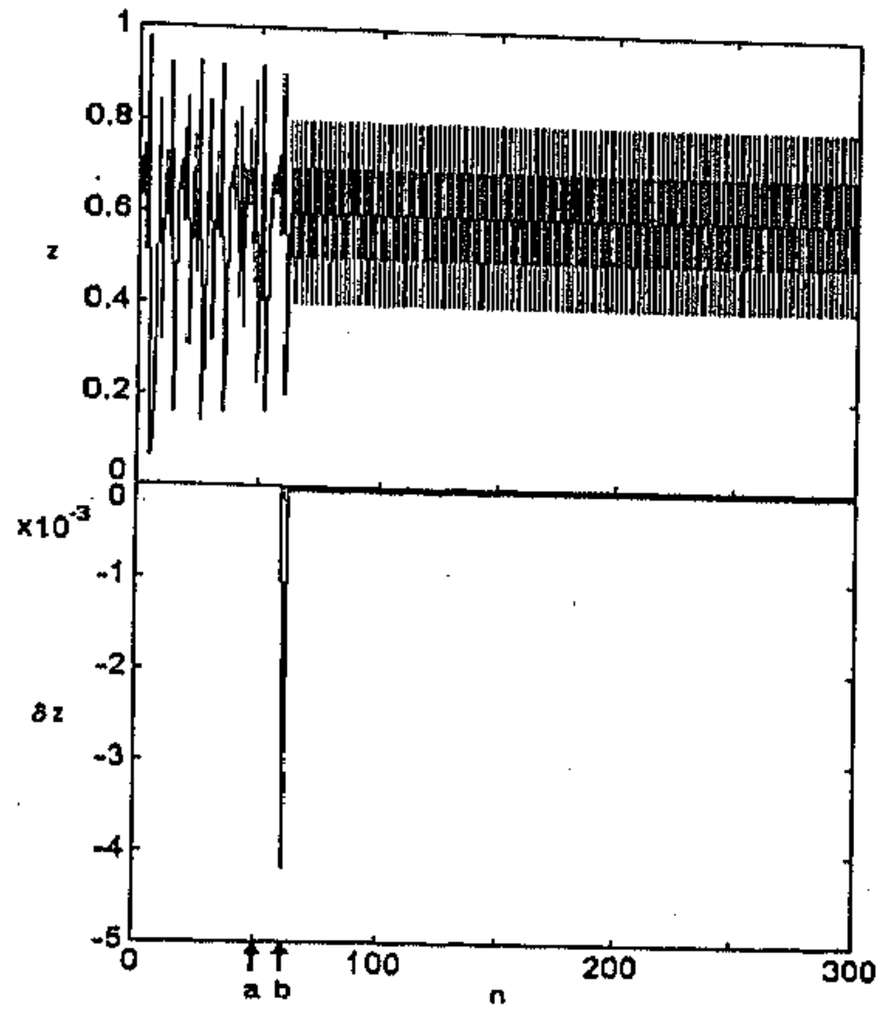

Figure 4.3: (Time series of the tent map subjected to control (top) and the magnitude of the control signal (bottom). The arrows a and b indicate the switching on of the control mechanism and the onset of controlled periodic cycles, respectively.

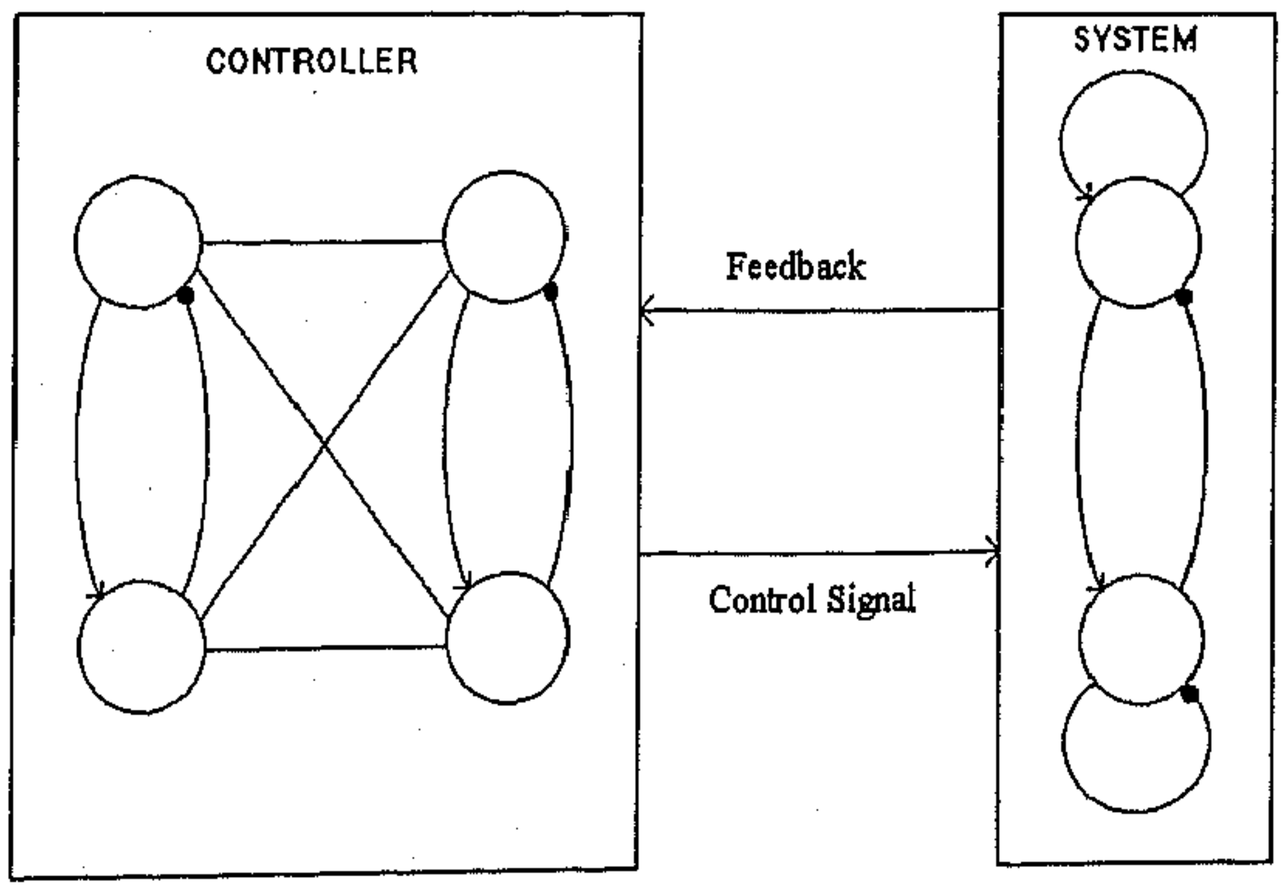

Figure 4.4: A biologically plausible mechanism for implementing the feedback control mechanism demonstrated for the tent map.

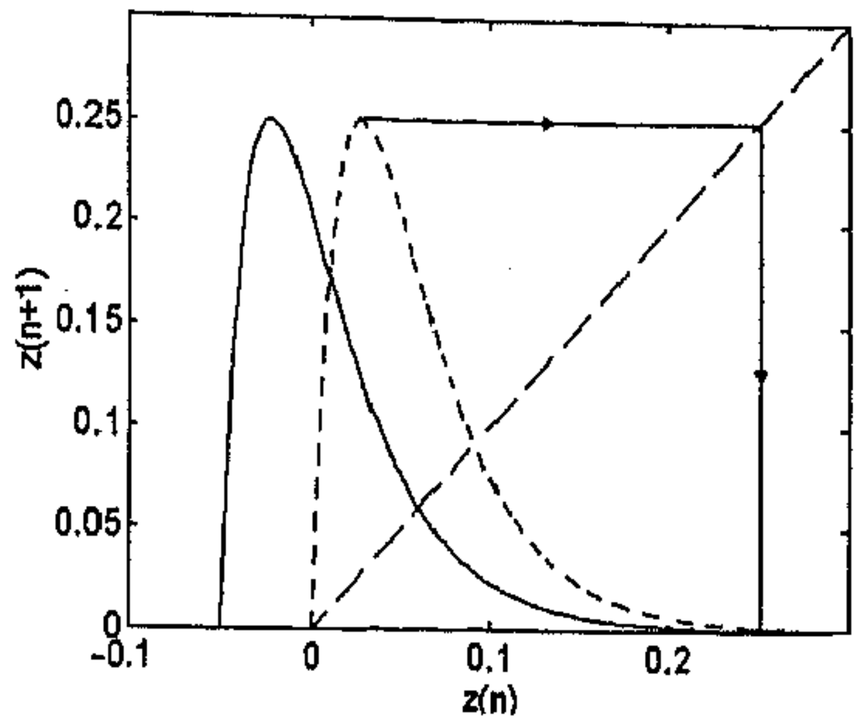

Figure 4.5: The map representing the dynamics of the excitatory-inhibitory neural pair ($a = 50, b = 25$) governed by sigmoid activation function subjected to control by a periodic external input of peak amplitude $\delta = 0.05$. The broken curve indicates the unperturbed map (F_1), while the solid curve indicates the shifted map (F_2) due to the periodic input.

Let the unperturbed map be chaotic in nature. On applying a periodic signal, the map is translated periodically, so that the slope at different points of the map is a function of time. Consider the case of a period-2 signal, which switches alternately between 0 and δ (Fig. 4.5). The trajectory from the critical point of the unperturbed map, F_1 (indicated by broken lines), iterates to the tail portion of the shifted map, F_2 (indicated by solid lines). Note that the slope, at this region, of the perturbed map, is much less than that of the original map. The stability of a period-2 cycle (z_1, z_2), is decided by the slope of the fixed point of the composite map, $F_1 * F_2$, given by:

$$m = \frac{dF_1}{dz}|_{z=z_1} \times \frac{dF_2}{dz}|_{z=z_2}.$$

Now, $|\frac{dF_2}{dz}|_{z=z_2} \ll 1 \Rightarrow |m| < 1$ (for sufficiently large δ), indicating the stabilization of the period-2 cycle.

4.3 Chaotic neural network model

We shall now consider a network comprising a larger number of elements for the purpose of controlling unstable periodic cycles. The present work has been done on an excitatory-inhibitory neural network model, which is a discrete-time version of a model proposed by Hayashi [80]. The system consists of N excitatory and N inhibitory elements, denoted by x_i and y_i, respectively (Fig. 4.6). The cells update

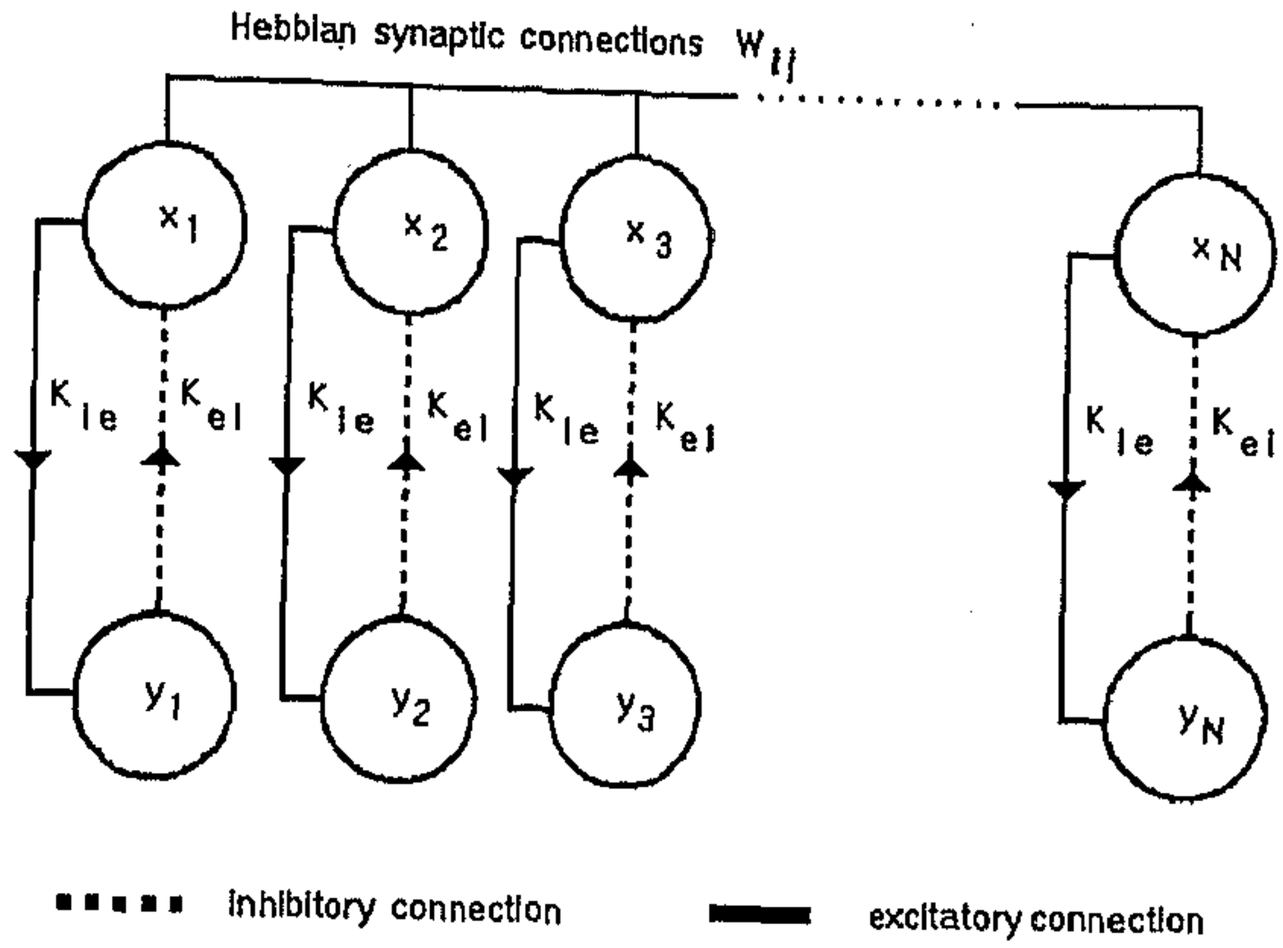

Figure 4.6: The oscillatory neural network model. Excitatory and inhibitory cells are labeled as x and y, respectively. W_{ij} represents the connection weights between the excitatory cells. K_{ei} is the strength of inhibitory connection from y to x and K_{ie} is the strength of excitatory connection from x to y.

their states in the $(n+1)$th iteration, according to the following transformations:

$$x_i(n+1) \;=\; G(\sum_{j=1}^{N} W_{ij}\, x_j(n) \;-\; K_{EI}\, y_i(n) \;+\; I_i(\omega)) \tag{4.10}$$

and,

$$y_i(n+1) \;=\; G(K_{IE}\, x_i(n) \;+\; I_i(\omega+\delta)) \tag{4.11}$$

where, $I(\omega)$ is an external periodic input or bias, δ is a phase difference between the inputs to x_i and y_i and, the function G is defined as,

$$G(z) \;=\; \frac{2}{\pi}\,\arctan(z/a) \tag{4.12}$$

a being the slope of the function. This parameter is analogous to 'temperature' in a physical system.

Thus, while excitatory cells are all connected to each other, inhibitory cells are connected only to the corresponding excitatory cells - K_{IE} being the weightage of the excitatory connection from x_i to y_i and K_{EI} being the inhibitory connection weightage from y_i to x_i. It is evident that x_i and y_i vary between +1 and -1. The activation values of the excitatory cells at time t, $x_i(t)$, is taken as the output of the network at that instant of time.

The synaptic connection weights W_{ij} between the excitatory cells, x_i, are evaluated by a modification of the standard Hebb rule,

$$W_{ij} = \frac{1}{N} \sum_{\mu} \xi_i^{\mu} \xi_j^{\mu} + \delta_{ij} \tag{4.13}$$

where ξ_i^{μ} is the ith component of the μth pattern vector being stored in the network and δ_{ij} is the Kronecker delta function.

It is easily seen that the pair of first-order difference equations (4-5) is equivalent to the second-order difference equation:

$$x_i(n+1) = G(\sum_{j=1}^{N} W_{ij}\, x_j(n) - K_{EI}\, G(K_{IE}\, x_i(n-1) + I_i(\omega+\delta)) + I_i(\omega)) \tag{4.14}$$

which resembles a Hopfield-like model with delay-dynamics.

4.3.1 Stability analysis

The stability of the fixed points of a single excitatory-inhibitory pair is investigated in this section. Let z^* denote a fixed point of the pair of evolution equations for x_i and y_i. The Jacobian in the neighborhood of the fixed point in the absence of any external input is given by

$$\mathrm{J} = \begin{vmatrix} G'(z)|_{z=z^*} W_{ii} & G'(z)|_{z=z^*} K_{EI} \\ G'(z)|_{z=z^*} K_{IE} & 0 \end{vmatrix} \tag{4.15}$$

where $G'(z)$ is the derivative of $G(z)$ w.r.t. z.

The eigenvalues are given by the solution of the equation

$$\mathrm{Det} \mid \mathrm{J} - \lambda\, \mathrm{I} \mid = 0 \tag{4.16}$$

where I is the identity matrix. This equation can be reduced to

$$\lambda^2 - \mathrm{Tr\ J}\, \lambda + \mathrm{Det\ J} = 0 \tag{4.17}$$

Thus,

$$\lambda_{1,2} = \frac{\mathrm{Tr\ J} \pm \sqrt{(\mathrm{Tr\ J})^2 - 4\ \mathrm{Det\ J}}}{2} \tag{4.18}$$

For $(\mathrm{Tr\ J})^2 - 4\ \mathrm{Det\ J} \geq 0$ the solutions eventually converges to the fixed point, which is thus stable. Evaluating J , $\mathrm{Tr\ J} = G'(z)|_{z=z^*} W_{ii}$ and $\mathrm{Det\ J} = (G'(z)|_{z=z^*})^2 K_{IE} K_{EI}$.

As $G'(z) = \frac{2\,a}{\pi\,(a^2+z^2)}$, the eigenvalues are given by,

$$\lambda_{1,2} = \frac{2\,a}{\pi\,(a^2+z^{*2})}\ (W_{ii} \pm \sqrt{W_{ii}^2 - 4\,K_{EI}\,K_{IE}}) \tag{4.19}$$

According to Eqn. (4.13), $W_{ii} = 2$. Therefore, the condition for stability of the fixed point is $K_{EI}\, K_{IE} \leq 1$. If this condition is not satisfied, all the fixed points of the second-order difference equation become unstable giving rise to periodic orbits.

4.3.2 Simulation results

For the present work, a network with N = 3 was used for carrying out computer simulations. The number of cells was kept low for ease of graphical analysis. The pattern vectors chosen for storage in the network were :

$$\xi^1 = (\ 1\ \ 1\ \ 1),\ \xi^2 = (\ 1\ \ -1\ \ -1),\ \xi^3 = (\ -1\ \ -1\ \ 1)$$

The memory patterns are, therefore, vertices of a cube, $-1 \leq x_i \leq 1$ (i=1,2,3). After evaluating the weight matrix, the network was made to evolve from a randomly chosen initial value. The initial states were taken as $x_i(0) = I_i$ and $y_i(0) = 0$. As pointed out above the condition for oscillations in a single excitatory-inhibitory pair is $K_{EI}\ K_{IE} \geq 1$. The system thus corresponds to three oscillators weakly coupled together through connection strengths $\sim$ O $(\frac{1}{N})$. If these three oscillators have independent periods of oscillations then, according to the results of Li and Yorke [110], the system is capable of chaotic behavior.

The simulation was carried out for the following set of parameters: $K_{EI} = 2.0$, $K_{IE} = 2.0$ and $a = 0.1$. An external sinusoidal input which completed one period every 300 iterations of the network with $\delta = 0$ was used to stimulate the network. The system showed chaotic activity when the input pattern vector was very different from any of the stored pattern vectors. The 3-dimensional plot of the trajectory of the network state in state space is shown in Fig. 4.7, while Fig. 4.8 shows the variation of the average activation of the excitatory cells with iteration number along with the corresponding logarithmic spectral density.

Another performance parameter to be noted is the overlap of the output of the network at a given time with each of the stored patterns. This is defined for the μth pattern vector at the nth iteration as

$$m^{\mu}(n) \ = \ \frac{1}{N} \sum_{i=1}^{N} x_i^{\mu}(n)\ \xi_i^{\mu} \tag{4.20}$$

In Fig. 4.9 the overlap values are plotted against the number of iterations, for each of the three ξ^{μ}.

This chaotic system was then subjected to control by modulating the amplitude of the external periodic input. The resulting system, starting from the same initial conditions and network parameters as in the previous chaotic case, showed a time-series repeating every 15 iterations, after the initial transients had died away. The trajectory of the system state over time in Fig. 4.10 shows a simple periodic orbit. Regular periodic behavior is clearly manifested in the plot of the average excitatory cell activation and the corresponding logarithmic spectral density curve in Fig. 4.11.

The overlap vs. iterations diagram in Fig. 4.12 shows that the network periodically comes close to each of the three stored patterns. Thus, on imposing control, the system state exhibits periodicity quite clearly.

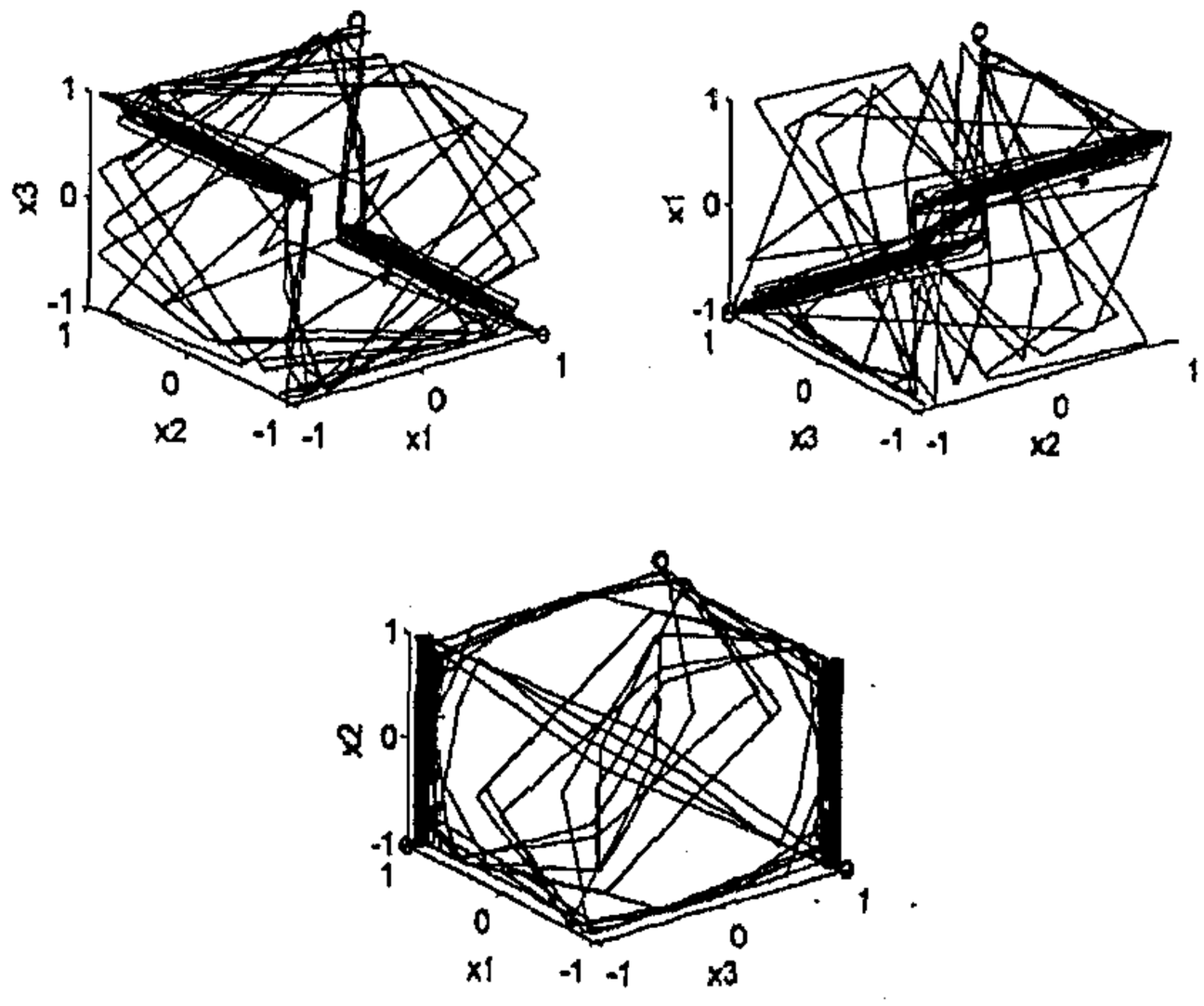

Figure 4.7: Trajectory of the network output in the chaotic state ($K_{ei} = 2.0$, $K_{ie} = 2.0$). The activation values for the cells $x(1)$, $x(2)$ and $x(3)$ are plotted along the three axes. The circles represent the locations of the stored patterns and the plus sign indicate the location of the input pattern.

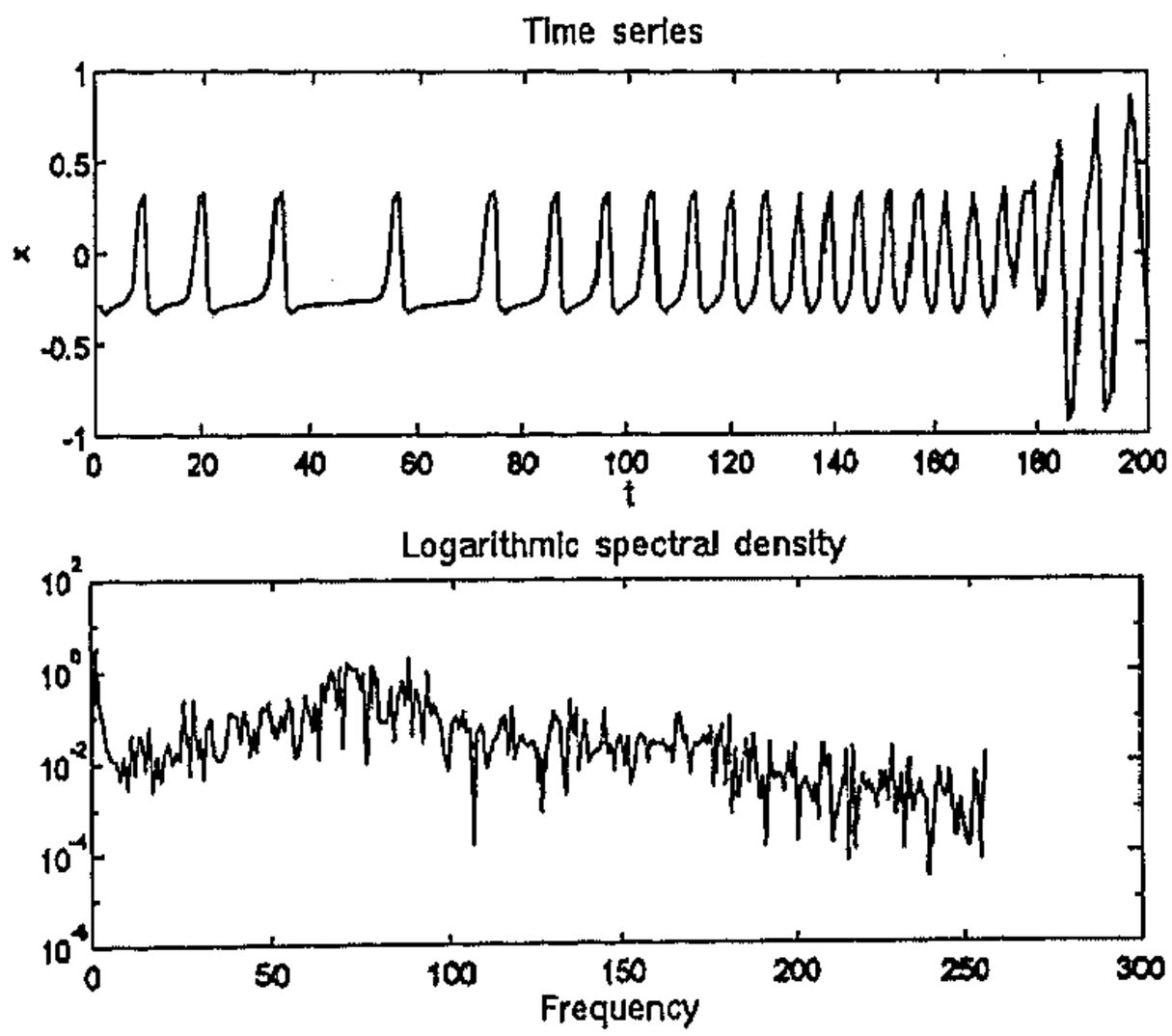

Figure 4.8: Temporal evolution of the average activation value of the excitatory cells in the chaotic state and the corresponding logarithmic spectral density.

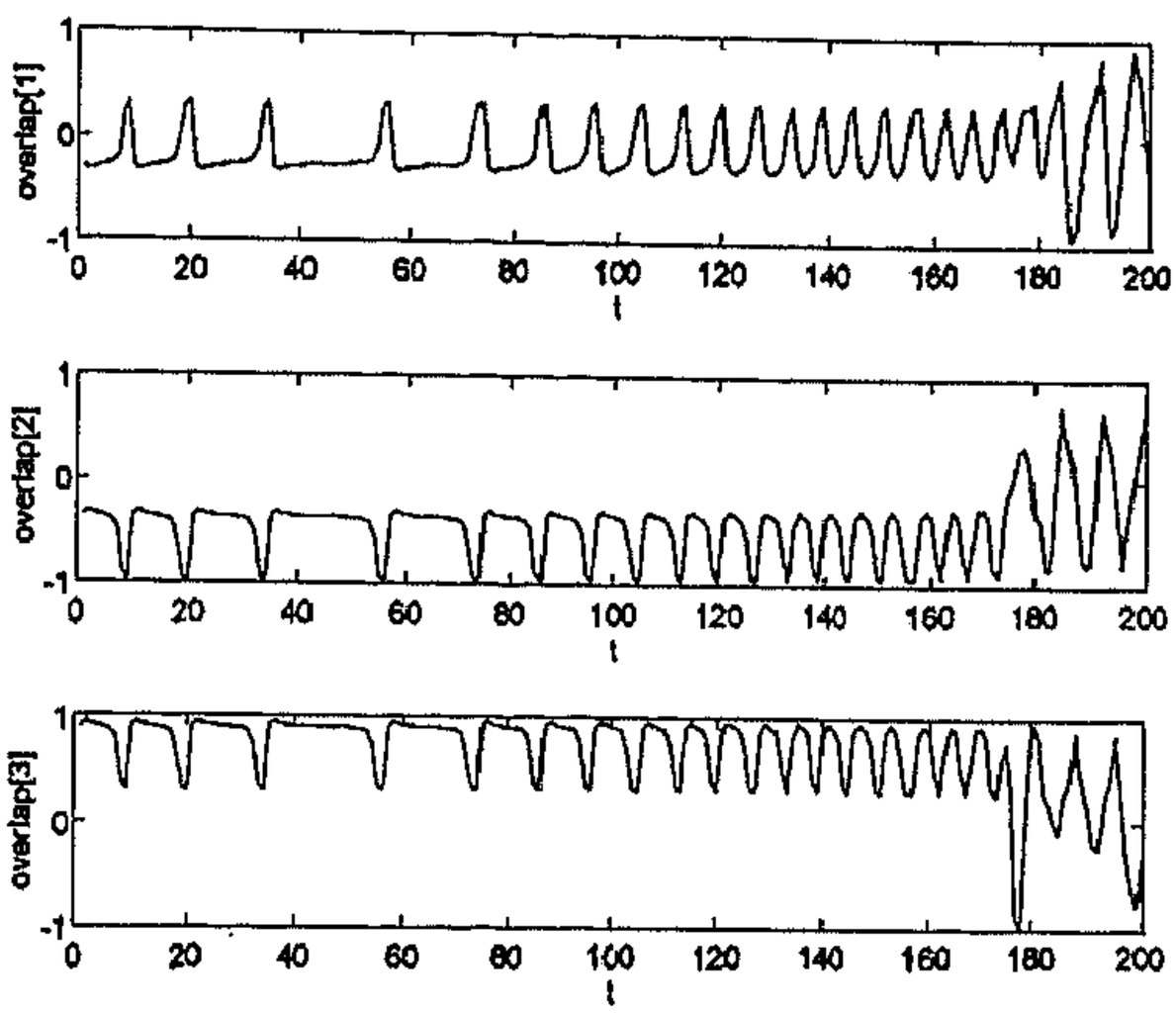

Figure 4.9: Temporal evolution of the overlap of the network output with the stored patterns in the chaotic state.

4.4 Neurobiological implications

The modeling of neurobiological chaos and its subsequent control to produce periodic behavior, points out several possible avenues for research aimed at understanding how the brain works. As Freeman has already pointed out [177], chaos is omnipresent in the brain - demonstrably so, in the somatosensory and the olfactory cortices. It has been suggested that the quiescent state of the brain is chaos, while during perception, i.e. when attention is focused on any sensory stimuli, brain activity becomes more periodic. From this perspective, the periodic orbits observed in the controlled state of the network model can be interpreted as specific memories. If the different spatio-temporal patterns stored in memory are identified with the infinite number of unstable periodic attractors that are embedded in the chaotic attractor, then the transition from quiescence to attention can be interpreted as the controlling of chaos to give rise to periodic behavior, culminating in the identification of the sensory stimulus that has been received. This control, of course, is not imposed by any external agency, but is an emergent property of the brain.

This identification is also indirectly supported by the clinical observations of hallucinations that are prevalent during sensory epileptic seizures [2]. Complex visual hallucinations are usually due to an epileptic focus in the posterior part of the temporal lobe, near its junction with the occipital lobe. Often the hallucinatory visual images are distorted, being too small or too large or unnaturally arranged. More

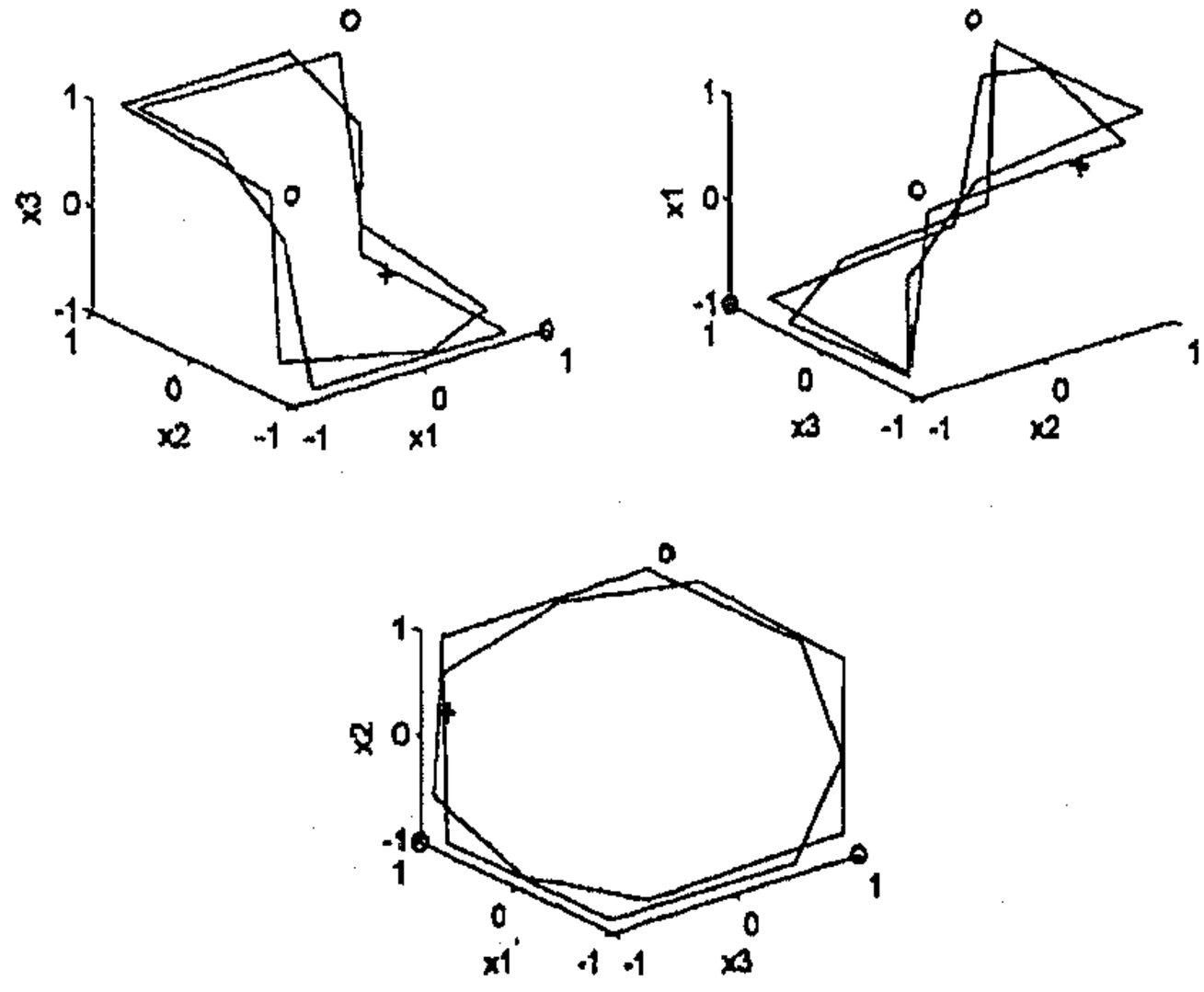

Figure 4.10: Trajectory of the network output in the controlled state for the same set of network parameters and input pattern as in Fig. 7.

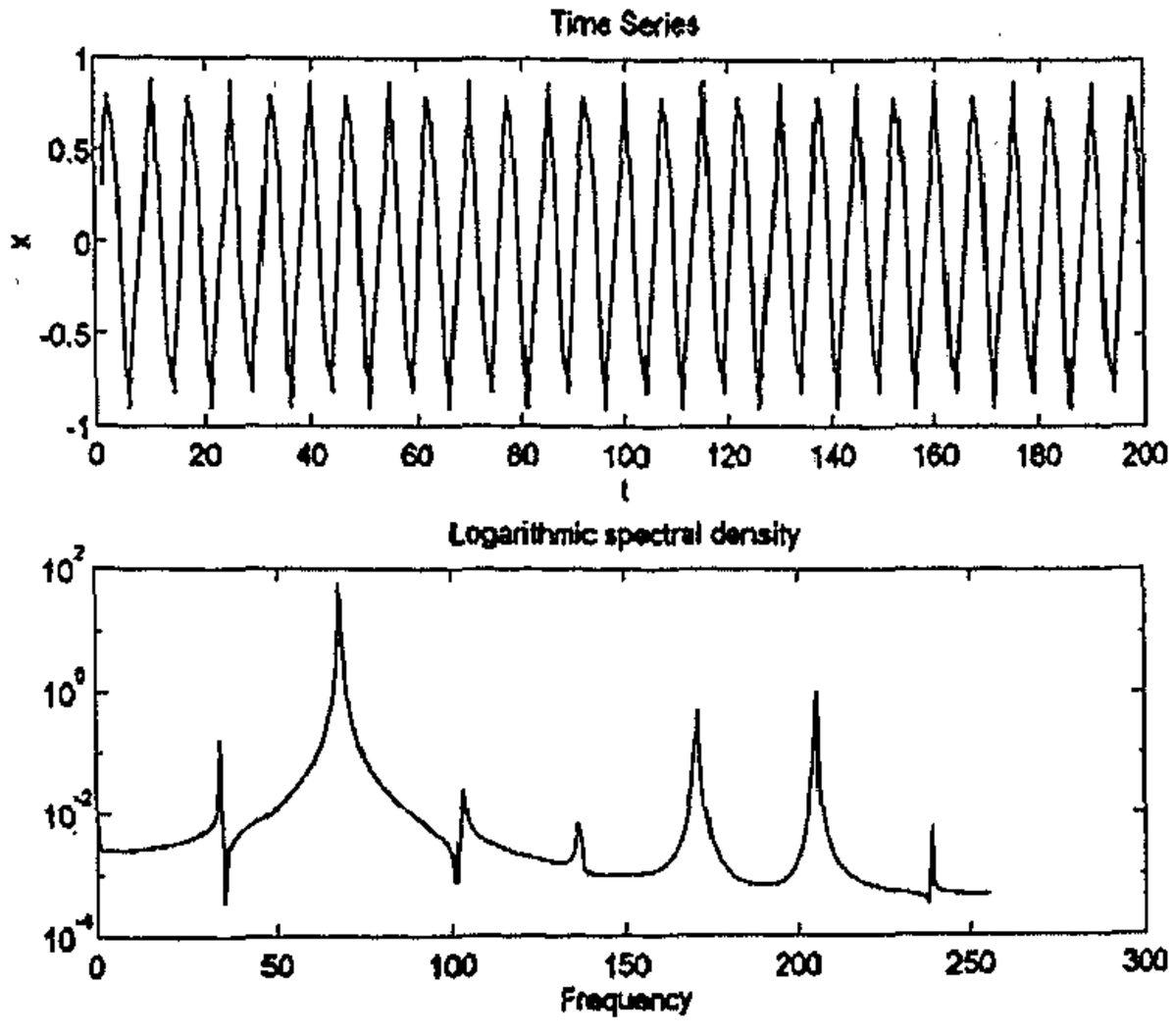

Figure 4.11: Temporal evolution of the average activation value of the excitatory cells in the controlled state and the corresponding logarithmic spectral density.

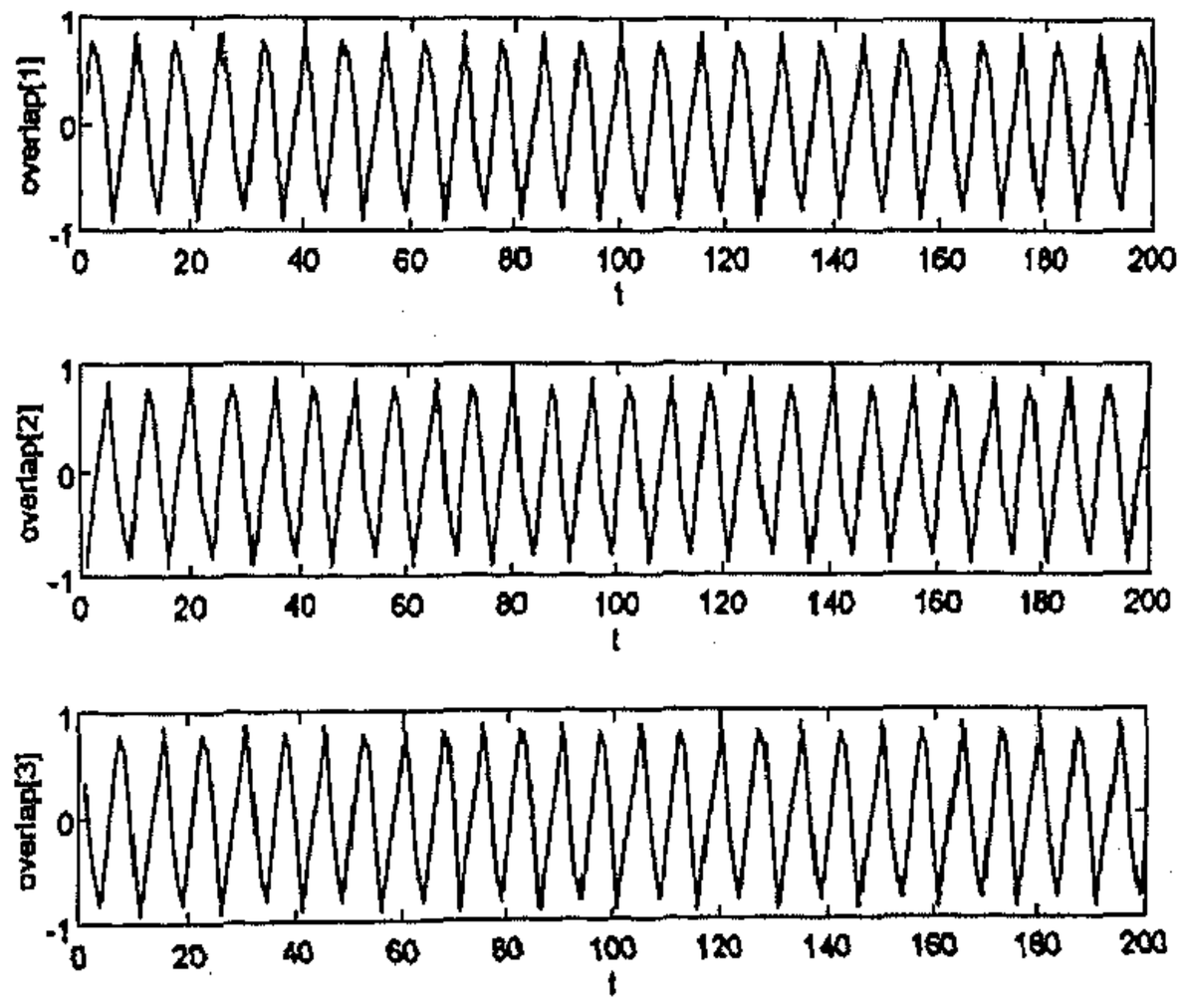

Figure 4.12: Temporal evolution of the overlap of the network output with the stored patterns in the controlled state.

striking is the case of olfactory hallucinations, that are often associated with disease of the inferior and medial parts of the temporal lobe, usually in the region of the hippocampal convolution. Commonly, the hallucinatory smell is thought by the subjects to come from some place in the environment and is described as disagreeable or foul, although otherwise unidentifiable. This can be explained in terms of the proposed picture of brain function by noting that during epilepsy, undesired control of the chaotic activity of the brain occurs as a result of the highly synchronized electrical stimulation of large parts of the brain. The stabilizing of an undesired periodic attractor results in the erroneous recognition of a sensory stimuli even when such a stimuli is absent from the immediate environment of the epileptic subject.

4.5 Discussion

In this investigation, we have confined our attention to small networks for convenience of analysis. The extension of the control methods to the situation of spatiotemporally extended systems [92] is a challenging task for the future.

The traditional neural network paradigm has been so far dominated by dynamics governed by a multitude of fixed point attractors [8]. Each such attractor is identified with a specific pattern which is desired to be classified appropriately and/or recalled associatively. But limitations of neural networks designed according to this prescription, as well as, recent neurobiological research, is now forcing this "fixed-point" approach to be replaced by a more dynamic interpretation of how cognitive tasks may actually be performed in the brain.

The use of chaos control can improve the performance of neural network models for processing information. The possibility of embedding an enormous amount of dynamic patterns (e.g., moving images, pieces of music, etc.) in a chaotic neural network and their systematic recognition will widen the scope of applications of neurocomputers. Rapid switching between various unstable periodic cycles, without large changes in the system dynamics, can be of use in tasks such as storing information and pattern classification. Temporal sequences can be associated with the unstable periodic attractors by suitable learning rules and then recalled on presentation of suitable stimulus as input to the network. The convergence to the stored patterns will be extremely rapid owing to the chaotic dynamics governing the network.

Although control of chaos (by the OGY method) has been demonstrated in the brain [155], it is still not clear whether a similar process is actually used in nature. In this situation, the investigation of different control processes in simple, biologically plausible neural models, can give us an insight on the possible functional role of such phenomena in the actual neurobiological situation.

Chapter 5

Collective Dynamics and Synchronization in Small Assemblies of Neural Pairs

The unique capabilities of the brain to perform cognitive tasks are an outcome of the collective global behavior of its constituent neurons. This is the motivation for investigating the dynamics of small networks of excitatory-inhibitory neural pairs, which have been studied in isolation so far. Recent neurobiological studies have shown that many cortical neurons respond to behavioral events with rapid modulations of discharge correlations, lasting between $\sim 10^{-2} - 10$ seconds [193]. This supports the notion that a neuron can intermittently participate in different computations by rapid synchronization and desynchronization with neighboring neurons. The mechanism of such dynamic correlations in the brain are as yet unknown.

Observation of transition between synchronized activity and incoherent activity in the brain during sensory perception [53], hints at a connection with phase-locking among coupled chaotic systems. Under certain conditions, such chaotic systems can synchronize, either through coupling, or by being linked to a common signal. However, the presence of multiple synchronizing interactions in a network of chaotic elements shows a variety of novel phenomena. The numerical observations reported in this chapter provide a glimpse of the possible range of collective behavior in small assemblies of chaotic neural pairs. Section 1 reviews some techniques for synchronizing chaotic systems. In Section 2 we briefly mention several interesting features observed during the synchronization of two or three coupled neural pairs (both unidirectional and bidirectional couplings have been considered). Section 3 introduces the model (based on the Lorenz system of equations) used for studying competition among synchronizing chaotic systems and includes a short analysis of the fixed points and their stability. Section 4 contains the results of computer simulations of the system. Finally, possible directions of future research and the relevance of this type of research to the theory of neural computation are discussed.

5.1 Synchronization of chaotic systems

The synchronization of chaotic systems is a difficult problem owing to their extremely sensitive dependence on initial conditions. Any initial correlation present between identical systems, starting from very close initial conditions, exponentially decrease to zero with time. Thus, for all practical purposes, any initial synchronization between the systems is bound to disappear rapidly. In recent times, however, some methods of achieving synchronized behavior between chaotic systems have been proposed. Pioneering work in this respect has been done by Pecora and Carroll [140], who used the concept of a response system locking on to a driver system. So far, such studies have been limited to driving a response system by a single driver system. However, the knowledge gained from studying such simple systems may not be adequate to give us an idea as to how systems consisting of multiple independent driver systems, competing with each other to synchronize the same response system, will behave. The Pecora-Carroll driving mechanism can be seen as the "strong-coupling" limit of a general scheme of directionally- oriented couplings in a network of chaotic elements.

The synchronization of bidirectionally coupled chaotic systems is stable provided the coupling strength is at least half the Lyapunov exponent of the system [55] (when the coupling includes all the components of the system equally). One-way coupling (or, driving one chaotic system by another) can also lead to synchronization, provided certain conditions are satisfied [140], [141], [81]. The drive-response method consist of the following steps. First an n-dimensional autonomous system

$$\frac{d\mathbf{x}}{dt} = \mathbf{F}(\mathbf{x}),$$

is divided into two parts, driving ($\mathbf{x}_d$) and responding ($\mathbf{x}_r$):

$$\frac{d\mathbf{x}_d}{dt} = \mathbf{g}(\mathbf{x}_d, \mathbf{x}_r), \quad \frac{d\mathbf{x}_r}{dt} = \mathbf{h}(\mathbf{x}_d, \mathbf{x}_r),$$

where, $\mathbf{x}_d = (x_1, \ldots, x_m)$, $\mathbf{g} = [f_1(\mathbf{x}), \ldots, f_m(\mathbf{x})]$, $\mathbf{x}_r = (x_{m+1}, \ldots, x_n)$ and $\mathbf{h} = [f_{m+1}(\mathbf{x}), \ldots, f_n(\mathbf{x})]$. A replica subsystem $\mathbf{x}'_r$ identical to $\mathbf{x}_r$ is then created and driven with the $\mathbf{x}_d$ variables of the original system. Therefore, the replica subsystem equations are,

$$\frac{d\mathbf{x}'_r}{dt} = \mathbf{h}(\mathbf{x}_d, \mathbf{x}'_r).$$

The responding subsystems $\mathbf{x}_r$ and $\mathbf{x}'_r$ will synchronize only if $\delta\mathbf{x}_r = |\mathbf{x}_r - \mathbf{x}'_r| \to 0$. According to Pecora and Carroll, this occurs if and only if the conditional Lyapunov exponents of the $\mathbf{x}_r$ subsystem are all negative.

Drive-response synchronization has been realized in various electrical circuit experiments. It has also been used in experiments of secure communication where a chaotic masking signal is added to the transmitted signal. It is then recovered at the receiving end by subtracting the chaotic signal regenerated by synchronization [42].

Besides the Pecora-Carroll method, other synchronization procedures have also been proposed. Of these, the Variable Control Feedback (VCF) method is of particular interest, as it can be used for both control and synchronization of chaos [92]. In fact, the Pecora-Carroll method turns out to be a special limiting case of this method. VCF consists of adding a feedback term to a dynamical system to guide it into some prescribed state. If $\frac{dx}{dt} = \mathrm{F}(\mathrm{x})$ be an n-dimensional dynamical system and x^* be the desired state to which the system has to be brought, then VCF involves modifying the system dynamics to:

$$\frac{dx}{dt} = \mathrm{F}(\mathrm{x}) - \lambda(\mathrm{x} - \mathrm{x}^*)$$

where λ is the set of n feedback multipliers. If x^* be the output of a chaotic system $\mathrm{F}'(\mathrm{x})$, then the system synchronizes with $\mathrm{F}(\mathrm{x})$. In the large-λ limit, VCF reduces to the Pecora-Carroll method. Specifically, the feedback parameters for the driving subsystem variables, $\lambda_d \to \infty$, while the remaining λs are set to zero.

5.2 Collective dynamics of neural assemblies

Synchronization among chaotic maps, with either unidirectional or bidirectional coupling, have been investigated previously in [46, 78, 189], while the effect of coupling on the chaotic dynamics has been studied in [115, 152, 63, 143]. In this section we briefly mention some results of numerical investigations of collective dynamics of N pairs of excitatory-inhibitory neural pairs (N=2,3), coupled to each other, either unidirectionally or bidirectionally. The cases considered are shown schematically in Fig. 5.1.

Case I: $N = 2$

In this case, synchronization occurs for both unidirectional and bidirectional coupling, when the magnitude of the coupling parameter is above a certain critical threshold. An interesting feature observed is the intermittent occurrence of desynchronization [56, 82] in an apparently synchronized situation, for a range of coupling values. The arrangements we have investigated numerically are given by the following set of equations:

$$z^1_{n+1} = I\!F(z^1_n),$$
$$z^2_{n+1} = I\!F(z^2_n + \lambda[z^1_n - z^2_n]),$$

for unidirectional coupling, and

$$z^1_{n+1} = I\!F(z^1_n + \lambda[z^2_n - z^1_n]),$$
$$z^2_{n+1} = I\!F(z^2_n + \lambda[z^1_n - z^2_n]),$$

for bidirectional coupling ($I\!F$ indicates the dynamical system representing an excitatory-inhibitory neural pair, with sigmoid activation function). Both systems show qualitatively similar behavior. In Fig. 5.2, we present the results of numerical simulation

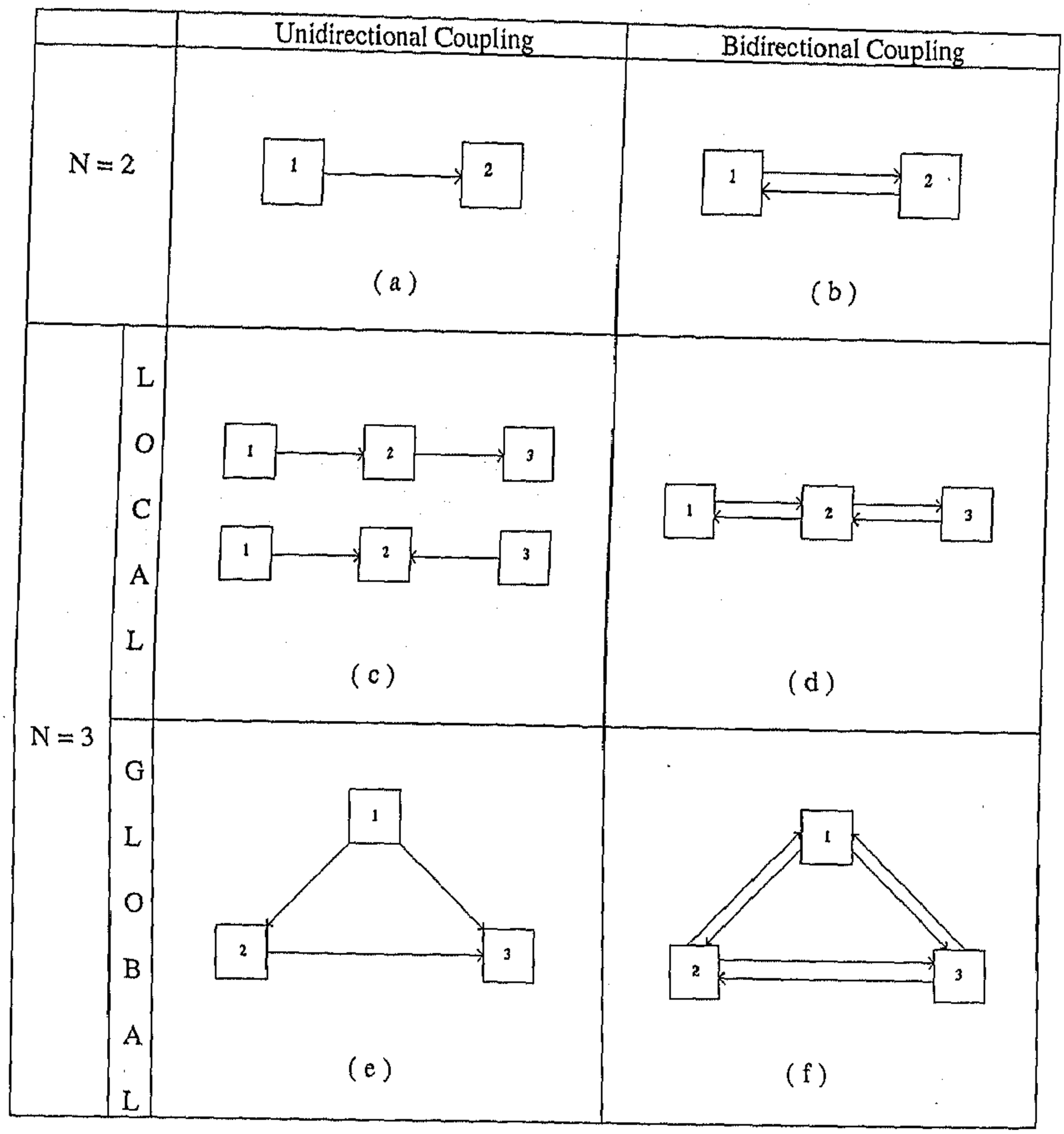

Figure 5.1: The coupling arrangements investigated for $N = 2$ ((a) unidirectional and (b) bidirectional) and $N = 3$ neural pairs. In the latter case, two further cases were considered: local coupling ((c) unidirectional and (d) bidirectional) and global coupling ((e) unidirectional and (f) bidirectional).

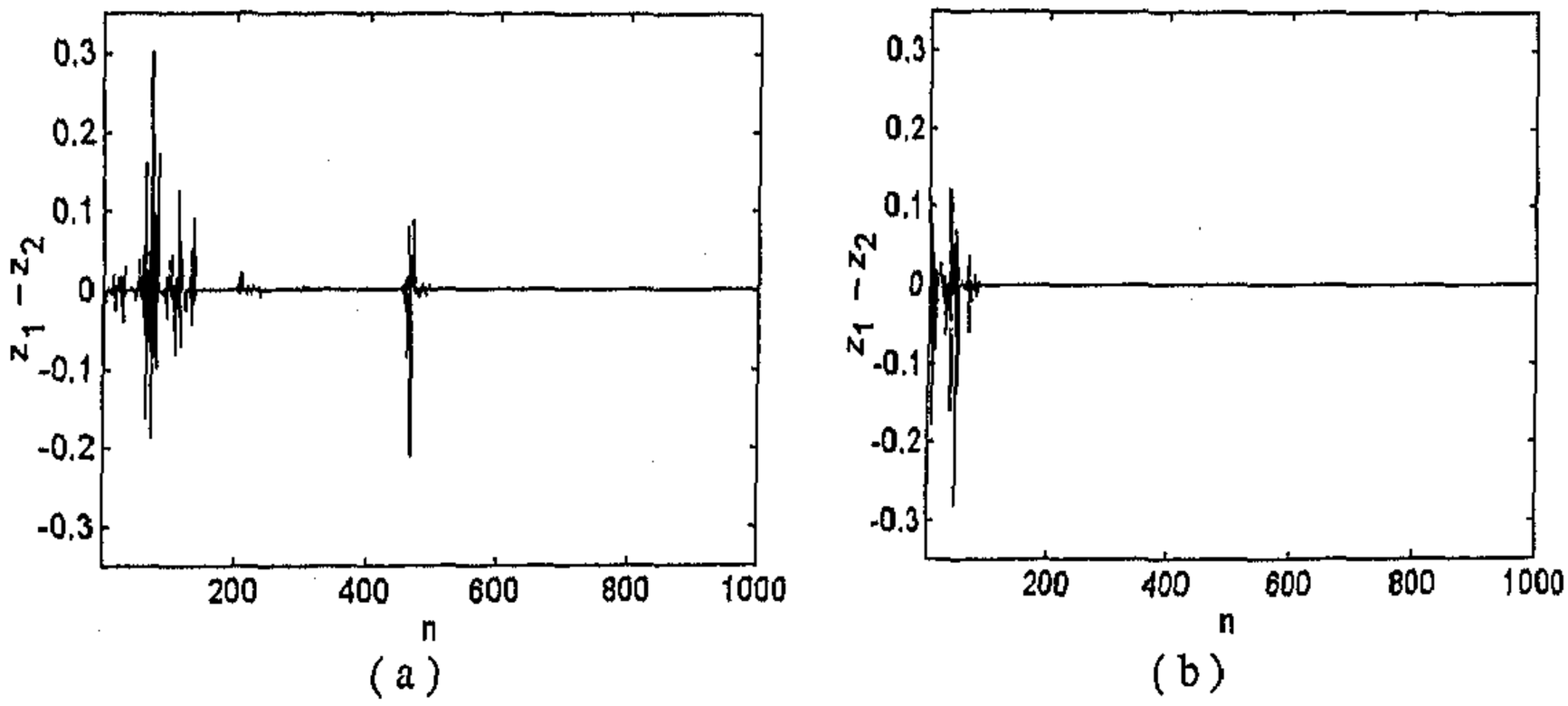

Figure 5.2: Intermittent synchronization for 2 bidirectionally coupled neural pairs (z_1, z_2) with coupling magnitude (a) $\lambda = 0.26$ and (b) $\lambda = 0.28$ ($a = 100, b = 25$, for both the pairs).

of a *bidirectionally coupled system*, where the component neural pairs have the activation function parameters $a = 100, b = 25$. As can be seen clearly, the presence of intermittent burst of desynchronization occurs as a function of the coupling parameter, λ.

Case II: $N = 3$

For $N = 3$, two coupling arrangements are possible for both unidirectional and bidirectional coupling: *local coupling*, where nearest neighbors are coupled to each other, and *global coupling*, where the elements are coupled in an all-to-all fashion.

In the case of unidirectional coupling, a certain type of local coupling arrangement can produce a situation, referred to as "frustrated synchronization", that has been analysed in detail later in this chapter. In the case of bidirectional coupling, we observe a new phenomenon, referred to as *mediated synchronization*. The equations governing the dynamics of the coupled system is given by:

$$z^1_{n+1} = I\!F(z^1_n + \lambda z^2_n),$$

$$z^2_{n+1} = I\!F(z^2_n + \lambda[z^1_n + z^3_n]),$$

$$z^3_{n+1} = I\!F(z^3_n + \lambda z^2_n).$$

For the set of activation parameters $a = 100, b = 25$, we observe the following feature over a range of values of the coupling parameter, λ: the neural pairs, z^1 and z^3 which have no direct connection between themselves synchronize, although z^2

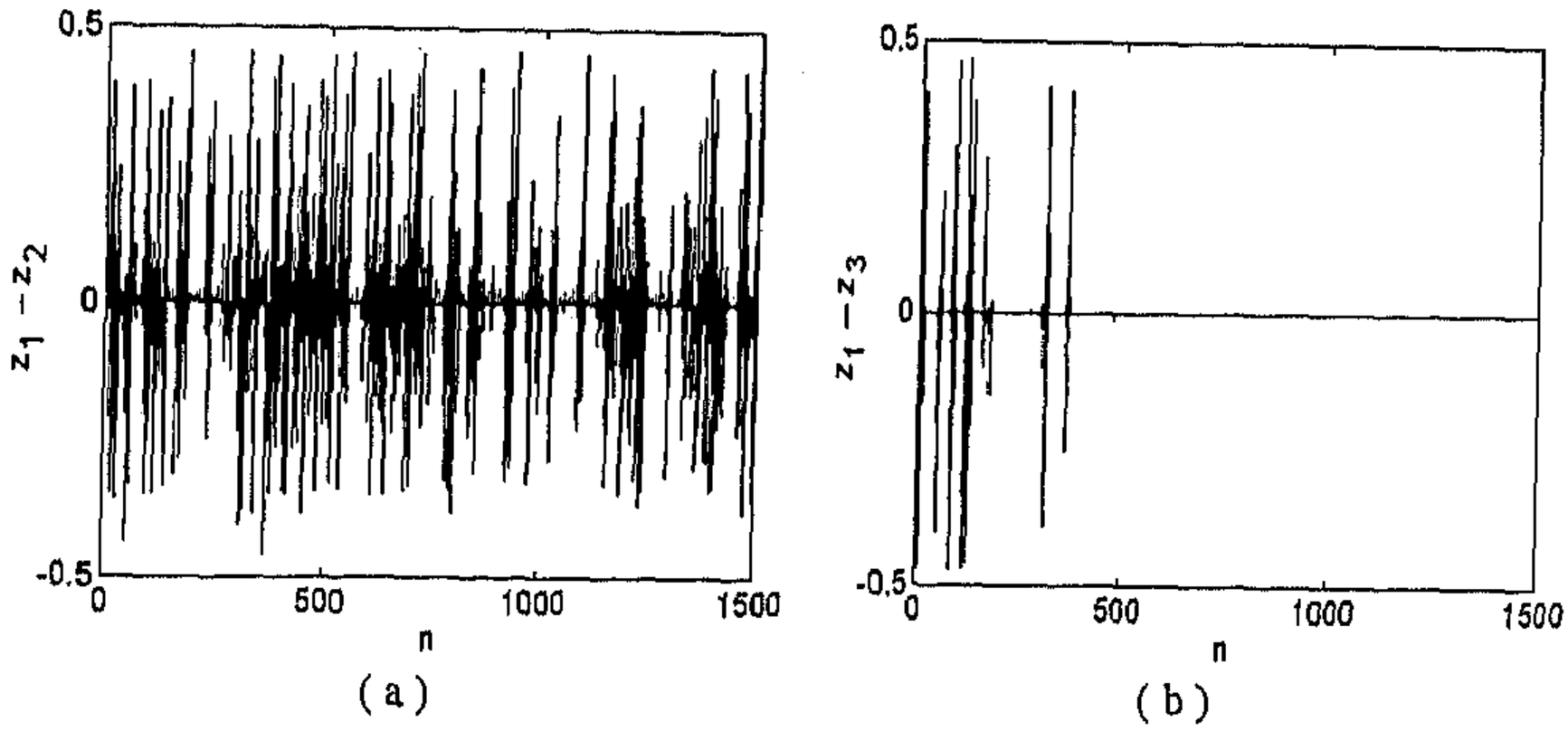

Figure 5.3: *Mediated synchronization* for 3 bidirectional, locally coupled neural pairs (z_1, z_2, z_3) with coupling magnitude $\lambda = 0.12$: (a) no synchronization between z_1 and z_2, while, (b) z_1 and z_3 synchronize after ~ 500 iterations ($a = 100, b = 25$ for all the pairs).

synchronizes with neither (Fig. 5.3). So, the system z^2 appears to be "mediating" the synchronization interaction, although not taking part in it by itself.

For a global coupling arrangement, no new feature is observed for unidirectional coupling (this arrangement is similar to that studied in [13] for continuous time systems) - but for bidirectional coupling, governed by the set of equations:

$$z^1_{n+1} = I\!F(z^1_n + \lambda[z^2_n + z^3_n]),$$

$$z^2_{n+1} = I\!F(z^2_n + \lambda[z^1_n + z^3_n]),$$

$$z^3_{n+1} = I\!F(z^3_n + \lambda[z^1_n + z^2_n]),$$

the phenomenon of "frustrated synchronization" is observed. The phase space of the entire coupled system is shown in Fig. 5.4. The time series plots in Fig 5.5 show that none of the component systems synchronize. This is because the 3 systems, each trying to synchronize the other, frustrate all attempts at collective synchronization. (Note that the introduction of structural disorder in chaotic systems can also lead to frustration [26].) To study this phenomenon in detail in the unidirectionally coupled situation, we have considered the well-known Lorenz system of equations in the following section.

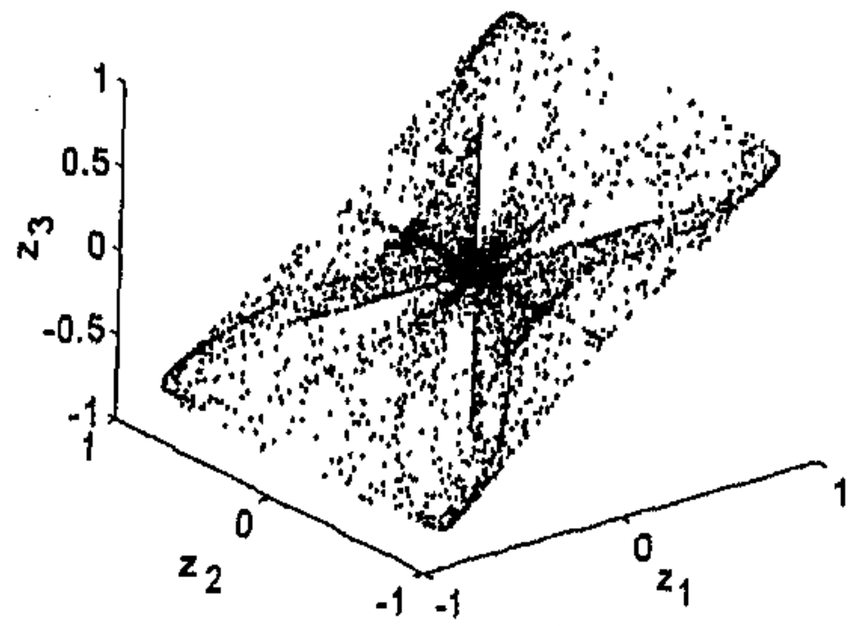

Figure 5.4: Phase space for 3 bidirectional, globally coupled neural pairs (z_1, z_2, z_3) with coupling magnitude $\lambda = 0.5$ ($a = 100, b = 5$ for all the pairs).

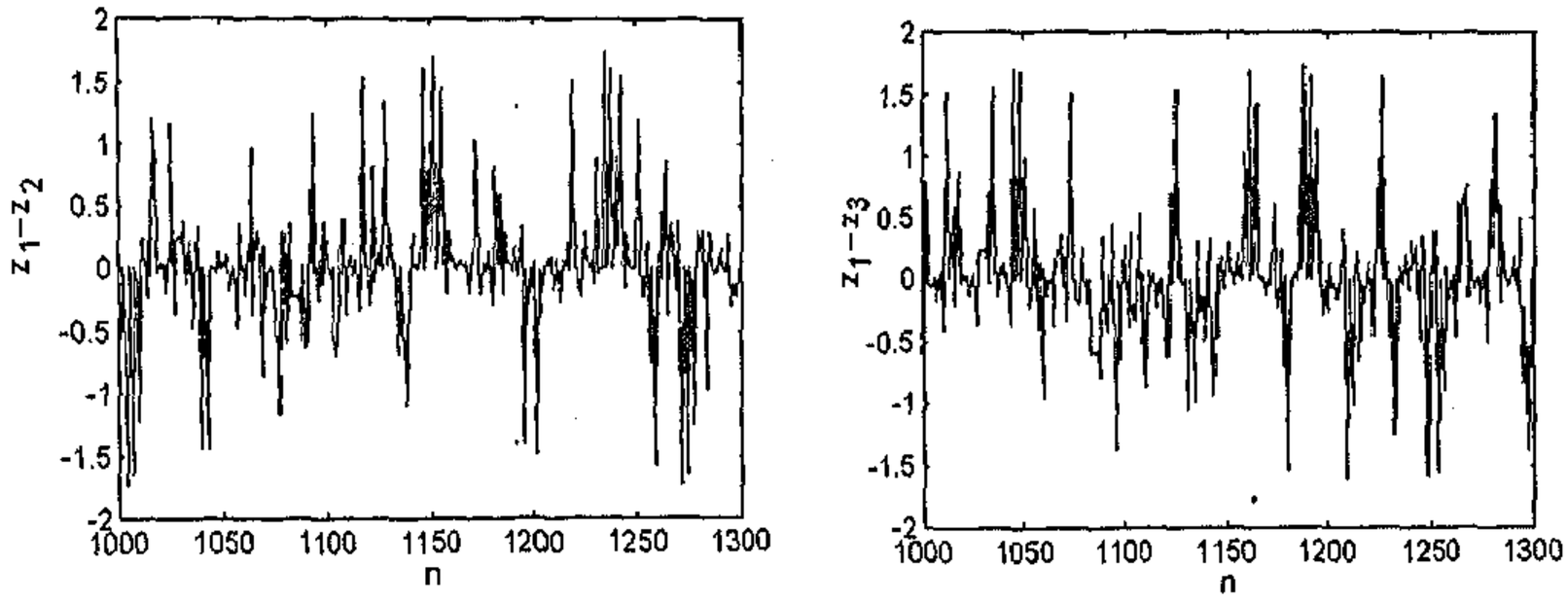

Figure 5.5: Frustrated synchronization for 3 bidirectional, globally coupled neural pairs (z_1, z_2, z_3) with coupling magnitude $\lambda = 0.5$: no synchronization between (a) z_1 and z_2, or, (b) z_1 and z_3 ($a = 100, b = 5$ for all the pairs).

5.3 Competition among synchronizing Lorenz systems

The investigation of competition among synchronizing chaotic systems was carried out using the Lorenz system of equations [114], [182]. This well-known paradigm of chaos is defined by the following set of equations:

$$\frac{dx}{dt} = \sigma\,(y - x), \tag{5.1}$$

$$\frac{dy}{dt} = rx - y - xz, \tag{5.2}$$

$$\frac{dz}{dt} = xy - bz, \tag{5.3}$$

where, σ, r and b are real, positive parameters. There are three fixed points for this system: $F_1 = (0,0,0)$, $F_2 = (\sqrt{b(r-1)}, \sqrt{b(r-1)}, r-1)$, and $F_3 = (-\sqrt{b(r-1)}, -\sqrt{b(r-1)}, r-1)$. The local stability of the fixed point $(x_f\ ,\ y_f\ ,\ z_f)$ is determined by the eigenvalues of the Jacobian

$$J = \begin{vmatrix} -\sigma & \sigma & 0 \\ (r - z_f) & -1 & -x_f \\ y_f & x_f & -b \end{vmatrix}. \tag{5.4}$$

Evaluation of the matrix shows that for $0 < r < 1$, F_1 is the only stable fixed point. For $r > 1$, F_1 becomes unstable and the phase-space trajectory of the system converges to either F_2 or F_3. For $r > r_c = \sigma(\sigma + b + 3)/(\sigma - b - 1)$ the system's trajectory perpetually wanders along the extremely complicated structure of the stable and unstable manifolds of the fixed points, exhibiting chaotic behavior.

For the present work the effect of two driving systems, designated as driving systems 1 (x_1, y_1, z_1) and 2 (x_2, y_2, z_2), competing to synchronize a responding system (x_3, y_3, z_3) was studied. The responding system was driven using the y variable. A competition parameter a was defined to indicate the strength of the driving systems relative to each other. The maximum value of a was normalized to unity. Therefore, the y variable of the responding system was defined in terms of the two driving systems as:

$$y_3 = ay_1 + (1 - a)y_2. \tag{5.5}$$

We consider first the case where the two driving systems have the same r-parameter value, and then, the more general case, where the two r-values are different (r_1 and r_2, say). The σ and b-parameter values are considered to be the same in all cases.

Case I: $r_1 = r_2 = r$

It is obvious that for $a = 1$ the responding system synchronizes with driver system 1, whereas for $a = 0$, it synchronizes with system 2. The attractor of the response

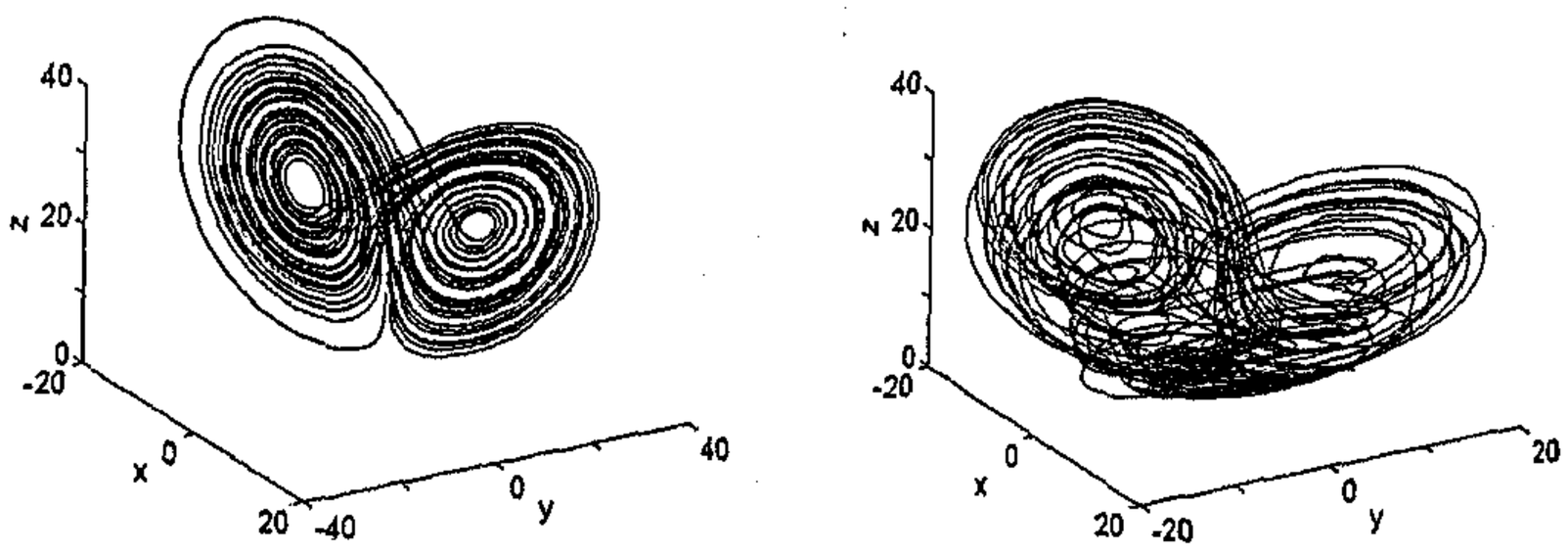

(a) (b)

Figure 5.6: The response system attractor for (a) $a = 1.0$ and (b) $a = 0.5$ ($r_1 = r_2 = 28, \sigma = 10, b = 8/3$).

system, is identical to that of the conventional Lorenz system (Fig. 5.6 (a)). For $0 < a < 1$, the responding system (x_3, y_3, z_3) has nine fixed points:

$$\begin{aligned}
\mathrm{F}_1 &= (0,0,0),\\
\mathrm{F}_2 &= (\sqrt{b(r-1)}, \sqrt{b(r-1)}, r-1),\\
\mathrm{F}_3 &= (-\sqrt{b(r-1)}, -\sqrt{b(r-1)}, r-1),\\
\mathrm{F}_4 &= (a\sqrt{b(r-1)}, a\sqrt{b(r-1)}, a^2(r-1)),\\
\mathrm{F}_5 &= ((1-a)\sqrt{b(r-1)}, (1-a)\sqrt{b(r-1)}, (1-a)^2(r-1)),\\
\mathrm{F}_6 &= (-a\sqrt{b(r-1)}, -a\sqrt{b(r-1)}, a^2(r-1)),\\
\mathrm{F}_7 &= (-(1-a)\sqrt{b(r-1)}, -(1-a)\sqrt{b(r-1)}, (1-a)^2(r-1)),\\
\mathrm{F}_8 &= ((2a-1)\sqrt{b(r-1)}, (2a-1)\sqrt{b(r-1)}, (2a-1)^2(r-1)),\\
\mathrm{F}_9 &= (-(2a-1)\sqrt{b(r-1)}, -(2a-1)\sqrt{b(r-1)}, (2a-1)^2(r-1)).
\end{aligned}$$

Note that the first three fixed points are those of the uncoupled Lorenz system. To find out about the stability of these fixed points we need to calculate the eigenvalues of the corresponding Jacobian, J′. The partially block-diagonal form of the matrix makes the calculation easy:

$$\mathrm{J}' = \begin{vmatrix} \mathrm{J} & 0_{3\times3} & 0_{3\times2} \\ 0_{3\times3} & \mathrm{J} & 0_{3\times2} \\ \mathrm{A} & \mathrm{B} & \mathrm{J}_R \end{vmatrix}, \tag{5.6}$$

where, J is the Jacobian (eqn. 4) of the unperturbed Lorenz system of equations, $0_{m\times n}$ is a null matrix having m rows and n columns, and the other matrices are defined as,

$$\mathrm{A} = \begin{vmatrix} 0 & a\,\sigma & 0 \\ 0 & a\,x_{f_3} & 0 \end{vmatrix}, \tag{5.7}$$

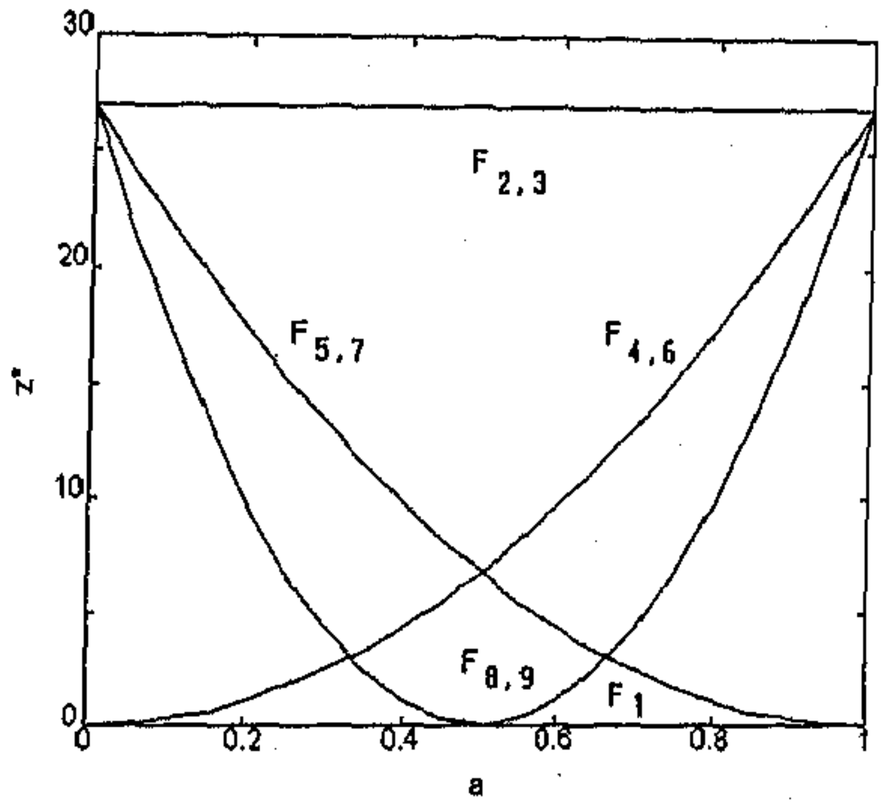

Figure 5.7: The z-coordinate of fixed points of the response system for $0 \leq a \leq 1$.

$$\mathrm{B} = \begin{vmatrix} 0 & (1-a)\,\sigma & 0 \\ 0 & (1-a)\,x_{f_3} & 0 \end{vmatrix}, \tag{5.8}$$

and,

$$\mathrm{J}_R = \begin{vmatrix} -\sigma & 0 \\ a\,y_{f_1} + (1-a)\,y_{f_2} & -b \end{vmatrix}. \tag{5.9}$$

Here f_k refers to the fixed point of the kth Lorenz system.

For $0 < r < 1$, the only stable fixed point is F_1. For $r > 1$, F_1 loses its stability, and there are four new stable fixed points: $\mathrm{F}_2, \mathrm{F}_3, \mathrm{F}_8$ and F_9. For $r > r_c = \sigma(\sigma + b + 3)/(\sigma - b - 1)$, these fixed points lose their stability and the system shows only chaotic behavior. The most interesting instance is that of $a = 0.5$, where maximal competition occurs. In this case, $\mathrm{F}_8 = \mathrm{F}_9 = \mathrm{F}_1$, $\mathrm{F}_4 = \mathrm{F}_5$ and $\mathrm{F}_6 = \mathrm{F}_7$ (Fig. 5.7). The attractor of the responding system is found to be stretched over its 3-dimensional phase space showing an extremely tangled structure (Fig. 5.6 (b)). This is due to the extremely complicated motion of the response system trajectory along the stable and unstable manifolds of the fixed points $\mathrm{F}_1, \mathrm{F}_2, \mathrm{F}_3, \mathrm{F}_4$ and F_6. The coupling with driver system 1 tries to force the response system into synchronization with it, but at the same time, the coupling with driver system 2 desynchronizes the trajectory. The synchronization is therefore 'frustrated' by the competition between the two driver systems. The "frustrated" response system attractor reduces to the conventional Lorenz attractor if $a \to 0$ or 1, when competition is absent.

The attractor structure is found to be quite robust. If we start from two different initial conditions for the responding system, (x, y, z) and (x', y', z'), say, then for stable synchronization, the two respective trajectories should converge rapidly. However, whereas in the Pecora-Carroll case, convergence occurs to the standard Lorenz attractor, in this case, both the trajectories converge to the "frustrated" attractor.

The stability of synchronization can be demonstrated analytically by linear stability analysis of the error dynamics. Defining the dynamical error between two response system trajectories (x and x′) which have different initial conditions, as e = x − x′, the error equations can be written as:

$$\frac{de_x}{dt} = -\sigma e_x, \tag{5.10}$$

$$e_y = 0, \tag{5.11}$$

$$\frac{de_z}{dt} = (ay_1 + (1-a)y_2)e_x - be_z. \tag{5.12}$$

Here we have assumed that the equation parameters for the two systems are identical. The error system of equations has an equilibrium point at e = (0, 0, 0), which corresponds to perfect synchronization. The local stability of synchronization can then be checked by looking at the eigenvalues of the Jacobian of the error equations:

$$J_R = \begin{vmatrix} -\sigma & 0 \\ a\,y_1 + (1-a)\,y_2 & -b \end{vmatrix} \tag{5.13}$$

The eigenvalues are $-\sigma$ and $-b$, which are the conditional Lyapunov exponents of the response system. As both eigenvalues are negative, the synchronization is locally stable, and any difference in initial conditions rapidly goes to zero. Note that, this does not prove the global stability of the synchronized state. However, simulations have verified that even in the presence of large deviations in initial conditions, synchronization with the "frustrated" trajectory is achieved. This indicates that, although exact synchronization with the driver system cannot be achieved, the "frustrated" system can still be used for secure communication through chaotic masking. This has been established through simulations reported below.

Case II: $r_1 \neq r_2$

When the value of the r-parameter of the two driving systems is not the same, the fixed points are given by:
$F_1 = (0, 0, 0)$,
$F_2 = (a\sqrt{b(r_1-1)} + (1-a)\sqrt{b(r_2-1)}, a\sqrt{b(r-1)} + (1-a)\sqrt{b(r_2-1)}, a^2(r_1-1) + (1-a)^2(r_2-1) + 2a(1-a)\sqrt{(r_1-1)(r_2-1)})$,
$F_3 = (-a\sqrt{b(r_1-1)} - (1-a)\sqrt{b(r_2-1)}, -a\sqrt{b(r-1)} - (1-a)\sqrt{b(r_2-1)}, a^2(r_1-1) + (1-a)^2(r_2-1) + 2a(1-a)\sqrt{(r_1-1)(r_2-1)})$,
$F_4 = (a\sqrt{b(r_1-1)}, a\sqrt{b(r_1-1)}, a^2(r_1-1))$,
$F_5 = ((1-a)\sqrt{b(r_2-1)}, (1-a)\sqrt{b(r_2-1)}, (1-a)^2(r_2-1))$,
$F_6 = (-a\sqrt{b(r_1-1)}, -a\sqrt{b(r_1-1)}, a^2(r_1-1))$,
$F_7 = (-(1-a)\sqrt{b(r_2-1)}, -(1-a)\sqrt{b(r_2-1)}, (1-a)^2(r_2-1))$,
$F_8 = (a\sqrt{b(r_1-1)} - (1-a)\sqrt{b(r_2-1)}, a\sqrt{b(r-1)} - (1-a)\sqrt{b(r_2-1)}, a^2(r_1-1) +$

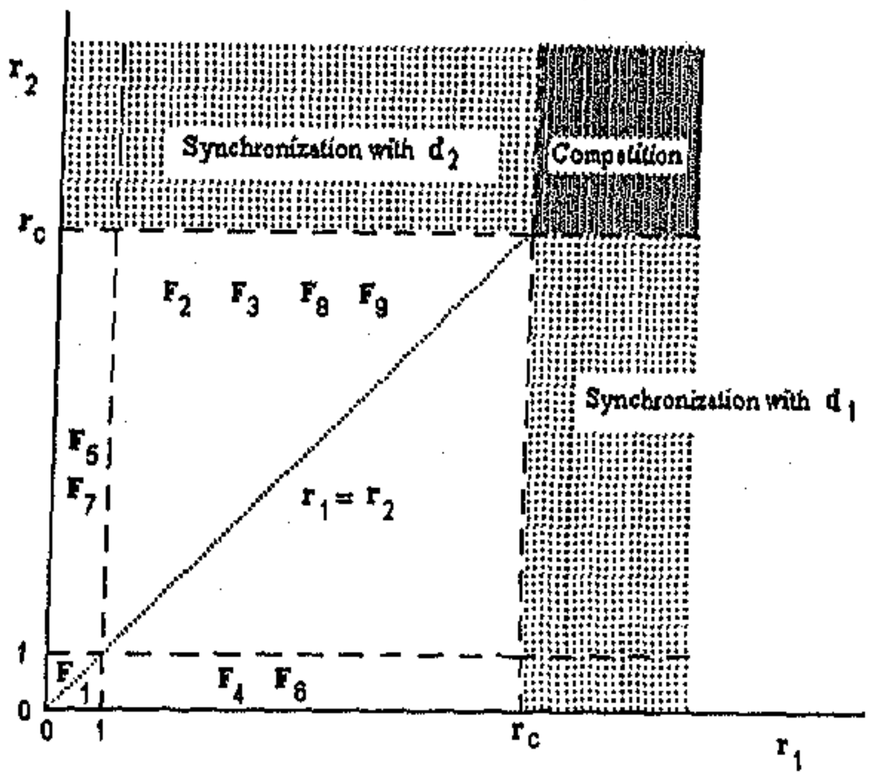

Figure 5.8: The (r_1, r_2)-parameter space showing the stable fixed points of the response system at different regions.

$(1-a)^2(r_2-1) - 2a(1-a)\sqrt{(r_1-1)(r_2-1)})$,
$\mathrm{F}_9 = (-a\sqrt{b(r_1-1)} + (1-a)\sqrt{b(r_2-1)}, -a\sqrt{b(r-1)} + (1-a)\sqrt{b(r_2-1)}, a^2(r_1 - 1) + (1-a)^2(r_2-1) - 2a(1-a)\sqrt{(r_1-1)(r_2-1)})$.

Fig. 5.8 shows the (r_1, r_2)-parameter space. The stable fixed points at different regions are indicated in the diagram. The dotted line corresponds to the special case $r_1 = r_2$ which has been considered above. Note that, whereas in the general case all the fixed points are stable in some region or other, in the special case of $r_1 = r_2$, four of the fixed points, *viz.*, $\mathrm{F}_4, \mathrm{F}_5, \mathrm{F}_6$ and F_7, are always unstable. When one of the r-values go over to the chaotic regime, while the other r-value remains fairly below it, asymptotic synchronization with the chaotic trajectory is observed [106]. The time required to ultimately synchronize with the chaotic attractor is a function of both the r-parameter values. The synchronization is phase- synchronization rather than state- synchronization, as the response system chaotic attractor is a scaled replica of the driver system attractor. The scaling factor is a for synchronization with driving system 1, and $(1-a)$, for driving system 2. When both the r-values are in the chaotic regime, the "frustrated synchronization" situation occurs.

5.4 Simulation results

For conducting simulations, the parameter values chosen were $r_1 = r_2 = 28$, $\sigma = 10$ and $b = 8/3$. The trace of the Jacobian (which is equal to the sum of the Lyapunov exponents) for the total system, including the driver and response systems, is

-40.0. So the overall system is diffusive and possesses an attractor. The competition parameter a was varied in the interval $[0, 1]$. The differential equations were numerically solved using the fourth-order Runge-Kutta method with step-size $= 0.025$. The phase-space trajectory of the responding system (x_3, y_3, z_3) was observed with different values of a from $t = 0$ to $t = 100$. At the limit $a = 0$ (or 1) the responding system trajectory is identical to that of a unperturbed Lorenz system (Fig. 5.6 (a)). However, as $a \rightarrow 0.5$ (where maximal competition occurs), the trajectory deviates more and more from the standard Lorenz form. At $a = 0.5$, the trajectory moves in a complicated path around the fixed points F_1, F_2 and F_3 (note that, at $a = 0.5$, $F_8 = F_9 = F_1$ (Fig. 5.6 (b)). It appears that for a=0.5, the z-variable time-series is much more correlated. This becomes clearer on taking a Fourier transform of the data. The power spectral density of the frustrated attractor time-series is low in the high-frequency end compared to the unperturbed system time-series.

The Lyapunov exponents were calculated using Gram-Schmidt technique [160] to create an orthonormal basis every 0.5 seconds of simulation time (this time interval being roughly half the "period" of the Lorenz system) and then averaging over 100 iterations. As expected, of the eight exponents, six correspond to those for the two unperturbed driving Lorenz systems (0.84, 0, -14.51). The remaining two exponents are the conditional Lyapunov exponents of the responding system : -8/3 and -10. This implies the robustness of the "frustrated" attractor - as any deviation from the attractor rapidly diminishes.

To study the degree of synchronization, z-coordinates of the responding system state (z_3)were plotted against the z-coordinates of each of the driver system states (z_1, z_2), for different values of a. If the two are synchronized, the plot gives a straight line. This suggests that the linear correlation coefficients, r, between the driver and response system time series, can be used to obtain a quantitative measure of synchronization. The linear correlation coefficient between two time series data $x(t)$ and $y(t)(t = 1, \ldots, n)$, is given by

$$r_{x,y} = \frac{1}{n} \frac{\sum_{i=1}^{n} (x(i) - \bar{x})(y(i) - \bar{y})}{\sigma_x \sigma_y},$$

where $\bar{x}$ and σ_x are the mean and standard deviation respectively, for the time series $x(t)$. A measure of desynchronization is defined as

$$\delta = 1 - r_{z_2,z_3}. \tag{5.14}$$

At a=0, where there is exact synchronization between driver system 2 and the response system, $\delta = 0$. This is a particularly robust measure, as $\delta \rightarrow 0$ for both state- and phase- synchronization. The variation of δ with a is shown in a logarithmic plot (Fig. 5.9). The linear nature of the curve over at least 3 orders of magnitude as $a \rightarrow 0$, indicates the presence of a power-law scaling relation of the form:

$$\delta \sim a^{\beta}, \tag{5.15}$$

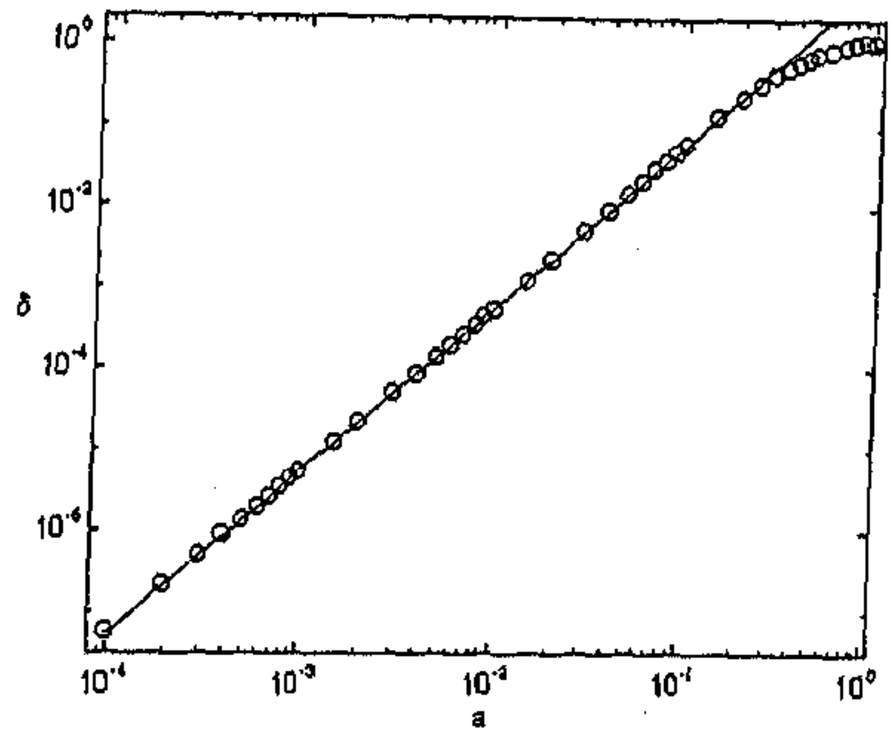

Figure 5.9: Log-scale plot of desynchronization (δ) for $0 < a \leq 1$. The power-law scaling relation (with characteristic exponent, $\beta \sim 2.0$) is indicated by the solid line fitted to the simulation data.

where the scaling exponent, $\beta \simeq 2.0$. The scaling exponent was also obtained for r= 50 and 70. In both cases, $\beta \simeq 2.0$ within simulation error. The scaling seems to be related to similar scaling phenomena due to intermittency induced by noise (in this case, the non-synchronized chaotic input) for motion on the invariant synchronization manifold [146, 136], that have been observed both theoretically [12, 83, 147, 45] and experimentally [207].

Another interesting feature studied was the fractal correlation dimension of the frustrated attractor (Fig. 5.10), calculated using the FD3 (ver. 0.3) software [154]. For the unperturbed Lorenz system, this is very close to 2, as the attractor is almost 2-dimensional. As a increases from 0 to 0.5, the attractor deviates from this two-dimensional shape, which can be quantitatively measured by the correlation dimension. As $a \rightarrow 0.5$, the attractor structure stretches out more and more over the three-dimensional space. This type of enhanced diffusion in phase space seems to be a generic feature of frustration in chaotic systems, and has been reported previously in the case of Coupled Map Lattices [20].

The simulations also showed the robustness of the "frustrated" attractor. Starting from different initial conditions, the response system trajectory was found to converge to the same attractor structure. This indicates that even in the absence of exact synchronization with any of the driver systems, the response system trajectory can be used as a chaotic masking signal for secure communication [42]. This was verified by adding a small amplitude periodic signal (e.g., a sine wave of frequency $\omega = 1/200$) to the response system y-variable time series. The resultant time series appears to be devoid of any periodic component (Fig. 5.11, top). It is then used to drive another

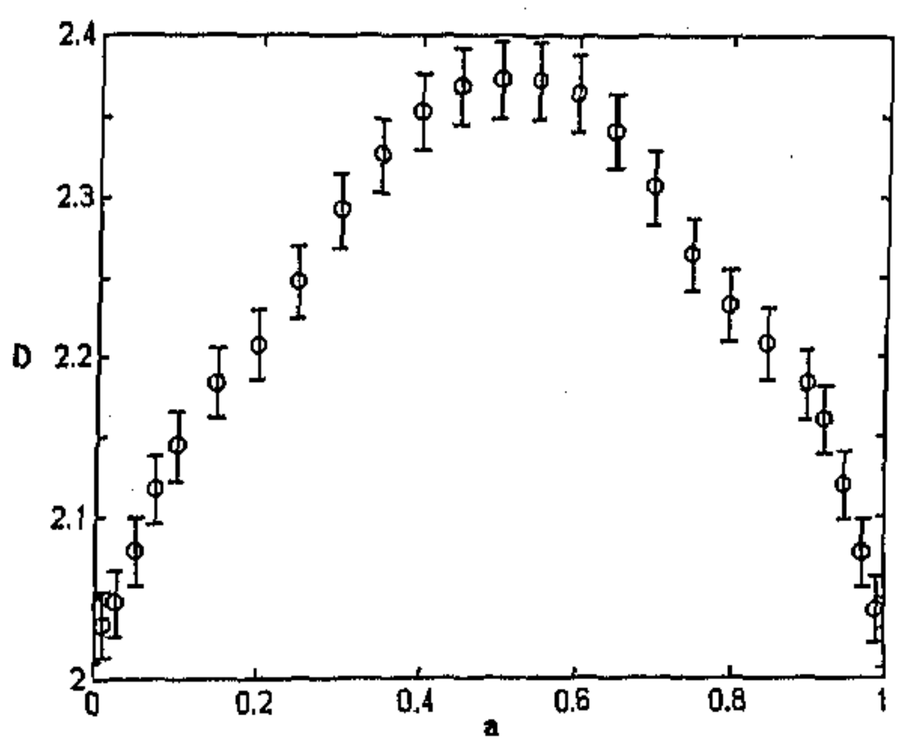

Figure 5.10: Correlation dimension of the response system attractor for $0 \leq a \leq 1$. The error is less than $\pm 10\%$.

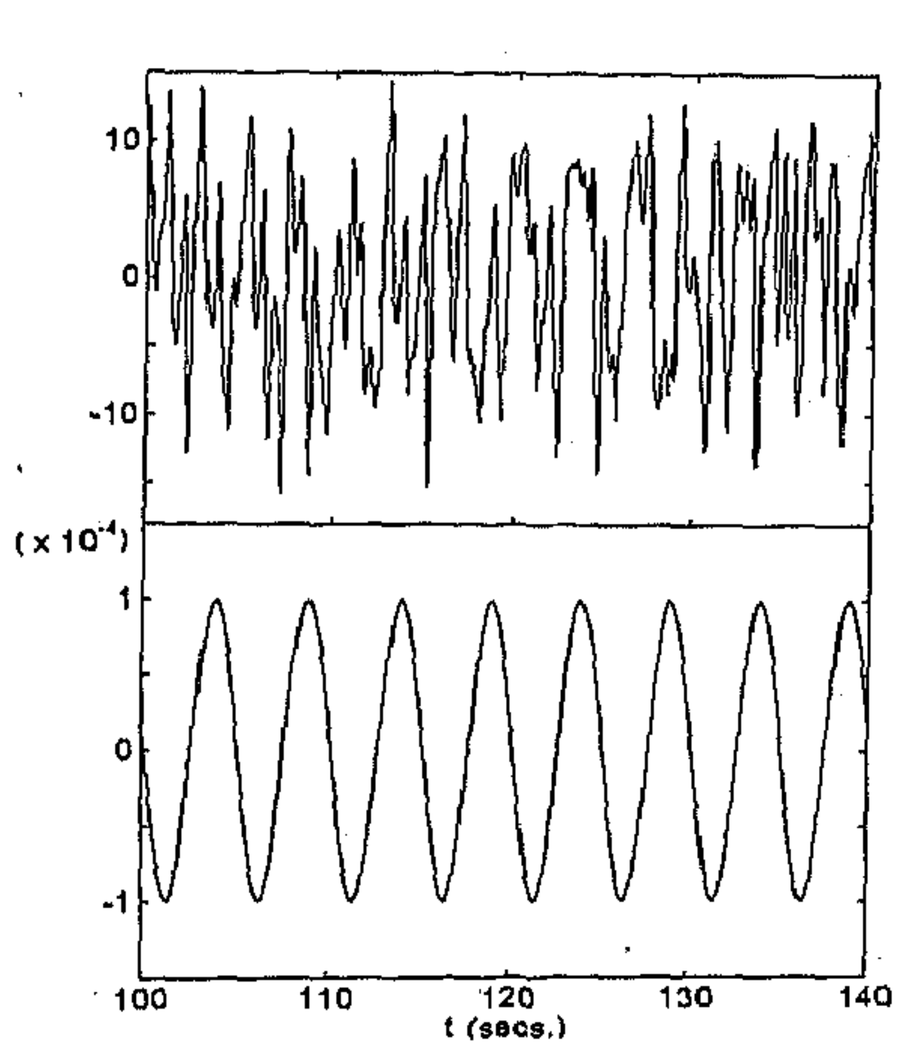

Figure 5.11: Chaotic masking: the x-variable time series of response system (top); the periodic signal obtained by subtracting the regenerated time series from the chaotic carrier wave (bottom).

Lorenz system, and the x-variable time series of the two systems are subtracted from each other to retrieve the original signal (Fig. 5.11, bottom). The modulation of the competition parameter,a, by a binary signal for chaotic switching, is another possibility of using the competitive scheme for secure communication.

5.5 Discussion

The competitive scheme described here for y-variable coupling was also implemented for x- and z-coupling of Lorenz systems. In the former, similar generalized attractor structure was observed, while in the latter, where the Pecora-Carroll synchronization does not work, no such structure could be observed. The work done here on coupled Lorenz systems can be extended to other systems defined by autonomous set of differential equations as well as discrete maps. However, it might be interesting to consider the result of competition in synchronizing non-autonomous systems (e.g., the Duffing oscillator). As such systems already have a forcing term present, which brings about the onset of chaos, the introduction of additional forcing terms can lead to qualitatively new behavior.

Competitive synchronization in extended systems might also lead to interesting phenomena. Lattices of (globally or diffusively) coupled chaotic elements, where each element can be used both to drive other elements, as well as respond to driving signals from yet another set of elements, and hence by a series of feedbacks drive its own driving systems, will serve to illustrate interactions between multiple competing synchronizing feedback loops. The motivation for such a study is that, in the human brain, synchronization of activity among different neurons appear to have an important functional role in the proper performance of perceptual tasks. It is to be noted that, single neurons are capable of chaotic behavior. As the brain is composed of densely connected networks of neurons, there is bound to be competitive synchronizing interactions between neural assemblies [193, 176]. A dynamic competition parameter, which causes synchronization-desynchronization transitions between various neural sub-assemblies, is a possible mechanism for information processing in biological systems. The resultant dynamics will be radically different from the one we are led to expect by observing the dynamics of single neurons or small groups of neurons.

The above work describes the simplest competitive scenario which can show a qualitatively different dynamics from that in the non-competitive situation. It is at present not known how the nature of synchronization and the attractor structure of the responding system might be altered by increasing the number of competing driver systems. In the brain, where each neuron is connected to $\sim 10^4$ other neurons, the competitive situation is bound to be far more complicated. The manner in which such an extremely competitive synchronization scenario might influence the way in which neural networks perform computations and process information is a very interesting problem for the future.

Chapter 6

Visual Information Processing with Excitatory-Inhibitory Networks

Upto now we have considered in detail only neural networks comprising a small number of processing elements, N - viz., the largest network examined so far, contains three excitatory and three inhibitory neurons (i.e., N = 6). This simplification has made it possible to investigate the properties of such networks as a function of several parameters, without making the attendant complexity too forbidding to allow any analysis. We shall now introduce relatively larger networks ($N \sim 10^4$) for the specific purpose of applying such systems to visual information processing. The specific tasks considered are those of segmentation and adaptive smoothing (followed by edge extraction), which form part of the phenomenon known as "early vision", the first stage in the visual processing path in the brain. At this level, the raw sensory data (intensity value) is the source from which the primitive features are obtained, to construct representations of objects present in the visual field. These are used by higher stages for further processing, ultimately leading to the act of "seeing". Several efforts have been made by the neural network community to model various aspects of vision. These models have been formulated at various levels of abstraction - from a detailed representation of the actual neurobiological structures employed for vision, to a phenomenological explanation. While low level processing can be investigated retaining a degree of fidelity to the biological apparatus, in the case of higher level processing, the enormous complexity of the neurobiological architecture (and the lack of complete understanding of the processes employed) forces one to invoke various simplification to model features such as object recognition [17] and visual memory [173].

In this chapter we have investigated certain features of early vision, using a couple of excitatory-inhibitory neural network models. The process of image segmentation, in particular, object-background segregation, has been examined with a network of

excitatory-inhibitory pairs, coupled over a local neighborhood. The other model introduced, has been inspired by the architecture of the retina and consists of three layers, comprising excitatory, inhibitory and excitatory elements respectively. It is used to implement adaptive smoothing on images - the resulting enhanced image being used for extracting edges.

The rest of the chapter is organized as follows: In Section 1, we have briefly reviewed some of the existing computational techniques used to implement "early vision" tasks, such as, segmentation and edge detection. In the next section, the network model used for dynamical segmentation of images is introduced. A theoretical analysis is presented for the case of an uncoupled network and results for different types of images are presented. In Section 3, we describe the three-layer network model used for adaptive smoothing. The results of applying the proposed method on a gray-level image are presented and compared with some existing techniques. Finally, we conclude with some comments on the relation of the models presented here to existing work reported in the image processing literature.

6.1 The problem of early vision

Early vision is the name given to that part of visual information processing where the principal features of an image are extracted (e.g., information concerning form, motion, color, etc.) and sent to higher brain areas for further processing. Although identification of the portion of the brain which is concerned with early vision is somewhat arbitrary (depending on an individual investigator's interpretation of the word 'early'), for our purpose we shall be concerned with the processing done in the *retina*. Note that, a considerable amount of processing appears to be involved before information from the photoreceptors in the eye reach higher visual centers in the brain, for further interpretation. It appears that this processing is done in subsequent stages so as to use the fewest possible number of active neurons to achieve an adequate representation of the stimulus. Such selective representations have the advantage of reducing considerably the volume of information that has to be propagated through the visual pathway, at any given time.

In this chapter, we shall be concerned with two specific tasks performed during early vision: (*i*) the detection of edges, and (*ii*) the segmentation of similar regions, in an image. We now briefly review a few existing techniques for achieving these objectives through computational means.

6.1.1 Edge detection

Edges are points of discontinuity in the gray level intensity values of an image - and hence, are local features, determined on the basis of local information. A large variety of edge detection methods are available in the image processing literature (e.g.

[118, 29, 23]). A good edge detector should be a filter with the following features:

- it should be a differential operator, taking either a first or second order spatial derivative of the image, and,
- it should be capable of being tuned to act at any desired scale (large filters for blurry edges and small ones to detect sharply focussed fine details).

The second requirement is very useful, as intensity changes occur at different scales in an image.

The simple differential operators used for edge detection are the first difference operators like Roberts gradient, Sobel gradient and Prewitt gradient and second difference operators like the Laplacian operator [64]. These not only respond to edges but also to isolated points. For a noisy picture, the Laplacian operator gives a higher response for noise than for a true edge, unless the noise has a low contrast. Marr and Hildreth [119] proposed the Laplacian of Gaussian (LOG) operator to alleviate this problem. To find intensity changes at a given scale, the image is first convolved with a two-dimensional Gaussian distribution with an appropriate standard deviation σ. This blurs the image, smoothing out all structures at scales much smaller than σ. The image is then filtered through a Laplacian operator and the zero-crossings obtained. The space described by the scale parameter σ and the zero-crossing curves is called the scale space.

Canny [29] has proposed an "optimal" edge detector in terms of good detection, good localization and single response. Good detection, i.e., low probability of detecting non-edges or not detecting the actual edges, is achieved by maximizing the signal-to-noise ratio (SNR), while, good localization (i.e. points marked as edges should be as close as possible to true edges) is achieved by maximizing the reciprocal of the (approximately) standard deviation of the displacement of edge points. Single response, i.e. one and only one response to a single edge point, is achieved by subjecting the optimal filter to a constraint that eliminates multiple responses. The Canny detector has been found to be extremely effective for a wide class of images. A neural network model implementation of Canny's method has also been reported [184].

All the edges produced by the operators discussed above, are normally not significant or relevant edges, when viewed by human beings. Therefore, one needs to extract prominent edges from the output of such edge detectors. Kundu and Pal [107] have suggested a method of thresholding, to extract the prominent edges, based on psychovisual phenomena.

6.1.2 Segmentation

Segmentation is an essential and important step of early vision [64]. It is a process of partitioning the image into some non-intersecting regions, such that, each region is

homogeneous and the union of no two adjacent regions is homogeneous. Segmentation may be formally defined as follows [139]:

> If F is the set of all pixels and $P(\quad)$ is a uniformity/ homogeneity predicate defined on groups of connected pixels, then segmentation is a partitioning of the set F into a set of connected subsets or regions $(S_1, S_2, ..., S_n)$ such that
>
> $$\cap_{(i=1)}^{n} S_i = F$$
>
> with $S_i \cap S_j = \emptyset, i \neq j$. The uniformity predicate $P(S_i)$ = true for all regions S_i, and $P(S_i \cup S_j)$ = false, when S_i, S_j are adjacent regions.

There are several approaches available for image segmentation. In addition to techniques based on histogram thresholding, edge detection, relaxation and semantic & syntactic approaches, several attempts have been made to develop segmentation methods using neural network models, particularly the Hopfield and Kohonen networks. Neural network based methods have the advantages of producing reasonable outputs even in highly noisy environments, as well as, generating results in real time.

Thresholding is an old and simple technique for image segmentation. It can be done based, either on global information (e.g. gray level histogram of the entire image), or on local information of the image. If only one threshold is used for the entire image, it is called global thresholding. On the other hand, when the image is partitioned into several sub-regions and a threshold is determined for each sub-region, it is referred to as local thresholding or adaptive thresholding. Thresholding techniques can also be classified into bi-level and multi-level thresholding. In the former case, the image is partitioned into two regions - object (say, black) and background (white). Thus, here thresholding can be viewed as a classification problem, with the pixels of the image being assigned to one of two classes: object and background. When the image is composed of several objects with different characteristics, one needs several thresholds for segmentation. This is multi-level thresholding.

Segmentation can also be obtained through detection of edges of various regions. A good strategy to produce meaningful segments would be to fuse region segmentation results and edge detector outputs.

Neural network based methods are attempts to achieve robustness with respect to random noise (or failure of processors) and to have real time output. Massive connectionist architecture makes the system robust while the parallel processing enables real time operation. Ghosh *et al* [61] used a Hopfield type network for extraction of objects from highly noise-corrupted scenes. The energy function of the network has been constructed in such a manner that in a stable state of the net, it extracts compact regions from a noisy scene.

6.2 The dynamical segmentation network

In this section, we investigate a model for performing bi-level image segmentation, comprising excitatory and inhibitory neurons, that are coupled to each other over a local neighborhood. The basic module of the proposed network is an excitatory-inhibitory neural pair. If x and y be the activities of the excitatory and the inhibitory elements respectively, then they evolve in time according to:

$$\begin{aligned} x_{n+1} &= F_a(w_{xx}x_n - w_{xy}y_n + I_n) \\ y_{n+1} &= F_b(w_{yx}x_n - w_{yy}y_n + I'_n), \end{aligned} \tag{6.1}$$

where, w_{ij} is the weight of synaptic coupling between elements i and j, F is the activation function defined by Eqn. (2.9) and I, I' are the external stimuli. By imposing the following restriction on the values of the synaptic weights:

$$\frac{w_{xy}}{w_{xx}} = \frac{w_{yy}}{w_{yx}} = k,$$

and absorbing w_{xx} and w_{yy} within a and b (respectively), we can simplify the dynamics to that of the following one-dimensional map:

$$z_{n+1} = F_a(z_n + I_n) - kF_b(z_n + I'_n). \tag{6.2}$$

Without loss of generality, we can take $k = 1$. In the following account we will be considering only time-invariant external stimuli, so that, for our purposes:

$$I_n = I'_n = I.$$

6.2.1 Analysis of response to constant magnitude external stimulus

We shall now consider how the dyanmics of the excitatory-inhibitory neural pair changes in response to external stimulus. Let us consider the isolated neural pair, whose time evolution is given by Eqn. (6.2). On replacing the expression of the transfer function from (2.9), we get

$$z_{n+1} = \exp(-b(z_n + I)) - \exp(-a(z_n + I)). \tag{6.3}$$

Now,

$$z_{n+1} = z_n = z^*$$

for a fixed point. It is stable if

$$\frac{dz_{n+1}}{dz_n} \geq -1,$$

i.e.,

$$(a - b)\exp(-a(z_n + I)) - bz_{n+1} \geq -1.$$

Therefore, for the fixed point to be marginally stable (i.e. $\frac{dz_{n+1}}{dz_n} = -1$), it must satisfy the following condition:

$$(a-b)\exp(-a(z^* + I_c)) = bz^* - 1, \tag{6.4}$$

where, I_c is the critical external stimulus for which z^* just attains stability. Let us define a new variable, α, as

$$\alpha = \frac{bz^* - 1}{a-b}. \tag{6.5}$$

Therefore, from (6.4), we get

$$\exp(-a(z^* + I_c)) = \alpha. \tag{6.6}$$

Also from (6.5),

$$z^* = \frac{1}{b} + \frac{1-\mu}{\mu}\alpha \tag{6.7}$$

where $\mu = b/a$. Now, from (6.3), a fixed point can be expressed as

$$z^* = -\exp(-a(z^* + I_c)) + \exp(-b(z^* + I_c)).$$

Therefore, from (6.6) and (6.7), the above expression can be written as

$$\alpha^\mu - \alpha = \frac{1}{b} + (\frac{1-\mu}{\mu})\alpha. \tag{6.8}$$

By simple algebraic manipulation, we get

$$\alpha = \frac{1}{b^{1/\mu}}(1 + a\alpha)^{1/\mu}. \tag{6.9}$$

Assuming $a\alpha << 1$, we need to consider only the first order terms in α in the right hand side, so that

$$b^{1/\mu}\alpha = 1 + \frac{a\alpha}{\mu}, \tag{6.10}$$

which gives the following expression for α:

$$\alpha = \frac{1}{b^{1/\mu} - \frac{a}{\mu}}. \tag{6.11}$$

For a real solution of z^* to exist, we must have $bz^* - 1 > 0$, since, otherwise, z^* will have an imaginary component (from (6.14)). In other words, $\alpha > 0$ (from (6.4)). Therefore, from (6.11), we must have

$$a < \mu b^{1/\mu}. \tag{6.12}$$

Since $b = \mu a$, we get

$$a > \mu^{\frac{\mu+1}{\mu-1}}. \tag{6.13}$$

For example, if $\mu = 0.5$, then $a > 8$, for z^* to be real. From (6.4) we get

$$\exp(aI_c) = \frac{a-b}{bz^* - 1}\exp(-az^*). \tag{6.14}$$

Taking logarithms on both sides, we have,

$$I_c = -z^* - \frac{1}{a}\log(\alpha).$$

Therefore replacing z^* from (6.7),

$$I_c = (\frac{\mu - 1}{\mu})\alpha - \frac{1}{\mu a} - \frac{1}{a}\log(\alpha). \tag{6.15}$$

The equation (6.15), together with (6.11), provides the critical value of the external stimulus, which leads the oscillatory neuron pair to a fixed stable state, subject to the restriction (6.13).

This expression can be further simplified. From (6.9), we can write

$$\mu\log(\alpha) = -\log(b) + \log(1 + a\alpha).$$

As before, assuming $a\alpha << 1$, we need to consider only the first order terms in α in the right hand side of the logarithmic expansion, which gives us

$$\log(\alpha) = \frac{a\alpha}{\mu} - \frac{1}{\mu}\log(b). \tag{6.16}$$

From (6.11), (6.15), and (6.16), the critical magnitude of the external stimulus is given as

$$I_c = \frac{1 - \frac{2}{\mu}}{(\mu a)^{1/\mu} - \frac{a}{\mu}} + \frac{1}{\mu a}\log(\frac{\mu a}{e}), \tag{6.17}$$

where $e = \exp(1)$. Fig. 6.1 shows the a vs. I_c curves for different values of μ, viz. μ=0.1, 0.25 and 0.5.

To make the network segment regions of different intensities ($I_1 < I_2$, say), one can fix μ and choose a suitable a, such that $I_1 < I_c < I_2$. So elements, which receive input of intensity I_1, will undergo oscillatory behavior, while elements receiving input of intensity I_2, will go to a fixed-point solution. Notice that, the curves obtained from Fig. 6.1 gives two values of a for the same I_c. This gives rise to an operational question: given a certain I_c, which value of a is more appropriate. Notice that the region of the a vs I_c curve, to the left of the maxima, has a very high gradient. This implies that, in the presence of wide variation in the possible value of I_c, choice of a from this region, will show very small variation - i.e., the system performance will be robust with respect to uncertainty in the determination of the appropriate value of I_c. This is possible in the case of any gray image, with a bimodal intensity distribution, having a long, almost uniform valley in between.

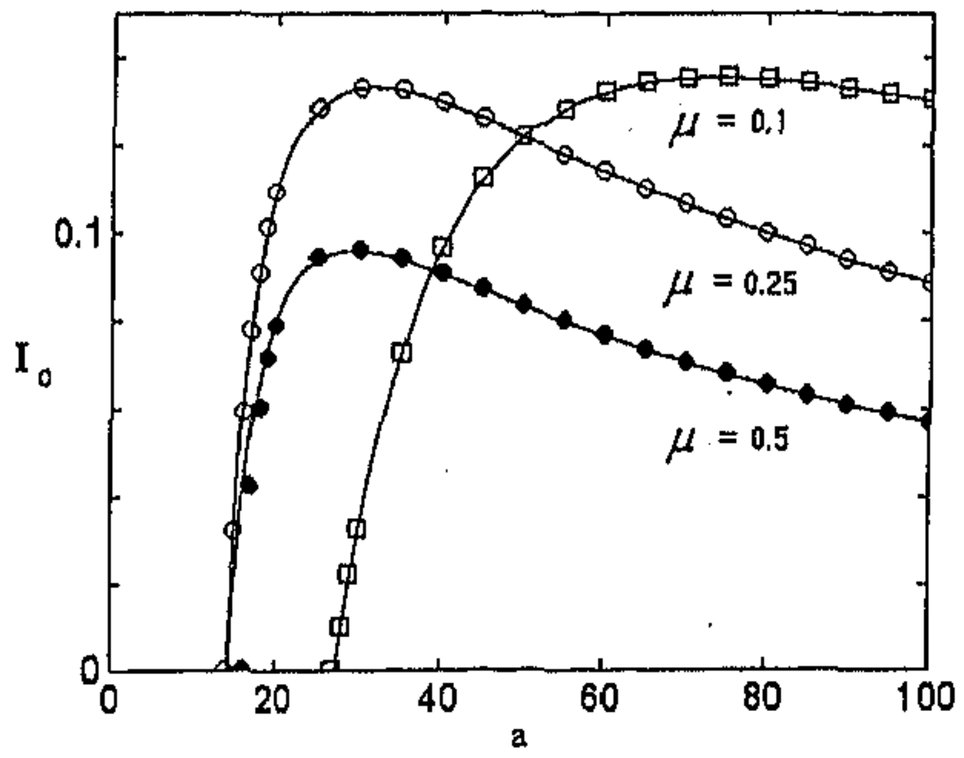

Figure 6.1: Critical magnitude (I_c) of the external stimulus, at which transition from periodic to fixed point behavior occurs. The circles (filled and blank) and squares represent the values obtained exactly through numerical procedures for $b/a = \mu =$ 0.5, 0.25 and 0.1, respectively. The curves indicate the theoretically predicted values.

On the other hand, the region of the curve to the right of the maxima has a very low gradient (almost approaching zero for high values of a). This implies structural stability in network performance, as wide variation in choice of a will give almost identical results. So, choice of a from this region is going to make the network performance stable against parametric variations. As both robustness against uncertain input, and, stability against parametric variations, are highly desirable properties in network computation, a trade-off seems to be involved here. The nature of the task in hand is going to be the determining factor of which value of a we should choose for a specific I_c.

6.2.2 The two-dimensional network

The introduction of spatial interactions over a local neighborhood in the above model produces some improvement in the segmentation performance. We have considered discrete approximations of circular neighborhoods [22] of radii r_{ex}, r_{in} $(r = 1, 2)$ in our simulations (Fig. 6.2).

There is an important feature to consider when choosing the neighborhoods of the excitatory and inhibitory neurons. Unless $r_{ex} < r_{in}$, the network activity becomes unstable owing to the unbounded increase in the activity of the excitatory elements. This is shown by looking at the averaged activity of the network $< z >_n = \frac{1}{N}\sum_{i=1}^{N} z_n(i)$, where $z(i)$ indicates the i-th excitatory-inhibitory neural pair (Fig. 6.3). For $r_{ex} \geq r_{in}$, $< z >$ shows an oscillatory behavior whose amplitude increases with n (Fig. 6.3 (b)). However, for the network to have stable behavior, the amplitude of the

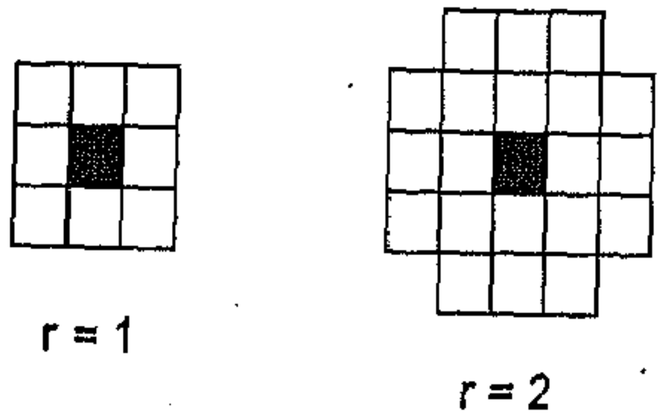

Figure 6.2: Discrete circular neighborhoods of radii $r = 1$ and $r = 2$.

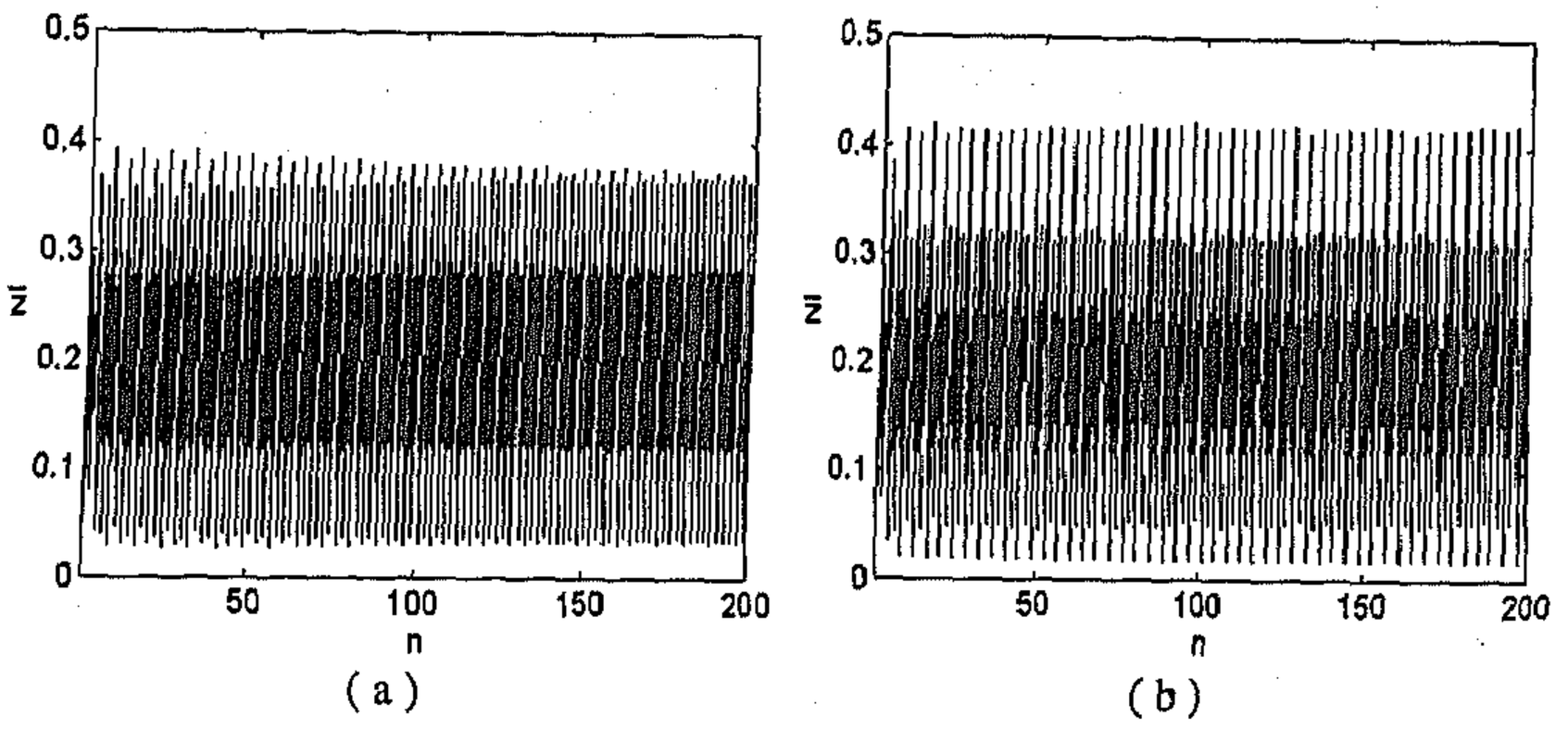

Figure 6.3: Average activity ($\bar{z}$) of a network of 100×100 elements, arranged in a two-dimensional plane, with coupling over a local neighborhood: (a) $r_{ex} = 1$, $r_{in} = 2$ and (b) $r_{ex} = 2$, $r_{in} = 2$.

oscillation should be constant in time. This is so for $r_{ex} < r_{in}$, as seen in Fig. 6.3 (a).

6.2.3 Simulation results

The network described above has been used to segment images, both synthetic and "real-life". The synthetic image chosen is that of a square of intensity I_2 (the "object") against a background of intensity I_1 ($I_1 < I_2$). Uniform noise of intensity ϵ is added to this image. The signal-to-noise ratio (SNR) is defined as the ratio of the range of gray levels in the original image to the range of noise added (given by ϵ). The image is then presented to the network, which is made to undergo 200 - 300 iterations. Afterwards, the elements which remain unchanged over successive iterations

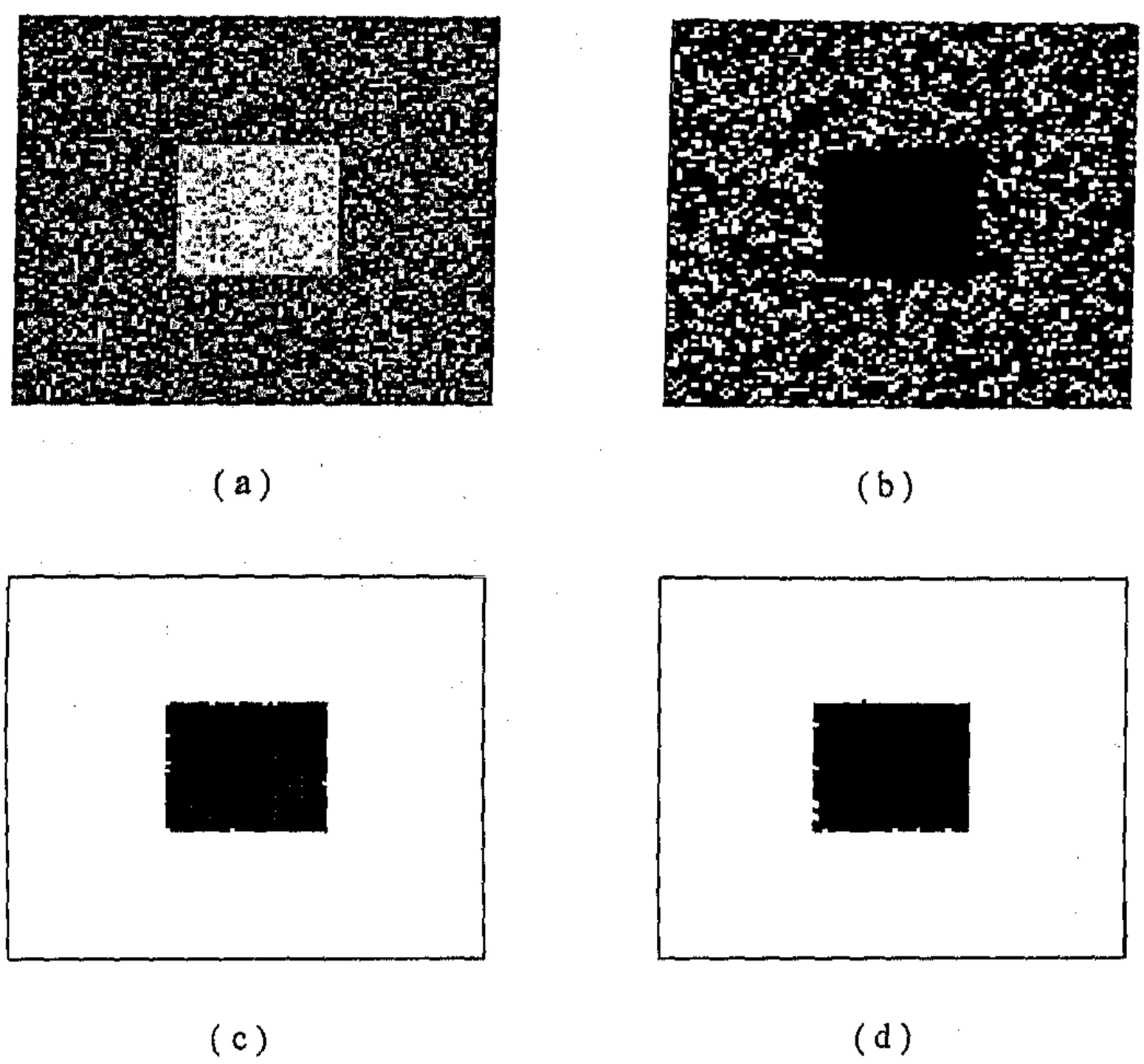

Figure 6.4: Results of implementing the proposed segmentation method on noisy synthetic image: (a) original image, (b) output by the uncoupled network, (c) output by the coupled network ($r_{ex} = 1, r_{in} = 2$), and (d) output by the coupled network ($r_{ex} = r_{in} = 2$), after 200 iterations (a=20, b/a=0.25 and threshold th=0.02).

(within a tolerance value, th) are labeled as the "object", the remaining being labeled the "background". For SNR = 1, the results of segmentation are shown in Fig. 6.4. Results for $r_{ex} = 1, r_{in} = 2$ and $r_{ex} = r_{in} = 2$ are shown. The two architectures show very similar segmentation results, at least upto the iterations considered here, although the latter is unstable (as discussed in the previous section). Excepting for the boundary of the "object", which is somewhat broken, the rest of the image has been assigned to the two different classes quite accurately.

We have also considered the 5-bit gray level "Lincoln" image as an example of a "real-life" picture. A suitable I_c has been estimated by looking at the histogram of the gray-level values, and taking the trough between two dominating peaks as the required value. Following the same procedure, as in the synthetic image, we have segmented the image. The results are shown in Fig. 6.5. Most of the image has been labeled accurately, except for a few regions (e.g., near the neck).

Note that, we have considered a single value of a (and hence I_c) for the entire image. This is akin to "global thresholding". By implementing local thresholding and choice of a on the basis of local neighborhood information, the performance of the network can be improved.

6.3 The retinal processing model

We next proceed to investigate image enhancement through adaptive smoothing in an excitatory-inhibitory network, followed by edge extraction from the processed image. The model used for this purpose has been inspired by the neural architecture of the retina.

6.3.1 Structure of the retina

The retina is where the physical image of a visual scene is converted to a neural representation, on being projected onto a receptor array. It is a thin sheet of neural tissue lining the rear hemisphere of the eyeball, being a projection of the brain itself. The basic design of a retina involves three interconnected layers and five broad classes of neurons: photoreceptor, bipolar, horizontal, amacrine and ganglion cells (Fig. 6.6). In all vertebrate retinas, the transformation from optical to neural image involves three stages [185]:

- phototransduction by a layer of receptor neurons,
- transmission of their signals by chemical synapses to a layer of bipolar neurons, and,
- transmission of these signals by chemical synapses to output neurons (ganglion cells).

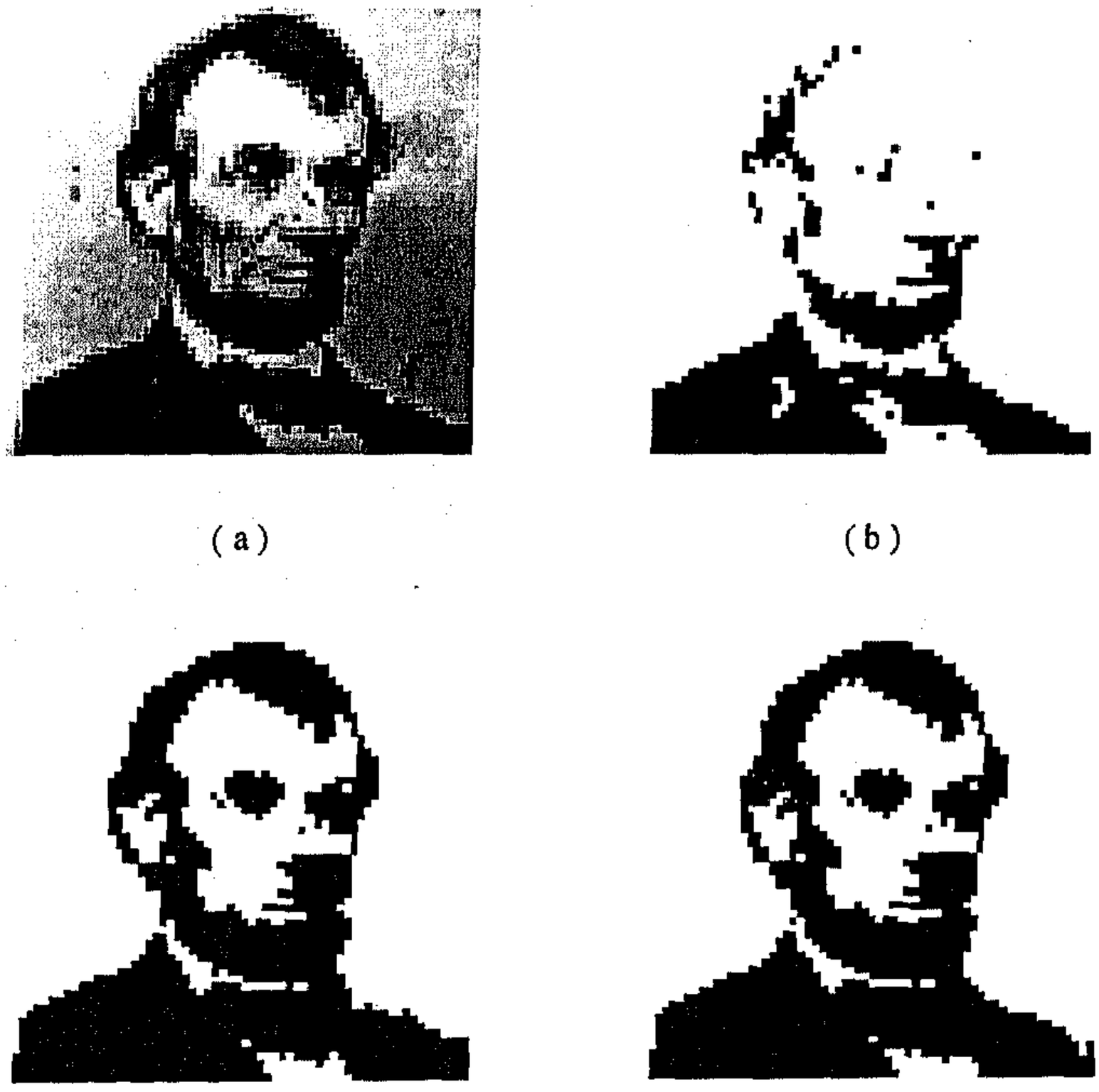

(a) (b)

(c) (d)

Figure 6.5: Results of implementing the proposed segmentation method on "Lincoln" image: (a) original image, (b) output by the uncoupled network, (c) output by the coupled network ($r_{ex} = 1, r_{in} = 2$), and (d) output by the coupled network ($r_{ex} = r_{in} = 2$), after 300 iterations (a=30, b/a=0.25 and threshold th=0.02).

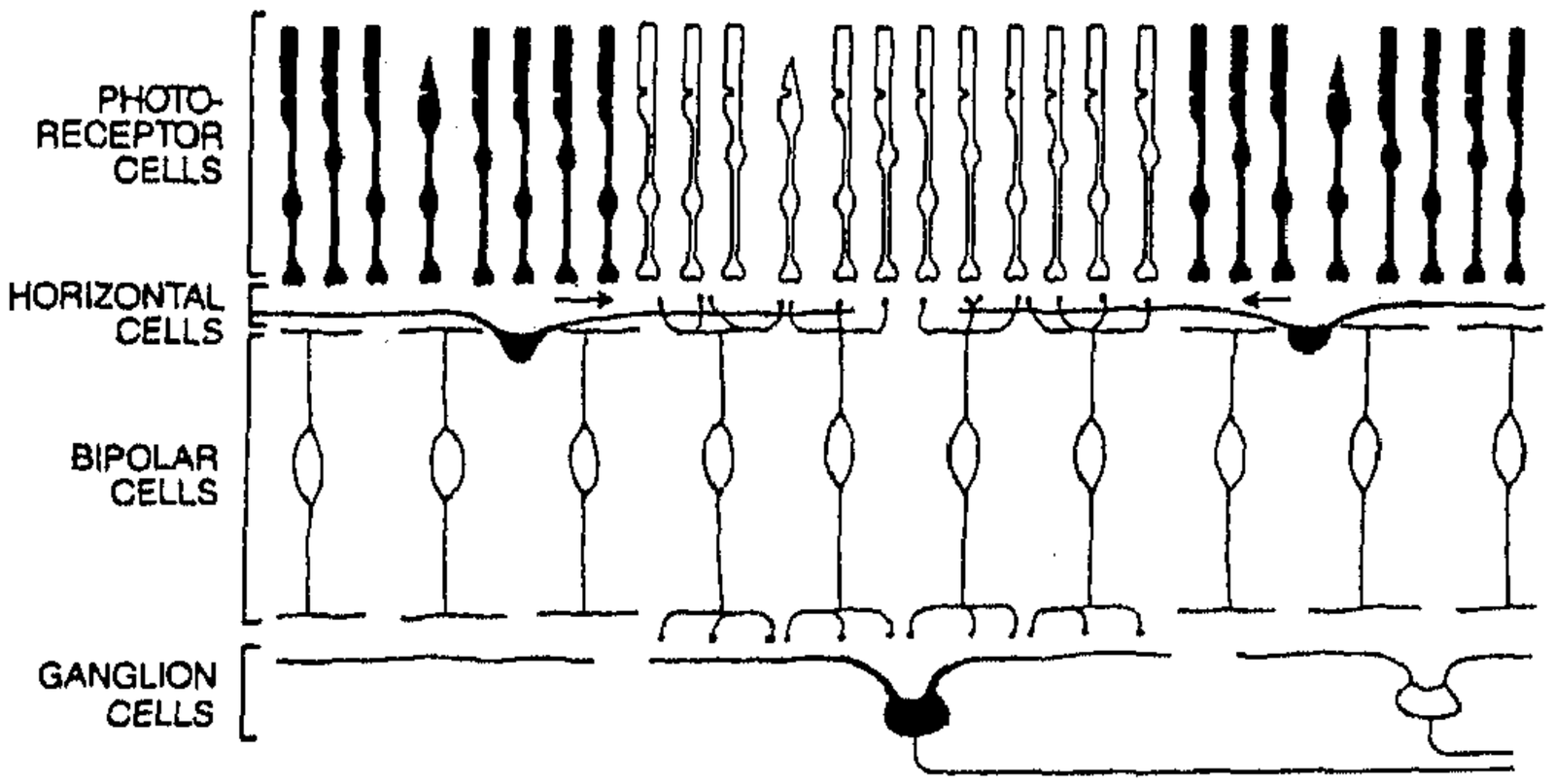

Figure 6.6: Structural organization of the retina. (Adapted from R. H. Masland, "The functional architecture of the retina", *Sci. Am.* **255**(6), 102-111 (1986).)

Synaptic connections in the retina are confined to two distinct zones: the outer plexiform layer (OPL) and the inner plexiform layer (IPL). The OPL contains the axon terminals of rods and cones, the dendritic processes of bipolar cells and the processes of horizontal cells. The IPL comprises the axon terminals of bipolar cells, the processes of amacrine cells and the dendrites of ganglion cells.

The two structurally similar systems of lateral interactions, at the OPL and the IPL, mediated by the horizontal and amacrine cells, respectively, modulate the signal transmitted along the input-output pathway. These interactions, which are inhibitory in nature [203], play an important role in retinal response, as they implement the process of *lateral inhibition*. This process is observed in a large variety of neural systems, whereby the stimulation of a neuron leads to the inhibition of other neurons lying in the surrounding area. Lateral inhibition in sensory systems has important functional significance, since, it provides for an enhancement of the acuity by increasing the contrasts of the pattern of the message carried to the brain [76, 137]. The modulation of the local input-output pathways due to the lateral interneurons (on the basis of an average signal received over a broad area) is used by the retina to adjust its operating characteristics to prevailing light conditions [200, 201, 178]. This ensures the generation of a high-contrast visual image. In this work, we have focussed on the interactions at the OPL, responsible for producing a high contrast response to visual stimuli.

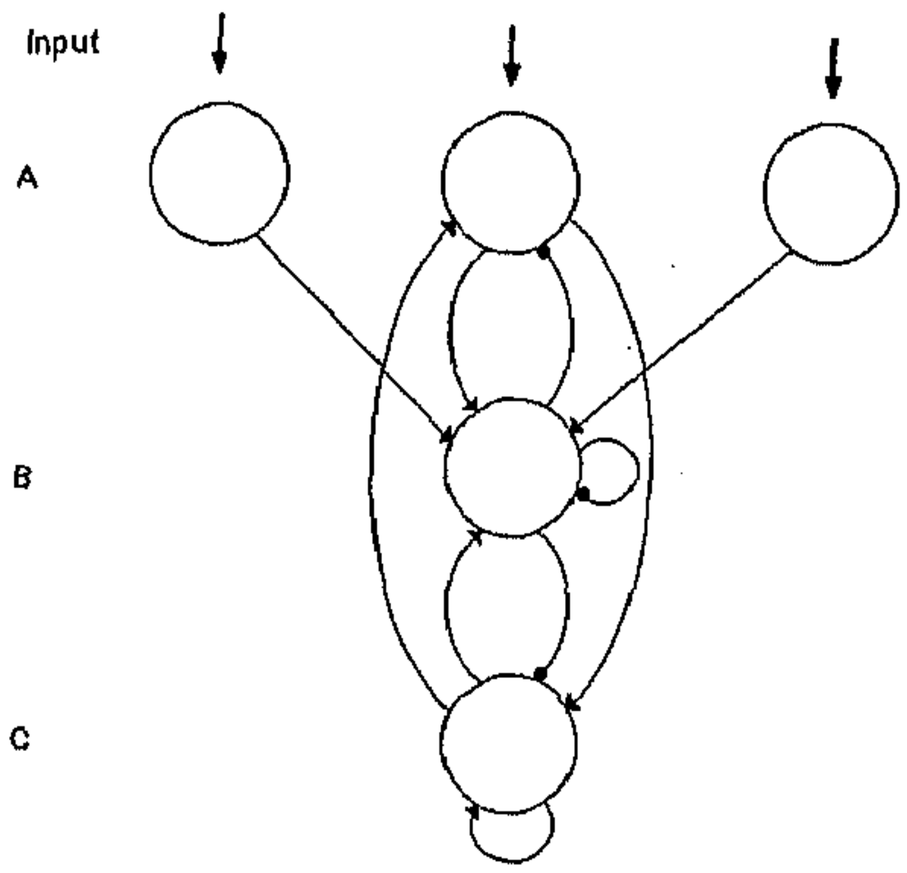

Figure 6.7: An excitatory-inhibitory neural network model for retinal information processing. Layers A, B and C correspond to the photoreceptor, horizontal cell and bipolar cell layers of the retina. Arrows indicate excitatory connections, while circles represent inhibitory synaptic couplings.

6.3.2 The model

A model comprising three layers of excitatory, inhibitory and excitatory elements (respectively), with anti-symmetric, sigmoid activation function, has been used to investigate the visual processing done in the outer plexiform layer of the retina. Figure 6.7 shows the arrangement of the network. Layers A and C consist of excitatory elements, while, layer B is composed of inhibitory elements. They correspond to the photoreceptor, horizontal cell and bipolar cell layers of the retina, respectively. The dynamics of the network is governed by the following set of equations:

$$x_{n+1} = F_b(I), \tag{6.18}$$

$$y_{n+1} = F_b(x_n + z_n - y_n - \lambda(x_n + z_n - \Sigma_{j\in R} y_n^j)), \tag{6.19}$$

$$z_{n+1} = F_a(x_n + z_n - y_n - \lambda(x_n + z_n - \Sigma_{j\in R} y_n^j)). \tag{6.20}$$

Here R indicates the local neighborhood in layer B, over which lateral connections are considered. In our simulations for a two-dimensional network, R is the 3×3 neighborhood around a given element. The external input to the network is denoted by I, while, the parameter, λ, controls the relative weightage of the lateral interactions. The activation functions, F, are given by Eqn. (2.10).

Initially (i.e. at $n = 0$), the input I is taken to be the input image, while x, y, z are all set equal to zero. The input image is then withdrawn, so that for all subsequent iterations, I, and hence, x, is zero. Therefore, for $n > 0$, if we neglect the lateral

interactions (i.e., $\lambda = 0$), the dynamics of the network reduces to that of the one dimensional map:

$$\xi_{n+1} = F_a(\xi_n) - F_b(\xi_n),$$

where, $\xi = z - y$. This is the map representing the dynamics of a single excitatory-inhibitory neural pair, that has been analyzed in Chapter 2. The additional features of the network that shall be reported here are, therefore, purely the result of lateral interactions.

The effect of the lateral interaction term is to enable computation of the local gradient of the intensity values in an image. This is used to generate an output, which is then added to the existing image. The result is *adaptive smoothing* [1] of the image. Note that, λ necessarily has to be small, as otherwise, the network becomes unstable, and the activity becomes spatially uniform.

The mechanism by which adaptive smoothing is implemented in the present model, can be easily understood by looking at the map governing the dynamics of an excitatory-inhibitory pair with sigmoid activation functions (Fig. 2.11). In the present context, the input is the gradient of the image. For edge regions, where the gradient is high, the resultant output is low, implying that there will be little or no change in these regions. However, isolated discontinuities, which are not part of any edge, also give high gradients. As a result of the selective smoothing process, they will be maintained almost unchanged, degrading the performance of the method. This can be avoided by decreasing b (keeping a fixed), which increases the output value of the map for high values of the gradient. Therefore, there will be smoothing of points having a very high gradient value.

Let us now consider the smooth regions of the image, for which the gradient is low. The neural map, considered above, gives a very high output value for these regions. Any small inhomogeneity present in these regions is, therefore, rapidly smoothed out. As the peak value of the map is a function of the parameter, a (with b fixed), the extent of smoothing is governed by the magnitude of a - i.e., a desired degree of smoothing can be obtained by a suitable choice of a.

6.3.3 Simulation results

The proposed model has been used to implement adaptive smoothing in several gray-level images, an example being shown in Fig. 6.8 (a). The results of adaptive smoothing is shown for various parameter values in Fig. 6.8 (b – d). The process was carried out for 30 iterations for all the parameter values considered. As is clear from the results, increasing the parameter a results in enhanced smoothing of the image, while, increasing b has the effect of increasing the gradient of isolated discontinuities of the image. This is in accordance with the qualitative understanding of the network behavior outlined previously.

[1] Adaptive smoothing is a nonlinear filtering mechanism that can achieve edge-preserving smoothing of an image [151]

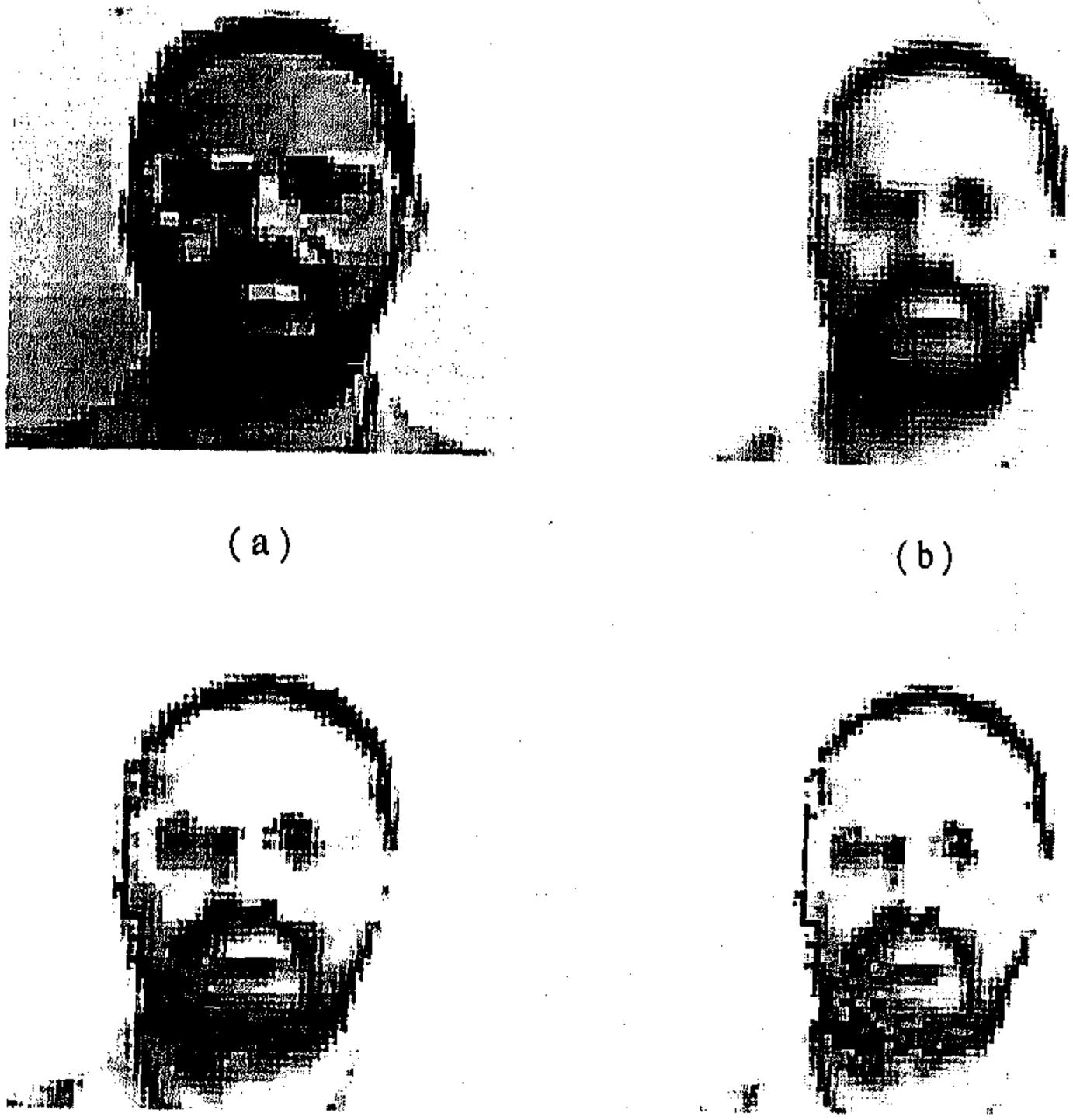

(a) (b) (c) (d)

Figure 6.8: Results of implementing the proposed adaptive smoothing method on "Uma" image: (a) original image, (b) output by the model with a=20, b=5, (c) output by the model with a=10, b=5, and (d) output by the model with a=10, b=8, after 30 iterations (λ=0.01). It is evident that increasing a produces greater blurring of the final image, while increasing b leads to enhancement of isolated discontinuities.

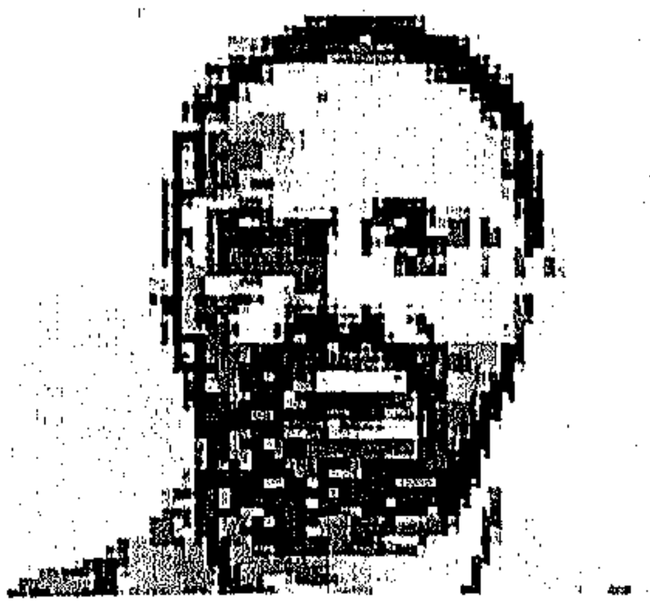

(a)

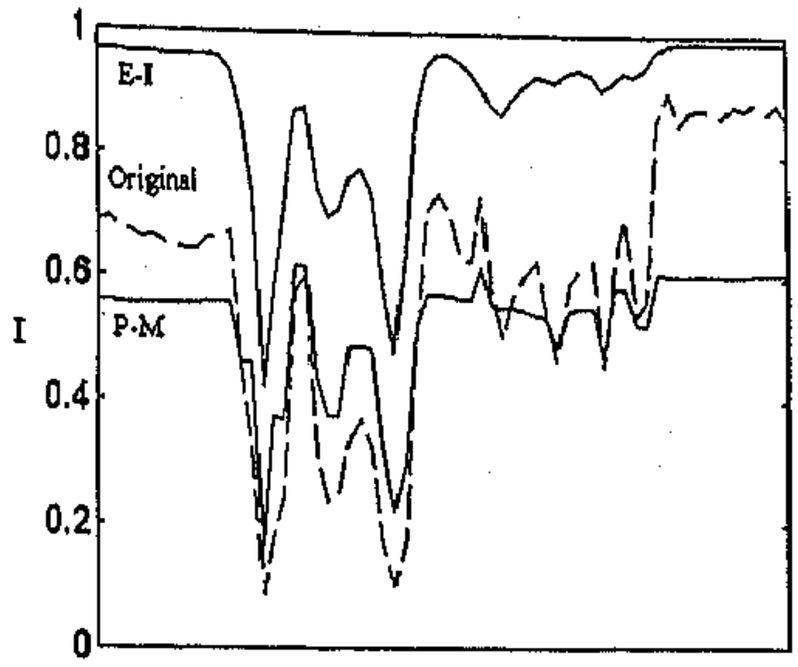

(b)

Figure 6.9: Comparison with Perona-Malik method: (a) output by the Perona-Malik variable conductance diffusion method, and (b) the relative smoothing of a one-dimensional signal extracted from "Uma" image by considering the 32nd row. The broken line shows the original signal, while outputs by the Perona-Malik method (P-M) and the proposed model (E-I) ($a = 10$, $b = 5$, $\lambda = 0.01$) are shown with solid curves (the intensity values have been scaled to lie in (0,1)).

We have compared the proposed method with the variable conductance diffusion (VCD) method proposed by Perona and Malik [144] in Fig. 6.9. As can be seen clearly, isolated points having a high local gradient have been enhanced by the VCD method, leading to a speckled image. By extracting a one-dimensional signal from the image (viz. the 32nd row) we demonstrate the relative performance of the VCD method and the proposed method. While the former seems to enhance small local discontinuities (which may be only due to noise), the latter retains the broad features of the original signal, while averaging out smaller discontinuities, thus giving a smoother image.

The output of the adaptive smoothing process has been used for extraction of edges by using a conventional gradient thresholding technique. Note that, alternatively, an extra pair of excitatory-inhibitory layers can also be used for this purpose. This is because, as mentioned earlier, the interaction between excitatory and inhibitory neurons results in the gradient of the intensity values of an image to be obtained. In Fig 6.10, the edges obtained from the output image of the proposed method is compared with the results of applying the Canny operator method [29] on the original image. No post-processing technique, such as thinning or linking, has been applied. The performance of the two methods appear to be comparable, although the former method leads to a few broken edges.

(a) (b)

Figure 6.10: Performance in edge extraction: edges obtained from the "Uma" image on implementing (a) *Canny's method* and (b) the proposed model ($a = 10$, $b = 5$).

6.4 Discussion

The segmentation of images, through dynamical activity in neural network models, have been investigated previously by a number of researchers [68, 181, 183, 70, 194, 156, 195, 28, 73]. However, all these efforts had been confined to using synchronization and desynchronization of oscillatory activity among neural assemblies. We have instead, concentrated on using *stimulus induced transitions* from periodic to fixed point behavior, in order to segment images. As Malsburg [194] has indicated, the reason oscillatory synchronization has been studied so far, as a mean of segmenting sensory stimuli, is its relative ease of analysis. However, with the developments in nonlinear dynamics and chaos theory, we can approach the problem of sensory segmentation using more general dynamical behavior.

The adaptive smoothing method proposed in this chapter is similar to the variable conductance diffusion method discussed in the image processing literature [144, 131, 21]. Although the continuous space version of this method, expressed in terms of partial differential equations, is ill-posed [32, 202], the discretised version appears to be quite robust [199]. As the proposed model is based on a discrete lattice of elements, a relation with discrete scale space methods [111] may not be far-fetched. However, this is an area for future investigation.

Chapter 7

Conclusions

The spirit within nourishes, and mind instilled
Throughout the living parts activates the whole mass
And mingles with the vast frame.
Virgil

Life is not so simple, man!
B. Uma Shankar

We have presented in this thesis some results of investigations, both theoretical and computational, which demonstrate some of the features of simple networks of excitatory and inhibitory neuron-type elements. The main goal was to study the behavior of the simplest network model capable of producing chaotic behavior. Initially, a single pair of an excitatory and an inhibitory neuron is described and analyzed in detail. Then small networks of such pairs are studied in the context of control and synchronization of their activity. Finally, an attempt is made to utilize such networks for some image processing tasks, specifically, segmentation and adaptive smoothing.

In the following section, the most important results are briefly summarized, while the final section provides an outlook to further problems which can be looked at in the future, as an extension to the investigation reported here.

7.1 Summary of Main Results

- The intrinsic properties of an excitatory-inhibitory neural pair have been studied with four types of nonlinear activation functions, distinct from each other in terms of their (*i*) asymmetric or anti-symmetric nature and (*ii*) sigmoid or piecewise linear characteristics. Fixed point, oscillatory and chaotic behaviors have been found to occur for various parameter values for these different types of functions, leading to the conclusion that this wide range of dynamics is a generic feature of excitatory-inhibitory neural pairs, evolving in discrete time.

- In addition to generic features, behavior specific to each type of transfer function has also been observed. For example, in the case of the piecewise linear functions, the presence of border-collision bifurcations and multifractal fragmentation of the phase space are noted. Neural pairs with sigmoidal activation functions exhibit a period-doubling route to chaos, which is an universal feature of unimodal one-dimensional chaotic maps [134, 188]. The anti-symmetric activation functions show a transition from symmetry-broken chaos (with multiple coexisting but disconnected chaotic attractors) to symmetric chaos (when only a single chaotic attractor exists).

- Varying a *threshold/ bias* parameter or equivalently, introducing a constant amplitude external stimulus, leads either to transition between chaos and periodic behavior or to coexistence of multiple attractors, depending on the nature of the variation. In the case of anti-symmetric functions, this causes previously distinct attractors to be dynamically connected. *Hysteresis* effect, a possible mechanism for short-term memory, is observed as the parameter is varied.

- Networks composed of elements having piecewise linear activation functions are found to be amenable to analytical treatment under some simplifying assumptions. This makes the resultant dynamics effectively equivalent to that of an one-dimensional piecewise linear map with multiple "folds". These "folds" permit the creation and maintenance of localized coherent structures within a global chaotic activity. This is of relevance to the use of such networks for information processing. Applications to problems of auto-associative recall, pattern classification, nonlinear function approximation and periodic sequence generation are outlined. This serves to indicate the versatility of such networks and possible areas where they maybe successfully used.

- In the presence of low-amplitude, low-frequency external stimulation, the chaotic neural pair with anti-symmetric activation function is found to exhibit a type of *nonlinear resonance* phenomenon, which can be looked upon as a deterministic analogue of "stochastic resonance" (SR) [59]. By introducing a piecewise linear system to study this phenomenon, a detailed understanding of the resonance process is obtained. The chaotic trajectory of the system is found to switch between two halves of the phase space at a rate which 'resonates' with the frequency of an externally applied periodic perturbation (both multiplicative and additive). By periodically modulating the parameter at a specific frequency, we observe the existence of resonance where the response of the system (in terms of the residence-time distribution) is maximum. The possible application of nonlinear resonance for the enhancement of subthreshold signals is indicated by showing that the excitatory- inhibitory neural pair shows similar resonance behavior when the external input is a small amplitude periodic signal. The "characteristic frequency" at which the system response is maximum is obtained explicitly in terms of the network parameters, in the case of the piecewise linear activation function. It is found that as the amplitude of

the signal increases, the response of the system also increases up to a limit. An expression for the "critical signal amplitude", above which the response saturates, is also obtained.

- Control mechanisms for the chaos observed in excitatory-inhibitory neural pairs have been studied. Two types of control have been proposed: (*i*) proportional variable feedback and (*ii*) small-amplitude periodic forcing. A physical understanding of the control mechanism is obtained in the case of a single excitatory-inhibitory pair. Control of a 3-neuron pair network has been studied through computer simulations. A possible connection between undesirable stabilization of periodic cycles by external periodic stimulus and the phenomenon of epileptic hallucination is suggested.

- Collective dynamics and synchronization of small assemblies of neural pairs are analyzed. Both unidirectional and bidirectional couplings between the neural pairs have been studied. For bidirectional coupling, intermittent synchronization is observed in the case of two coupled neural pairs, while the case of three coupled neural pairs show the more interesting feature of "mediated" synchronization. For unidirectional coupling, the phenomena of "frustrated synchronization" has been studied in detail. The well-known Lorenz system of equations has been used as a model system for ease of theoretical analysis. A 'desynchronization' parameter has been defined, which shows a scaling relation with the scaled coupling parameter.

- The utility of chaotic dynamics in certain image processing tasks such as, segmentation and adaptive smoothing, has been studied. A two-dimensional network of locally coupled excitatory-inhibitory pairs is used to study *segmentation.* Bilevel segmentation is achieved through different dynamical responses of neural pairs corresponding to "object" and "background". An approximate expression for the critical input stimulus magnitude, that leads to transition between the two different dynamical responses, is obtained in the case of an isolated neural pair. Noisy, synthetic images as well as "real-life" images are used to show the effectiveness of the segmentation procedure.

- *Adaptive smoothing* of gray-level images is achieved with a three layer network of excitatory, inhibitory and excitatory neurons, respectively. The output of this network is then used to find the edges of the input image by using a standard difference operator. The network has been used on several "real-life" images, and the results compare favorably to those of some standard methods of edge detection. The network architecture has been inspired by the structure of the outer plexiform layer of the retina and it has been proposed as a model for retinal information processing.

7.2 Outlook

In this work, we have stressed on 'simple' network models: 'simple' not only in terms of the size of the networks considered when compared to the brain (consisting of $\sim 10^{11}$ neurons and $\sim 10^{15}$ synapses), but 'simple' also in terms of the properties of the constituent elements (i.e., the 'neurons') themselves, in that, most of the physiological details of real neurons are ignored. Biological neurons are far more complicated, and a lot of computation is achieved at the level of the single neuron itself [105].

The point is to see what is essential and what is unnecessary detail for the proper functioning of biological neuronal networks. To do that one has to throw away as much of the complexity as possible to make the model tractable - while at the same time retaining those features of the system which make it interesting. So, while our modeling is indeed inspired by neuroscience, we are not concerned with actually mimicking the activity of real neuronal systems.

Our prime concern is what functional role chaos might be playing in the brain. As the brain itself is still a relatively poorly understood system, we have instead tried to look at what *artificial* networks can do with chaos. Hopefully, this will give us a clearer understanding of how chaos might actually be used in the brain to perform cognitive tasks. By resorting to a simple model, where we can perform detailed theoretical analysis, we can obtain a deep understanding of its behavior. This can then be used fruitfully to study the more complex entity, that is the brain.

In the work reported here, many interesting features were observed. However, to see their relevance to the actual biological situation, we have to make a connection between our results and the behavior of the brain. Such attempts have already been made, as for example, in Chapter 4, where, undesired control of neurobiological chaos is sought to be connected to the phenomenon of epileptic hallucinations. However, to take these efforts further, the complexity of the model needs to be increased systematically in a step-by-step manner, with detailed analysis of the new features thus revealed, in each step of the way.

For example, in this work we have been concerned exclusively with 'neurons' evolving in discrete time intervals. Biological neurons are better modeled by differential equations which evolve in continuous time. However, this is not really a limitation as any N-dimensional discrete-time dynamical system may be related to a corresponding $(N+1)$-dimensional continuous-time dynamical system through the concept of *Poincare sections* [188]. It follows that the discrete-time model we have studied has a higher dimensional differential equation analogue, which will show qualitatively similar behavior. Several differential equation models already exist which describe the activity of single neurons, with varying degrees of fidelity. A popular model which is biologically motivated and yet simple enough for ease of analysis is the Bonhoeffer-van der Pol (BVP) system of equations. Such systems have been shown to exhibit chaos when subjected to forced oscillations of specific amplitude and frequency [148].

However, large networks of BVP or similar systems have, as yet, not been studied in detail. Investigation of the collective behavior of such continuous-time neural network models, and linking the results to those reported here, should go a long way in establishing the genericity of our findings.

Real biological systems reside in an extremely noisy environment. This is incorporated in neural models by using stochastic updating rule and/or explicit introduction of a term representing external noise. The former can be represented as a form of multiplicative noise, whereas the latter is a strictly additive form of noise [192]. Physiologically, additive noise may originate from threshold fluctuations of a dendritic potential, while multiplicative noise could be due to stimulus-induced stochastic release of vescicles, containing neurotransmitter chemicals, from the synapses. We plan to introduce similar features in our model in the future. In dissipative chaotic systems, the effect of external noise seems to be limited to destroying the fine structure of the bifurcation sequence [41]. The interaction of deterministic chaos and stochastic noise in the network will be interesting to study.

One important point not addressed here is the issue of *learning*. The connection weights $\{ W_{ij} \}$ have been assumed constant, as they change at a much slower time scale compared to that of the neural activation states. However, modification of the weights due to learning will also cause changes in the dynamics. Such bifurcation behavior, induced by weight changes, will have to be taken into account when devising learning rules for specific purposes. The interaction of chaotic activation dynamics at a fast time scale and learning dynamics on a slower time scale might yield richer behavior than that seen in the present model [47]. The first step towards such a program would be to incorporate time-varying connection weights in the model. In [196], time-dependence of a suitable system parameter was shown to give rise to interesting dynamical behaviors, e.g., transition between periodic oscillations and chaos. This suggests that varying the environment can facilitate memory retrieval if dynamic states are used for storing information in a neural network. The introduction of temporal variation in the connection weights, independent of the neural state dynamics, should allow us to develop an understanding of how the dynamics at two time-scales interact with each other.

Parallel to this we have to look at the *learning dynamics* itself. Freeman [54], among others, has suggested an important role of chaos in the Hebbian model of learning [84]. This is one of the most popular learning models in the neural network community and is based on the following principle postulated by Hebb [84] in 1949:

> When an axon of cell A is near enough to excite cell B and repeatedly or consistently takes part in firing it, some growth process or metabolic change takes place in one or both cells such that A's efficiency, as one of the cells firing B, is increased.

According to the principle known as *synaptic plasticity*, the synapse between neurons A and B increase its "weight", if the neurons are simultaneously active. By

invoking an "adiabatic approximation", we can separate the time scale of updating the connection weights from that of neural state updating. This will allow us to study the dynamics of the connection weights in isolation.

The final step will be to remove the "adiabatic approximation", so that the neural states will evolve, guided by the connection weights (as studied in the thesis), while the connection weights themselves will also evolve, depending on the activation states of the neurons, as:

$$W_{ij}(n+1) = \mathcal{F}_\epsilon(W_{ij}(n), X_i(n), X_j(n)),$$

where $X(n)$ and $W(n)$ denote the neuron state and connection weight at the nth instant, $\mathcal{F}$ is a nonlinear function that specifies the learning rule, and ϵ is related to the time-scale of the synaptic dynamics. The cross-level effects of such synaptic dynamics interacting with the chaotic network dynamics might lead to significant departure from the overall behavior of the network described here.

The proposed extensions and modifications of the neural network model presented here will most probably lead to behavior yet unexpected. Considering that the model already exhibits such complex behavior, the incorporation of the details suggested above should provide results, which will be comparable to actual neurobiological data.

On a broader front, chaos may play a substantial role in resolving the *stability-plasticity dilemma* that confronts a wide range of complex adaptive systems, including neural networks. This dilemma can be framed in terms of the following questions:

- How can a learning system be designed to remain plastic (adaptive) in response to significant events and yet remain stable in response to irrelevant events ?
- How does the system know when to switch between its stable and plastic modes to achieve stability without rigidity and plasticity without disorder ?

Transitions between chaotic and ordered behavior are a general feature of complex adaptive systems and form the subject matter of the recently emerged discipline of Artificial Life (A-Life). It studies how local rules of interaction between elements of a complex system can give rise to collectively emergent global behavior of the system. This phenomena has been studied in the relatively simple system of cellular automata (CA) models by Langton [109]. CA are rule driven systems, defined by specifying the transformation rules that map a given initial state of the system to the final state. They can show a wide variety of behavior, ranging from highly ordered to totally chaotic. By using a variable parameter, changing which alters the behavior of the system, it has been seen that, at the region where transition from ordered to chaotic behavior occurs, the system exhibits complexity in the sense that it is capable of universal computation. Langton has extended this finding to the generalization that *"complexity occurs at the edge of chaos"*. The substance of this assertion is that

while an ordered system is too rigid to learn from experience, and chaotic systems are too unstable to exist in a competitive environment, complexity arises only in those systems having the right blend of order and chaos. Only systems poised at the "edge of chaos" , the critical state at which complexity is most likely to emerge, are rigid enough to survive, while being capable of suitably adapting themselves to a changing environment. While these findings are only for the specific system of CA, and not yet universally accepted, they are nonetheless highly suggestive. The brain, being a complex adaptive system also, might be indulging in a similar kind of tradeoff between order and chaos. Studying chaotic models of neural activity thus might provide us with an an understanding of how complexity emerges not only in the brain, but in a broad family of complex adaptive systems, of which it is a member.

Bibliography

[1] M. Adachi and K. Aihara. Associative dynamics in a chaotic neural network. *Neural Networks*, 10:83–98, 1997.

[2] R. D. Adams and M. Victor. *Principles of Neurology.* McGraw-Hill, New York, 1977.

[3] K. Aihara, G. Matsumoto, and Y. Ikegaya. Periodic and non-periodic responses of a periodically forced Hodgkin-Huxley oscillator. *J. Theo. Biol.*, 109:249–269, 1984.

[4] K. Aihara, T. Takabe, and M. Toyoda. Chaotic neural networks. *Phys. Lett. A*, 144:333–340, 1990.

[5] S. Amari. Characteristics of random nets of analog neuron-like elements. *IEEE Trans. Systems, Man and Cybernetics*, 2:643–657, 1972.

[6] S. Amari and M. Arbib, editors. *Competition and Cooperation in Neural Nets.* Springer-Verlag, New York, 1982.

[7] S. Amari and K. Maginu. Statistical neurodynamics of associative memory. *Neural Networks*, 1:63–73, 1988.

[8] D. J. Amit. *Modeling Brain Function.* Cambridge University Press, Cambridge, 1989.

[9] Y. V. Andreyev, Y. L. Belsky, A. S. Dmitriev, and D. A. Kuminov. Information processing using dynamical chaos: neural networks implementation. *IEEE Trans. Neural Networks*, 7:290–299, 1996.

[10] Y. V. Andreyev, A. S. Dmitriev, and S. O. Starkov. Information processing in one-dimensional systems with chaos. *IEEE Trans. Circuits and Systems - I*, 44:21–28, 1997.

[11] V. S. Anishchenko, A. B. Neiman, and M. A. Safanova. Stochastic resonance in chaotic systems. *J. Stat. Phys.*, 70:183–196, 1993.

[12] P. Ashwin, J. Buescu, and I. Stewart. Bubbling of attractors and synchronisation of chaotic oscillators. *Phys. Lett. A*, 193:126–139, 1994.

[13] A. Atiya and P. Baldi. Oscillations and synchronizations in neural networks: An exploration of the labeling hypothesis. *Int. J. Neural Systems*, 1:103–124, 1989.

[14] A. Babloyantz and A. Destexhe. Low-dimensional chaos in an instance of epilepsy. *Proc. Natl. Acad. Sci. USA*, 83:3513–3517, 1986.

[15] A. Babloyantz, J. M. Salazar, and C. Nicolis. Evidence of chaotic dynamics of brain activity during the sleep cycle. *Phys. Lett. A*, 111:152–156, 1985.

[16] P. Baldi and A. Atiya. How delays affect neural dynamics and learning. *IEEE Trans. Neural Networks*, 5:612–621, 1994.

[17] J. Basak. *Connectionist models for certain tasks related to object recognition.* PhD thesis, Indian Statistical Institute, Calcutta, 1994.

[18] C. Beck and F. Schlögl. *Thermodynamics of Chaotic Systems.* Cambridge University Press, Cambridge, 1993.

[19] R. Benzi, A. Sutera, and A. Vulpiani. The mechanism of stochastic resonance. *J. Phys. A*, 14:L453–L457, 1981.

[20] H. Bersini and V. Calenbuhr. Frustrated chaos in biological networks. *J. Theo. Biol.*, 188:187–200, 1997.

[21] S. Biswas, N. R. Pal, and S. K. Pal. Smoothing of digital images using the concept of diffusion process. *Pattern Recognition*, 29:497–510, 1996.

[22] S. N. Biswas and B. B. Chaudhuri. On the generation of discrete circular objects and their properties. *Computer Vision, Graphics and Image Processing*, 32:158–170, 1985.

[23] A. Blake and A. Zisserman. *Visual Reconstruction.* MIT Press, Cambridge, Mass., 1987.

[24] E. K. Blum and X. Wang. Stability of fixed points and periodic orbits and bifurcations in analog neural networks. *Neural Networks*, 5:577–587, 1992.

[25] Y. Braiman and I. Goldhirsch. Taming chaotic dynamics with weak periodic perturbations. *Phys. Rev. Lett.*, 66:2545–2548, 1991.

[26] Y. Braiman, J. F. Lindner, and W. L. Ditto. Taming spatiotemporal chaos with disorder. *Nature*, 378:465–467, 1995.

[27] D. S. Broomhead and R. Jones. Time-series analysis. *Proc. Roy. Soc. Lond. A*, 423:103–121, 1989.

[28] S. Campbell and D. L. Wang. Synchronization and desynchronization in a network of locally coupled Wilson-Cowan oscillators. *IEEE Trans. Neural Networks*, 7:541–554, 1996.

[29] J. Canny. A computational approach to edge detection. *IEEE Trans. Pattern Analysis and Machine Intelligence*, 8:679–698, 1986.

[30] T. W. Carr and I. B. Schwartz. Controlling high-dimensional unstable steady states using delay, duration and feedback. *Physica D*, 96:17–25, 1996.

[31] T. L. Carroll and L. M. Pecora. Stochastic resonance and crises. *Phys. Rev. Lett.*, 70:576–579, 1993.

[32] F. Catté, P. L. Lions,. J. M. Morel, and T. Coll. Image selective smoothing and edge detection by nonlinear diffusion. *SIAM J. Num. Anal.*, 29:182–193, 1992.

[33] Z. Chang-song, C. Tian-lun, and H. Wu-qun. Chaotic neural network with nonlinear self-feedback and its application to optimization. *Neurocomputing*, 14:209–222, 1997.

[34] T. R. Chay. Chaos in a three-variable model of an excitable cell. *Physica D*, 16:233–242, 1985.

[35] L. Chen and K. Aihara. Chaotic simulated annealing by a neural network model with transient chaos. *Neural Networks*, 8:915–930, 1995.

[36] M. Y. Choi and B. A. Huberman. Digital dynamics and the simulation of magnetic systems. *Phys. Rev. B*, 28:2547–2554, 1983.

[37] D. J. Christini and J. J. Collins. Controlling nonchaotic neuronal noise using chaos control techniques. *Phys. Rev. Lett.*, 75:2782–2785, 1995.

[38] M. Conrad. What is the use of chaos ? In A. V. Holden, editor, *Chaos*, pages 3–14. Manchester University Press, Manchester, 1986.

[39] M. Cosnard and D. Moumida. Dynamical properties of an automaton with memory. In F. Fogelman Soulié, Y. Robert, and M. Tchuente, editors, *Automata Networks in Computer Science*, pages 82–100. Manchester University Press, Manchester, 1987.

[40] A. Crisanti, M. Falcioni, G. Paladin, and A. Vulpiani. Stochastic resonance in deterministic chaotic systems. *J. Phys. A*, 27:L597–L603, 1994.

[41] J. Crutchfield, M. Nauenberg, and J. Rudnick. Scaling for external noise at the onset of chaos. *Phys. Rev. Lett.*, 46:933–935, 1981.

[42] K. M. Cuomo, A. V. Oppenheim, and S. H. Strogatz. Synchronization of Lorenz-based chaotic circuits with applications to communications. *IEEE Trans. Circuits & Systems II*, 40:626–633, 1993.

[43] V. Deshpande and C. Dasgupta. A neural network storing individual patterns in a limit cycle. *J. Phys. A*, 24:5105–5119, 1991.

[44] A. Destexhe. Oscillations, complex spatiotemporal behavior and information transport in networks of excitatory and inhibitory neurons. *Phys. Rev. E*, 50:1594–1606, 1994.

[45] M. Ding and W. Yang. Stability of synchronous chaos and on-off intermittency in coupled map lattices. *Phys. Rev. E*, 56:4009–4016, 1997.

[46] A. S. Dmitriev, M. Shirokov, and S. O. Starkov. Chaotic synchronization in ensembles of coupled maps. *IEEE Trans. Circuits and Systems-I*, 44:918–926, 1997.

[47] D. Dong. *Dynamic properties of neural networks*. PhD thesis, California Institute of Technology, 1991.

[48] J. K. Douglass, L. Wilkens, E. Pantazelou, and F. Moss. Noise enhancement of information transfer in crayfish mechanoreceptors by stochastic resonance. *Nature*, 365:337–340, 1993.

[49] B. Doyon, B. Cessac, M. Quoy, and M. Samuelides. Control of the transition to chaos in neural networks with random connectivity. *Int. J. Bif. Chaos*, 3:279–291, 1993.

[50] R. M. Everson. Scaling of intermittency period with dimension of a partition boundary. *Phys. Lett. A*, 122:471–475, 1987.

[51] W. J. Freeman. Simulation of chaotic EEG patterns with a dynamic model of the olfactory system. *Biol. Cybern.*, 56:139–150, 1987.

[52] W. J. Freeman. The physiology of perception. *Scientific American*, 264 (2):78–85, 1991.

[53] W. J. Freeman. Tutorial on neurobiology: From single neurons to brain chaos. *Int. J. Bif. Chaos*, 2:451–482, 1992.

[54] W. J. Freeman. Chaos in the brain: Possible roles in biological intelligence. *Int. J. Intelligent Systems*, 10:71–88, 1995.

[55] H. Fujisaka and T. Yamada. Stability theory of synchronized motion in coupled-oscillator systems. *Prog. Theor. Phys.*, 69:32–47, 1983.

[56] H. Fujisaka and T. Yamada. Stability theory of synchronized motion in coupled-oscillator systems IV. Instability of synchronized chaos and new intermittency. *Prog. Theor. Phys.*, 75:1087–1104, 1986.

[57] T. Fukai and M. Shiino. Asymmetric neural networks incorporating the Dale hypothesis and noise-driven chaos. *Phys. Rev. Lett.*, 64:1465–1468, 1990.

[58] P. M. Gade, R. Rai, and H. Singh. Stochastic resonance in maps and coupled map lattices. *Phys. Rev. E*, 56:2518–2526, 1997.

[59] L. Gammaitoni, P. Hänggi, P. Jung, and F. Marchesoni. Stochastic resonance. *Rev. Mod. Phys.*, 70:223–287, 1998.

[60] L. Gammaitoni, F. Marchesoni, and S. Santucci. Stochastic resonance as a *bona fide* resonance. *Phys. Rev. Lett.*, 74:1052–1055, 1995.

[61] A. Ghosh, N. R. Pal, and S. K. Pal. Object-background classification using Hopfield type neural network. *Int. J. Patt. Rec. Artif. Int.*, 6:989–1008, 1992.

[62] L. Glass and M. C. Mackey. *From Clocks to Chaos: The Rhythms of Life.* Princeton University Press, Princeton, N. J., 1988.

[63] L. Glass and C. P. Malta. Chaos in multilooped negative feedback systems. *J. Theo. Biol.*, 145:217–223, 1990.

[64] R. C. Gonzalez and R. E. Woods. *Digital Image Processing.* Addison-Wesley, Reading, Mass., 1992.

[65] P. Grassberger. Generalized dimensions of strange attractors. *Phys. Lett. A*, 97:227–230, 1983.

[66] P. Grassberger. New mechanism for deterministic diffusion. *Phys. Rev. A*, 28:3666–3667, 1983.

[67] P. Grassberger and I. Procaccia. Characterization of strange attractors. *Phys. Rev. Lett.*, 50:346–349, 1983.

[68] C. M. Gray, P. König, A. K. Engel, and W. Singer. Oscillatory responses in cat visual cortex exhibit inter-columnar synchronization which reflects global stimulus properties. *Nature*, 338:334–337, 1989.

[69] C. Grebogi, E. Ott, and J. A. Yorke. Crises, sudden changes in chaotic attractors and chaotic transients. *Physica D*, 7:181–200, 1983.

[70] S. Grossberg and D. Somers. Synchronized oscillations during cooperative feature linking in a cortical model of visual perception. *Neural Networks*, 4:453–466, 1991.

[71] S. Grossman and H. Fujisaka. Diffusion in discrete nonlinear dynamical systems. *Phys. Rev. A*, 26:1779–1782, 1982.

[72] M. R. Guevara, L. Glass, M. C. Mackey, and A. Shrier. Chaos in neurobiology. *IEEE Trans. Systems, Man and Cybernetics*, 13:790–798, 1983.

[73] S. K. Han, W. S. Kim, and H. Kook. Temporal segmentation of the stochastic oscillator neural network. *Phys. Rev. E*, 58:2325–2334, 1998.

[74] D. Hansel and H. Sompolinsky. Synchronization and computation in a chaotic neural network. *Phys. Rev. Lett.*, 68:718–721, 1992.

[75] E. Harth. Order and chaos in neural systems: An approach to the dynamics of higher brain functions. *IEEE Trans. Systems, Man and Cybernetics*, 13:782–789, 1983.

[76] E. Harth and G. Pertile. The role of inhibition and adaptation in sensory information processing. *Kybernetik*, 10:32–37, 1972.

[77] M. Hasegawa, T. Ikeguchi, T. Matozaki, and K. Aihara. Improving image segmentation by chaotic neurodynamics. *IEICE Trans. Fundamentals E*, 79-A:1630–1637, 1996.

[78] M. Hasler and Y. L. Maistrenko. An introduction to the synchronization of chaotic systems: coupled skew tent maps. *IEEE Trans. Circuits and Systems -I*, 44:856–866, 1997.

[79] H. Hayashi, M. Nakao, and K. Hirakawa. Chaos in the self-sustained oscillation of an excitable biological membrane under sinusoidal stimulation. *Physics Letters A*, 88:265–266, 1982.

[80] Y. Hayashi. Oscillatory neural network and learning of continuously transformed patterns. *Neural Networks*, 7:219–231, 1994.

[81] R. He and P. G. Vaidya. Analysis and synthesis of synchronous periodic and chaotic systems. *Phys. Rev. A*, 46:7387–7392, 1992.

[82] J. F. Heagy, T. L. Carroll, and L. M. Pecora. Desynchronization by periodic orbits. *Phys. Rev. E*, 52:R1253–R1256, 1995.

[83] J. F. Heagy, N. Platt, and S. M. Hammel. Characterization of on-off intermittency. *Phys. Rev. E*, 49:1140–1150, 1994.

[84] D. O. Hebb. *The Organization of Behavior.* Wiley, New York, 1949.

[85] J. Hertz, A. Krogh, and R. G. Palmer. *Introduction to the Theory of Neural Computation.* Addison-Wesley, Reading, Mass., 1991.

[86] M. W. Hirsch. Convergent activation dynamics in continuous time networks. *Neural Networks*, 2:331–349, 1989.

[87] A. V. Holden, editor. *Chaos.* Manchester University Press, Manchester, 1986.

[88] A. V. Holden, W. Winlow, and P. G. Haydon. The induction of periodic and chaotic activity in a molluscan neuron. *Biol. Cybern.*, 43:169–173, 1982.

[89] D. Holton and R. May. The chaos of disease response and competition. In T. Mullin, editor, *The Nature of Chaos*, pages 183–200. Oxford University Press, Oxford, 1993.

[90] J. J. Hopfield. Neural networks and physical systems with emergent collective computational abilities. *Proc. Natl. Acad. Sci. (USA)*, 79:2554–2558, 1982.

[91] J. J. Hopfield. Neurons with graded response have collective computational properties like those of two-state neurons. *Proc. Natl. Acad. Sci. (USA)*, 81:3088–3092, 1984.

[92] G. Hu, Z. Qu, and K. He. Feedback control of chaos in spatiotemporal systems. *Int. J. Bif. Chaos*, 5:901–936, 1995.

[93] E. R. Hunt. Stabilizing high-period orbits in a chaotic system: The diode resonator. *Phys. Rev. Lett.*, 67:1953–1955, 1991.

[94] M. Inoue and S. Fukushima. A neural network of chaotic oscillators. *Prog. Theor. Phys.*, 87:771–774, 1992.

[95] E. Ippen, J. Lindner, and W. L. Ditto. Chaotic resonance: a simulation. *J. Stat. Phys.*, 70:437–450, 1993.

[96] S. Ishii, K. Fukumizu, and S. Watanbe. A network of chaotic elements for information processing. *Neural Networks*, 9:25–40, 1996.

[97] L. Jin, P. N. Nikiforuk, and M. M. Gupta. Absolute stability conditions for discrete-time recurrent neural networks. *IEEE Trans. Neural Networks*, 5:954–964, 1994.

[98] L. Jin, P. N. Nikiforuk, and M. M. Gupta. Approximation of discrete-time state space trajectories using dynamic recurrent neural networks. *IEEE Trans. Automatic Control*, 40:169–176, 1995.

[99] K. Kaneko. Pattern dynamics in spatiotemporal chaos. *Physica D*, 34:1–41, 1989.

[100] K. Kaneko. Spatiotemporal chaos in one- and two-dimensional coupled map lattices. *Physica D*, 37:60–82, 1989.

[101] K. Kaneko. Clustering, coding, switching, hierarchical ordering and control in a network of chaotic elements. *Physica D*, 41:137–172, 1990.

[102] O. Kinouchi and M. H. R. Tragtenberg. Modeling neurons by simple maps. *Int. J. Bif. Chaos*, 6:2343–2360, 1996.

[103] S. Kirkpatrick, C. D. Gelatt, and M. P. Vecchi. Optimization by simulated annealing. *Science*, 220:671–680, 1983.

[104] R. Klages. *Deterministic diffusion in one-dimensional chaotic dynamical systems*. PhD thesis, Technische Universitat Berlin, 1995.

[105] C. Koch. Computation and the single neuron. *Nature*, 385:207–210, 1997.

[106] J. M. Kowalski, G. L. Albert, and G. W. Gross. Asymptotically synchronous chaotic orbits in systems of excitable elements. *Phys. Rev. A*, 42:6260–6263, 1990.

[107] M. K. Kundu and S. K. Pal. Edge detection based on human visual response. *Int. J. Systems Sci.*, 19:2523–2542, 1988.

[108] K. E. Kurten and J. W. Clark. Chaos in neural systems. *Phys. Lett. A*, 114:413–418, 1986.

[109] C. G. Langton. Computation at the edge of chaos: phase transitions and emergent computation. *Physica D*, 42:12–37, 1990.

[110] T. Y. Li and J. A. Yorke. Period three implies chaos. *Am. Math. Monthly*, 82:985 – 992, 1975.

[111] T. Lindeberg. Scale-space for discrete signals. *IEEE Trans. Pattern Analysis and Machine Intelligence*, 12:234–254, 1990.

[112] J. F. Lindner, B. K. Meadows, W. L. Ditto, M. E. Inchiosa, and A. R. Bulsara. Array enhanced stochastic resonance and spatiotemporal synchronization. *Phys. Rev. Lett.*, 75:3–6, 1995.

[113] W. A. Little. The existence of persistent states in the brain. *Math. Biosci.*, 19:101–120, 1974.

[114] E. N. Lorenz. Deterministic nonperiodic flow. *J. Atm. Sci.*, 20:130–141, 1963.

[115] J. Losson and M. C. Mackey. Coupling induced statistical cycling in two diffusively coupled maps. *Physica D*, 72:324–342, 1994.

[116] P. K. Maiti, P. K. Dasgupta, and B. K. Chakrabarti. Improved performance of the Hopfield and Little neural network models with time delayed dynamics. *Int. J. Mod. Phys. B*, 9:3025–3037, 1995.

[117] C. M. Marcus and R. M. Westervelt. Dynamics of iterated-map neural networks. *Phys. Rev. A*, 40:501–504, 1989.

[118] D. Marr. *Vision: A computational investigation into the human representation and processing of visual information.* W. H. Freeman, New York, 1982.

[119] D. Marr and E. Hildreth. Theory of edge-detection. *Proc. Roy. Soc. Lond. B*, 207:187–217, 1980.

[120] M. A. Matias and J. Güemez. Stabilization of chaos by proportional pulses in the system variables. *Phys. Rev. Lett.*, 72:1455–1458, 1994.

[121] G. Matsumoto, K. Aihara, Y. Hanyu, N. Takahashi, S. Yoshizawa, and J. Nagumo. Chaos and phase locking in normal squid axons. *Phys. Lett. A*, 123:162–166, 1987.

[122] R. M. May. Bifurcations and dynamic complexity in ecological systems. *Ann. N. Y. Acad. Sci.*, 316:517–529, 1978.

[123] J. L. McCauley. *Chaos, Dynamics and Fractals.* Cambridge University Press, Cambridge, 1993.

[124] W. S. McCulloch and W. Pitts. A logical calculus of the ideas immanent in nervous activity. *Bull. Math. Biophys.*, 5:115–133, 1943.

[125] B. McNamara and K. Wiesenfeld. Theory of stochastic resonance. *Phys. Rev. A*, 39:4854–4869, 1989.

[126] M. Mezard, G. Parisi, and M. A. Virasoro. *Spin Glass Theory and Beyond.* World Scientific, Singapore, 1987.

[127] J. Nagumo and S. Sato. On a response characteristic of a mathematical neuron model. *Kybernetik*, 10:155–164, 1972.

[128] G. Nicolis, C. Nicolis, and D. McKernan. Stochastic resonance in chaotic dynamics. *J. Stat. Phys.*, 70:125–139, 1993.

[129] J. S. Nicolis. Should a reliable information processor be chaotic ? *Kybernetes*, 11:269–274, 1982.

[130] J. S. Nicolis and I. Tsuda. Chaotic dynamics of information processing: The magic number "seven plus minus two" revisited. *Bull. Math. Biol.*, 47:343–365, 1985.

[131] K. N. Nordström. Biased anisotropic diffusion – A unified regularization and diffusion approach to edge detection. Technical Report CSD-89-514, Dept. of Computer Science, Univ. of California, Berkeley, 1989.

[132] H. E. Nusse and J. A. Yorke. Border-collision bifurcations including "period-two to period-three" for piecewise smooth systems. *Physica D*, 57:39–57, 1992.

[133] H. E. Nusse and J. A. Yorke. Border-collision bifurcations for piecewise smooth one-dimensional maps. *Int. J. Bif. Chaos*, 5:189–207, 1995.

[134] E. Ott. *Chaos in Dynamical Systems.* Cambridge University Press, Cambridge, 1993.

[135] E. Ott, C. Grebogi, and J. A. Yorke. Controlling chaos. *Phys. Rev. Lett.*, 64:1196–1199, 1990.

[136] E. Ott and J. C. Sommerer. Blowout bifurcations: The occurrence of riddled basins and on-off intermittency. *Phys. Lett. A*, 188:39–47, 1994.

[137] D. Ottoson. *Physiology of the Nervous System.* Macmillan, London, 1983.

[138] N. H. Packard, J. P. Crutchfield, J. D. Farmer, and R. S. Shaw. Geometry from a time series. *Phys. Rev. Lett.*, 47:712–715, 1980.

[139] N. R. Pal and S. K. Pal. A review of image segmentation techniques. *Pattern Recognition*, 26:1277–1294, 1993.

[140] L. M. Pecora and T. L. Carroll. Synchronization in chaotic systems. *Phys. Rev. Lett.*, 64:821–824, 1990.

[141] L. M. Pecora and T. L. Carroll. Driving systems with chaotic signals. *Phys. Rev. A*, 44:2374–2383, 1991.

[142] X. Pei and F. Moss. Characterization of low-dimensional dynamics in the crayfish caudal photoreceptor. *Nature*, 379:618–621, 1996.

[143] C. J. Perez, A. Corral, A. Diaz-Guilera, K. Christensen, and A. Arenas. On self-organized criticality and synchronization in lattice models of coupled dynamical systems. *Int. J. Mod. Phys. B*, 10:1111–1151, 1996.

[144] P. Perona and J. Malik. Scale-space and edge detection using anisotropic diffusion. *IEEE Trans. Pattern Analysis and Machine Intelligence*, 12:629–639, 1990.

[145] J. P. Pijn, J. Van Neerven, A. Noest, and F. H. Lopes da Silva. Chaos or noise in EEG signals: Dependence on state and brain site. *Electroenceph. Clin. Neuropsych.*, 79:371–381, 1991.

[146] A. S. Pikovsky and P. Grassberger. Symmetry breaking bifurcation for coupled chaotic attractors. *J. Phys. A*, 24:4587–4597, 1991.

[147] N. Platt, S. M. Hammel, and J. F. Heagy. Effects of additive noise on on-off intermittency. *Phys. Rev. Lett.*, 72:3498–3501, 1994.

[148] S. Rajasekar and M. Lakshmanan. Period-doubling bifurcations, chaos, phase-locking and devil's staircase in a Bonhoeffer - Van der Pol oscillator. *Physica D*, 32:146–152, 1988.

[149] D. H. Rao and M. M. Gupta. Chaotic behavior of a dynamic neural network. In *Proc. Third Int. Conf. Fuzzy Logic, Neural Nets and Soft Computing, (IIZUKA-94)*, pages 533–534, 1994.

[150] E. Reibold, W. Just, J. Becker, and H. Benner. Stochastic resonance in chaotic spin-wave dynamics. *Phys. Rev. Lett.*, 78:3101–3104, 1997.

[151] P. Saint-Marc, J. S. Chen, and G. Medioni. Adaptive smoothing : a general tool for early vision. *IEEE Trans. Pattern Analysis and Machine Intelligence*, 13:514–529, 1991.

[152] H. Sakaguchi and K. Tomita. Bifurcations of the coupled logistic map. *Prog. Theo. Phys.*, 78:305–315, 1987.

[153] P. P. Saratchandran, V. M. Nandakumaran, and G. Ambika. Dynamics of the logistic map under discrete parametric perturbation. *Pramana - J. Phys.*, 47:339–345, 1996.

[154] J. Sarraille and Peter DiFalco. FD3, ver 0.3 (fractal dimension estimation software), 1992. (available at ftp:// ftp.immt.pwr.wroc.pl/ pub/ fractal).

[155] S. J. Schiff, K. Jerger, D. H. Duong, T. Chang, M. L. Spano, and W. L. Ditto. Controlling chaos in the brain. *Nature*, 370:615–620, 1994.

[156] T. B. Schillen and P. König. Binding by temporal structure in multiple feature domains of an oscillatory neuronal network. *Biol. Cybern.*, 70:397–405, 1994.

[157] N. J. Schulmann. Chaos in piecewise linear systems. *Phys. Rev. A*, 28:477–479, 1983.

[158] C. Seko and K. Takatsuka. Rhythmic hopping in a one-dimensional crisis map. *Phys. Rev. E*, 54:956–959, 1996.

[159] D. Sherrington. Spin glasses and neural networks. In J. G. Taylor and C. L. T. Mannion, editors, *New Developments in Neural Computing*, pages 15–30. Adam Hilger, Bristol, 1989.

[160] I. Shimada and T. Nagashima. A numerical approach to ergodic problems of dissipative dynamical systems. *Prog. Theor. Phys.*, 61:1605–1616, 1979.

[161] T. Shinbrot, C. Grebogi, E. Ott, and J. A. Yorke. Using small perturbations to control chaos. *Nature*, 363:411–417, 1993.

[162] T. Shinbrot and J. M. Ottino. Using horseshoes to create coherent structures. *Phys. Rev. Lett.*, 71:843–846, 1993.

[163] S. W. Sides, R. A. Ramos, P. A. Rikvold, and M. A. Novotny. Kinetic Ising system in an oscillating external field: stochastic resonance and residence-time distributions. *J. Appl. Phys.*, 81:5597–5599, 1997.

[164] S. W. Sides, P. A. Rikvold, and M. A. Novotny. Stochastic hysteresis and resonance in a kinetic Ising system. *Phys. Rev E* (to appear), 1998. (http:// xxx.lanl.gov/ abs/ cond-mat/ 9712021).

[165] S. Sinha. Unidirectional adaptive dynamics. *Phys. Rev. E*, 49:4832–4842, 1994.

[166] S. Sinha. Chaos control in an oscillatory neural network model. *J. IETE*, 42:205–213, 1996.

[167] S. Sinha. Controlled transition from chaos to periodic oscillations in a neural network model. *Physica A*, 224:433–446, 1996.

[168] S. Sinha. Geometry of chaos control in a one-dimensional map. In *Proc. Int. Conf. Dynamical Systems, Bangalore*, page 61, 1997.

[169] S. Sinha. Chaos and synchronization in simple excitatory-inhibitory neural network models. In *Proc. Int. Conf. Nonlinear Dynamics and Brain Functioning, Bangalore*, page 54, 1998.

[170] S. Sinha. Chaotic dynamics in iterated map neural networks with piecewise linear activation function. *Fundamenta Informaticae* (to appear), 1998.

[171] S. Sinha. Frustrated synchronization in competing drive-response coupled chaotic systems. LANL e-print, 1998. (http:// xxx.lanl.gov/ abs/ chao-dyn/ 9808017).

[172] S. Sinha and J. Basak. Response of an excitatory-inhibitory neural network to external stimulation: An application to image segmentation. LANL e-print, 1998. (http:// xxx.lanl.gov/ abs/ cond-mat/).

[173] S. Sinha and S. Biswas. Associative memory for gray-level images. In *Proc. IEEE Int. Conf. Image Processing*, Santa Barbara, Calif., pages 871–873, 1997.

[174] S. Sinha and B. K. Chakrabarti. Deterministic SR in a piecewise linear chaotic map. *Phys. Rev. E* (to appear), 1998. (available at http:// xxx.lanl.gov/ abs/ chao-dyn/ 9803033).

[175] S. Sinha and P. K. Das. Dynamics of simple one-dimensional maps under perturbation. *Pramana - J. Phys.*, 48:87–98, 1997.

[176] S. Sinha and S. Kar. Competition among synchronizing chaotic systems: Implications for neural computation. In T. Yamakawa and G. Matsumoto, editors, *Methodologies for the conception, design and application of intelligent systems*, pages 700–703. World Scientific, Singapore, 1996.

[177] C. A. Skarda and W. J. Freeman. How brains make chaos in order to make sense of the world. *Behavioral and Brain Sciences*, 10:161–195, 1987.

[178] S. M. Smirnakis, M. J. Berry, D. K. Wayland, W. Bialek, and M. Meister. Adaptation of retinal processing to image contrast and spatial scale. *Nature*, 386:69–73, 1997.

[179] R. V. Sole and L. M. de la Prida. Controlling chaos in discrete neural networks. *Phys. Lett. A*, 199:65–69, 1995.

[180] H. Sompolinsky, A. Crisanti, and H. J. Sommers. Chaos in random neural networks. *Phys. Rev. Lett.*, 61:259–262, 1988.

[181] H. Sompolinsky, D. Golomb, and D. Kleinfeld. Global processing of visual stimuli in a neural network of coupled oscillators. *Proc. Natl. Acad. Sci. USA*, 87:7200–7204, 1990.

[182] C. Sparrow. *The Lorenz Equations: Bifurcations, Chaos, and Strange Attractors.* Springer-Verlag, New York, 1982.

[183] O. Sporns, G. Tononi, and G. M. Edelman. Modeling perceptual grouping and figure-ground segregation by means of active reentrant connections. *Proc. Natl. Acad. Sci. USA*, 88:129–133, 1991.

[184] V. Srinivasan, P. Bhatia, and S. H. Ong. Edge detection using a neural network. *Pattern Recognition*, 27:1653–1662, 1994.

[185] P. Sterling. The Retina. In G. M. Shepherd, editor, *The Synaptic Organization of the Brain*, pages 170–213. Oxford University Press, Oxford, 1990.

[186] N. Stollenwerk. Self-controlling chaos in neuromodules. In H. Herrmann, E. Pöppel, and D. Wolf, editors, *Supercomputing in Brain Research: From Tomography to Neural Networks*, pages 421–426. World Scientific, Singapore, 1995.

[187] L. Stone. Period-doubling reversals and chaos in simple ecological models. *Nature*, 365:617–620, 1993.

[188] S. H. Strogatz. *Nonlinear Dynamics and Chaos.* Addison-Wesley, Reading, Mass., 1994.

[189] M. M. Sushchik, N. F. Rulkov, and H. D. I. Abarbanel. Robustness and stability of synchronized chaos: An illustrative model. *IEEE Trans. Circuits and Systems-I*, 44:867–873, 1997.

[190] J. Testa and G. A. Held. Study of a one-dimensional map with multiple basins. *Phys. Rev. A*, 28:3085–3089, 1983.

[191] C. M. Thomas, W. G. Gibson, and J. Robinson. Stability and bifurcations in an associative memory model. *Neural Networks*, 9:53–66, 1996.

[192] I. Tsuda. Dynamic link of memory: Chaotic memory map in nonequilibrium neural networks. *Neural Networks*, 5:313–326, 1992.

[193] E. Vaadia, I. Haalman, M. Abeles, H. Bergman, Y. Prut, H. Slovin, and A. Aertsen. Dynamics of neuronal interactions in monkey cortex in relation to behavioral events. *Nature*, 373:515–518, 1995.

[194] C. von der Malsburg and J. Buhmann. Sensory segmentation with coupled neural oscillators. *Biol. Cybern.*, 67:233–242, 1992.

[195] D. L. Wang. Emergent synchrony in locally coupled neural oscillators. *IEEE Trans. Neural Networks*, 6:941–948, 1995.

[196] L. Wang. Oscillatory and chaotic dynamics in neural networks under varying operating conditions. *IEEE Trans. Neural Networks*, 7:1382–1388, 1996.

[197] X. Wang. Period-doublings to chaos in a simple neural network: An analytical proof. *Complex Systems*, 5:425–441, 1991.

[198] X. Wang and E. K. Blum. Discrete time vs continuous time models of neural networks. *J. Comp. Syst. Sci.*, 45:1–19, 1992.

[199] J. Weickert and B. Benhamouda. Why the Perona-Malik filter works. Technical Report DIKU-TR-97/22, Dept. of Computer Science, Univ. of Copenhagen, 1997. (available at http:// www.diku.dk/ users/ joachim/).

[200] F. S. Werblin. Functional organization of a vertebrate retina: sharpening up in space and intensity. *Ann. N. Y. Acad. Sci.*, 190:75–85, 1972.

[201] F. S. Werblin. The control of sensitivity in the retina. *Sci. Am.*, 228 (1):71–79, 1973.

[202] R. T. Whitaker and S. M. Pizer. A multi-scale approach to nonuniform diffusion. *CVGIP: Image Understanding*, 57:99–110, 1993.

[203] I. C. Whitfield. *Neurocommunications: An Introduction.* John Wiley, Chichester, 1984.

[204] H. R. Wilson and J. D. Cowan. Excitatory and inhibitory interactions in localized populations of model neurons. *Biophys. J.*, 12:1–24, 1972.

[205] T. Yamakawa, M. Shimono, and T. Miki. Design criteria for robust associative memory employing non-equilibrium network. In T. Yamakawa and G. Matsumoto, editors, *Methodologies for the conception, design and application of intelligent systems*, pages 688–691. World Scientific, Singapore, 1996.

[206] T. Yoshida, H. Mori, and H. Shigematsu. Analytic study of the tent map: band structures, power spectra and critical behaviors. *J. Stat. Phys.*, 31:279–308, 1983.

[207] Y. H. Yu, K. Kwak, and T. K. Lim. On-off intermittency in an experimental synchronization process. *Phys. Lett. A*, 198:34–38, 1995.

LIST OF PUBLICATIONS OF THE AUTHOR

1. S. Sinha, "Influence of asymmetric initial configurations on the recall properties of the Hopfield net", *J. IE(I)*, vol. 74, pp. 28–31, 1993.

2. S. Sinha, "The evolution of adaptability: the artificial life approach", *Ind. J. Phys.*, vol. 69 B, pp. 625–640, 1995.

3. S. Sinha, "Controlled transition from chaos to periodic oscillations in a neural network model", *Physica A*, vol. 224, pp. 433–446, 1996.

4. S. Sinha, "Chaos control in an oscillatory neural network model", *J. IETE*, vol. 42, pp. 205–213, 1996.

5. S. Sinha and S. Kar, "Competition among synchronizing chaotic systems: Implications for neural computation", in T. Yamakawa and G. Matsumoto (eds.), *Methodologies for the conception, design and application of intelligent systems*, pp. 700–703, (World Scientific, Singapore) 1996.

6. S. Sinha, "Adaptive walks in fitness landscapes", *Ind. J. Theo. Phys.*, vol. 44, pp. 63–73, 1996.

7. S. Sinha, "Geometry of chaos control in a one-dimensional map", in *Proc. Int. Conf. Dynamical Systems, Bangalore*, pg. 61, 1997.

8. S. Sinha and S. Biswas, "Associative memory for gray-level images", in *Proc. IEEE Int. Conf. Image Processing, Santa Barbara, Calif.*, pp. 871–873, 1997.

9. S. Sinha and B. K. Chakrabarti, "Deterministic stochastic resonance in a piecewise linear chaotic map", *Phys. Rev. E* (to appear), 1998.

10. S. Sinha, "Chaotic dynamics in iterated map neural networks with piecewise linear activation function", *Fundamenta Informaticae* (to appear), 1998.

11. S. Sinha, "Chaos and synchronization in simple excitatory-inhibitory neural network models", in *Proc. Int. Conf. Nonlinear Dynamics and Brain Functioning, Bangalore*, pg. 54, 1998.

12. S. Sinha, "Frustrated synchronization in competing drive-response coupled chaotic systems", LANL e-print (http:// xxx.lanl.gov/ abs/ chao-dyn/ 9808017), 1998.

13. S. Sinha and J. Basak, "Response of an excitatory-inhibitory neural network to external stimulation: An application to image segmentation", LANL e-print (http:// xxx.lanl.gov/ abs/ cond-mat/), 1998.